Investigating the Impact of Lead Exposure on Epigenetic Regulation During Neural Differentiation and Neurodevelopment: Focus on piRNA and Transposable Element Regulation

by

Rachel Kelley Morgan

A dissertation submitted in partial fulfillment
of the requirements for the degree of
Doctor of Philosophy
(Environmental Health Sciences)
in the University of Michigan
2023

Doctoral Committee:

Associate Professor Justin A. Colacino, Co-Chair
Professor Dana C. Dolinoy, Co-Chair
Research Associate Professor Jackie M. Goodrich
Professor Maureen A. Sartor
Assistant Professor Laurie K. Svoboda

Rachel K. Morgan

rkmorgan@umich.edu

ORCID iD: 0000-0002-0157-7755

Dedication

This dissertation is dedicated to my mom, Mary. Your generosity, honesty, and humor are things I miss every day.

Acknowledgements

I would like to thank my primary research mentors, Dr. Dana Dolinoy and Dr. Justin Colacino, for all their help and guidance over the last five years. Whenever I felt overwhelmed or unsure of my footing, they both provided support and confidence. Their consistent passion and excitement for all things science reminds me that there is fun in the work. I would also like to thank my committee members, Dr. Laurie Svoboda, Dr. Jackie Goodrich, and Dr. Maureen Sartor, all of whom shared their time and expertise with me throughout this process. This dissertation was also made possible by support from Dr. Claudia Lalancette and Dr. Jonny Sexton, both of whom helped ensure these projects were completed. I am also immensely grateful for my funding sources, including the NIEHS Environmental Toxicology and Epidemiology Program (ETEP) T32 ES007062, the NICHD Career Training in Reproductive Biology (CTRB) training grant T32 HD079342, and the University of Michigan Rackham One Term Dissertation Fellowship.

Thanks are also due to the many friends and family who have supported me during this experience. My dad, Steve, has supported my interest in science for as long as I can remember. Nothing compares to going out in the middle of winter to collect water samples from the Milwaukee River for a 6th grade science project. Katelyn Polemi and Tomoko Ishikawa are wonderful friends who have always been willing to listen, be it to ideas for a new experiment or to stressors of the week, and they both went above and beyond in the lab, helping me to complete many of the projects in this dissertation.

The last five years would have been a whole lot less fun without my best friend, Emma. Thank you for always taking the time to build me up when I needed it. Finally, an immense amount of love and gratitude also goes to my husband, Peter. Thank you for the encouragement when I was unsure, the humor when I was upset, and the constant assurance that the work would pay off. I am so fortunate to have a partner in you.

Table of Contents

List of Tables

List of Figures

Abstract

Neurodegenerative disease (ND) constitutes a substantial public health burden as roughly 50 million people globally have some form of dementia, and this number is expected to triple by 2050. ND risk may be partially attributable to early developmental exposures, as described by the Developmental Origins of Health and Disease hypothesis. One avenue by which developmental exposures modulate the risk of disease is through perturbations to the epigenome, broadly defined as mitotically heritable modifications to the genome that are independent of the DNA sequence. Of these, DNA methylation (DNAm) and small non-coding RNAs (ncRNA) such as PIWI-interacting RNA (piRNA) work to control the expression of transposable elements (TEs). TEs are elements of the genome with the capacity to mobilize and pose a threat to genomic integrity if not properly controlled. Lead (Pb) has been associated with hypomethylation of these elements, and TE hypomethylation has also been documented in persons with ND. It is hypothesized that Pb-induced disruption of TE regulation may contribute to ND risk and progression.

The objective of this dissertation was to evaluate epigenetic regulation of TEs in the developing brain and to what extent Pb exposure disrupts this process. In Aim 1, we utilized a mouse developmental exposure model to evaluate changes in DNAm throughout the genome in adulthood following perinatal Pb exposure. We found Pb exposure to be associated with differentially methylated regions in the brain and blood at LINE-1 elements, an active class of TEs, the majority of which were hypomethylated.

Additionally, we identified imprinted genes as a class of interest, and two such genes with differential methylation included *Gnas* and *Grb10*, both known to be important to neurodevelopment. We identified the imprinting control region of *Grb10* as a candidate for future biomarker work, in that Pb-induced changes in DNAm were replicated in the blood and brain. In Aims 2 and 3, we utilized the SH-SY5Y cell model to investigate the relationships between Pb exposure and neural differentiation. In Aim 2, we found Pb exposure was associated with markers of cellular stress during early differentiation and that consistent exposure resulted in impaired differentiation by later stages. In Aim 3, we found preliminary evidence that Pb exposure disrupts epigenetic regulation of LINE-1 TEs during neural differentiation, with decreased DNAm and *PIWIL* expression, as well as increased LINE-1 mRNA expression. However, these results were somewhat inconclusive and need further exploration. Given the role of piRNA in regulating TEs, it is likely that this class of ncRNA will continue to be a focus of toxicological work. In Aim 4, we characterized the expression of *PIWIL* mRNA and piRNA transcripts in several human somatic tissues from early development. We found comparable levels of *PIWIL3* and 4 mRNA and piRNA expression in all tissues, with distinct profiles identified in males and females. Additionally, we found that the genomic targets of both muti- and uniquely mapping piRNA in the soma mirrored those of the gonads, suggesting the presence and function of piRNA may not be as unique to the germline as has previously thought, particularly during early development. This work demonstrates that the impact of Pb exposure on the neural epigenome may be stage-specific and that effects persist into later life stages, and that continued assessment of how Pb exposure perturbs

piRNA expression and function may elucidate relevant mechanisms behind this relationship.

Chapter 1
Introduction

Lead

Lead (Pb) is a metal with which humans have a long history of use and exposure. In recent years, most exposures to Pb have occurred via drinking water, Pb-based paint, contaminated soil, with less occasional exposures occurring via children's toys, jewelry, candy, and ceramics.[1] Historically, leaded gasoline was a prolific source of exposure, as its combustion resulted in vast amounts of Pb being released into the air.[2] Despite advances in legislation that have reduced or eliminated the use of Pb in paints and gasoline, Pb exposures continue to occur, most commonly through legacy homes and infrastructure.[3,4] Homes built before 1978 often contain one or more Pb-associated hazards, as regulations pertaining to the use of Pb in plumbing and paint, as well as the proper disposal of Pb-containing waste, were not enforced up until that year.[5,6] Pb from these household sources primarily results in ingested exposures, via either drinking water or ingestion of Pb-containing paint, dust, or soil, and these routes of exposure are much more likely in children as they frequently engage in hand-to-mouth behaviors.[7] Inhalation is another common route of exposure when Pb-containing particles from dust, paint, and soil become airborne and are deposited in the lungs.[8]

Once absorbed into the blood, Pb has a half-life of roughly 28 days, but this varies depending on age, health factors such as pregnancy, and occupation.[9,10] Pb is distributed and stored in soft tissues such as the liver, neural tissue, and the kidneys,

however the most significant site of Pb storage is bone.[9] It is estimated that as much as 95% of Pb in adult tissues is stored within bone, and this measure is roughly 70% in children.[11,12] The half-life of Pb once it has been taken up into the bone is estimated to be 25-30 years.[13] Once stored there, Pb is largely considered to be inert, however the remobilization of Pb from bone storage is accelerated during periods of pregnancy and lactation, disease, and calcium deficiencies.[14]

Standards for what is deemed an actionable blood lead level (BLL) have changed dramatically over the last fifty years in the US. In 1971, a BLL of 80μg/dL was considered the threshold for Pb poisoning. In 1991, this was reduced to 10μg/dL and re-termed a BLL of concern. In 2012, the Center for Disease Control (CDC) set the blood lead reference value (BLRV) at 5μg/dL and reduced it once again in 2021 to 3.5μg/dL.[15] These modifications in standards and thresholds have only occurred over the last several decades, meaning much of the US population has lived some portion of their lives in the presence of what we now consider to be unacceptable levels of Pb exposure. The vast majority of people in the US have been exposed to Pb at some point in their life, with nearly 54% of people estimated to have had BLLs greater than 5μg/dL at some point during their childhood.[16] Roughly 1.23 million children in the US today have BLLs >5μg/dL,[17] and major disparities in exposure exist.[18,19] Significant delineations in exposure follow socioeconomic trends in the US, with children living in low-income communities and older homes bearing the brunt of this public health burden.[20] Moreover, given the extensive history of structural racism throughout the US, trends of greater childhood Pb exposure among those of low socioeconomic status ensures that non-Hispanic black, Hispanic, and non-Hispanic Asian children have a

significantly higher risk of Pb exposure and poisoning relative to their non-Hispanic white counterparts.[21] Pb exposure in the US therefore represents a significant environmental justice issue, and continued research that may promote stricter and more productive legislation pertaining to minimizing exposure events is warranted.

Neurodegenerative Disease

Neurodegenerative disease (ND) constitutes a substantial public health burden, and the number of individuals in the US with such conditions is only expected to increase in the coming years as the proportion of elderly rises.[22,23] Globally, roughly 50 million people have some form of dementia, and this number is expected to more than triple by 2050.[24] In the US, nearly 7 million people are living with Alzheimer's disease (AD), with rates expected to double by 2050,[25] and as many as 90,000 people are diagnosed with Parkinson's disease (PD) each year.[26] In 2020, it was estimated that the totality of NDs in the US constitute $655 billion in health care, social and caregiver, and economic costs.[27]

The risk of developing NDs has been associated with several environmental exposures, including Pb, though this area of research is still relatively understudied.[28,29] This compounds the issue of an aging population as the incoming generation of individuals over the age of 65 largely grew up during the 1960s and 70s, that is, during decades of heavy Pb use prior to its restriction. For these reasons, the National Institute of Aging has made it a priority to understand the environmental risk factors associated with NDs such as AD and other dementias, as outlined in the 2018 strategic plan *Understanding the Impact of the Environment to Advance Disease Prevention*, which aims to improve our ability to treat and prevent AD by 2025.[30] Research into the

mechanisms by which Pb exposure contributes to ND is a major opportunity, not only to further motivate legislative efforts to reduce and eliminate Pb exposure, but also in the search for therapeutic avenues. If we better understand the pathways by which Pb exposure contributes to neurological disease risk, we may identify novel therapeutic targets.

Developmental Origins of Health and Disease

The health risks associated with Pb exposure are significantly influenced by exposure timing, as the type and intensity of cognitive impacts of Pb exposure appear to be dependent on when exposure occurs, as neurodevelopment is a dynamic process that occurs across multiple developmental stages.[31,32] The Developmental Origins of Health and Disease (DOHaD) hypothesis postulates that environmental exposures that occur during critical windows of development can have significant impacts on long term health and disease risk.[33] Such critical windows are prime opportunities for Pb exposure to occur, as they coincide with underdeveloped barriers and unique physiology. Placental transfer of Pb during pregnancy happens readily, as Pb is able to cross the placenta and maternal BLLs have been positively associated with umbilical cord BLLs as well as Pb levels in offspring.[34,35] Pb is also able to cross and impair the blood brain barrier, this being particularly true during early life when this barrier is not yet fully formed.[36,37] Additional physiological barriers across which Pb can travel, including the gastrointestinal tract, are also still developing during early years of life, and children are estimated to absorb as much as 5 times the amount of Pb via ingestion as their adult counterparts.[13] These greater rates of absorption in children are compounded by the fact that children engage in much higher rates of hand-to-mouth behaviors as they

interact with their environment, meaning their chances of ingesting Pb-containing materials such as dust and paint is much higher than that of adults.[38] Taken together, the ability of Pb to efficiently cross these barriers makes early development and childhood particularly vulnerable periods for Pb exposure.[39]

There is ample evidence of the association between early developmental Pb exposure and adverse cognitive outcomes. Much of the epidemiological work quantifies exposure during infancy and early childhood and has found that Pb exposure is associated with adverse neurodevelopmental outcomes, such as neurobehavioral symptoms.[40,41] Complementary *in vivo* work has demonstrated a relationship between developmental Pb exposures and ND-like phenotypes, including tau protein expression and the accumulation of amyloid plaques in mice,[42,43] as well as ND-pathology in cortical tissue of primates.[44]

Mechanistic *in vitro* work demonstrates some of the cellular dysfunction associated with Pb exposure and ND, such as increased oxidative stress and apoptosis.[45,46] One of the primary ways in which Pb disrupts normal cellular function is through competition with calcium cations, thereby gaining access to cells via calcium transporters and subsequently altering calcium homeostasis, which has direct effects on neural signaling.[47] Pb is also able to compete with zinc cations, thereby disrupting the ability of zinc-finger proteins, a major transcription factor class, to bind to nucleic acid.[48] The disordered function of many of these zinc-finger proteins, such as dopamine and NDMA receptors, have in turn been implicated in ND risk.[49] Pb also inhibits thiol groups in the mitochondria, leading to a reduction in glutathione levels, which normally acts as an antioxidant.[50] This alteration to mitochondrial homeostasis leads to an increase in

oxidative stress, to which the brain is particularly susceptible given its need for a continuous supply of ATP.[51] Finally, Pb exposure has been shown to have toxic effects on cellular membranes through lipid peroxidation via the creation of reactive oxygen species during periods of oxidative stress.[52] Taken together, these mechanisms of Pb toxicity pose a substantial threat to developing neural populations and are suspected to contribute to ND risk later in life.[53]

Epigenetic Gene Regulation and piRNA

One avenue by which early developmental exposures are thought to modulate one's risk for ND later in life is through perturbation of epigenetic mechanisms.[54,55] Epigenetics is broadly defined as mitotically heritable modifications to the genome that are independent of the DNA sequence itself, and these mechanisms play important roles in the regulation of gene expression.[56] Epigenetic mechanisms are typically classified under three categories: DNA methylation (DNAm), histone modifications, and small, non-coding RNA (ncRNA).[57] DNAm is the most abundantly studied epigenetic mechanism and entails the addition of a methyl group to the fifth position of a cytosine (5mC) that is adjacent to a guanine (CpG). CpG sites are enriched in certain regions of the genome, such as gene promoters, and increased presence of 5mC within such regions is generally associated with reduced transcription from that location.[58] Histone modifications largely regulate chromatin conformation, loosening or tightening the structure of chromosomes, thus making transcription more or less likely in a given region.[59]

Regulation by small ncRNA encompasses several classes, each with their own unique biology and function. Along with microRNA (miRNA) and short interfering RNA

(siRNA), PIWI-interacting RNA (piRNA) are a class of short ncRNA that, along with PIWI proteins, regulate gene expression, and this has been extensively characterized germline.[60] piRNA is best known for its regulation of transposable elements (TEs), genetic elements that contains the capacity for mobility, i.e., the ability to change position within the genome.[61] This mobility poses a substantial risk to genomic integrity as replication and reinsertion of TEs can introduce genetic mutations that have deleterious effects on cellular health and longevity.[62] Studies examining several classes of TEs found that the expression of transposon-derived piRNA transcripts increased during early development and this expression was upstream and required for *de novo* DNAm of these elements by DNA methyltransferases (DNMTs).[60,63] Additional work has found that suppression of the piRNA system results in increased transposition mutagenesis, whereas overexpression of this system results in greater DNMT expression and inhibition of TE activity.[64]

While much of the work on piRNA function focuses on the germline, recent work has characterized the expression of piRNA within the mouse soma and found notable levels of expression in several brain regions during adulthood.[65] A small but growing body of literature suggests that piRNA may play a role in neural differentiation and development via piRNA-directed regulation of TEs. LINE-1 retrotransposons have been shown to retrotranspose within neural precursor cells, and this activity has the capacity to alter the expression of neural genes, thus impacting cell fate.[66,67] LINE-1 regulation has also been shown to influence experience-dependent neural plasticity within the mouse hippocampus.[68] These results taken together motivate continued evaluation of

the role of piRNA and TE epigenetic regulation in the development of ND, as well as its response to classic neurotoxicants.

These epigenetic mechanisms work in close collaboration to regulate gene expression throughout the genome and their dynamics are constantly changing depending on cell type, developmental period, and their environment.[69,70] The epigenome undergoes massive reprogramming during early development, with nearly the entirety of DNAm marks erased and then replaced as differentiation takes off and cellular populations expand.[71] Environmental exposures during critical windows of development can alter the epigenome, with effects lasting into childhood and adulthood.[72,73] Epidemiological work had found persistent changes in DNAm patterns in peri-adolescent blood samples following gestational Pb exposure, as measured via maternal BLLs, with changes seen at genes important for neurodevelopment.[74] Additional work in the mouse model has identified similar results, with perinatal Pb exposure associated with aberrant DNAm patterns in the brain.[75,76]

Aberrant Epigenetic Patterns and Neurodegenerative Disease Risk

These results highlight the epigenome as a potential mechanistic link between developmental Pb exposure and adverse neurological outcomes later in life. A growing body of literature demonstrates that several epigenetic mechanisms may play a role in ND risk. Loss of heterochromatin with age, as well as increased levels of histone marks associated with a more open chromatin conformation, have been associated with increased rates of cellular apoptosis and inflammation, as well as reductions in neural signaling and plasticity.[77] Regarding ncRNAs, differential expression of miRNA has also been documented in individuals with NDs such as AD, several of which have been

linked to amyloid plaque accumulation and inflammatory pathways.[78,79] Recent work has also shown depletion of piRNA in human tissues with ND-like phenotypes (namely the accumulation of tau protein) and increased TE expression.[80] Outside of TEs, piRNA has also been shown to regulate the expression of *CREB2*, a major inhibitor of memory formation,[81] and there is evidence of differential piRNA expression in the cortical tissue of individuals diagnosed with AD.[82] Finally, DNA methylation and hydroxymethylation have been linked to ND risk as well.[83] Hypomethylation of the *APOE* gene has been documented in several epidemiological cohorts of ND, increased expression of which is closely associated with AD.[84,85]

Two gene classes that require finely tuned epigenetic regulation, both during early development as well as throughout life, are TEs and imprinted genes. As stated, TEs require consistent regulation to prevent deleterious effects to the genome, as has been documented in several neural models. In addition to this, aberrant DNAm of several TE classes has been implicated in ND risk, as individuals with AD, PD, and ALS have been shown to have differential methylation at these repetitive elements.[86–88] Additionally, imprinted genes are a class of interest with regard to neurodevelopment and ND risk. Imprinted genes are defined by their mono-allelic expression that is determined in a parent-of-origin manner, meaning that either the maternal or paternal allele is expressed in a given tissue or cell population, while the other is epigenetically repressed.[89] Aberrant epigenetic patterns within several imprinted genes has been associated with several NDs.[90,91] Continued work is needed evaluating whether aberrant epigenetic patterns that are established during early periods of development in such gene classes contribute to ND risk.

Experimental Design

The research in this dissertation utilizes mouse and cell models of developmental Pb exposure in order to 1) ascertain how early Pb exposure affects the epigenome in the developing brain and 2) elucidate possible mechanisms by which Pb exposure perturbs gene regulation during neural differentiation. Additionally, this dissertation employs a human tissue model to characterize the presence of piRNA in the soma, which will be important to future toxicoepigenomic studies assessing the impact of Pb exposure in various developing tissues, including the brain. An overview of these experimental aims can be found in **Figure 1.1**.

Aim 1

The first aim of this dissertation examines the associations between perinatal Pb exposure and changes in DNAm throughout the genome in blood and cortex within a mouse model. Previous work has found perinatal Pb exposure in mice is associated with differential gene expression in several cell types within the brain during adulthood (>3 months of age).[42,92,93] There is a growing body of work assessing the impact of Pb exposure on DNAm in this model system, and while notable associations have been detected, much of this work is either limited to males[75] or uses gene-specific methods of DNAm quantification (i.e., pyrosequencing)[76] to study individual genes or gene classes. To date, there is limited work exploring genome-wide associations between developmental Pb exposure and DNAm in males and females in the mouse model. This work is also one of few attempts to assess whether Pb-associated changes of DNAm in the brain are replicated in the blood.

Animals were obtained from wild-type non-agouti *a/a* mice from an over 230-generation colony of viable yellow agouti (A^{vy}) mice, which are genetically invariant mice 93% identical to the C57BL/6J strain.[75] Virgin *a/a* females (6-8 weeks old) were randomly assigned to control or Pb-acetate water two weeks prior to mating with virgin *a/a* males (7-9 weeks old). The Pb concentration was set at 32 ppm to model human relevant perinatal exposure, where we have previously measured murine maternal BLLs of 16-60μg/dL (mean: 32.1μg/dL).[94] Pb exposure continued through weaning at post-natal day 21 (PND21) and offspring were maintained for 5 months, at which point blood and cortex tissue was collected from 1 male and 1 female per litter (n = 6 males and n = 6 females per exposure group). Whole genome bisulfite sequencing (WGBS) was utilized to quantify changes in DNAm throughout the mouse genome in these tissues.

This study seeks to address several gaps in knowledge: 1) whether developmental Pb exposure is associated with altered DNAm in blood and cortex in adulthood, 2) if changes in DNAm are similar between these two tissues, 3) if there are sex-specific effects of Pb exposure on DNAm, and 4) whether there are certain gene classes that are particularly affected by Pb exposure and what implications this has for neurodevelopment. Based on available literature, we hypothesized that perinatal exposure to Pb would be largely associated with hypomethylated differentially methylated regions (DMRs) in both cortex and blood, and that there would be notable overlap in DNAm signatures between cortex and blood.

Aim 2

There is ample *in vitro* evidence of the effects of Pb on neurons as well as neuronal support cells, such as microglia and astrocytes,[95,96] which highlights significant

disruption of cellular metabolism, synaptic communication, and the balance of reactive oxygen species.[95,97,98] Cellular models of Pb neurotoxicity have helped elucidate the mechanisms by which Pb disrupts normal processes. However, much of this work entails exposing cells only after they have fully developed, rather than modeling exposures that occur during the process of neural differentiation. The latter is much more reflective not only of human developmental exposures, which often occur during gestational as well as post-natal periods of development,[35,99] but also of the exposure models we employ *in vivo*, wherein Pb exposure begins preconception and is sustained through gestation and lactation.[75,76] Neural differentiation and development are long and complex processes, beginning in the early periods of gestation when neurulation and neural proliferation occur, followed by weeks of neural migration and synaptogenesis. These processes continue after birth, as neural networks are remodeled and myelinated.[100,101] It is therefore pertinent that cellular models of neurotoxicity employ exposure paradigms that cover neurogenesis.

Aims 2 utilizes the SH-SY5Y neuroblastoma (5Y) cell model, which is a robust and tractable model of neural differentiation and produces dopaminergic-like neurons in 18 days. This model is commonly employed in toxicological research given the extensive characterization of these cells throughout differentiation, making it efficient to measure deviations in this process.[102] This model is also more likely to be used in studies characterizing the effects of toxicant exposures that occur during differentiation, rather than only before or after, likely due to their being a relatively hardy cell model.[103,104] Given Pb's ability to cross the blood brain barrier, we designed the dose range in this study to reflect various BLLs from the past fifty years. The lowest dose of

0.16μM is analogous to a BLL of 3.5μg/dL, the current actionable level set by the CDC, while the moderate dose of 1.26μM is reflective of BLLs seen in the 1960s and 70s, and therefore represents exposures that occurred in people who are now 55-65 years of age in the US. Finally, we included 10μM as our highest dose, as it represents an acute exposure and was also determined to be the maximum concentration these cells could tolerate.

Aim 2 assesses the impact of Pb exposure on morphological measures of 5Y differentiation. At multiple time points during differentiation, cells were fixed and stained with fluorescently tagged antibodies for imaging. Images were then analyzed using CellProfiler software, which quantified the intensity of markers of neural differentiation (β-tubulin III, GAP43, and MAP2), as well as the nucleus (Hoechst). The location and structure of these markers was further utilized in the characterization of neuronal morphology (i.e., cell size, degree of neuron branching, etc.). These measures taken together give us a good sense of how Pb exposure during differentiation affects cell health and morphology. This aim seeks assess 1) if Pb exposure during 5Y differentiation disrupts neural morphology in a dose-dependent manner, 2) whether exposure also alters the expression of classic markers of 5Y differentiation, and 3) if these effects are more pronounced during early or late stages of differentiation. We hypothesized that Pb exposure will significantly alter neural morphology (i.e., enlarged nuclei, reduced neuron branching) and will decrease the expression of signatures of 5Y differentiation in a dose-dependent manner, and that these effects will be more pronounced during later stages of differentiation (e.g., post-Day 12).

Aim 3

Aim 3 examines associations between Pb exposure and LINE-1 epigenetic regulation and expression in differentiating neurons. Alongside the examination of how Pb exposure affects classic markers of neural differentiation and cell morphology in Aim 2, we sought to employ this same exposure design with regard to LINE-1 elements. There is evidence to suggest that Pb exposure is associated with aberrant epigenetic regulation of LINE-1 elements, though much of this data comes from studies that evaluated this relationship in occupational and adult populations,[105,106] and regardless of population, these studies typically have had access to blood samples.[107,108] As such, the specific effects of developmental Pb exposure on LINE-1 in the brain cannot be ascertained based on the available literature alone. What this review of the literature does demonstrate is that, generally, Pb exposure is associated with hypomethylation of LINE-1 elements,[109] and that, to our knowledge, there is no corresponding analysis of this relationship in a neural cell model. Given the documented associations between decreased LINE-1 methylation,[110,111] as well as increased LINE-1 expression and retrotransposition,[112,113] with ND risk, we sought to evaluate this relationship specifically in an *in vitro* model of neural differentiation.

Cells cultured and collected using the same experimental design, and Pb dose range, described in Aim 2 were used for genomic extractions to assess gene expression and DNAm of piRNA-related genes as well as LINE-1 TEs. Genomic extractions were performed every 3 days on cells differentiated in the presence of Pb. RNA was converted to cDNA, which was then utilized for gene expression analysis of *PIWIL* mRNA as well as that of LINE-1 regions (*5'UTR* and *ORF2*) via qRT-PCR. Genomic

DNA was bisulfite converted and DNAm of LINE-1 was measured via pyrosequencing. This aim seeks to assess 1) if Pb exposure alters the expression of PIWIL mRNA, 2) if this disruption is associated with concurrent changes in DNAm of LINE-1, and 3) if changes in LINE-1 DNAm status are accompanied by changes in *LINE-1* mRNA expression. We hypothesized that Pb exposure will be associated with a decrease in *PIWIL* mRNA expression and of LINE-1 DNAm, and an increase in *LINE-1* mRNA expression.

Aim 4

The previous aims of this dissertation focus on the toxicological impacts of Pb exposure on epigenetic gene regulation during neurodevelopment and neural differentiation. This work explores changes in DNAm, LINE-1 regulation and expression, and begins to assess the impact of exposure on the piRNA system. Taken together, these experiments highlight a need for continued evaluation of the impact of toxicant exposure on the piRNA system in the developing brain and whether perturbations to this form of epigenetic regulation have consequences for LINE-1 regulation and ND risk.

However, much of our understanding of the piRNA system comes from the germline, given its important role in gametogenesis where it ensures the regulation of TEs as well as coordinates the translation of mRNAs during spermatid formation.[114,115] Much of the limited toxicological work on piRNA also focuses on the germline, where differential piRNA expression has been observed with exposures like dichlorodiphenyltrichloroethane (DDT), vinclozolin, flame retardants, and endocrine drisruptors,[116–119] but to date, limited work exists in somatic tissues or corresponding models.[120] In order to adequately assess the impact of the environment on this system,

it is vital that a comprehensive description of its presence in various somatic tissues is completed. Previous work has characterized the expression of piRNA and *PIWIL* mRNA in somatic tissues of the adult mouse, wherein detectable expression was measured in several somatic tissues.[65] Interestingly, relatively few detected piRNA found in the soma were also detected in the gonadal tissues, suggesting there may be independent functions of this class of ncRNA in the soma during adulthood.

Aim 4 of this dissertation characterizes the expression of this system in human somatic tissues from an early developmental time point (gestational days 90-105), in an attempt to build upon the work begun in the mouse model. Brain, heart, lung, liver, kidney, and gonadal tissues were acquired from an NIH-funded biobank and processed for nucleic acid extraction. Total RNA was utilized in the analysis of *PIWIL* mRNA expression via qRT-PCR, whereas smRNA was further processed prior to smRNA sequencing. During their biogenesis, piRNAs acquire 2'-O-methylation at their 3' end by the methyltransferase HEN1, which confers stability and is regarded as the mark of a mature piRNA.[121] Treatment of smRNA with sodium periodate, which elicits a β-elimination reaction and to which piRNA with this 2'O-methylation are resistant, enriches piRNA within the sample prior to sequencing.[122] This approach will create a comprehensive profile of piRNA and *PIWIL* mRNA expression across these somatic tissue types and will address several gaps in knowledge, including: 1) whether the piRNA system is expressed in the soma during early human development and how this expression compares to the gonads, 2) whether the somatic tissues have unique profiles of piRNAs relative to the gonads, and 3) if there are sex-specific profiles of this expression. We hypothesized that the piRNA system will be expressed in the soma, but

to a lesser degree than that seen in the gonads, and that piRNA transcript profiles will be unique between tissue types as well as between the sexes.

References

1. Common Sources of Lead Poisoning. *Washington State Department of Health* https://doh.wa.gov/community-and-environment/contaminants/lead/common-sources-lead-poisoning.

2. Dignam, T., Kaufmann, R. B., LeStourgeon, L. & Brown, M. J. Control of Lead Sources in the United States, 1970-2017: Public Health Progress and Current Challenges to Eliminating Lead Exposure. *J. Public Health Manag. Pract. JPHMP* **25**, S13–S22 (2019).

3. CDC - National Childhood Blood Lead Surveillance Data. https://www.cdc.gov/nceh/lead/data/national.htm (2022).

4. Lead (Pb) Toxicity: Where is Lead Found? | Environmental Education | ATSDR. https://www.atsdr.cdc.gov/csem/leadtoxicity/lead_found.html (2021).

5. Jacobs, D. E., Mielke, H. & Pavur, N. The high cost of improper removal of lead-based paint from housing: a case report. *Environ. Health Perspect.* **111**, 185–186 (2003).

6. US EPA, O. Basic Information about Lead in Drinking Water. https://www.epa.gov/ground-water-and-drinking-water/basic-information-about-lead-drinking-water (2016).

7. Wilson, A. M. *et al.* Frequency of hand-to-head, -mouth, -eyes, and -nose contacts for adults and children during eating and non-eating macro-activities. *J. Expo. Sci. Environ. Epidemiol.* **31**, 34–44 (2021).

8. Roy, A. *et al.* Lead exposure and behavior among young children in Chennai, India. *Environ. Health Perspect.* **117**, 1607–1611 (2009).

9. Rădulescu, A. & Lundgren, S. A pharmacokinetic model of lead absorption and calcium competitive dynamics. *Sci. Rep.* **9**, 14225 (2019).

10. Rabinowitz, M. B. Toxicokinetics of bone lead. *Environ. Health Perspect.* **91**, 33–37 (1991).

11. Barry, P. S. A comparison of concentrations of lead in human tissues. *Occup. Environ. Med.* **32**, 119–139 (1975).

12. Barry, P. S. Concentrations of lead in the tissues of children. *Occup. Environ. Med.* **38**, 61–71 (1981).

13. *Toxicological Profile for Lead*. (Agency for Toxic Substances and Disease Registry (US), 2020).

14. Lead (Pb) Toxicity: What is the Biological Fate of Lead in the Body? | Environmental Medicine | ATSDR. https://www.atsdr.cdc.gov/csem/leadtoxicity/biologic_fate.html (2021).

15. Timeline of CLPPP Highlights | Lead | CDC. https://www.cdc.gov/nceh/lead/about/timeline.html (2022).

16. McFarland, M. J., Hauer, M. E. & Reuben, A. Half of US population exposed to adverse lead levels in early childhood. *Proc. Natl. Acad. Sci.* **119**, e2118631119 (2022).

17. CDC changes its definition of lead poisoning in young children - The Washington Post. https://www.washingtonpost.com/health/lead-poisoning-children-cdc-definition/2021/11/05/0a8af132-3cc7-11ec-a493-51b0252dea0c_story.html.

18. O'Shea, M. J. *et al.* Lead Pollution, Demographics, and Environmental Health Risks: The Case of Philadelphia, USA. *Int. J. Environ. Res. Public. Health* **18**, 9055 (2021).

19. Egendorf, S. P., Mielke, H. W., Castorena-Gonzalez, J. A., Powell, E. T. & Gonzales, C. R. Soil Lead (Pb) in New Orleans: A Spatiotemporal and Racial Analysis. *Int. J. Environ. Res. Public. Health* **18**, 1314 (2021).

20. Hauptman, M., Rogers, M. L., Scarpaci, M., Morin, B. & Vivier, P. M. Neighborhood disparities and the burden of lead poisoning. *Pediatr. Res.* 1–11 (2023) doi:10.1038/s41390-023-02476-7.

21. Yeter, D., Banks, E. C. & Aschner, M. Disparity in Risk Factor Severity for Early Childhood Blood Lead among Predominantly African-American Black Children: The 1999 to 2010 US NHANES. *Int. J. Environ. Res. Public. Health* **17**, 1552 (2020).

22. Yang, W. *et al.* Current and projected future economic burden of Parkinson's disease in the U.S. *Npj Park. Dis.* **6**, 1–9 (2020).

23. Nandi, A. *et al.* Global and regional projections of the economic burden of Alzheimer's disease and related dementias from 2019 to 2050: A value of statistical life approach. *eClinicalMedicine* **51**, (2022).

24. GBD 2019 Dementia Forecasting Collaborators. Estimation of the global prevalence of dementia in 2019 and forecasted prevalence in 2050: an analysis for the Global Burden of Disease Study 2019. *Lancet Public Health* **7**, e105–e125 (2022).

25. 2023 Alzheimer's disease facts and figures. *Alzheimers Dement. J. Alzheimers Assoc.* (2023) doi:10.1002/alz.13016.

26. Willis, A. W. *et al.* Incidence of Parkinson disease in North America. *Npj Park. Dis.* **8**, 1–7 (2022).

27. Evans, J. A., Mendonca, P. & Soliman, K. F. A. Neuroprotective Effects and Therapeutic Potential of the Citrus Flavonoid Hesperetin in Neurodegenerative Diseases. *Nutrients* **14**, 2228 (2022).

28. Xu, W. *et al.* Meta-analysis of modifiable risk factors for Alzheimer's disease. *J. Neurol. Neurosurg. Psychiatry* **86**, 1299–1306 (2015).

29. Reuben, A. Childhood Lead Exposure and Adult Neurodegenerative Disease. *J. Alzheimers Dis. JAD* **64**, 17–42 (2018).

30. Recommendations from the NIH AD Research Summit 2018. *National Institute on Aging* https://www.nia.nih.gov/research/administration/recommendations-nih-ad-research-summit-2018.

31. Anderson, D. W., Mettil, W. & Schneider, J. S. Effects of Low Level Lead Exposure on Associative Learning and Memory in the Rat: Influences of Sex and Developmental Timing Of Exposure. *Toxicol. Lett.* **246**, 57–64 (2016).

32. Singh, G. *et al.* Effects of Developmental Lead Exposure on the Hippocampal Methylome: Influences of Sex and Timing and Level of Exposure. *Toxicol. Lett.* **290**, 63–72 (2018).

33. Heindel, J. J., Skalla, L. A., Joubert, B. R., Dilworth, C. H. & Gray, K. A. Review of developmental origins of health and disease publications in environmental epidemiology. *Reprod. Toxicol. Elmsford N* **68**, 34–48 (2017).

34. Gundacker, C. *et al.* Gene Variants Determine Placental Transfer of Perfluoroalkyl Substances (PFAS), Mercury (Hg) and Lead (Pb), and Birth Outcome: Findings From the UmMuKi Bratislava-Vienna Study. *Front. Genet.* **12**, 664946 (2021).

35. Esteban-Vasallo, M. D., Aragonés, N., Pollan, M., López-Abente, G. & Perez-Gomez, B. Mercury, cadmium, and lead levels in human placenta: a systematic review. *Environ. Health Perspect.* **120**, 1369–1377 (2012).

36. Michaelson, I. A. & Bradbury, M. Effect of early inorganic lead exposure on rat blood-brain barrier permeability to tyrosine or choline. *Biochem. Pharmacol.* **31**, 1881–1885 (1982).

37. Lidsky, T. I. & Schneider, J. S. Lead neurotoxicity in children: basic mechanisms and clinical correlates. *Brain* **126**, 5–19 (2003).

38. Miranda, M., Yarger, L. & Dolinoy, D. Childhood Lead Exposure: Effects and Policy Options. (2000).

39. Populations, N. R. C. (US) C. on M. L. in C. *Biologic Markers of Lead Toxicity*. *Measuring Lead Exposure in Infants, Children, and Other Sensitive Populations* (National Academies Press (US), 1993).

40. Liu, C. *et al.* Association of both prenatal and early childhood multiple metals exposure with neurodevelopment in infant: A prospective cohort study. *Environ. Res.* **205**, 112450 (2022).

41. Dórea, J. G. Environmental exposure to low-level lead (Pb) co-occurring with other neurotoxicants in early life and neurodevelopment of children. *Environ. Res.* **177**, 108641 (2019).

42. Dash, M. *et al.* Developmental exposure to lead (Pb) alters the expression of the human tau gene and its products in a transgenic animal model. *Neurotoxicology* **55**, 154–159 (2016).

43. vonderEmbse, A. N., Hu, Q. & DeWitt, J. C. Developmental toxicant exposure in a mouse model of Alzheimer's disease induces differential sex-associated microglial activation and increased susceptibility to amyloid accumulation. *J. Dev. Orig. Health Dis.* **8**, 493–501 (2017).

44. Wu, J. *et al.* Alzheimer's Disease (AD)-Like Pathology in Aged Monkeys after Infantile Exposure to Environmental Metal Lead (Pb): Evidence for a Developmental Origin and Environmental Link for AD. *J. Neurosci.* **28**, 3–9 (2008).

45. Su, P. *et al.* Genistein alleviates lead-induced neurotoxicity in vitro and in vivo: Involvement of multiple signaling pathways. *Neurotoxicology* **53**, 153–164 (2016).

46. Ayyalasomayajula, N., Ajumeera, R., Chellu, C. S. & Challa, S. Mitigative effects of epigallocatechin gallate in terms of diminishing apoptosis and oxidative stress generated by the combination of lead and amyloid peptides in human neuronal cells. *J. Biochem. Mol. Toxicol.* **33**, e22393 (2019).

47. Westerink, R. H. S. & Vijverberg, H. P. M. Ca(2+) -independent vesicular catecholamine release in PC12 cells by nanomolar concentrations of Pb(2+). *J. Neurochem.* **80**, 861–873 (2002).

48. Hanas, J. S., Rodgers, J. S., Bantle, J. A. & Cheng, Y.-G. Lead Inhibition of DNA-Binding Mechanism of Cys2His2 Zinc Finger Proteins. *Mol. Pharmacol.* **56**, 982–988 (1999).

49. Ordemann, J. M. & Austin, R. N. Lead neurotoxicity: exploring the potential impact of lead substitution in zinc-finger proteins on mental health. *Metallomics* **8**, 579–588 (2016).

50. Virgolini, M. B. & Aschner, M. MOLECULAR MECHANISMS OF LEAD NEUROTOXICITY. *Adv. Neurotoxicology* **5**, 159–213 (2021).

51. Ahamed, M. & Siddiqui, M. K. J. Low level lead exposure and oxidative stress: Current opinions. *Clin. Chim. Acta* **383**, 57–64 (2007).

52. Verstraeten, S. V., Aimo, L. & Oteiza, P. I. Aluminium and lead: molecular mechanisms of brain toxicity. *Arch. Toxicol.* **82**, 789–802 (2008).

53. Lee, J. & Freeman, J. L. Zebrafish as a model for investigating developmental lead (Pb) neurotoxicity as a risk factor in adult neurodegenerative disease: a mini-review. *Neurotoxicology* **43**, 57–64 (2014).

54. Park, S. S., Skaar, D. A., Jirtle, R. L. & Hoyo, C. Epigenetics, obesity and early-life cadmium or lead exposure. *Epigenomics* **9**, 57–75 (2017).

55. Dolinoy, D. C. & Jirtle, R. L. Environmental epigenomics in human health and disease. *Environ. Mol. Mutagen.* **49**, 4–8 (2008).

56. Jirtle, R. L. Epigenetics: How Genes and Environment Interact. in *Environmental Epigenomics in Health and Disease: Epigenetics and Disease Origins* (eds. Jirtle, R. L. & Tyson, F. L.) 3–30 (Springer, 2013). doi:10.1007/978-3-642-23380-7_1.

57. Skvortsova, K., Iovino, N. & Bogdanović, O. Functions and mechanisms of epigenetic inheritance in animals. *Nat. Rev. Mol. Cell Biol.* **19**, 774–790 (2018).

58. Mattei, A. L., Bailly, N. & Meissner, A. DNA methylation: a historical perspective. *Trends Genet. TIG* **38**, 676–707 (2022).

59. Morgan, M. A. J. & Shilatifard, A. Reevaluating the roles of histone-modifying enzymes and their associated chromatin modifications in transcriptional regulation. *Nat. Genet.* **52**, 1271–1281 (2020).

60. Aravin, A. A. & Bourc'his, D. Small RNA guides for de novo DNA methylation in mammalian germ cells. *Genes Dev.* **22**, 970–975 (2008).

61. Wells, J. N. & Feschotte, C. A Field Guide to Eukaryotic Transposable Elements. *Annu. Rev. Genet.* **54**, 539–561 (2020).

62. Burns, K. H. Our Conflict with Transposable Elements and Its Implications for Human Disease. *Annu. Rev. Pathol. Mech. Dis.* **15**, 51–70 (2020).

63. Aravin, A. A. *et al.* A piRNA Pathway Primed by Individual Transposons Is Linked to De Novo DNA Methylation in Mice. *Mol. Cell* **31**, 785–799 (2008).

64. Du, W. W. *et al.* Reciprocal regulation of miRNAs and piRNAs in embryonic development. *Cell Death Differ.* **23**, 1458–1470 (2016).

65. Perera, B. P. U. *et al.* Somatic expression of piRNA and associated machinery in the mouse identifies short, tissue-specific piRNA. *Epigenetics* **14**, 504–521 (2019).

66. Muotri, A. R. *et al.* Somatic mosaicism in neuronal precursor cells mediated by L1 retrotransposition. *Nature* **435**, 903–910 (2005).

67. Coufal, N. G. *et al.* L1 retrotransposition in human neural progenitor cells. *Nature* **460**, 1127–1131 (2009).

68. Siomi, M. C., Mannen, T. & Siomi, H. How does the Royal Family of Tudor rule the PIWI-interacting RNA pathway? *Genes Dev.* **24**, 636–646 (2010).

69. Aluru, N. Epigenetic effects of environmental chemicals: Insights from zebrafish. *Curr. Opin. Toxicol.* **6**, 26–33 (2017).

70. Tran, N. Q. V. & Miyake, K. Neurodevelopmental Disorders and Environmental Toxicants: Epigenetics as an Underlying Mechanism. *International Journal of Genomics* vol. 2017 e7526592 https://www.hindawi.com/journals/ijg/2017/7526592/ (2017).

71. Ivanova, E. *et al.* DNA methylation changes during preimplantation development reveal inter-species differences and reprogramming events at imprinted genes. *Clin. Epigenetics* **12**, 64 (2020).

72. Bara, A., Ferland, J.-M. N., Rompala, G., Szutorisz, H. & Hurd, Y. L. Cannabis and synaptic reprogramming of the developing brain. *Nat. Rev. Neurosci.* **22**, 423–438 (2021).

73. Bale, T. L. Epigenetic and transgenerational reprogramming of brain development. *Nat. Rev. Neurosci.* **16**, 332–344 (2015).

74. Rygiel, C. A. *et al.* Prenatal Lead (Pb) Exposure and Peripheral Blood DNA Methylation (5mC) and Hydroxymethylation (5hmC) in Mexican Adolescents from the ELEMENT Birth Cohort. *Environ. Health Perspect.* **129**, 67002 (2021).

75. Dou, J. F. *et al.* Perinatal Lead (Pb) Exposure and Cortical Neuron-Specific DNA Methylation in Male Mice. *Genes* **10**, (2019).

76. Montrose, L., Faulk, C., Francis, J. & Dolinoy, D. C. Perinatal lead (Pb) exposure results in sex and tissue-dependent adult DNA methylation alterations in murine IAP transposons. *Environ. Mol. Mutagen.* **58**, 540–550 (2017).

77. Lu, X., Wang, L., Yu, C., Yu, D. & Yu, G. Histone Acetylation Modifiers in the Pathogenesis of Alzheimer's Disease. *Front. Cell. Neurosci.* **9**, 226 (2015).

78. Schonrock, N. *et al.* Neuronal MicroRNA Deregulation in Response to Alzheimer's Disease Amyloid-β. *PLoS ONE* **5**, e11070 (2010).

79. Li, J. J. *et al.* In vivo evidence for the contribution of peripheral circulating inflammatory exosomes to neuroinflammation. *J. Neuroinflammation* **15**, 8 (2018).

80. Sun, W., Samimi, H., Gamez, M., Zare, H. & Frost, B. Pathogenic tau-induced piRNA depletion promotes neuronal death through transposable element dysregulation in neurodegenerative tauopathies. *Nat. Neurosci.* **21**, 1038–1048 (2018).

81. Rajasethupathy, P. *et al.* A Role for Neuronal piRNAs in the Epigenetic Control of Memory-Related Synaptic Plasticity. *Cell* **149**, 693–707 (2012).

82. Qiu, W. *et al.* Transcriptome-wide piRNA profiling in human brains of Alzheimer's disease. *Neurobiol. Aging* **57**, 170–177 (2017).

83. Nikolac Perkovic, M. *et al.* Epigenetics of Alzheimer's Disease. *Biomolecules* **11**, 195 (2021).

84. Shao, Y. *et al.* DNA methylation of TOMM40-APOE-APOC2 in Alzheimer's disease. *J. Hum. Genet.* **63**, 459–471 (2018).

85. Tulloch, J. *et al.* Glia-specific APOE epigenetic changes in the Alzheimer's disease brain. *Brain Res.* **1698**, 179–186 (2018).

86. Sae-Lee, C. *et al.* DNA methylation patterns of LINE-1 and Alu for pre-symptomatic dementia in type 2 diabetes. *PloS One* **15**, e0234578 (2020).

87. Ravel-Godreuil, C. *et al.* Perturbed DNA methylation by Gadd45b induces chromatin disorganization, DNA strand breaks and dopaminergic neuron death. *iScience* **24**, 102756 (2021).

88. Tam, O. H. *et al.* Postmortem Cortex Samples Identify Distinct Molecular Subtypes of ALS: Retrotransposon Activation, Oxidative Stress, and Activated Glia. *Cell Rep.* **29**, 1164-1177.e5 (2019).

89. Prickett, A. R. & Oakey, R. J. A survey of tissue-specific genomic imprinting in mammals. *Mol. Genet. Genomics MGG* **287**, 621–630 (2012).

90. Joseph, R. M. Neuronatin gene: Imprinted and misfolded: Studies in Lafora disease, diabetes and cancer may implicate NNAT-aggregates as a common downstream participant in neuronal loss. *Genomics* **103**, 183–188 (2014).

91. Baulina, N., Kiselev, I. & Favorova, O. Imprinted Genes and Multiple Sclerosis: What Do We Know? *Int. J. Mol. Sci.* **22**, 1346 (2021).

92. Masoud, A. M., Bihaqi, S. W., Machan, J. T., Zawia, N. H. & Renehan, W. E. Early-Life Exposure to Lead (Pb) Alters the Expression of microRNA that Target Proteins Associated with Alzheimer's Disease. *J. Alzheimers Dis. JAD* **51**, 1257–1264 (2016).

93. Bakulski, K. M. *et al.* Single-Cell Analysis of the Gene Expression Effects of Developmental Lead (Pb) Exposure on the Mouse Hippocampus. *Toxicol. Sci. Off. J. Soc. Toxicol.* **176**, 396–409 (2020).

94. Faulk, C., Barks, A., Liu, K., Goodrich, J. M. & Dolinoy, D. C. Early-life lead exposure results in dose- and sex-specific effects on weight and epigenetic gene regulation in weanling mice. *Epigenomics* **5**, 487–500 (2013).

95. Zou, R.-X. *et al.* Pb exposure induces an imbalance of excitatory and inhibitory synaptic transmission in cultured rat hippocampal neurons. *Toxicol. Vitro Int. J. Publ. Assoc. BIBRA* **63**, 104742 (2020).

96. Peng, J. *et al.* Differential response to lead toxicity in rat primary microglia and astrocytes. *Toxicol. Appl. Pharmacol.* **363**, 64–71 (2019).

97. Oberto, A., Marks, N., Evans, H. L. & Guidotti, A. Lead (Pb+2) promotes apoptosis in newborn rat cerebellar neurons: pathological implications. *J. Pharmacol. Exp. Ther.* **279**, 435–442 (1996).

98. Huang, H., Bihaqi, S. W., Cui, L. & Zawia, N. H. In vitro Pb exposure disturbs the balance between Aβ production and elimination: The role of AβPP and neprilysin. *NeuroToxicology* **32**, 300–306 (2011).

99. Lin, X. *et al.* Infant exposure to trace elements in breast milk, infant formulas and complementary foods from southern China. *Sci. Total Environ.* **838**, 156597 (2022).

100. Tau, G. Z. & Peterson, B. S. Normal development of brain circuits. *Neuropsychopharmacol. Off. Publ. Am. Coll. Neuropsychopharmacol.* **35**, 147–168 (2010).

101. Bayer, S. A., Altman, J., Russo, R. J. & Zhang, X. Timetables of neurogenesis in the human brain based on experimentally determined patterns in the rat. *Neurotoxicology* **14**, 83–144 (1993).

102. Agholme, L., Lindström, T., Kågedal, K., Marcusson, J. & Hallbeck, M. An In Vitro Model for Neuroscience: Differentiation of SH-SY5Y Cells into Cells with Morphological and Biochemical Characteristics of Mature Neurons. *J. Alzheimers Dis.* **20**, 1069–1082 (2010).

103. Li, X., Li, X., Xiang, C. & Ye, F. Lead exposure represses mitochondrial metabolism by activation of heme-binding protein BACH1 in differentiated SH-SY5Y cell. *Sci. Total Environ.* **853**, 158665 (2022).

104. Lin, L. F. *et al.* Low dose lead exposure induces alterations on heterochromatin hallmarks persisting through SH-SY5Y cell differentiation. *Chemosphere* **264**, 128486 (2021).

105. Li, C., Yang, X., Xu, M., Zhang, J. & Sun, N. Epigenetic marker (LINE-1 promoter) methylation level was associated with occupational lead exposure. *Clin. Toxicol. Phila. Pa* **51**, 225–229 (2013).

106. Issah, I. *et al.* Global DNA (LINE-1) methylation is associated with lead exposure and certain job tasks performed by electronic waste workers. *Int. Arch. Occup. Environ. Health* **94**, 1931–1944 (2021).

107. Yohannes, Y. B. *et al.* Methylation profiles of global LINE-1 DNA and the GSTP1 promoter region in children exposed to lead (Pb). *Epigenetics* **17**, 2377–2388 (2022).

108. Goodrich, J. M. *et al.* Adolescent epigenetic profiles and environmental exposures from early life through peri-adolescence. *Environ. Epigenetics* **2**, (2016).

109. Wright, R. O. *et al.* Biomarkers of lead exposure and DNA methylation within retrotransposons. *Environ. Health Perspect.* **118**, 790–795 (2010).

110. Neven, K. Y. *et al.* Repetitive element hypermethylation in multiple sclerosis patients. *BMC Genet.* **17**, 84 (2016).

111. Hernández, H. G., Mahecha, M. F., Mejía, A., Arboleda, H. & Forero, D. A. Global Long Interspersed Nuclear Element 1 DNA Methylation in a Colombian Sample of Patients With Late-Onset Alzheimer's Disease. *Am. J. Alzheimers Dis. Dementias®* **29**, 50–53 (2014).

112. Peze-Heidsieck, E. *et al.* Retrotransposons as a Source of DNA Damage in Neurodegeneration. *Front. Aging Neurosci.* **13**, (2022).

113. Ravel-Godreuil, C., Znaidi, R., Bonnifet, T., Joshi, R. L. & Fuchs, J. Transposable elements as new players in neurodegenerative diseases. *FEBS Lett.* **595**, 2733–2755 (2021).

114. Gan, H. *et al.* piRNA profiling during specific stages of mouse spermatogenesis. *RNA* **17**, 1191–1203 (2011).

115. Dai, P. *et al.* A Translation-Activating Function of MIWI/piRNA during Mouse Spermiogenesis. *Cell* **179**, 1566-1581.e16 (2019).

116. Skinner, M. K. *et al.* Alterations in sperm DNA methylation, non-coding RNA and histone retention associate with DDT-induced epigenetic transgenerational inheritance of disease. *Epigenetics Chromatin* **11**, 8 (2018).

117. Nilsson, E. *et al.* Environmental toxicant induced epigenetic transgenerational inheritance of ovarian pathology and granulosa cell epigenome and transcriptome alterations: ancestral origins of polycystic ovarian syndrome and primary ovarian insufiency. *Epigenetics* **13**, 875–895 (2018).

118. Suvorov, A. *et al.* Aging Induces Profound Changes in sncRNA in Rat Sperm and These Changes Are Modified by Perinatal Exposure to Environmental Flame Retardant. *Int. J. Mol. Sci.* **21**, 8252 (2020).

119. Toth, G. P. *et al.* Development of omics biomarkers for estrogen exposure using mRNA, miRNA and piRNAs. *Aquat. Toxicol. Amst. Neth.* **235**, 105807 (2021).

120. Pierce, L. M., Kurata, W. E., Matsumoto, K. W., Clark, M. E. & Farmer, D. M. Long-term epigenetic alterations in a rat model of Gulf War Illness. *Neurotoxicology* **55**, 20–32 (2016).

121. Kirino, Y. & Mourelatos, Z. Mouse Piwi-interacting RNAs are 2′-O-methylated at their 3′ termini. *Nat. Struct. Mol. Biol.* **14**, 347–348 (2007).

122. Ohara, T. *et al.* The 3′ termini of mouse Piwi-interacting RNAs are 2′-O-methylated. *Nat. Struct. Mol. Biol.* **14**, 349–350 (2007).

Figures

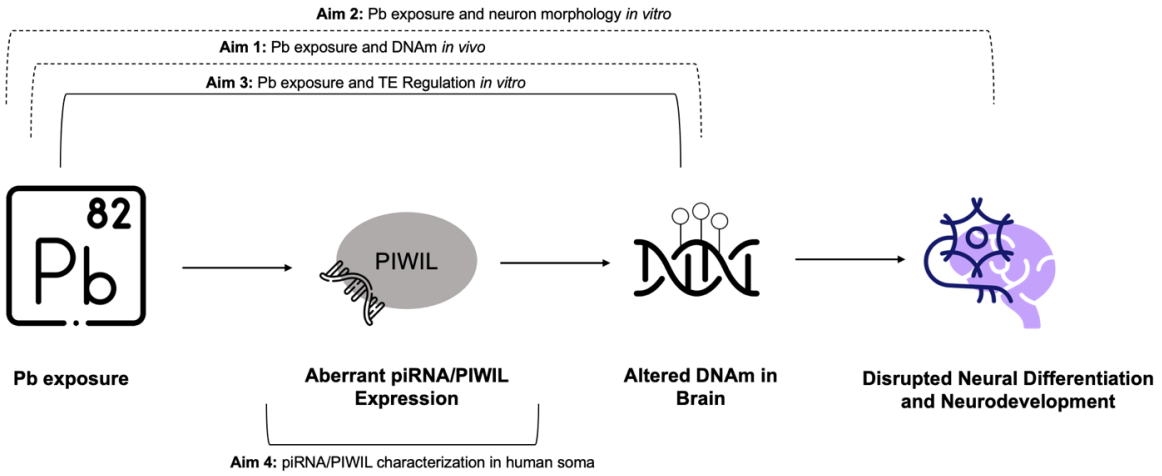

Figure 1.1: Schematic of Dissertation Aims. Solid lines represent aims that assess all components under the bracket (e.g., Aim 3 measures changes in PIWIL expression as well as DNAm), whereas dotted lines represent aims that only assess the two components connected by the bracket (e.g., Aim 2 measures only Pb exposure and neural differentiation morphology, with no assessment of piRNA/PIWIL expression or DNAm).

Chapter 2

Aim 1: Evaluation of Effects of Developmental Lead (Pb) Exposure on Epigenome-Wide DNA Methylation in Mouse Brain and Blood in Adulthood Identifies Tissue- and Sex-Specific Changes with Implications for Genomic Imprinting and Transposable Elements

Abstract

Maternal lead (Pb) exposure can cause adverse effects to neurodevelopment and cognition in offspring, and it is theorized that one avenue by which this relationship occurs is through perturbation to epigenetic mechanisms governing relevant gene classes. This study examines tissue- and sex-specific changes in DNA methylation (DNAm) associated with human-relevant Pb exposure during the perinatal period in cortex and blood tissue from a mouse model. Female mice were exposed to either 32ppm Pb-acetate or control drinking water for two weeks prior to mating through offspring weaning. Whole genome bisulfite sequencing (WGBS) was utilized to examine DNAm changes in offspring cortex and blood at 5 months of age. Differentially methylated regions (DMRs) were identified using metilene and MethylSig. The genomic annotations and gene set enrichment of detected DMRs were determined using annotatr and chipenrich, respectively. The cortex contained the majority of DMRs detected (73%) across males and females with a limited number also detected in blood (5 in males and 7 in females). In both tissues, detected DMRs were preferentially found at genomic regions associated with gene expression regulation (e.g., CpG islands and

shores, 5' UTRs, promoters, and exons). An analysis of GO terms associated with DMR-containing genes identified imprinting genes as a class of interest. Of these, *Gnas* and *Grb10* contained DMRs in both tissues and sexes. Furthermore, DMRs were enriched in the imprinting control regions (ICRs) of *Gnas* and *Gbr10*. The *Grb10* ICR provided evidence of DNAm signatures in a target tissue (cortex) being replicated in a surrogate tissue (blood), a pattern that was not seen to a significant degree in the total summation of all DMRs detected in this study, suggesting ICRs may be potential candidates in the utilization of DNAm changes as biomarkers. Given previous assessment from our group which has found Pb exposure to be associated with aberrant methylation of transposable elements, further evaluation of LINE-1 elements was also conducted and a number of LINE-1 DMRs were detected in the cortex of males (32) and females (46), the majority of which were hypomethylated (24 and 28, respectively). Conversely of trends seen at large, LINE-1 DMRs were typically found in non-regulatory regions, such as the open sea and introns. There were few LINE-1 DMRs detected in blood, relative to the total detected, and none in blood were found to overlap with those in brain, suggesting this gene class may not be as suitable as others in providing surrogate measures of epigenetic changes in target tissues. Assessment of both gene classes highlighted in this study emphasizes the importance of considering the sex-specific effects of environmental exposures on epigenetic mechanisms.

Introduction

Developmental exposure to Pb has been extensively linked to adverse cognitive outcomes for decades,[1] with major legislative action aimed at reducing Pb exposure enacted in the U.S. in the latter half of the 20th century.[2] Despite this, Pb exposures

continue[3] and so it is essential that we understand the mechanisms by which Pb exposure affects neurodevelopment, so that we might identify potential avenues for therapeutics.[4] Continued research into this relationship is also useful from the perspective of identifying potential biomarkers of exposure so that we can be better prepared to make conclusions as to what effects Pb exposure has in difficult-to-study human tissues, such as the brain, when we are limited to surrogate tissues, such as blood.

A substantial amount of neurotoxicological research on Pb highlights its effects on various neuronal cell populations and brain regions, which effectively demonstrates the functional impact of exposure.[5–7] However, this work would be appropriately complimented by research that assesses the impact of Pb exposure on cell types and/or pathways that are present in and outside of the brain, so that a concrete biomarker of exposure that also has functional relevance might be ascertained. Many current biomarkers are used with the intention of concluding that Pb exposure has occurred, not necessarily that it has had a neurotoxicological effect,[8] and there is a continued need for more sensitive markers that may also reflect the effects of exposure, particularly those that occur at environmentally relevant doses and can be detected in easily accessible tissues.

One avenue by which developmental Pb exposure is thought to disrupt typical neurodevelopmental processes is through perturbations of epigenetic mechanisms.[9] Developmental exposures of many kinds can impact gene expression long-term through alterations to the epigenome, which in turn can have significant repercussions for health and disease.[10,11] Epigenetics refers to mitotically heritable and potentially reversible

mechanisms modulating gene expression that are independent of the DNA sequence, with the most abundantly studied mechanism being DNA methylation (DNAm).[12] DNAm entails the addition of a methyl group to the fifth position of a cytosine base (5mC) adjacent to a guanine base (CpG) by DNA methyltransferases (DNMTs). Increased levels of 5mC within promoters and enhancers are typically associated with decreased transcription factor binding and subsequent changes in gene expression.[13,14] Patterns of 5mC undergo waves of reprogramming (i.e., global demethylation and re-methylation) during critical windows of development, such as gestation, making these periods potentially susceptible targets of developmental exposures.[15]

Tight epigenetic regulation of several gene classes, such as imprinted genes and repetitive elements, is critical for proper growth and development.[16–18] Imprinted genes can be expressed in a mono-allelic fashion, which is determined in a parent-of-origin manner.[19] For instance, a paternally expressed gene will contain an active paternal allele and an inactive (methylated or imprinted) maternal allele. The DNAm patterns of imprinted genes expressed at specific developmental stages are important during growth and early development.[20,21] Once DNAm patterns have been established for these genes, often within imprinting control regions (ICRs) in gametes, they are maintained through fertilization and the aforementioned extensive epigenetic reprogramming events.[22,23] The specificity required to maintain patterns of genomic imprinting and re-establish DNAm in a parent-of-origin manner following waves of global demethylation make gestational periods ideal timeframes for studying the impact of environmental exposures as environmentally induced disruption of epigenetic processes

during gestation has been associated with changes in imprinted gene regulation and expression.[24,25]

Transposable elements (TEs) are repetitive elements within our genomes that can propagate independently of the host genome.[26] They are sequences of our DNA with the capacity to mobilize and reinsert themselves back into the genome, potentially to the detriment of genome stability.[27] Generally, TEs are regarded as elements that require tight regulation, so as to not disrupt the integrity of the genome through induced genomic mutations (such as when a TE is reinserted into a protein coding region) or disruption to gene expression regulatory mechanisms (such as through the induction of chromatin modifications).[27,28] This regulatory capacity is particularly important during early development and embryogenesis, wherein these forms of genomic disruption often have significant repercussions for rapidly differentiating and dividing cells.[29] It should be noted that TEs can and do provide a benefit to their host genomes. Some retroviral TEs have been co-opted into gene expression regulatory networks, and early, regulated TE activity is associated with increasing genetic plasticity.[30,31] While a certain degree of TE activity has been shown to be beneficial during developmental processes, as their activity contributes to cellular diversity, mobilization that exceeds normal levels is often associated with genome instability, cellular stress, and developmental dysfunction.[29] LINE-1 is a class I family of TEs that make up roughly 17% and 18% of the human and mouse genomes, respectively, and their activation has been extensively studied with regard to its impact on genome integrity and cellular development, particularly within the developing brain.[32]

Pb has been previously associated with differential gene regulation and expression of both gene classes explored here (imprinted genes and LINE-1 TEs) in various organ systems and models. *In vitro* work has found aberrant DNA methylation and increased imprinted gene expression in kidney cells[33], while *in vivo* models have demonstrated changes in imprinted gene regulation in the liver following gestational Pb exposure.[34,35] This work is further complimented by epidemiological work which has quantified associations between maternal blood lead levels and imprinted gene DNAm in infants and children.[36,37] Pb exposure has also been associated with altered regulation of LINE-1 elements in humans, including children and those occupationally exposed.[38–40] There is additional, but limited, evidence from *in vitro* and *in vivo* models that exposure to various metals, including Pb, is associated with increased TE activity as well as with reduced TE regulation.[41–43]

As a part of the Toxicant Exposures and Responses by Genomic and Epigenomic Regulators of Transcription (TaRGET II) Consortium, we utilized a mouse model of human-relevant perinatal Pb exposure to investigate genome-wide tissue- and sex- specific associations with changes in DNAm.[44] Whole genome bisulfite sequencing (WGBS) quantified DNAm changes in blood (and easily accessible and therefore considered a “surrogate” tissue) as well as brain (a tissue often difficult to access, and therefore considered a “target” tissue) collected from male and female 5-month-old mice, with and without perinatal Pb exposure. We assessed whether perinatal Pb-exposed mice displayed changes in DNAm across the genome and identified imprinted genes and TEs as relevant gene classes to this exposure. We additionally assessed whether DNAm patterns in the surrogate tissue (blood) correlated with those seen in the

target tissue (cortex), to determine if blood provides a viable signature of Pb-induced epigenetic changes in this target tissue, and how these patterns differed between males and females.

Methods

Animal Exposure Paradigm and Tissue Collection

Mice were obtained from wild-type non-agouti *a/a* mice from an over 230-generation colony of viable yellow agouti (A^{vy}) mice, which are genetically invariant mice 93% identical to the C57BL/6J strain.[45] Virgin *a/a* females (6-8 weeks old) were randomly assigned to control or Pb-acetate water two weeks prior to mating with virgin *a/a* males (7-9 weeks old). Pb exposure was conducted *ad libitum* via distilled drinking water mixed with Pb-acetate. The Pb concentration was set at 32 ppm to model human relevant perinatal exposure, where we have previously measured murine maternal BLLs around 16-60μg/dL (mean: 32.1μg/dL).[46] All animals were maintained on a phytoestrogen-free modified AIN-93 G diet (Td.95092, 7% corn oil diet, Harlan Teklad) while housed in polycarbonate-free cages. Animal exposure to Pb continued through gestation and lactation until weaning at post-natal day 21 (PND21), when pups were switched to Pb-free drinking water. *In utero* exposure, thus occurred in offspring throughout fetal development and the first three weeks after birth. Offspring were maintained until 5 months of age. This study included n = 6 males and n = 6 females for Pb-exposed and control groups, each containing 1 male and 1 female mouse per litter; and a final samples size of n = 48 once tissues (i.e., cortex and blood) were collected. Immediately following mouse euthanasia with CO2 asphyxiation, blood was collected through cardiac puncture, followed by dissection of the cortex, which was immediately

flash frozen in liquid nitrogen and stored at -80ºC. All mouse procedures were approved by the University of Michigan Institutional Animal Care and Use Committee (IACUC). All experiments were conducted according to experimental procedures outlined by the NIEHS TaRGET II Consortium.[44]

DNA Extraction and Whole Genome Bisulfite Sequencing

DNA extraction was performed using the AllPrep DNA/RNA/miRNA Universal Kit (Qiagen, Cat. #80224). Additional details about the animal exposures, blood collection, and blood DNA extraction can be found in previously published protocols.[34] Genomic DNA (gDNA) was used in the preparation of WGBS libraries at the University of Michigan Epigenomics Core. gDNA was quantified using the Qubit BR dsDNA Kit (Fisher, Cat. #Q32850), and quality assessed using Agilent's Genomic DNA Tapestation Kit (Agilent, Cat. #A63880). For each sample, 200 ng of gDNA was spiked with 0.5% of unmethylated lambda DNA and sheared using a Covaris S220 (10% duty factor, 140W peak incident power, 200 cycle/burst, 55s). A 2µL aliquot of processed gDNA was taken to assess shearing using an Agilent High Sensitivity D1000 Kit (Agilent, Cat. #G2991AA). Once shearing was assessed, the remaining gDNA was concentrated using a Qiagen PCR Purification column and processed for end-repair and A-tailing. Ligation of cytosine-methylated adapters was done overnight at 16ºC. Following this, ligation products were cleaned using AMPure XP Beads (Fisher, Cat. #NC9933872) before processing for bisulfite conversion using the Zymo EZ DNA Methylation Kit (Zymo, Cat. #D5001), and by amplifying the bisulfite converted products over 55 cycles of 95ºC for 30 seconds, followed by 55ºC for 15 minutes, according to the manufacturer's guidelines. After cleanup of the bisulfite converted products, final

libraries were amplified over 10 cycles of PCR using KAPA Uracil+ Ready Mix (Fisher, Cat. #501965287) and NEB dual indexing primers. Final libraries were cleaned with AMPure XP Beads, concentration assessed using the Qubit BR dsDNA Kit and library size assessed on the Agilent High Quantification Kit (Fisher, Cat. #501965234). A total of 27 libraries were pooled together for sequencing on a NovaSeq6000 S4 200 cycle flow cell (PE-100) at the University of Michigan Advanced Genomics Core. Unless otherwise stated, all enzymes used in library generation were purchased from New England Biolabs. Adapters with universally methylated cytosines were synthesized by Integrated DNA Technologies (IDT).

Data Processing, Quality Control, and Differential DNA Methylation Analysis

FastQC[47] (v0.11.5) and MultiQC[48] (v1.8) were used to assess the quality of all sequenced samples. Sequencing adapters and low-quality bases were removed by Trim Galore[49] (v0.4.5). After trimming, reads shorter than 20 bp were removed from further analysis. Bismark[50] (v0.19.0) with bowtie 2[51] (v2.3.4) as backend alignment software were used for read alignment and methylation calling with Genome Reference Consortium Mouse Build 38 (mm10) as the reference genome. All alignments were performed with 0 mismatches and multi-seed length of 20 bp. The bisulfite conversion rates were calculated through the unmethylated lambda phage DNA. Metilene[52] (v0.2.8) and R Bioconductor package methylSig[53] (v1.4.0) were used to identify the differentially methylated regions (DMRs) independently. Any CpG sites with less than 10 reads or more than 500 reads were excluded from DMR detection. For methylSig, CpG sites that have reads covered in less than 4 samples within a treatment group were filtered out for DMR identification. Tiling windows were used with methylSig to identify DMRs, with a

window size of 100 bp. For metilene, DMRs were identified de novo with at least 5 CpGs in a single DMR. For both methods, an FDR cutoff of < 0.05 and a DNAm difference of >5% were applied to select significant DMRs. Overlapping DMRs from methylSig and metilene were merged, then all DMRs were combined for downstream analysis. The combined DMRs that had the same directional change in DNAm (i.e., hyper- or hypomethylated) were merged as one DMR (**Table 2.A1**). The annotatr Bioconductor package[54] was used to annotate all significant DMRs associated with genes and genomic locations, including CpG islands, CpG shores, CpG shelves, promoters, exons, introns, 5' UTRs, 3' UTRs, enhancers, and regions 1-5kb upstream of transcription start sites (TSSs). Random genomic regions were generated and annotated with annotatr for each tissue using the mm10 reference genome. These random regions were used as background information to show the distribution of the genomic annotation of the DMRs. An overview of the complete methods is illustrated in **Figure 2.1**. In addition, a minimum overlap cutoff ≥10bp was applied to identify overlapping DMRs between tissues, sexes, and exposures. As a secondary analysis, murine LINE-1 elements were annotated using the UCSC Genome Browser.[55] Total detected DMRs were intersected with this annotation to curate a list of LINE-1 DMRs for use. As with the initial analysis, tiling windows were used with methylSig to identify DMRs, with a window size of 100 bp and an FDR cutoff of < 0.05 and a DNAm difference of >5% were applied to select significant DMRs.

Geneset Enrichment Test

R Bioconductor package Chipenrich[56] (v2.16.0) was used to perform geneset enrichment testing of Gene Ontology (GO) terms enriched with significant DMRs. Eight

analyses were performed stratified by each tissue and sex (i.e., male cortex, male blood, female cortex, and female blood) with hyper- and hypomethylation determined in Pb versus control samples. Gene assignments were determined with the nearest_tss locus definition in the chipenrich function to find all three categories of ontology (i.e., Biological Process (BP), Cellular Component (CC), and Molecular Function (MF)). An FDR cutoff of < 0.05 was applied for selecting significantly enriched GO terms. GO terms containing fewer than 15 genes or more than 500 genes were removed from analysis.

Mouse Imprinted Genes, Imprinting Control Regions and LINE-1 Elements

DMRs were compared to mouse imprinted genes and imprinting control regions (ICRs). Imprinted genes used for this study were derived from Williamson et al.[57] and Tucci et al.[17], while ICRs were collected from Wang et al.[58]. The valr R package[59] (0.6.4) was used to identify overlapping regions between the DMRs and ICRs. A Binomial test was used to assess whether the DMRs were significantly enriched in ICRs or LINE-1 elements and an adjusted p-value < 0.05 cutoff was utilized for identifying significant results.

Results

Cortex and Blood Share Relatively Few DMRs in Pb-Exposed Mice

Of the two tissues studied, the majority of DMRs were detected in the cortex (M = 688, F = 746) compared to the blood (M = 243, F = 292) (**Figure 2.2A**). There was relatively little overlap between these two tissues compared to the total number of DMRs detected, with 5 common DMRs between cortex and blood in males, and 7 in

females (**Figure 2.2B**). We also assessed to what degree males and females shared DMRs in the same tissue and found 17 and 10 shared DMRs in the cortex and blood, respectively (**Figure 2.2C**). There was some similarity between tissues when quantifying the direction of DNAm changes. DMRs in male cortex and blood were largely hypomethylated (80% and 56%, respectively), while in females DMRs were more likely to be hypermethylated (48% in cortex and 71% in blood) when compared to their male counterparts (**Figure 2.2D**).

Distribution of Differentially Methylation Regions Across Genomic Regions

The DMRs detected in this study occurred in specific genomic regions to a greater degree than would have been expected by chance, given known patterns of CpG sites in the C57BL/6J genome. Detected DMRs correlated to CpG islands to a greater degree than would have been expected by chance (10.01-19.07% of all DMRs across sexes and tissues, compared to 0.12-0.23% at random). Several transcriptional regulatory regions demonstrated significant derivation from what would be expected by chance as well. In both blood and cortex and in both sexes, more DMRs were detected in 5' UTRs than expected (4.03-8.79%, compared to 0.18-0.4% under a random distribution) as well as promoter regions (8.82-14.41% compared to 1.74-2.18% at random). Exons were another notable location of DMRs, constituting 14.36 -17.8% compared to 3.37-3.84% at random. Conversely, there were fewer DMRs detected in the open sea (11.02-20.15% in blood and 21.41-25.87% in cortex) than would have been expected by chance (54.83-58.09%) (**Figure 2.3**, **Table 2.A2**).

Gene Ontology Terms Associated with Differentially Methylated Regions

DMRs were annotated using annotatr R Bioconductor package, and a summary of the overlap in DMR-containing genes across sexes and tissues can be found in **Figure 2.A1**. Chipenrich was used to perform geneset enrichment tests and Gene Ontology (GO) Resource was used to identify DMR-related GO terms. The number of DMR-containing genes associated with each GO result are summarized in **Table 2.A3**.

Gene Ontology Biological Pathway (GOBP) terms were the most commonly associated class of terms with Pb-associated DMRs (212 DMR-containing genes across 29 terms), and cortex had the greatest number of GOBP-related DMR-containing genes in both males (85) and females (106). DMR-associated GOBPs in female cortex were dominated by metabolic processes (35 out of 106 genes), whereas male cortex contained an abundance of DMR-containing genes related to gene expression regulation (e.g., DNA methylation or demethylation and miRNA silencing) (16 out of 85). The most common biological process associated with Pb exposure was genomic imprinting (GO:0071514), which appeared in male and female cortex samples, as well as male blood samples, and this was the only GO term to be returned in more than one tissue-sex category. In total, DMRs were detected in 17 genes associated with genetic imprinting in these tissues (**Figure 2.4**).

DNA Methylation Changes at Imprinted Genomic Locations

The appearance of imprinted genes in both tissues during pathway analysis (**Figure 2.4**) was motivation to take a closer look at the effects of Pb exposure on imprinted genes. When we examined this class of genes specifically, cortex and blood, in males and females, had detectable changes in DNAm within multiple imprinted genes (**Figures 2.A2**). A reference list of imprinted genes used in this analysis can be found in

Table 2.A4, and genes that did not contain a DMR in either tissue were omitted from the final figures. Cortex had the greatest number of DMRs as well as magnitude of methylation changes in assessed imprinted genes. 73 Pb-associated DMRs were detected in cortex in imprinted genes (46 in males and 27 in females, with magnitude changes of 5.03-23.77%) and 36 were detected in blood (16 in males and 20 in females, with magnitude changes of 5.04-20.1%). Blood from Pb-exposed females largely contained hypermethylated sites at imprinted genes at large (15/20 DMRs), while cortex from the same animals was largely hypomethylated in the same gene class (20/27 DMRs) (**Table 2.A5**).

Two imprinted genes, *Gnas* and *Grb10*, contained a notable number of exposure associated DMRs throughout the span of each gene. A complete overview of these DMRs is summarized in **Figure 2.5** and **Table 2.A5**. In the cortex, *Gnas* DMRs were largely hypomethylated in both females (3/4) and males (3/5), whereas in blood, DMRs within the *Gnas* locus were entirely hypermethylated in females (1/1) and hypomethylated in males (3/3). *Gbr10* DMRs in the cortex were largely hypomethylated in females (2/3) and hypermethylated in males (2/3). *Gbr10* DMRs detected in male blood were entirely hypermethylated (2/2), and there were no DMRs detected within this locus in female blood samples.

Exposure-Associated Changes in Imprinting Control Regions

Imprinted genes are regulated in part through imprinting control regions (ICRs), which are elements that regulate gene expression and subsequent functions of imprinted gene clusters. Changes in the DNAm status of these regions can impact the expression of imprinted and non-imprinted genes within a given cluster, thus magnifying

the regulatory effects of what would otherwise be a single-gene effect. *Gnas* contains two ICRs, the *Gnas* ICR and the *Nespas* ICR, while *Grb10* contains one ICR. This analysis identified multiple DMRs within the ICRs of both *Gnas* (3 in ICR *Nespas*) and *Grb10* (9 in ICR *Grb10*) across both tissues and sexes (**Figure 2.6**). A binomial test was conducted to assess whether exposure associated DMRs occurred in these ICRs to a greater degree than would have been expected by random chance. Both the *Gnas* and *Grb10* ICRs contained more DMRs than would have been expected by chance and a summary of these findings can be found in **Table 2.A6**.

In the *Grb10* ICR, Pb exposure was largely associated with hypomethylation (2/3) in female cortex and hypermethylation (2/3) in male cortex. Similar patterns presented in Pb-exposed blood, wherein female samples were hypomethylated at this locus (1/1) while male samples were entirely hypermethylated (2/2) (**Figure 2.6B and Table 2.A7**), suggesting this ICR may be a viable candidate for a target-surrogate biomarker of Pb exposure with regard to the brain. In the *Nespas* ICR, Pb exposure was associated with hypermethylation in female cortex (1/1 DMR) and a mix of hyper- (1/2) and hypomethylation (1/2) in male cortex, with no DMRs detected within *Gnas* ICRs in female blood (**Figure 2.6A and Table 2.A7**). These patterns provided little evidence that *Gnas* ICRs were as strong of a biomarker candidate as that of *Grb10*.

Exposure-Associated Changes in Methylation of LINE-1 Elements

This analysis was further expanded to the DNAm of LINE-1 elements, as previous work from our group has found TEs are often hypomethylated following developmental Pb exposure, in both mouse models in the cortex as well as epidemiological cohorts which utilize blood measurements.[39,43] There was a modest

difference in the total number of DMRs detected at LINE-1 regions between the two tissues studied, with 46 and 32 LINE-1 DMRs detected in female and male cortex, respectively, and 8 and 18 were found in the same gene class in female and male blood, respectively (**Table 2.1**).

Given that LINE-1 elements make up roughly 18% of the murine genome, we would expect the percent of DMRs mapped to these elements in each sex and tissue combination to also be roughly 18%. We conducted a binomial test, with a p-value cut off of 0.05, to assess whether DMRs occurred in these elements to a greater degree than would have been expected given by chance. We used the total number of DMRs detected in the initial analysis in each sex and tissue (**Figure 2.2**) and added the number of LINE-1 DMRs to these totals to obtain the number of DMRs in this analysis. Surprisingly, we found fewer DMRs in LINE-1 elements in this sample set than expected by chance ($p < 0.05$) (**Table 2.A8**), with less than 10% of total DMRs detected in this study mapping to LINE-1 elements.

Of the LINE-1 DMRs detected, there was no overlap detected between either cortex and blood of the same sex, nor between sexes within the same tissue type (**Figure 2.7**). Of those detected in female cortex, nearly two-thirds were hypomethylated (28/46, 61%), while three-quarters of LINE-1 DMRs in male cortex were hypomethylated (24/32, 75%). In the limited number of LINE-1 DMRs detected in blood, there was an even split among both females and males as to the proportion that were hypomethylated (9 in males and 4 in females) and hypermethylated (9 in males and 4 in females) (**Table 2.1**).

The annotation of LINE-1 DMRs revealed that, in both cortex and blood, as well as in both males and females, the majority of changes occurred within the open sea (CpG-inter regions) (**Figure 2.8A** and **2.8C**). Within the cortex, there was a notable number of LINE-1 DMRs that fell within intron regions, in both males and females, and this pattern was replicated in male blood (**Figure 2.8B** and **2.8D**). Overall, there were fewer DMRs within regulatory regions relative to the total, as was seen in this broader dataset. Magnitude changes in DNAm ranged from 5-45%, and maximum observed percent changes in methylation were slightly higher in blood samples (45% in males) compared to that of the cortex (35-36% in males and females). While the highest percent changes in DNAm in each sex and tissue represented hypermethylated sites, there were hypomethylated sites with percent methylation differences of 18-32% as well. A summary of this data is available in **Table 2.A9**.

Discussion

Toxicant exposures that occur during critical periods of development can have ramifications for health and well-being throughout the life-course.[60] Perinatal Pb exposure has been linked to aberrant brain development and cognitive function at environmentally relevant doses,[61] with substantial epidemiological evidence supported by growing toxicological work. With regard to epigenetic mechanisms governing gene expression, Pb has been associated with differential DNAm in human populations, most notably within blood samples.[62–64] Concurrently, it is unknown if toxicant-induced changes in difficult to study organs, such as the brain, are reflected in more easily accessible (surrogate) tissues, such as blood. However, given that epigenetic reprogramming during embryogenesis precedes that of germ line differentiation, it

stands to reason that patterns of DNAm would be promising candidates for this association.[65] It is therefore pertinent to examine how this potent neurodevelopmental toxicant affects epigenetic gene regulation (i.e., DNAm) in this target-surrogate tissue pairing in order to assess whether blood could be utilized as a biomarker of changes in the brain.

Pb Exposure Associated with Sex- and Tissue-Specific General Changes in DNA Methylation. The majority of detected DMRs were located in the cortex (73%) and relatively few were also detected in the blood, for either sex (5/910 in males, 7/1027 in females). These results mirror that of other toxicological work that found limited overlap in DMRs (<7%) between blood and brain tissue following glucocorticoid exposure,[66] highlighting that general trends in exposure-associated DMRs in the blood may not be reflective of changes occurring in the brain. There was also relatively little overlap in Pb-associated DMRs between the sexes in either tissue (1.2% of all DMRs detected in the cortex and 1.9% of those detected in blood) which parallels the existing literature which has routinely documented sex-specific changes in DNAm following environmental exposures.[67,68] When considering the added complexity of whether the direction of changes in DNAm is consistent between the target-surrogate or male-female comparisons, there was also little similarity. There were no appreciable trends in common between the cortex and blood, or males and females, in terms of whether DMRs were more hyper- or hypomethylated (**Figure 2.2**). These results taken together suggest limited overlap in Pb-associated DNAm signatures, either between a target and surrogate tissue or the sexes, when examining broad trends in DMRs. While broad trends in exposure associated DMRs do not appear to qualify as robust biomarkers, it

may be that closer inspection of specific gene classes or genomic regions may provide stronger evidence of changes replicated in surrogate and target tissues.

Exposure-Associated DMRs Occur to a Notable Degree in Imprinted Genes. An analysis of GO terms associated with DMR-containing genes identified genomic imprinting as a common category across cortex and blood (**Figures 2.4**). Imprinted genes are an important class with regard to early growth and development, and their epigenetically-controlled mono-allelic parent-of-origin nature of expression may confer particular susceptibility to the impacts of environmental exposures.[25,36] Early disruption of imprinted gene expression and function can result in developmental disorders (e.g., Beckwith-Wiedmann syndrome and Silver-Russel syndrome),[69,70] all of which have neurodevelopmental and/or cognitive components to their symptomology. The methylation status of imprinted genes is susceptible to environmental exposures, including Pb,[33,34,43] during early development and epidemiological work has linked early Pb exposures to altered methylation in imprinted genes such as insulin-like growth factor 2 (*IGF2*) and maternally expressed gene 3 (*MEG3*).[36]

Potential Functional Relevance of DNA Methylation Changes in Gnas and Grb10 Regulatory Regions. Gnas encodes for the G-protein alpha-subunit protein, which contributes to signal transduction via cAMP generation,[71] and its imprinting dysregulation has been associated with increased insulin sensitivity, neural tube defects, and hypothyroidism.[72,73] The imprinted expression of *Gnas* is complex, as this gene gives rise to several maternal- and paternal-specific gene products, and these patterns of expression have been shown to be tissue-specific in mice and humans.[74,75] In this work, *Gnas* contained a mix of hyper- and hypomethylated DMRs in the cortex,

making the prediction of observed sustained effects at 5 months difficult to ascertain. However, given the importance of maintained imprinted expression of this locus and its various gene products in the brain, it is reasonable to expect that there may be functional relevance to the Pb-associated changes in DNAm reported here and that continued evaluation of the impact of these changes and any downstream physiological ramifications is warranted. Changes in DNAm within *Gnas* were much more uniform in the blood, where biallelic expression is considered to be the norm in adult mice.[71] Distinct differences in *Gnas* DMR direction appeared between the sexes in this study when focused on blood, with hypomethylation observed in males and hypermethylation in females (**Figure 2.6**). Previous work has documented differential methylation at *Gnas* following environmental exposures, though much of this work focuses on either dietary or disease states,[76–78] and to our knowledge, this is one of few studies that has identified changes associated with a toxicant.[34]

Grb10 encodes for an insulin receptor-binding protein involved in growth and insulin response and is imprinted in a tissue- and sometimes cell-specific manner. This is especially true during development as changes in *Grb10* expression across time are tissue-specific. For example, *Grb10* is thought to be biallelically expressed in much of the brain until adulthood when it becomes paternally expressed.[81] There were several DMRs detected in *Grb10* in Pb-exposed male and female cortex at the adult time point of 5 months in this study. Furthermore, *Grb10* methylation appears to be cell-type specific during early brain development, with paternal expression in cortical neurons and maternal expression in glial cells.[80] While this study was unable to assess cell-type specific changes in DNAm within the cortex, future single cell analyses could help

determine whether exposure-associated DMRs are specific to certain cellular populations.[6] Pb exposure was associated with hypermethylation in male blood and hypomethylation in female blood. *Grb10* is thought to be maternally expressed during early development and completely repressed during adulthood in blood,[82] meaning that, at least in females, Pb exposure may be related to reactivation of this gene during an inappropriate time point. Future evaluation of the impact of *Grb10* hypomethylation in blood during adulthood would contribute to our understanding of the potential functional impact of this change.

Grb10 Provide Evidence of DNA Methylation Signatures in Target-Surrogate Tissue Pairs. ICRs are environmentally sensitive regulatory regions, and changes to their methylation status can have consequences for more than one imprinted gene product.[83] The ICRs of both *Gnas* and *Grb10* contained Pb-associated DMRs, with relatively more detected in the *Grb10* ICR (9) compared to that of *Gnas* (3). The ICR of *Grb10*, but not *Gnas*, displayed some changes in DNAm that were replicated in both target and surrogate tissues, suggesting that this regulatory region may be of significance when attempting to identify DNAm-related biomarkers of exposure effects in difficult to access tissues. Pb exposure was associated with multiple hypermethylated DMRs in the *Grb10* ICR within male cortex and blood samples, suggesting that, at least for this exposure, the *Grb10* ICR may be a potential region to consider when exploring male-specific DNAm surrogate measures. At this same locus in females, there were hypomethylated DMRs in both cortex and blood, however female cortex displayed a much more even distribution of hyper- and hypomethylated DMRs compared to males,

suggesting that the correlation between these tissues in this sex may not be as strong as in males.

Changes in LINE-1 Methylation Provide Little Evidence of Consistent Patterns Across Target-Surrogate Tissue Pairs. LINE-1 elements are a gene class with immense potential for their use in biomarker and target-surrogate research as they appear in the human genome as well as that of commonly used animal models.[84] The mobility of LINE-1 elements also has significant relevance to the risk of neurodegenerative disease, as increased mobility has been associated with neural cell death and physical symptoms including ataxia.[85] Additionally, LINE-1 hypomethylation has been documented in several epidemiological populations with neurodegenerative diseases including Alzheimer's disease, and it is suspected that this relationship arises from LINE-1-induced DNA damage and a depletion of neurons in certain regions of the brain, leading to these health outcomes.[86] Surprisingly, we found significantly fewer DMRs within LINE-1 elements than we would have expected based on chance. This may reflect the fact that there are a multitude of regulatory mechanisms working in concert to keep these repetitive elements repressed, including repressive histone marks and heterochromatin conformations, in addition to DNAm.[87,88]The results in this study are limited to that of Pb-induced changes in DNAm, and further assessment of exposure related changes on these other LINE-1 regulatory mechanisms may provide insight as to why we saw fewer changes in this gene class than expected.

This work found no concrete similarities between LINE-1 DMR signatures between males or females, either in terms of general trends in DMR number and direction, or with regard to specific DMR overlap. Generally, significantly more DMRs

were detected in the cortex of Pb-exposed mice relative to those discovered in blood, and this held true for both sexes. In males, the majority of DMRs in the cortex were hypomethylated (75%) and this proportion was slightly lower in females (61%), which may suggest sex-specific effects of Pb exposure on LINE-1 regulation. The almost even distribution in hyper- and hypomethylated DMRs in female cortex may mean there are negligible effects on neurodevelopment in this sex, especially when one considers that only a very small number of those that were hypomethylated were annotated to gene expression regulatory regions, such as enhancers and promoters. There were no overlapping LINE-1 DMRs detected within the cortex and blood in either males or females. Furthermore, there was no overlap in specific DMRs between males and females.

Limitations

DNAm patterns vary across cell types within a given tissue.[6,89] This study was unable to account for cell type and therefore, changes in DNAm as the result of Pb exposure may be due to exposure-induced changes in cell type proportions or changes in a specific cell type that drove observed trends.[90] Additionally, we were not able to evaluate changes in hydroxymethylation (5hmC) in these samples. This study was conducted using bisulfite conversion, which accounts for both 5mC and 5hmC, and the resulting data is unable to differentiate between these two signatures.[91] This epigenetic modification is particularly relevant to the brain, and it would be pertinent to include in future studies of this nature.[92] Imprinted genes are typically 50% methylated (accounting for mono-allelic expression or repression), and this data represents DNAm averages for both alleles.[93] Any allele-specific changes in gene regulation by Pb could not be

detected. It is also worth noting that the approach used in assessing the statistical significance of DMRs detected in LINE-1 regions does not account for reads that were unused due to multimapping, and future work would do well to examine the proportion of mapped reads that map to LINE-1 elements, as opposed to utilizing only the DMR data. A final limitation is the use of a relatively small sample size, and the assessment of the effects of only one dose at one timepoint.

Conclusion

This study systematically evaluated changes in DNAm in cortex and blood from mice at 5 months of age following developmental exposure to Pb. Pb-specific DNAm changes were observed via DMRs, with limited similarity in general DMR patterns seen between cortex and blood, or males and females. Genomic imprinting was impacted by Pb exposure, as determined by GO term analysis, and imprinted genes *Gnas* and *Grb10* indicated changes in DNAm at their respective DMRs. The *Grb10* ICR provided novel evidence of specific DMR signatures that were replicated between a target (cortex) and surrogate (blood) tissue and should be validated as well as expanded to other exposure types in future work. LINE-1 DMRs demonstrated no similarities between the tissue studied and is likely a less viable candidate for this paradigm.

While previous work has explored the relationships between Pb exposure and LINE-1 methylation in blood as well as brain, to our knowledge this is the first study to assess this in both tissues simultaneously and is therefore the first to identify specific gene classes (i.e., imprinted genes) that may carry signatures of Pb exposure in both tissues from the same animal. Environmental epidemiology as a field bears an incredible burden of attempting to measure the effects of toxicant exposures while often

limited to the use of surrogate tissue types, limiting what conclusions can be drawn. Toxicological work such as this has a unique opportunity to support this endeavor by exploring whether there is similarity in toxicant response between surrogate tissues and those that are inaccessible in epidemiological work but are also often the locations of the functional impacts of such exposures. These experiments identified one such loci with potential (*Grb10* ICR), but it remains to be seen if additional gene classes hold such promise or if this relationship is applicable to other exposure types.

Acknowledgements

Special thanks are due to Dr. Kai Wang who was a huge contributor to this work. Dr. Wang completed much of the data wrangling and bioinformatic analysis of the WGBS data and generated many of the impressive figures used in this chapter, and he was a wonderful source of support in the preparation of this manuscript. Additionally, Dr. Claudia Lalancette at the University of Michigan Epigenomics Core generated the WGBS libraries for sequencing and provided ample advice and expertise on sample preparation and data analysis, and Tamara Jones and Dr. Kari Neier led efforts to collect the samples utilized here as part of the TaRGET II Consortium. This work was supported by funding from the following sources: National Institute of Environmental Health Sciences (NIEHS) TaRGET II Consortium (ES026697), NIEHS Grant R35 (ES031686), NIEHS Grant K01 (ES032048), NIEHS Grant R01 (ES028802), the Michigan Lifestage Environmental Exposures and Disease (M-LEEaD) NIEHS Core Center (P30 ES017885), Institutional Training Grant T32 (ES007062), Institutional Training Grant T32 (HD079342), and National Institute of Aging (NIA) Grant R01 (AG072396).

References

1. Senut, M.-C. *et al.* Epigenetics of early-life lead exposure and effects on brain development. *Epigenomics* **4**, 665–674 (2012).

2. Dignam, T., Kaufmann, R. B., LeStourgeon, L. & Brown, M. J. Control of Lead Sources in the United States, 1970-2017: Public Health Progress and Current Challenges to Eliminating Lead Exposure. *J. Public Health Manag. Pract. JPHMP* **25**, S13–S22 (2019).

3. Hanna-Attisha, M., LaChance, J., Sadler, R. C. & Champney Schnepp, A. Elevated Blood Lead Levels in Children Associated With the Flint Drinking Water Crisis: A Spatial Analysis of Risk and Public Health Response. *Am. J. Public Health* **106**, 283–290 (2016).

4. Pichery, C. *et al.* Childhood lead exposure in France: benefit estimation and partial cost-benefit analysis of lead hazard control. *Environ. Health Glob. Access Sci. Source* **10**, 44 (2011).

5. Peng, J. *et al.* Differential response to lead toxicity in rat primary microglia and astrocytes. *Toxicol. Appl. Pharmacol.* **363**, 64–71 (2019).

6. Bakulski, K. M. *et al.* Single-Cell Analysis of the Gene Expression Effects of Developmental Lead (Pb) Exposure on the Mouse Hippocampus. *Toxicol. Sci. Off. J. Soc. Toxicol.* **176**, 396–409 (2020).

7. Chibowska, K. *et al.* Pre- and Neonatal Exposure to Lead (Pb) Induces Neuroinflammation in the Forebrain Cortex, Hippocampus and Cerebellum of Rat Pups. *Int. J. Mol. Sci.* **21**, 1083 (2020).

8. Gundacker, C. *et al.* Lead (Pb) and neurodevelopment: A review on exposure and biomarkers of effect (BDNF, HDL) and susceptibility. *Int. J. Hyg. Environ. Health* **238**, 113855 (2021).

9. Rygiel, C. A. *et al.* DNA methylation at birth potentially mediates the association between prenatal lead (Pb) exposure and infant neurodevelopmental outcomes. *Environ. Epigenetics* **7**, dvab005 (2021).

10. Park, J. H., Yoo, Y. & Park, Y. J. Epigenetics: Linking Nutrition to Molecular Mechanisms in Aging. *Prev. Nutr. Food Sci.* **22**, 81–89 (2017).

11. Siddeek, B., Mauduit, C., Simeoni, U. & Benahmed, M. Sperm epigenome as a marker of environmental exposure and lifestyle, at the origin of diseases inheritance. *Mutat. Res. Rev. Mutat. Res.* **778**, 38–44 (2018).

12. Fitz-James, M. H. & Cavalli, G. Molecular mechanisms of transgenerational epigenetic inheritance. *Nat. Rev. Genet.* **23**, 325–341 (2022).

13. Siegfried, Z. & Simon, I. DNA methylation and gene expression. *Wiley Interdiscip. Rev. Syst. Biol. Med.* **2**, 362–371 (2010).

14. Lyko, F. The DNA methyltransferase family: a versatile toolkit for epigenetic regulation. *Nat. Rev. Genet.* **19**, 81–92 (2018).

15. Zeng, Y. & Chen, T. DNA Methylation Reprogramming during Mammalian Development. *Genes* **10**, 257 (2019).

16. SanMiguel, J. M. & Bartolomei, M. S. DNA methylation dynamics of genomic imprinting in mouse development. *Biol. Reprod.* **99**, 252–262 (2018).

17. Tucci, V. *et al.* Genomic Imprinting and Physiological Processes in Mammals. *Cell* **176**, 952–965 (2019).

18. Friedli, M. & Trono, D. The developmental control of transposable elements and the evolution of higher species. *Annu. Rev. Cell Dev. Biol.* **31**, 429–451 (2015).

19. Kalish, J. M., Jiang, C. & Bartolomei, M. S. Epigenetics and imprinting in human disease. *Int. J. Dev. Biol.* **58**, 291–298 (2014).

20. Piedrahita, J. A. The role of imprinted genes in fetal growth abnormalities. *Birt. Defects Res. A. Clin. Mol. Teratol.* **91**, 682–692 (2011).

21. Moore, G. E. *et al.* The role and interaction of imprinted genes in human fetal growth. *Philos. Trans. R. Soc. B Biol. Sci.* **370**, 20140074 (2015).

22. Jima, D. D. *et al.* Genomic map of candidate human imprint control regions: the imprintome. *Epigenetics* **17**, 1920–1943 (2022).

23. Horsthemke, B. Mechanisms of imprint dysregulation. *Am. J. Med. Genet. C Semin. Med. Genet.* **154C**, 321–328 (2010).

24. Robles-Matos, N., Artis, T., Simmons, R. A. & Bartolomei, M. S. Environmental Exposure to Endocrine Disrupting Chemicals Influences Genomic Imprinting, Growth, and Metabolism. *Genes* **12**, 1153 (2021).

25. Kappil, M., Lambertini, L. & Chen, J. Environmental Influences on Genomic Imprinting. *Curr. Environ. Health Rep.* **2**, 155–162 (2015).

26. Wells, J. N. & Feschotte, C. A Field Guide to Eukaryotic Transposable Elements. *Annu. Rev. Genet.* **54**, 539–561 (2020).

27. Slotkin, R. K. & Martienssen, R. Transposable elements and the epigenetic regulation of the genome. *Nat. Rev. Genet.* **8**, 272–285 (2007).

28. Siomi, M. C., Sato, K., Pezic, D. & Aravin, A. A. PIWI-interacting small RNAs: the vanguard of genome defence. *Nat. Rev. Mol. Cell Biol.* **12**, 246–258 (2011).

29. Burns, K. H. Our Conflict with Transposable Elements and Its Implications for Human Disease. *Annu. Rev. Pathol. Mech. Dis.* **15**, 51–70 (2020).

30. Chuong, E. B., Elde, N. C. & Feschotte, C. Regulatory activities of transposable elements: from conflicts to benefits. *Nat. Rev. Genet.* **18**, 71–86 (2017).

31. Lanciano, S. & Cristofari, G. Measuring and interpreting transposable element expression. *Nat. Rev. Genet.* **21**, 721–736 (2020).

32. Suarez, N. A., Macia, A. & Muotri, A. R. LINE-1 retrotransposons in healthy and diseased human brain. *Dev. Neurobiol.* **78**, 434–455 (2018).

33. Nye, M. D., Hoyo, C. & Murphy, S. K. In vitro lead exposure changes DNA methylation and expression of IGF2 and PEG1/MEST. *Toxicol. Vitro Int. J. Publ. Assoc. BIBRA* **29**, 544–550 (2015).

34. Svoboda, L. K. *et al.* Tissue and sex-specific programming of dna methylation by perinatal lead exposure: implications for environmental epigenetics studies. *Epigenetics* **16**, 1102–1122 (2021).

35. K, W. *et al.* Tissue- and Sex-Specific DNA Methylation Changes in Mice Perinatally Exposed to Lead (Pb). *Front. Genet.* **11**, (2020).

36. Nye, M. D. *et al.* Maternal blood lead concentrations, DNA methylation of MEG3 DMR regulating the DLK1/MEG3 imprinted domain and early growth in a multiethnic cohort. *Environ. Epigenetics* **2**, dvv009 (2016).

37. Goodrich, J. M. *et al.* Quality control and statistical modeling for environmental epigenetics: a study on in utero lead exposure and DNA methylation at birth. *Epigenetics* **10**, 19–30 (2015).

38. Yohannes, Y. B. *et al.* Methylation profiles of global LINE-1 DNA and the GSTP1 promoter region in children exposed to lead (Pb). *Epigenetics* **17**, 2377–2388 (2022).

39. Goodrich, J. M. *et al.* Adolescent epigenetic profiles and environmental exposures from early life through peri-adolescence. *Environ. Epigenetics* **2**, (2016).

40. Issah, I. *et al.* Global DNA (LINE-1) methylation is associated with lead exposure and certain job tasks performed by electronic waste workers. *Int. Arch. Occup. Environ. Health* **94**, 1931–1944 (2021).

41. Habibi, L., Shokrgozar, M. A., Tabrizi, M., Modarressi, M. H. & Akrami, S. M. Mercury specifically induces LINE-1 activity in a human neuroblastoma cell line. *Mutat. Res. Genet. Toxicol. Environ. Mutagen.* **759**, 9–20 (2014).

42. Karimi, A., Madjd, Z., Habibi, L. & Akrami, S. M. Evaluating the extent of LINE-1 mobility following exposure to heavy metals in HepG2 cells. *Biol. Trace Elem. Res.* **160**, 143–151 (2014).

43. Montrose, L., Faulk, C., Francis, J. & Dolinoy, D. C. Perinatal lead (Pb) exposure results in sex and tissue-dependent adult DNA methylation alterations in murine IAP transposons. *Environ. Mol. Mutagen.* **58**, 540–550 (2017).

44. Wang, T. *et al.* The NIEHS TaRGET II Consortium and environmental epigenomics. *Nat. Biotechnol.* **36**, 225–227 (2018).

45. Waterland, R. A. & Jirtle, R. L. Transposable Elements: Targets for Early Nutritional Effects on Epigenetic Gene Regulation. *Mol. Cell. Biol.* **23**, 5293–5300 (2003).

46. Faulk, C., Barks, A., Liu, K., Goodrich, J. M. & Dolinoy, D. C. Early-life lead exposure results in dose- and sex-specific effects on weight and epigenetic gene regulation in weanling mice. *Epigenomics* **5**, 487–500 (2013).

47. Andrews. FastQC A Quality Control tool for High Throughput Sequence Data. https://www.bioinformatics.babraham.ac.uk/projects/fastqc/ (2010).

48. Ewels, P., Magnusson, M., Lundin, S. & Käller, M. MultiQC: summarize analysis results for multiple tools and samples in a single report. *Bioinforma. Oxf. Engl.* **32**, 3047–3048 (2016).

49. Krueger, F. Trim Galore. https://www.bioinformatics.babraham.ac.uk/projects/trim_galore/ (2015).

50. Krueger, F. & Andrews, S. R. Bismark: a flexible aligner and methylation caller for Bisulfite-Seq applications. *Bioinforma. Oxf. Engl.* **27**, 1571–1572 (2011).

51. Langmead, B. & Salzberg, S. L. Fast gapped-read alignment with Bowtie 2. *Nat. Methods* **9**, 357–359 (2012).

52. Jühling, F. *et al.* metilene: fast and sensitive calling of differentially methylated regions from bisulfite sequencing data. *Genome Res.* **26**, 256–262 (2016).

53. Park, Y., Figueroa, M. E., Rozek, L. S. & Sartor, M. A. MethylSig: a whole genome DNA methylation analysis pipeline. *Bioinforma. Oxf. Engl.* **30**, 2414–2422 (2014).

54. Cavalcante, R. G. & Sartor, M. A. annotatr: genomic regions in context. *Bioinforma. Oxf. Engl.* **33**, 2381–2383 (2017).

55. The Human Genome Browser at UCSC. https://genome.cshlp.org/content/12/6/996.abstract.

56. Welch, R. P. *et al.* ChIP-Enrich: gene set enrichment testing for ChIP-seq data. *Nucleic Acids Res.* **42**, e105 (2014).

57. Williamson, C. M. *et al.* Identification of an imprinting control region affecting the expression of all transcripts in the Gnas cluster. *Nat. Genet.* **38**, 350–355 (2006).

58. Wang, L. *et al.* Programming and inheritance of parental DNA methylomes in mammals. *Cell* **157**, 979–991 (2014).

59. Riemondy, K. A. *et al.* valr: Reproducible genome interval analysis in R. *F1000Research* **6**, 1025 (2017).

60. Dolinoy, D. C., Weidman, J. R. & Jirtle, R. L. Epigenetic gene regulation: linking early developmental environment to adult disease. *Reprod. Toxicol. Elmsford N* **23**, 297–307 (2007).

61. Thomason, M. E. *et al.* Prenatal lead exposure impacts cross-hemispheric and long-range connectivity in the human fetal brain. *NeuroImage* **191**, 186–192 (2019).

62. Childebayeva, A. *et al.* Blood lead levels in Peruvian adults are associated with proximity to mining and DNA methylation. *Environ. Int.* **155**, 106587 (2021).

63. Rygiel, C. A. *et al.* Trimester-Specific Associations of Prenatal Lead Exposure With Infant Cord Blood DNA Methylation at Birth. *Epigenetics Insights* **13**, 2516865720938669 (2020).

64. Bozack, A. K. *et al.* Prenatal metal exposure, cord blood DNA methylation and persistence in childhood: an epigenome-wide association study of 12 metals. *Clin. Epigenetics* **13**, 208 (2021).

65. Seisenberger, S. *et al.* Reprogramming DNA methylation in the mammalian life cycle: building and breaking epigenetic barriers. *Philos. Trans. R. Soc. B Biol. Sci.* **368**, 20110330 (2013).

66. Seifuddin, F. *et al.* Genome-wide Methyl-Seq analysis of blood-brain targets of glucocorticoid exposure. *Epigenetics* **12**, 637–652 (2017).

67. Murphy, S. K. *et al.* Gender-specific methylation differences in relation to prenatal exposure to cigarette smoke. *Gene* **494**, 36–43 (2012).

68. Li, Y. *et al.* Lead Exposure during Early Human Development and DNA Methylation of Imprinted Gene Regulatory Elements in Adulthood. *Environ. Health Perspect.* **124**, 666–673 (2016).

69. Brioude, F. *et al.* Expert consensus document: Clinical and molecular diagnosis, screening and management of Beckwith-Wiedemann syndrome: an international consensus statement. *Nat. Rev. Endocrinol.* **14**, 229–249 (2018).

70. Wakeling, E. L. *et al.* Diagnosis and management of Silver-Russell syndrome: first international consensus statement. *Nat. Rev. Endocrinol.* **13**, 105–124 (2017).

71. Weinstein, L. S., Xie, T., Zhang, Q.-H. & Chen, M. Studies of the regulation and function of the Gsα gene Gnas using gene targeting technology. *Pharmacol. Ther.* **115**, 271–291 (2007).

72. Hanna, P., Francou, B., Delemer, B., Jüppner, H. & Linglart, A. A Novel Familial PHP1B Variant With Incomplete Loss of Methylation at GNAS-A/B and Enhanced Methylation at GNAS-AS2. *J. Clin. Endocrinol. Metab.* **106**, 2779–2787 (2021).

73. Turan, S. & Bastepe, M. The GNAS complex locus and human diseases associated with loss-of-function mutations or epimutations within this imprinted gene. *Horm. Res. Paediatr.* **80**, 10.1159/000355384 (2013).

74. Wroe, S. F. *et al.* An imprinted transcript, antisense to Nesp, adds complexity to the cluster of imprinted genes at the mouse Gnas locus. *Proc. Natl. Acad. Sci. U. S. A.* **97**, 3342–3346 (2000).

75. Hayward, B. E. *et al.* The human GNAS1 gene is imprinted and encodes distinct paternally and biallelically expressed G proteins. *Proc. Natl. Acad. Sci. U. S. A.* **95**, 10038–10043 (1998).

76. Chen, D. *et al.* Increased methylation at differentially methylated region of GNASin infants born to gestational diabetes. *BMC Med. Genet.* **15**, 108 (2014).

77. He, J. *et al.* Methylation levels at IGF2 and GNAS DMRs in infants born to preeclamptic pregnancies. *BMC Genomics* **14**, 472 (2013).

78. Wang, L. *et al.* Altered GNAS imprinting due to folic acid deficiency contributes to poor embryo development and may lead to neural tube defects. *Oncotarget* **8**, 110797–110810 (2017).

79. Desbuquois, B., Carré, N. & Burnol, A.-F. Regulation of insulin and type 1 insulin-like growth factor signaling and action by the Grb10/14 and SH2B1/B2 adaptor proteins. *FEBS J.* **280**, 794–816 (2013).

80. Plasschaert, R. N. & Bartolomei, M. S. Tissue-specific regulation and function of Grb10 during growth and neuronal commitment. *Proc. Natl. Acad. Sci. U. S. A.* **112**, 6841–6847 (2015).

81. Hikichi, T., Kohda, T., Kaneko-Ishino, T. & Ishino, F. Imprinting regulation of the murine Meg1/Grb10 and human GRB10 genes; roles of brain-specific promoters and mouse-specific CTCF-binding sites. *Nucleic Acids Res.* **31**, 1398–1406 (2003).

82. Blagitko, N. *et al.* Human GRB10 is imprinted and expressed from the paternal and maternal allele in a highly tissue- and isoform-specific fashion. *Hum. Mol. Genet.* **9**, 1587–1595 (2000).

83. Doshi, T., D'souza, C. & Vanage, G. Aberrant DNA methylation at Igf2-H19 imprinting control region in spermatozoa upon neonatal exposure to bisphenol A and its association with post implantation loss. *Mol. Biol. Rep.* **40**, 4747–4757 (2013).

84. Richardson, S. R., Morell, S. & Faulkner, G. J. L1 retrotransposons and somatic mosaicism in the brain. *Annu. Rev. Genet.* **48**, 1–27 (2014).

85. Takahashi, T. *et al.* LINE-1 activation in the cerebellum drives ataxia. *Neuron* **110**, 3278-3287.e8 (2022).

86. Peze-Heidsieck, E. *et al.* Retrotransposons as a Source of DNA Damage in Neurodegeneration. *Front. Aging Neurosci.* **13**, 786897 (2022).

87. Montoya-Durango, D. E. *et al.* Epigenetic Control of Mammalian LINE-1 Retrotransposon by Retinoblastoma Proteins. *Mutat. Res.* **665**, 20–28 (2009).

88. Protasova, M. S., Andreeva, T. V. & Rogaev, E. I. Factors Regulating the Activity of LINE1 Retrotransposons. *Genes* **12**, 1562 (2021).

89. Armand, E. J., Li, J., Xie, F., Luo, C. & Mukamel, E. A. Single-Cell Sequencing of Brain Cell Transcriptomes and Epigenomes. *Neuron* **109**, 11–26 (2021).

90. Campbell, K. A., Colacino, J. A., Park, S. K. & Bakulski, K. M. Cell types in environmental epigenetic studies: Biological and epidemiological frameworks. *Curr. Environ. Health Rep.* **7**, 185–197 (2020).

91. Kochmanski, J. J. *et al.* Longitudinal Effects of Developmental Bisphenol A Exposure on Epigenome-Wide DNA Hydroxymethylation at Imprinted Loci in Mouse Blood. *Environ. Health Perspect.* **126**, (2018).

92. Zhang, M. *et al.* Ten-eleven translocation 1 mediated-DNA hydroxymethylation is required for myelination and remyelination in the mouse brain. *Nat. Commun.* **12**, 5091 (2021).

93. Murphy, S. K., Huang, Z. & Hoyo, C. Differentially methylated regions of imprinted genes in prenatal, perinatal and postnatal human tissues. *PloS One* **7**, e40924 (2012).

Figures and Tables

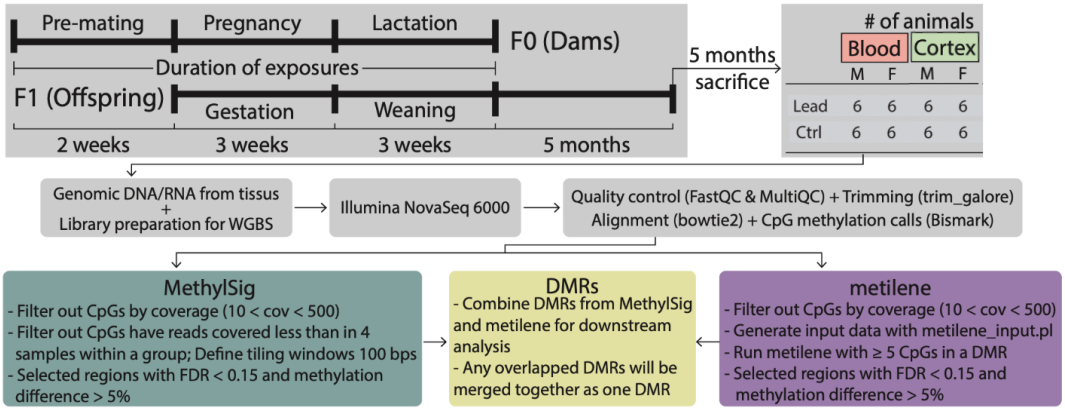

Figure 2.1: Overview of Experimental Workflow. F0 generation females (6-8 weeks of age) were exposed to 32 ppm Pb or control drinking water, beginning two weeks prior to mating using virgin males (8-10 weeks of age). Exposure to Pb or control water continued through gestation and weaning, when F1 mice were removed from the dams and placed on control water. At 5 months of age, F1 mice were sacrificed, and genomic DNA was extracted from cortex and blood tissues. DNA was used to prepare libraries for Whole Genome Bisulfite Sequencing (WGBS) Following initial data processing, Differentially Methylated Regions (DMRs) were called using MethylSig and metilene.

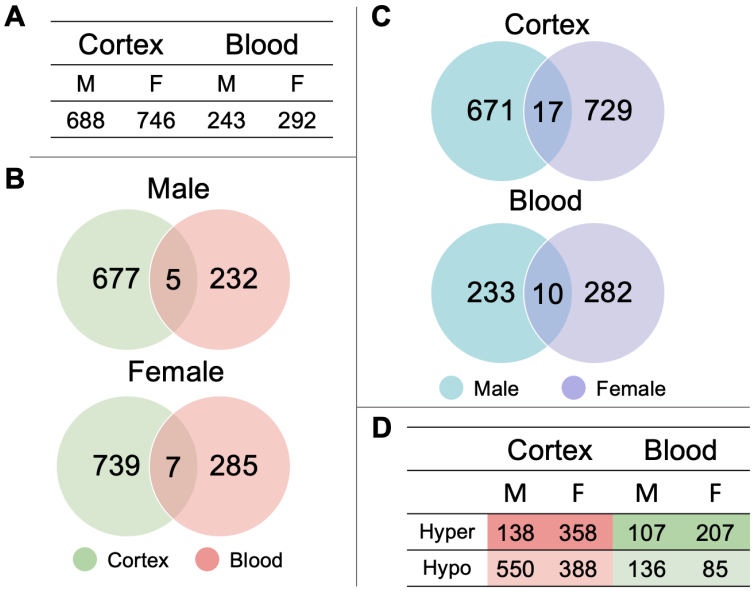

Figure 2.2: Summary of Detected Differentially Methylated Regions. Differentially Methylated Regions (DMRs) were categorized by tissue (cortex, blood) and sex (M: male, F: female) (**2.2A**), and DMRs detected in more than one tissue type were further categorized by sex (**2.2B**). DMRs shared by both sexes were quantified and broken down by tissue type (**2.2C**). The proportion of DMR directional changes were generally summarized for each tissue-sex combination, designated by hyper (more methylated in exposed) or hypo (less methylated in exposed), in comparison to controls (**2.2D**).

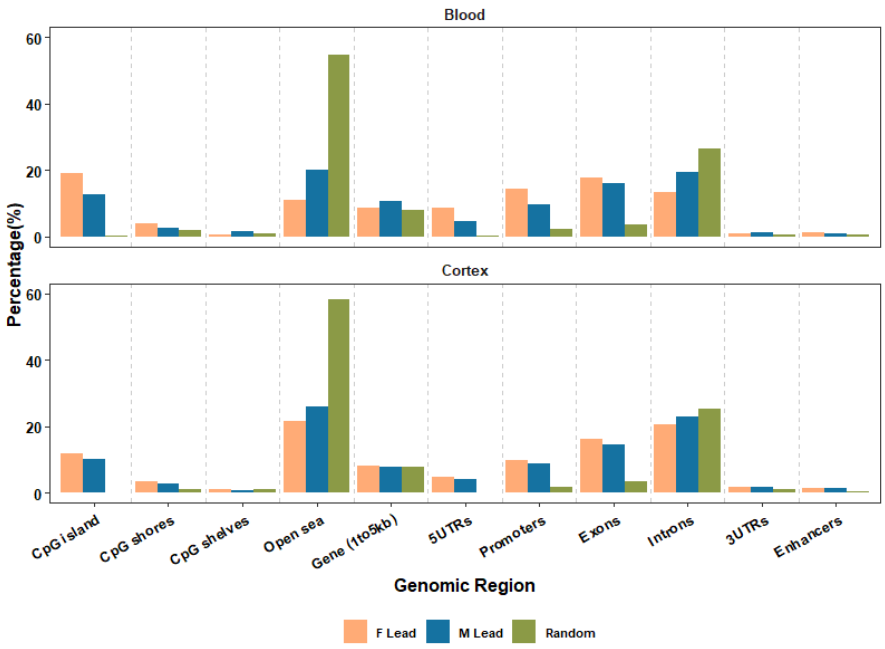

Figure 2.3: Genomic Regions of Detected Differentially Methylated Regions. Differentially Methylated Regions (DMRs) were mapped to the mouse reference genome (mm10) and their genomic region annotated as percentage of total DMRs (comparing control and exposed samples) for that sex and exposure within each tissue. This distribution was compared to what would be expected in a random distribution.

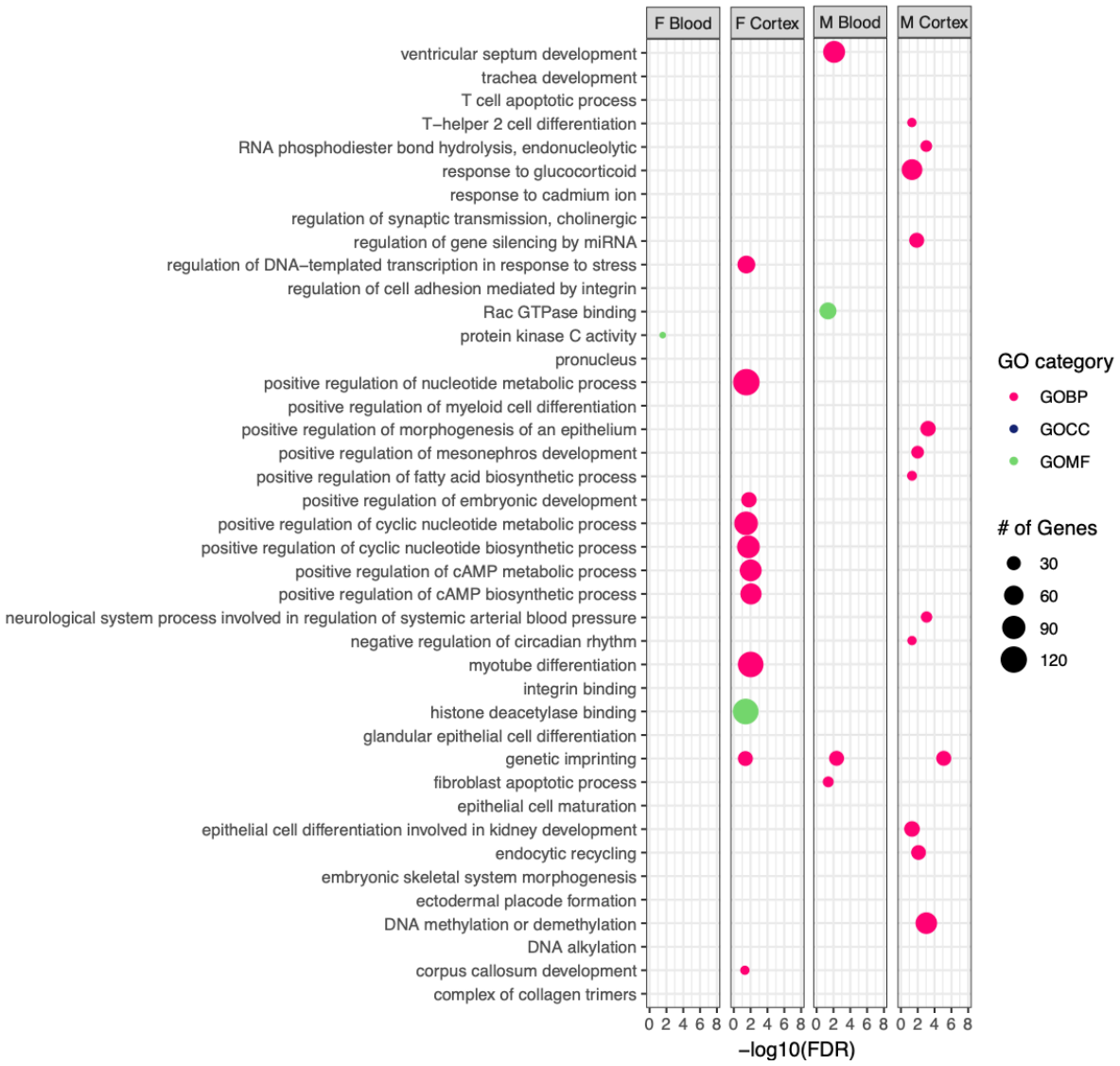

Figure 2.4: GO-terms Associated with Differentially Methylated Region-Containing Genes. Differentially Methylated Region-containing genes found in Pb-exposed tissues were submitted for Gene Ontology (GO) term analysis across three categories: Biological Process (GOBP), Cellular Component (GOCC), and Molecular Function (GOMF).

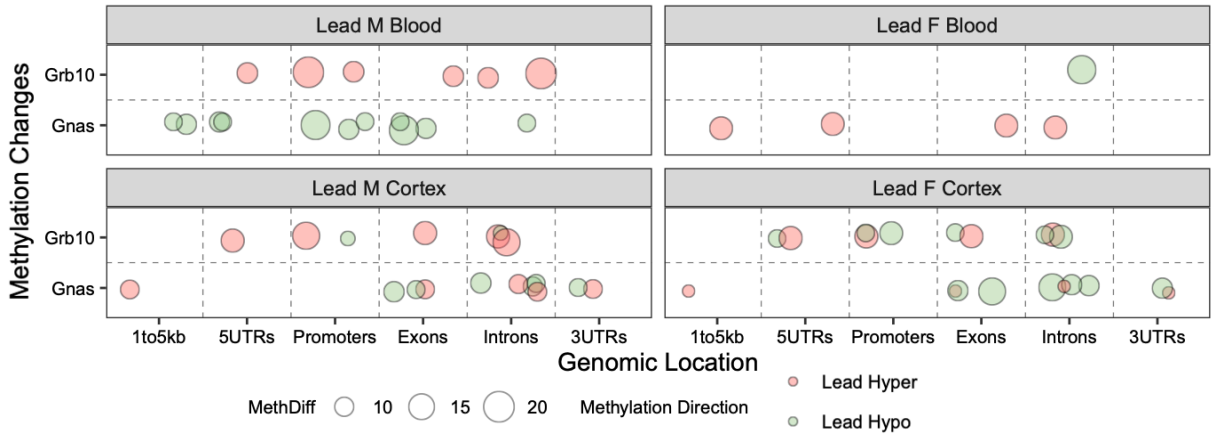

Figure 2.5: Genomic Location and Direction of Lead-Associated Differentially Methylated Regions in the Gnas and Grb10 Loci. Differentially Methylated Regions (DMRs) detected in the Gnas and Grb10 were classified as to their genomic location within each gene. Percent change in methylation is denoted by size and direction of methylation change by color (red = hypermethylation among Pb samples, green = among hypomethylation among Pb samples).

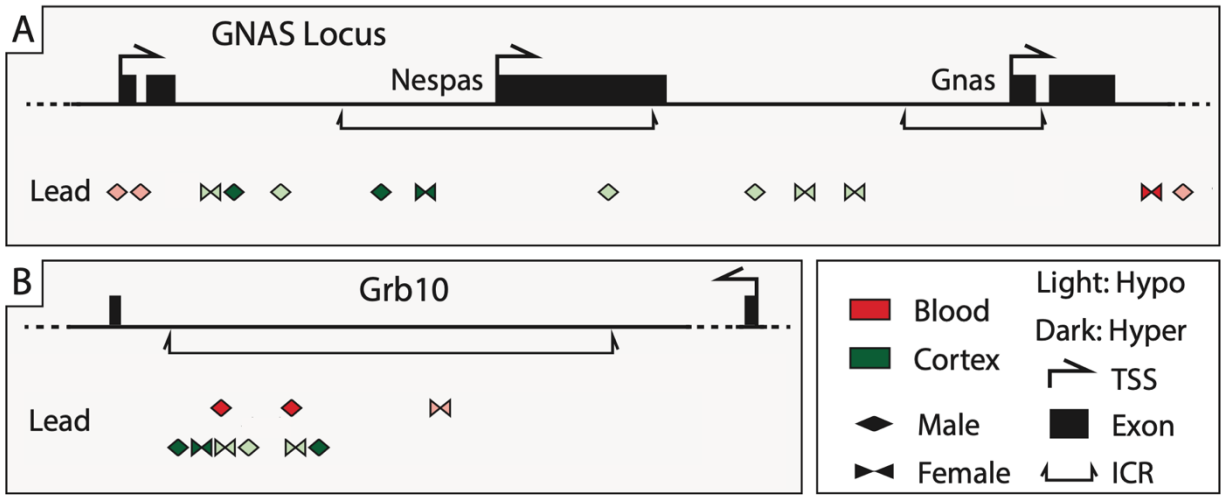

Figure 2.6: Differentially Methylated Regions Detected within Gnas and Grb10 Imprinting Control Regions. (A) Differentially Methylated Regions (DMRs) overlap with Gnas. (B) DMRs overlap with Grb10. DMRs only represents the related genomic locations corresponding to the genomic coordinates of ICRs. The genomic coordinates of these DMRs can be found in Table 2.A5.

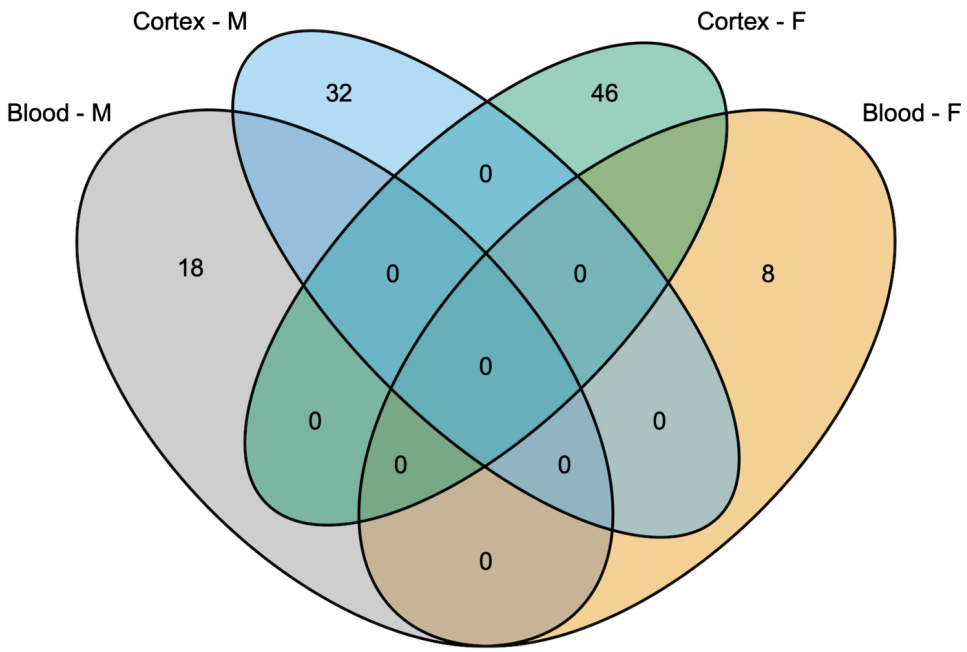

Figure 2.7: Overlap of Differentially Methylated Regions in LINE-1 Elements. Differentially methylated regions were identified in LINE-1 elements and overlap between sexes and tissues quantified using GenomicRanges (v 4.2).

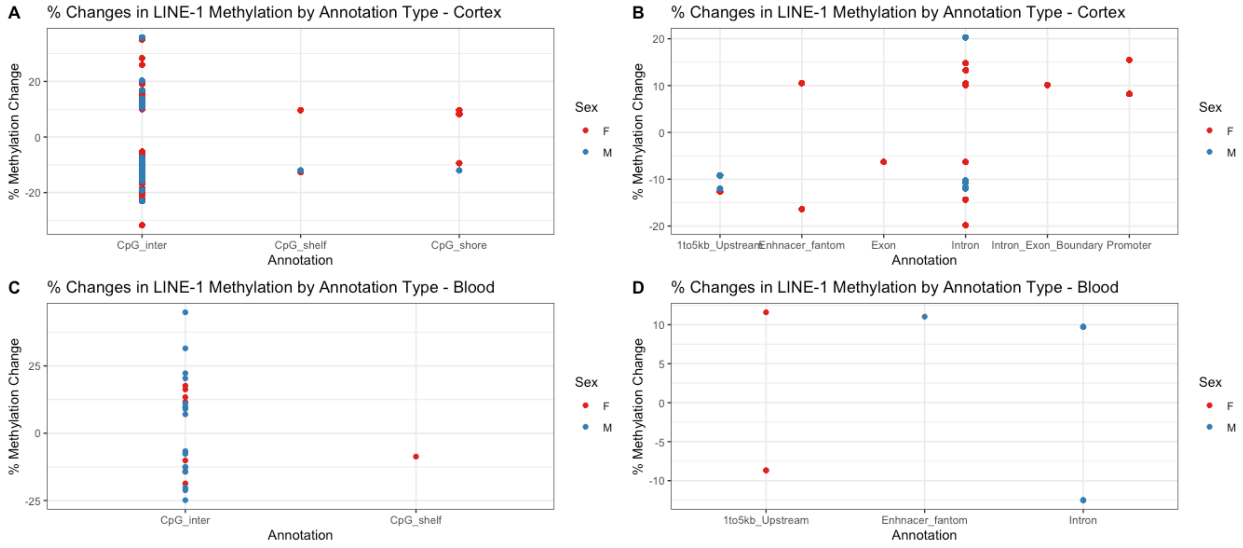

Figure 2.8: Genomic Regions of Detected Differentially Methylated Regions in LINE-1 Elements. Differentially Methylated Regions (DMRs) within LINE-1 elements were mapped to the mouse reference genome (mm10) and their genomic region annotated. Percent methylation changes for each DMR are reported here for each sex and tissue.

Cortex		
	Hypomethylated	Hypermethylated
Male	24	8
Female	28	18
Blood		
	Hypomethylated	Hypermethylated
Male	9	9
Female	4	4

Figure 2.9: Summary of Differentially Methylated Regions that Intersect with LINE-1 Elements.

Appendix

Sex	Tissue	Method		Overlap	After merge
		MethylSig	Metilene	DMRs	DMRs
Male	Blood	93	153	3	243
	Cortex	220	500	32	688
Female	Blood	58	241	7	292
	Cortex	209	567	31	746

Table 2.A1: Summary of Differentially Methylated Regions Detected by metilene and methylsig.

Table 2.A2: Summary of Differentially Methylated Region Annotation within the Mouse Genome.

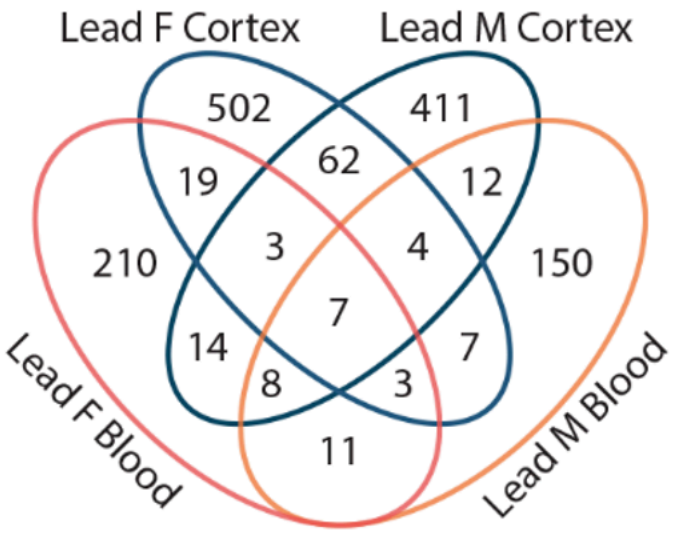

Figure 2.A1: Differentially Methylated Region-Containing Genes Shared Between Tissues.

Table 2.A3: Summary of GO-Terms Associated with Detected Differentially Methylated Regions.

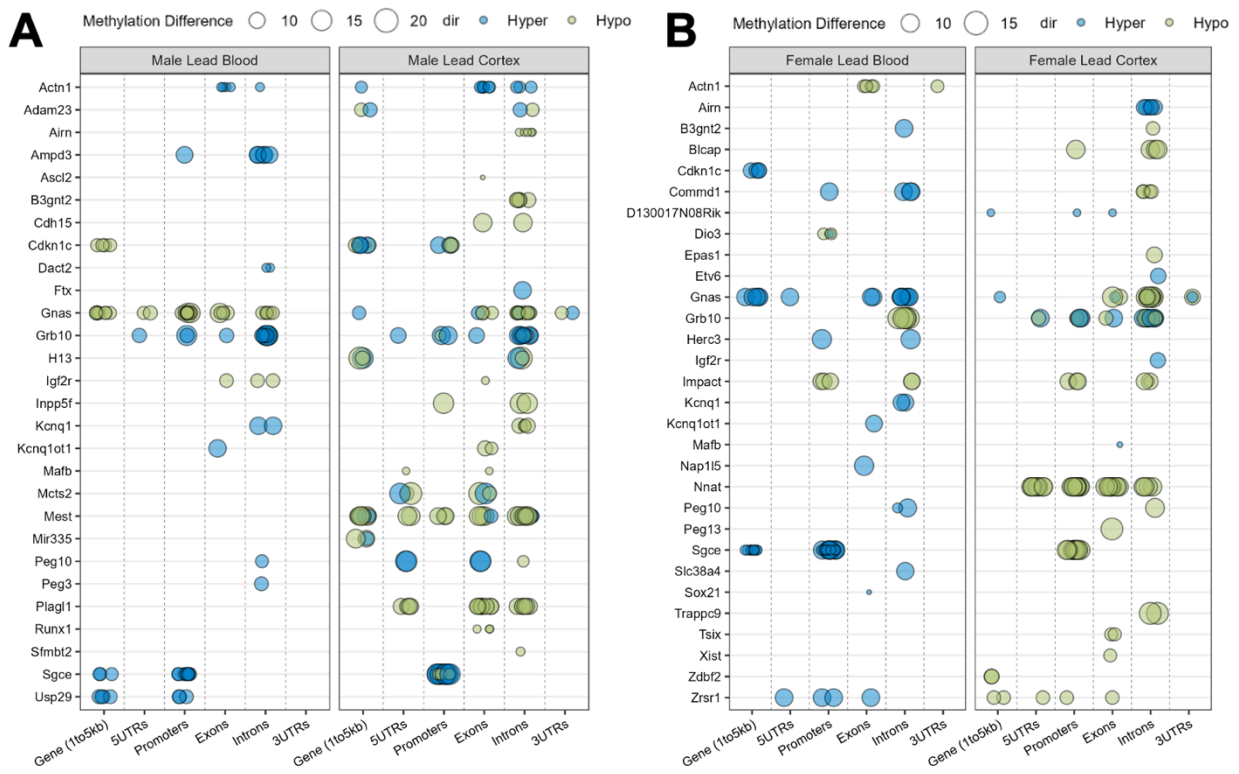

Figure 2.A2: Differentially Methylated Region Containing Imprinted Genes in Male (A) and Female (B) Tissues.

Table 2.A4: Reference List of Imprinted Genes. Type refers to mode of imprinting, either paternal (P) or maternal (M).

Table 2.A5: Summary of Differentially Methylated Regions Detected in Imprinted Genes.

Table 2.A6: Summary of Binomial Test Examining whether Differentially Methylated Regions Occur in Imprinting Control Regions to a Significant Degree.

Table 2.A7: Summary of Differentially Methylated Regions Detected within Imprinting Control Regions.

		Total DMR	LINE-1 DMR	Probability	Actual Occurrence	pvalBino
Cortex	Male	714	32	0.18	0.04	2.2E-16
	Female	792	46	0.18	0.06	2.2E-16
Blood	Male	237	18	0.18	0.08	0.0000062
	Female	292	8	0.18	0.03	1.17E-15

Table 2.A8: Summary of Bionomial Test Examining Differentially Methylated Regions in LINE-1 Elements.

Table 2.A9: Summary of LINE-1 Differentially Methylated Regions.

Chapter 3

Aim 2: Morphological Effects of Environmentally Relevant Lead (Pb) Exposure in Differentiating SH-SY5Y-Derived Dopaminergic-Like Neurons

Abstract

Neural stem cells (NSCs) are important sources of neurons involved in learning and memory not only during early development, but also throughout the life. Perturbation of these cell populations has been heavily documented with regard to neurodegenerative disease (ND) risk, and developmental origins of NSC decline are associated with earlier onset and more rapid ND progression. NSCs are impacted significantly by environmental exposures, with associated outcomes such as dysregulated proliferation, oxidative stress and mitochondrial dysfunction, and increased rates of apoptosis regularly documented. The majority of toxicological work on NSCs execute an exposure paradigm wherein exposure happens before and/or after cellular differentiation, as ESC-derived NSCs are difficult to maintain in culture, especially in the presence of dual stressors such as differentiation and a toxicant. This means much of this research misses out on documenting the effects of real-world exposure scenarios, ones in which exposure continues throughout this developmental process. This aim employs the SH-SY5Y neuroblastoma cell model as a robust model of neural differentiation in order to assess the impact of environmentally relevant Pb exposure on cellular morphology and neural differentiation. During early differentiation,

1.26μM Pb exposure was associated with elevated cellular markers of neural differentiation (GAP43, and MAP2). By late differentiation, the expression of these markers (β-tubulin III and GAP43) decreased with 1.26μM and 10μM Pb exposure, along with measures of neuron branching, indicating exposure perturbed the formation of terminal neurons. Benchmark dose analysis revealed changes in cellular response to Pb, with cells in later stages of differentiation less equipped to efficiently differentiate in the presence of low to moderate Pb exposure, compared to those of earlier time points. This work is one of relatively few examining the effects of Pb exposure during the course of differentiation and reveals time point-specific effects that may contribute to our understanding of how developmental exposures alter the risks of adverse neurodevelopmental outcomes.

Introduction

Neural stem cells (NSCs) are multipotent cells that give rise to neurons and glial cells beginning in fetal development.[1] Prior to this, stem cells in what will eventually develop into the brain in the embryo are much more pluripotent in nature, beginning with embryonic stem cells (ESCs) and neuroepithelial progenitors (NEPs). As fetal development begins in earnest, NEPs give rise to specific populations of NSCs in various regions of the brain.[2] Each of these populations have some capacity for self-renewal and thus, can differentiate into neurons and support cells specific for that brain region not only during development but also, in the case of a few regions, into adulthood.[3,4] In adulthood, these NSCs are largely located in the subventricular zone (SVZ) and subgranular zone (SGZ), which are positioned in the outer wall of the lateral ventricle and the hippocampus, respectively. NSCs of the SVZ largely give rise to

neurons that will eventually migrate to the olfactory bulb, whereas those of the SGZ will differentiate into excitatory (dopaminergic) neurons that are involved in learning and memory as well as motor function.[5] It is these latter cells of the SGZ that are of particular interest with regard to neurodegenerative disease (ND) risk, as a significant reduction in their proliferation and neurogenesis has been observed in individuals diagnosed with NDs such as Alzheimer's (AD) and Parkinson's disease (PD).[6–8]

Truly multipotent NSCs derived from ESCs are difficult to culture in a laboratory setting. Their sensitivity to nutrient balance and their environment increases the incidence of spontaneous differentiation into non-target cell types as well as the risk of cell death if conditions are not properly calibrated.[9–11] This is even more true when it comes to differentiating these cells into a terminal cell type, as this process is taxing on its own, making cells increasingly sensitive to the factors mentioned here.[12] For this reason, much of the available literature on Pb exposure and NSCs focuses on exposure paradigms that are limited to either the pre- or post-differentiation period, allowing cells to differentiate in the absence of a toxicant exposure.[13] However, this experimental design limits our ability to assess the effects of a real-world scenario, one in which exposure happens prior to, during, and after NSC differentiation. Here, we employ the SH-SY5Y (5Y) cell model, a robust and tractable model of neural differentiation in order to quantify changes that occur while both stressors occur simultaneously.

NSCs are environmentally sensitive, both during development as well as in adulthood. *In vivo* work demonstrates a relationship between maternal exposures to high fat diet and anesthetics during gestation and reduced NSC populations and neurogenesis in offspring.[14,15] Developmental origins of compromised NSCs within the

SGZ may contribute to ND risk later in life, as a reduction in these cellular populations may be permanent and would likely accelerate the rate at which ND develops, due to inadequate neurogenesis in this region.[16] Several studies have identified relationships between environmentally relevant Pb exposure and differential expression of genes involved in neurodevelopment and ND in NSCs.[17,18] Additional work has found NSC exposure to Pb is associated with abnormal cell morphology, as well as aberrant patterns of cellular apoptosis and proliferation.[19,20] While assessment of gene expression regulation and morphological changes in NSCs exposed to Pb during differentiation has been done, there is little research exploring these two outcomes in the same cells, which prevents any assessment of correlations between these two outcome categories. As such, this dissertation examines the effects of Pb exposure during SH-SY5Y differentiation on cellular morphology and differentiation success, as well as on mechanistic pathways related to epigenetic gene regulation in Chapters 3 and 4, respectively.

This aim attempts to assess the impact of environmentally relevant doses of Pb on the morphology of differentiating 5Ys. 5Ys are an NSC-like stem cell model derived from a neuroblastoma cell line (SK-N-SH) and are commonly used as a robust and tractable model of neural differentiation into dopaminergic-like neurons. At multiple time points during 5Y differentiation, cells were fixed and stained with fluorescently labeled

antibodies of markers of neural differentiation. Images of these cells were further quantified to assess changes in differentiation success as well as cellular morphology.

Methods

Cell Culture and Exposure Conditions

5Y cells were obtained from ATCC (Cat. #CRL-2266) at passage 28 (P28) and were stored in liquid nitrogen upon arrival. According to manufacturer recommendations, maintenance of 5Ys should not exceed 10-15 passages, and thus, cells were not used past P40. Cells were expanded according to manufacturer protocols in a mixture of EMEM (ATCC, Cat. #30-2003), F-12 (Thermo, Cat. #11765-054), antibiotics (Thermo, Cat. #15140-122), and 10% heat-inactivated fetal bovine serum (hiFBS) (Thermo, Cat. #A3840001). P39 5Ys were differentiated into dopaminergic-like neurons according to previously published protocols.[21] Briefly, beginning on Day 0 (D0), cells were seeded at 10,000 cells per well of a 24 well plate and allowed to attach overnight. Once attached, cells were maintained for one week in serum-deprivation conditions (2.5% hiFBS) and 10μM retinoic acid (RA) (Sigma, Cat. # R2625). After one week, on D7, cells were split 1:1 onto new 24 well plates and maintained for a further three days in 1% hiFBS and 10μM RA. Cells were split once again 1:1 on D10 onto extracellular matrix (ECM)-coated plates and maintained in hiFBS-free media containing Neurobasal Medium (Thermo, Cat. #21103049), brain-derived neurotrophic factor (BDNF) (Thermo, Cat. #10908-010), and dibutyryl cyclic-AMP (db-cAMP) (Fisher, Cat. #16980-89-5). A full description of media conditions and differentiation protocol can be found in **Table 3.A1** and **Figure 3.1**. Cells were considered fully differentiated on D18.

Beginning on D5, 5Ys were exposed to a range of Pb acetate (hence forth referred to as Pb) (Sigma, Cat. # 316512) concentrations via cell culture media. Exposure did not begin until D5 in order to give 5Ys the opportunity to begin differentiating in the absence of any additional stressors, but once introduced, Pb exposure continued for the duration of 5Y differentiation. Exposure conditions included 0μM Pb (control), 0.16μM Pb, 1.26μM Pb, and 10μM Pb. These exposure conditions are thought to reflect current and historical exposures, wherein 0.16μM corresponds to the current actionable blood lead level (BLL) set by the CDC (3.5μg/dL), 1.26μM corresponds to BLLs common in the US prior to the phase out of leaded-gasoline and Pb-based paint in the 1970s (16-30μg/dL), and 10μM corresponds to an acute exposure event that would occur in limited circumstance in the U.S. today, but does still occur elsewhere in the world.[22] The 10 μM dose was also determined to be the highest exposure the cells could handle while still differentiating in preliminary experiments. Fresh Pb was added to the cells with each media change (i.e., every 2-3 days).

Immunofluorescence and Imaging

Immunofluorescence (IF) of β-tubulin III, GAP43, and MAP2 were quantified on D6, D12, D15, and D18. D9 was omitted as a time point due to it falling between the two steps in which the cells were split 1:1 into new environments. Cells on D9 were precariously attached to the bottom of the plates and so, many were inevitably lost during the fixation step, limiting our ability to effectively stain and image them. Fixing and staining cells resumed on Day 12, as this was 48 hours following the final split and cells had largely recovered from these steps.

Cells were fixed with 4% paraformaldehyde (PFA) solution (Thermo, Cat. #AA433689M) and incubated at room temperature for 20 minutes. PFA was removed and cells were rinsed once with 1% solution of Tween 20 (Thermo, Cat. #85113) diluted in PBS (pH 7.4) (Thermo, Cat. #10010023). Cells were then permeabilized with a 1% solution of Triton-X (Thermo, Cat. #85111), incubated at room temperature for 15 minutes. After incubation, Triton-X solution was removed, and cells were rinsed twice with the 1% Tween-PBS solution. Primary staining consisted of Hoechst 33342 (Hoechst, 1:2000) (Thermo, Cat. #H3570), anti-β-tubulin III (mouse, 1:150) conjugate antibody (eFluor660) (Thermo, Cat. #50-4510-82), anti-GAP43 (rabbit, 1:200) antibody (Abcam, Cat. #ab75810), and anti-MAP2 (chicken, 1:500) antibody (Thermo, Cat. #PA1-10005) in normal goat serum (NGS) (Thermo, Cat. #50062Z). A full description of staining conditions can be found in **Table 3.A2**. β-tubulin III, GAP43, and MAP2 were selected for use in these experiments due to their prior use and validation in the assessment of 5Y-derived neurons.[21,23] Hoechst binds to AT-rich regions of double stranded DNA, thus providing a reliable visual of the nucleus.[24] β-tubulin localizes to the axonal growth throughout the course of differentiation, whereas GAP43 and MAP2 localize to cell body-adjacent axonal and dendritic growth, respectively, and begin to appear around D6 of differentiation.[25–27] Primary stain was applied to cells and left to incubate at room temperature in the dark for 1 hour. Following this, primary stain was removed, and cells were rinsed three times with the 1% Tween-PBS solution. Secondary staining consisted of anti-rabbit (1:333, Alexa Fluor 488) antibody (Abcam, Cat. #150077) and anti-chicken (1:1000, Alexa Fluor 568) antibody (Thermo, Cat. #A11041). The secondary stain solution was added to cells and allowed to incubate for

one hour in the dark at room temperature. Secondary stain was removed, and cells were rinsed three times with 1% Tween-PBS solution. Stained cells were stored in 1% Tween-PBS at 4°C until imaging.

Cells were imaged using the Yokogawa CellVoyager CV8000 High-Content Screening System and CellVoyager CQ1 Benchtop High-Content Analysis System. Acquired images were processed, quality controlled, and analyzed using CellProfiler (v.4.2.1) and CellProfiler Analyst (v.3.0.4) software. Images were loaded into CellProfiler along with metadata and underwent quality control and processing, including illumination correction. Primary objects were defined as nuclei (quantified using Hoechst/DAPI) and soma (quantified using the GAP43/488). Once primary objects had been identified, they were used as an anchor point for identifying secondary objects, these being the axon/dendritic projections from each cell. These were quantified using β-tubulin III/660. Once secondary objects were identified, they were converted to images which represented the morphological skeleton that could be quantified. An overview of the Cell Profiler pipeline as well as representative images from each step are illustrated in **Figure 3.A1**.

Benchmark Dose Analysis

Benchmark doses and best fit benchmark dose models were identified according to best practices for dose-response modeling using BMDExpress v.3.0., a free software package available through NIEHS, the EPA, Health Canada, and Sciome[28,29]. Original, untransformed data for each time point was uploaded and prefiltered step using a One-Way ANOVA, with significance accepted at $p < 0.05$ to identify measures with significant increasing or decreasing concentration response. Filtered data were modeled in

BMDExpress with exponential (2, 3, 4, 5), linear, polynomial (2º, 3º, 4º), hill, and power, and the best fit model was chosen based on the lowest Akaike information criteria (AIC). The Benchmark Response (BMR) type was set to 1 standard deviation relative to control with a confidence level of 0.95. Best fit models were chosen for each measure using nested chi square. Hill models were flagged if its 'k' parameter was 1/3 of the lowest possible dose. BMDs initially provided in μM were converted to μg/dL to facilitate comparisons to BLLs using a standard conversion and the molecular weight of Pb (μg/dL = (μM * 207.2g/mol)/(10dL/L).

Statistical Analysis

Six replicates for each exposure condition (n = 4) at each time point (n = 4) were included in each analysis. Replicates refer to wells of a 24-well plate, in which each row of 6 wells corresponds to one dose condition, and one 24-well plate corresponds to one time point. Average values for each measure of each replicate were obtained by taking the mean value per object and aggregating that data by replicate, thus data represents the median value for a given measure across a given well. Data are represented graphically as boxplots, with the median and mean indicated in the box as a horizontal line and dot, respectively, using ggplot2.[30] The size of the box represents the interquartile range (IQR), with the 25th and 75th percentile indicated by the lower and upper limits, respectively. The lines extending above and below these plots represent measures that fall within 1.5 times the IQR in either direction, and values that fall beyond these points are those that lie outside of this limit and are represented by dots. Comparisons between each experimental group and control was performed using a

two-sided t-test in R (v.4.1.2). Statistical significance was accepted with $p < 0.05$ and is designated in figures as * $p < 0.05$, ** $p < 0.01$, *** $p < 0.005$, **** $p < 0.001$.

Results

Lead Exposure Associated with Changes in Cell Number and Structural Changes

Cell number was totaled for each image and the number of cells per image was averaged across each well (n = 6 per exposure condition). There was a marked decrease in the number of cells per well (and image) for the control, 0.16μM Pb, and 1.26μM Pb exposure groups, on Days 12-18, as the splitting steps are harsh for all cells and only a subset survive the process. Prior to D12, the number of cells per image averaged between 118 and 140 cells, whereas on D12, this was reduced to between 17 and 88 cells per image. As differentiation progressed through D15 and D18, cell number recovered across control, 0.16μM, and 1.26μM conditions as cells recovered from the splitting process (average cells per image = 31-86) (**Table 3.1**).

Control cells appeared to recover from passaging steps more efficiently than exposed cells, with notable presence of axonal networks on D15 while exposed cells had much more truncated projections at this same time point (**Figure 3.2C**). By D18, control cells as well as those exposed to 0.16μM and 1.26μM Pb had developed extensive axonal networks, however those of the control cells were much more refined, with several processes per cell extending out and connecting with those of several neighboring cells. 0.16μM and 1.26μM Pb exposed cells on the other hand had axonal networks that were much more dysregulated in appearance. These projections were much more tangled and matted, suggesting their development was significantly perturbed by Pb exposure (**Figure 3.2D**). The combination of 10μM Pb exposure and

differentiation proved to be quite toxic to the 5Y cells, and the vast majority did not recover following the two passaging steps. These wells were largely void of any healthy cells, with the occasional nucleus detected, but no identifiable axonal projections from any cells and additional results from this group should be interpreted with caution.

Lead Exposure Associated with Alterations in β-Tubulin III, GAP43, and MAP2 Expression in Differentiating SH-SY5Y Cells

D6 corresponded to 24 hours after Pb exposure was introduced and was also 5 days into RA exposure, which resulted in cells that had begun to take on a neuronal phenotype (i.e., longer projections, more oblong cell bodies) (**Figure 3.2**). There were no detectable changes in Hoechst signal or β-tubulin III expression, though the 10 μM Pb exposed cells did display significantly more variation in these two markers (**Figure 3.3A-B**). Expression of the two 5Y differentiation-specific markers, GAP43 and MAP2, were significantly less than that of the control cells on D6 with 0.16μM Pb exposure ($p < 0.01$). Interestingly, there were no detectable differences in GAP43 expression in the 1.26μM and 10μM Pb conditions, and MAP2 expression was actually greater than that of the control cells in the 1.26μM Pb group ($p < 0.01$). There was no detectable difference in MAP2 expression in the 10μM Pb group (**Figure 3.3C-D)**.

D12 corresponds to 48 hours after the last passage in the 5Y differentiation protocol, thus marks a period of significant recovery for cells. It also corresponds to 24 hours after terminal differentiation factors have been added to 5Y media (e.g., neurobasal, BDNF, db-cAMP) and marks the beginning of the last week of differentiation, when the cells begin to take on their terminal form. On D12, there were no significant changes in Hoechst signal at the 0.16μM or 1.26μM Pb doses, relative to

control, but expression within the 10μM Pb condition was notably less than that of the control cells ($p < 0.005$) (**Figure 3.4A**). The remaining IF markers demonstrated similar patterns in expression, wherein the low or medium Pb doses resulted in greater expression relative to control, whereas the 10μM Pb condition resulted in much less expression. β-tubulin III expression was significantly increased in the 0.16μM Pb cells ($p < 0.05$) and decreased in the 10μM Pb cells ($p < 0.005$) (**Figure 3.4B**). GAP43 and MAP2 both had greater expression relative to control cells in the 1.26μM Pb condition ($p < 0.01$ and $p < 0.005$, respectively), whereas both were lowly expressed in the 10μM Pb condition (GAP43 $p < 0.001$, MAP2 $p < 0.01$) (**Figure 3.4C-D**).

By D15 of differentiation, cells have recovered completely from passaging steps and have been provided nutrient-rich media that contains terminal differentiation factors for 4 days. Their axonal projections have extended significantly relative to D6, and they have begun to form neural networks within in their environment, with cells migrating closer together and creating synapses with neighboring clusters (**Figure 3.2C**).[21] There was no detectable difference in the expression of Hoechst, β-tubulin III, or GAP43 in the 0.16μM and 1.26μM Pb exposure conditions, relative to control. There was a significant reduction in the expression of Hoechst ($p < 0.001$), β-tubulin III ($p <0.001$), and GAP43 ($p < 0.005$) in the 10μM Pb exposed cells, relative to control (**Figure 3.5A-C**).

5Y differentiation concludes on D18, with reduced cell clumping (>10 cells per group), slender cell bodies, and axonal connections between neighboring cells, which constitute mature neuronal networks.[21] There were no significant changes in Hoescht expression in the 0.16μM or 1.26μM Pb cells, though quantified expression patterns do suggest the beginnings of dose-response relationships (**Figure 3.6A**). We began to see

a more linear relationship between dose and β-tubulin III and GAP43 expression at D18, compared to the earlier time points. The expression of both these markers was significantly reduced with the 1.26μM Pb condition (β-tubulin III $p < 0.05$, GAP43 $p < 0.01$) as well as with the 10μM Pb condition (β-tubulin III $p < 0.001$, GAP43 $p < 0.005$) (**Figure 3.6B-C**).

Dose-Response Modeling of Immunofluorescence During SH-SY5Y Differentiation in the Presence of Lead

Benchmark dose (BMD) analyses were conducted using BMDExpress where significant differences between treatments was determined via One-Way ANOVA and data were analyzed for best model fit. The BMD represents the dose of Pb exposure that is predicted to produce a significant change in the response rate of a given measure, based on the modeled data. Analysis of D6 data produced a BMD for MAP2 (0.437μM Pb), which corresponds to a BLL of 9.06μg/dL (**Table 3.2, Figure 3.7**). D12 produced BMDs for all for included IF measures, including a Hoechst BMD of 9.2μM Pb (191.6μg/dL), β-tubulin III BMD of 1.1μM Pb (24.5μg/dL), a GAP43 BMD of 9.6μM Pb (199.4μg/dL), and a MAP2 BMD of 9.9μM Pb (205.1μg/dL) (**Table 3.2**, **Figure 3.8**). On D15, all included IF measures again had significant BMDs predicted by BMDExpress, the lowest again being that of β-tubulin III which was 1.9μM Pb (41.2μg/dL), followed by GAP43, the BMD of which fell sharply from that of D12 to 2.2μM Pb (47.4μg/dL). The dose at which Pb exposure was predicted to cause an adverse change in Hoechst expression remained similar to what was seen on D12, at 9.3μM Pb (192.8μg/dL) (**Table 3.2**, **Figure 3.9**). By D18, the BMDs for all three IF measures had dropped to similar levels, with the β-tubulin III BMD predicted to be 1.1μM Pb (23.9μg/dL), the

Hoechst BMD predicted to be 1.9μM (40.6μg/dL), and the BMD of GAP43 predicted to be 1.1μM Pb (23.2μg/dL) (**Table 3.2**, **Figure 3.10**).

Lead Exposure Associated with Changes in Cell Morphology During Neural Differentiation

IF imaging was used to quantify morphological measures of 5Y cells as they differentiated, in order to assess if there were structural changes associated with Pb exposure in a time-dependent manner using CellProfiler (**Figure 3.A1**). D6 cells, corresponding to 24 hours of Pb exposure, resulted in enlarged nuclei in the 10 μM Pb exposed cells, relative to control. There were no corresponding changes in at any dose in overall cell size or cytoplasm size (**Figure 3.11A-C**). Additional measures of morphology were quantified that were specific to neuron differentiation, including number of axon branches, axon endpoints, and total length of axon branching per cell. On D6, there were no significant changes in these measures at any dose (**Figure 3.10D-F**).

D12 demonstrated increased changes in cellular morphology associated with Pb exposure relative to D6, with effects seen at lower doses. Overall cell size and cytoplasmic size were both markedly reduced at 1.26μM ($p < 0.05$) and 10μM ($p < 0.001$) Pb exposure, relative to control (**Figure 3.12** and **3.12C**). Nuclei size was only significantly reduced in the 10μM Pb cells (**Figure 3.12B**). There were no significant changes in degree of branching at the 0.16μM or 1.26μM Pb doses, but there was marked decrease in all three measures in the 10μM Pb cells, relative to control (**Figure 3.12D-F**). The significant decrease in cell size at D12 in the 10μM Pb exposed cells is likely the result of their inability to survive the combined stressors of Pb exposure and

passaging during the differentiation process, and this trend holds true for remaining morphological measurements and remaining days.

Measures of morphological changes at D15 demonstrated similar patterns to those seen on D12, with the most significant changes in cell, nuclei, and cytoplasmic size seen in the 1μM Pb cells ($p < 0.05$) (**Figure 3.13A-C**). There was also a detectable increase in nuclei size in the 1.26μM Pb cells ($p < 0.01$) relative to control at this time point. As with D6 and D12, the most significant changes in axonal growth were seen in the 10μM Pb cells, with significant ($p < 0.005$) decreases in number of and total length of branching, as well as of the number of endpoints (**Figure 3.13D-F**). There were no detectable changes in these measures at D15 in the lower exposure conditions.

It is not until D18 that we begin to see a more robust dose-response relationship between Pb exposure and morphological measures. Cell, nuclei, and cytoplasm size all decreased significantly in the 1.26μM Pb exposed cells, relative to control ($p < 0.05$). A greater reduction in nuclei size was seen in the 10μM Pb cells, however nonsignificant results were returned for changes in cell and cytoplasm size in this same group, likely driven by the greater degree of variability in these measures (**Figure 3.14A-C**). Similar patterns were seen among morphological measures of neuron differentiation, wherein 1.26μM Pb exposure was associated with a decrease in the number of neuron branches and endpoints, as well as total length of neuron branching ($p < 0.05$). A greater decrease in these measures was observed in the 10μM Pb cells ($p < 0.05$) (**Figure 3.14D-F**).

Dose-Response Modeling of Morphological Features of Differentiating SH-SY5Ys in the Presence of Lead

There were no BMDs detected for morphological measures on D6 based on available data. As with IF measures, D12 and D15 saw significant model and BMD fit for all six morphological measures. On D12, measures including cell cytoplasm, and nuclei area all decreased with Pb exposure, with BMDs of 1μM Pb (20.7μg/dL), 0.38μM Pb (7.9μg/dL), and 2.06μM Pb (42.7μg/dL), respectively (**Table 3.2**, **Figure 3.15A-C**). Measures of neural outgrowth also decreased with increasing Pb exposure, and the number of endpoints, branches, and total length of branching had BMDs of 2.1μM Pb (45.3μg/dL), 1.7μM Pb (36.05μg/dL), and 1.7μM Pb (36.5μg/dL), respectively (**Table 3.2**, **Figure 3.15D-F**).

D15 saw significant BMD fit for these same measures, although they increased notably from those predicted on D12. Cell, cytoplasm, and nuclei area all had BMDs of roughly 9.1μM (189μg/dL) (**Table 3.2, Figure 3.16A-C**), whereas those of neural projections were somewhat lower. The BMDs of number of endpoints, number of branches, and total branching length per cell were predicted to be 7.6μM Pb (158.5μg/dL), 5.4μM Pb (112.9μg/dL), and 7.4μM Pb (153.6μg/dL), respectively. These models generally predicted increases in these measures at the lower doses of 0.16μM and 1.26μM and decreases at the highest dose of 10μM Pb (**Table 3.2, Figure 3.16D-F**). BMDs for these measures decreased on Day 18, but significant findings were limited to nuclei area (2.5μM, or 53.4μg/dL), number of end points per cell (0.38μM, or 8.02μg/dL), number of branches per cell (2.02μM, or 41.8μg/dL), and total branching

length (0.63μM, or 13.2μg/dL). At this time point, all modeling predicted decreases in these measures with increasing Pb exposure (**Table 3.2, Figure 3.17A-D**).

Discussion

Lead exposure and dysregulated cellular proliferation of differentiating SH-SY5Ys. Pb exposure was associated with elevated rates of cellular proliferation, as measured by cell number per well, during early differentiation (D6 and D12), and this effect was not as prominent on D15 and D18. Previous work has documented a decrease in neural proliferation in the presence of Pb and it is possible the same effect would have been observed here had the terminal neurons been kept in culture with Pb after D18. It is suspected that the stem-like state of these cells during the earlier days of differentiation may help explain the increased rate of proliferation seen here, as previous studies have identified stem cell-specific pathways that are upregulated during periods of stress (such as during toxicant exposures) that correlated with increased rates of cellular division and proliferation.[31,32] However, this relationship is not universal, with some literature showing a reduction in cell number in the face of other toxicant types, meaning the effects seen here may be specific to Pb and/or the experimental model used.[33,34]

Lead exposure associated with elevated expression of neural markers during early differentiation of SH-SY5Ys. Low and moderate Pb exposure, that which correlates with current and historical exposure levels, was largely associated with an increase in β-tubulin III, GAP43, and MAP2 expression during the earlier time points of 5Y differentiation (i.e., D6 and D12). This was in direct contrast with our hypothesis that the expression of these markers would decrease in a dose-dependent fashion, as we theorized that Pb exposure would hinder differentiation and it would take longer for 5Ys

to take on a neuronal phenotype and there would be corresponding reductions in the expression of these proteins.

β-tubulin III is a microtubule protein encoded by the human gene *TUBB3* and is predominantly expressed in neural and testicular cells.[35,36] We observed greater variability in β-tubulin III expression in 10μM Pb exposed cells on D6 and a non-monotonic relationship with exposure on D12, with lowly expressed cells demonstrating increased β-tubulin III expression, no change seen in the 1.26μM group, and a significant decrease in expression at 10μM Pb exposure. Previous toxicological work assessing this marker in differentiating neurons has also documented increases in its expression alongside exposures such as sevoflurane and indibulin, suggesting the cytoskeletal structure of these cells is developing in a dysregulated manner.[15,37] Chen et al., 2022 supports the idea that Pb exposure contributes to aberrant cytoskeletal development and organization *in vitro*, concluding that cytoskeletal development decreases with increasing Pb exposure.[38] However, it should be noted that this work employed a higher Pb exposure range (0μM to 50μM Pb exposure, with the majority of effects seen at the highest dose of 50μM) and examined effects in stable, undifferentiated cells. It is possible that the effects seen here are unique to the differentiation period and that cytoskeletal development may initially increase in the presence of Pb, while additional pathways promoting its expansion are also active, and that upon the conclusion of differentiation, sustained Pb exposure compromises what has been established. It would be prudent to expand this work in the future, employing multiple models of exposure timing, to assess how cytoskeletal structures adapt to exposures that begin and end at varying times.

GAP43 is commonly referred to as a growth or plasticity protein and has been well documents during neural differentiation as essential for neuronal plasticity and axon regeneration.[39] Previous work has demonstrated a robust decrease in GAP43 in differentiating 5Ys exposed to 5μM Pb for 24 hours, and these results are thought to be related to Pb-induced decreases in cellular calcium concentrations.[40] Our study also saw a decrease in GAP43 expression after 24 hours of Pb exposure, though this effect was only seen at 0.16μM Pb exposure and not either of the higher doses. We were also able to evaluate the effects of continuous Pb exposure on these cells throughout differentiation and saw a recovery in GAP43 expression by D12 at 0.16μM Pb exposure, as expression was indistinguishable from control cells, and overexpression at the moderate dose of 1.26μM Pb. It is possible that the low and moderate Pb doses employed in this study induced increased expression of GAP43 during early differentiation because they were high enough to trigger pathways related to cellular plasticity and resilience, thus increasing GAP43 activity, but not so high as to trigger cytotoxic effects, as has been documented with other stressors.[41–43]

MAP2 is a cytoskeletal protein specific to neurons thought to coordinate the organization and stabilization of microtubules and actin filaments.[44] Interestingly, MAP2 is closely related to Tau, both being Class II MAP proteins, with the former expressed in dendritic projections and the latter in axonal.[45] While Tau proteins have garnered most of the attention as to their role in ND, MAP2 has also been shown to be aberrantly expressed and phosphorylated in these conditions. Additionally, dysregulation of MAP2 is thought to drive that of Tau, and vice versa, meaning both should be considered in the context of ND development and progression.[46] This work saw a decrease in MAP2

in 0.16μM Pb cells and an increase in 1.26μM Pb cells on D6, the latter of which was maintained into D12. Previous work assessing the relationship between Pb exposure and MAP2 expression demonstrates an inverse relationship between the two, however this work occurs in differentiated SH-SY5Y cells, meaning the effects of exposure during early differentiation are not ascertainable.[47] The data presented here suggests MAP2 expression may be dysregulated in the presence of Pb and increased MAP2 during early differentiation may prime neurons for ND-like phenotypes after development.[48] When we consider the effects of other toxicants on 5Y differentiation, we see evidence that effects on MAP2 may be toxicant-specific, as graphene oxide has been associated with increases in MAP2 expression[49] whereas inorganic mercury exposure is associated with an impairment of 5Y differentiation as quantified by reduced MAP2 expression.[50] MAP2 expression was unable to be quantified during late 5Y differentiation and future experiments evaluating its expression as this process concludes will help determine whether Pb-induced overexpression is maintained or if there is an eventual reduction in expression, as was seen with the other two markers.

These results taken together suggest Pb exposure may induce greater than normal expression of neural markers, at least during the early stages of differentiation, in that exposure induces compensatory mechanisms to offset any cellular damage and manifests as the appearance of acceleration differentiation, via the cellular marker used here. By late differentiation, there is a decrease in the expression of GAP43 and β-tubulin III, suggesting sustained Pb exposure suppresses neurogenesis in this model, as has been quantified with other exposure types in this model, including cadmium and mercury.[50,51] In exposing cells to Pb as they are differentiating, we were able to detect

surprising changes in protein expression as this process was being initiated, a finding often missed in corresponding literature that typically evaluates the effects of exposure either prior to differentiation or once this process has concluded.

Lead exposure associated with dose-dependent declines in morphological signatures of SH-SY5Y differentiation. The effects of Pb exposure (i.e., elevated expression of neural markers) were not consistent throughout 5Y differentiation and dose-dependent decreases in β-tubulin III and GAP43 expression, as well as neuron branching and total outgrowth length, were detected by D18. As 5Y differentiation concluded, significant decreases in these measures were detected in cells exposed to the moderate Pb dose of 1.26μM, that which correlates to BLLs commonly seen in US children in the 1960s and 70s. While the experiment ended at D18, it is possible that these effects would have been maintained, and perhaps intensified, in these moderately exposed cells. Previous work has found similar results in neurons exposed to various metals for a sustained period (>7 days), in that neurite outgrowth significantly declined with exposure.[50,52,53]

It is also possible that significant effects would begin to appear in the lowest exposure condition, that which correlates with the current actional BLL set by the CDC, had the experiment continued past the conclusion of differentiation. Aberrant expression of β-tubulin III, GAP43, and MAP2, as well as dendritic and axonal recession, have all been documented with respect to various NDs,[54–56] and it is possible that Pb-induced decreases in their expression may contribute to disease risk. Future experiments would do well to elongate the experimental period to assess whether toxicological effects appear when lower dose exposures continue.

Benchmark Dose Analysis Reveals Changes in Cell Response as Differentiation Progresses. BMD analysis was conducted via BMDExpress and provided models of significant fit for multiple measures at each timepoint included in this study. Only one BMD was identified on D6, for MAP2 expression (0.4μM). By D12, all four IF and all six morphological measures elicited significant dose-response relationships with Pb exposure. Generally, BMDs associated with IF measures decreased over the course of differentiation, ranging from 1-9μM on D12 while on D18 they had decreased to 1-2μM overall. It should also be noted that fold changes in expression of these markers were a mix of positive and negative between D6 and D15. Taken together, these trends support the idea that Pb exposure has significant effects during early differentiation (correlating with positive fold changes in protein expression during this time point), while also suggesting that regardless of the direction of response, differentiating 5Ys become less equipped to resist adverse changes following Pb exposure as it persists and differentiation continues, as evident by the reduced BMDs on D18. This may be due in part to changes in neural physiology that make them less equipped to handle Pb-induced stress, but could also simply reflect that long-term Pb exposure will have greater effects on cells than shorter exposures of the same concentration.[57]

BMDs related to neural projection development also changed noticeably during the course of 5Y differentiation. D6 data provided no BMDs for these measures, however by D12 BMDs for parameters of size and projection growth were already fairly low (>2.2μM). Given that BMDs associated with most IF measures were so much higher at this same time point, it is hypothesized that cell growth is significantly hindered by Pb exposure during the early stages of differentiation, whereas processes related to

stemness such as GAP43, may be more resistant, as has been suggested in previously published work on other stem cell populations.[58,59] Interestingly, BMDs for these morphological measures increased in cells analyzed on D15, with 0.16μM and 1.26μM Pb exposure associated with increased cell and projection growth. Contrary to this, previous work has documented an increase in synaptic pruning and a reduction in projection growth in neurons exposed to Pb.[60,61] It may be that opposite effects were observed at this time point due to time-specific effects that are typically missed in studies that examine neurons once they have fully developed. Indeed, BMD analysis on D18 demonstrated that as neurons completed the differentiation process, their resistance to Pb decreased to levels seen on D12 (BMD range of 0.3μM – 2.5μM), and fold changes in these measures were negative with each increase in Pb dose.

This summary of BMD analysis, relative to time point, is in stark contrast to much of the limited literature exploring the effects of various toxicants on undifferentiated versus differentiated 5Ys. Most studies found either similar results between the two cell types or determined that the undifferentiated cells, those more like D6-D12 5Ys, to be more heavily impacted by Pb exposure, while differentiated 5Ys were more resistant to exposure.[62–64] This may be best explained by the fact that this study assessed impacts during differentiation, rather than before or after, and so dose-response relationships will be modified by the developmental process at hand.

While it is interesting to consider how dose-response relationships change during the course of neural differentiation, there is limited literature to compare these results to in a meaningful way. However, given that D18 cells are considered to be fully mature differentiated neurons, and that terminally differentiated neurons are regarded as non-

dividing cells,[65] it is reasonable to interpret relationships seen at this time point with currently available risk assessment literature. In comparing the modeling results from D18 to available risk assessment data, we see that there is notable overlap between the lower limit of BMDs calculated in this study (0.54-40.15μg/dL) and those associated with 1 point loss in IQ (0.355-8.061μg/dL).[66] This previous work goes on to recommend a reduction in the current actionable BLL set by the CDC to 1μg/dL, which corresponds to one fourth of the lowest dose included in this study (0.04μM). Given the concordance between these results, it is theorized that Pb exposures that occur during the process of neural differentiation contribute to the associated decrease in IQ through inadequately developed neurons, though future work assessing these two outcomes in an *in vivo* model would provide firmer conclusions.

These results also highlight that while more stringent policy regarding Pb exposure will no doubt protect children moving forward, past exposures are likely taking a toll on our healthcare system and economy in ways that are not fully appreciated. The average BLL in the late 1970s was 12.8μg/dL; 50% higher than the highest BMD predicted in the risk assessment discussed here.[67] Individuals who were born in those years are now in their mid to late 40s, meaning the lasting impact of Pb exposure from the mid-20th century has not yet been fully realized. Furthermore, much of our appreciation of the effects of Pb exposure on the US at large pertain to intelligence measures.[68] However, it would be prudent to conduct similar risk assessments of Pb exposure on ND incidence and progression, as the measures reported in this study were found to be significantly altered at exposure levels reminiscent of those seen forty to fifty years ago, and these same measures have been implicated in ND risk.[55,69,70]

Limitations

The 5Y cell model is inherently limited given its origin from cancerous tissue, and the effects measured here may be due in part to the increased plasticity and robustness of cancer cells.[71] 5Y cells also exist in both an adherent and non-adherent state, with both types considered viable.[72] This study did not consider differences in outcomes between these two cellular populations, and it is possible that these two groups may have demonstrated different responses to Pb exposure. This work also did not account for the possibility of epithelial-like cells in culture.[73] Future work would benefit from the inclusion of markers of epithelial phenotypes in order to assess the purity of 5Y neural differentiation, as well as whether Pb exposure pushes cells towards one of these phenotypes. Interpretations of this data are also limited by the marked decrease in cells after D12 in the 10 μM exposure group. This dose proved too toxic for these cells during this process and no firm conclusions can be drawn from their data. Future BMD analysis would benefit from a range of doses in which all cells could survive the differentiation process. Finally, the exposure paradigm utilized here introduced Pb exposure on D5 in order to ensure sufficient cell numbers during the experimental period, and thus does not represent a true real-world scenario in which exposure was present prior to as well as during neural differentiation.

Acknowledgements

Lots of gratitude is due to Dr. Justin Colacino who was a major influence on the development and execution of these experiments. The science conducted as a part of this aim was thoughtfully designed with his input and advice. Prior to this study, I had very little *in vitro* experience, and Dr. Colacino provided me with ample opportunity and

resources to expand my skillset and pursue what was interesting to me. I would also like to thank Katelyn Polemi who was a major source of support and assistance in the execution of these experiments, and who stepped in when I needed an extra set of hands. Finally, I'd like to thank Dr. Jonny Sexton who graciously allowed us to image these cells on the Yokogawa and Anagha Tapaswi who helped design the Cell Profiler analysis pipelines used in the data analysis of the cell images. This work was supported by funding from the following sources: NIEHS Grant R35 (ES031686), NIEHS Grant K01 (ES032048), Institutional Training Grant T32 (ES007062), Institutional Training Grant T32 (HD079342), and National Institute of Aging (NIA) Grant R01 (AG072396).

References

1. Zhao, X. & Moore, D. Neural stem cells: developmental mechanisms and disease modeling. *Cell Tissue Res* **371**, 1–6 (2018).

2. Conti, L. & Cattaneo, E. Neural stem cell systems: physiological players or in vitro entities? *Nat Rev Neurosci* **11**, 176–187 (2010).

3. Eze, U. C., Bhaduri, A., Haeussler, M., Nowakowski, T. J. & Kriegstein, A. R. Single-cell atlas of early human brain development highlights heterogeneity of human neuroepithelial cells and early radial glia. *Nat Neurosci* **24**, 584–594 (2021).

4. Gonzalez-Perez, O. Neural stem cells in the adult human brain. *Biol Biomed Rep* **2**, 59–69 (2012).

5. Obernier, K. & Alvarez-Buylla, A. Neural stem cells: origin, heterogeneity and regulation in the adult mammalian brain. *Development* **146**, dev156059 (2019).

6. Rodríguez, J. J. & Verkhratsky, A. Neurogenesis in Alzheimer's disease. *J Anat* **219**, 78–89 (2011).

7. Camicioli, R. *et al.* Parkinson's disease is associated with hippocampal atrophy. *Movement Disorders* **18**, 784–790 (2003).

8. Small, S. A., Schobel, S. A., Buxton, R. B., Witter, M. P. & Barnes, C. A. A pathophysiological framework of hippocampal dysfunction in ageing and disease. *Nat Rev Neurosci* **12**, 585–601 (2011).

9. Aulicino, F. *et al.* Canonical Wnt Pathway Controls mESC Self-Renewal Through Inhibition of Spontaneous Differentiation via β-Catenin/TCF/LEF Functions. *Stem Cell Reports* **15**, 646–661 (2020).

10. Millman, J. R., Tan, J. H. & Colton, C. K. The effects of low oxygen on self-renewal and differentiation of embryonic stem cells. *Curr Opin Organ Transplant* **14**, 694–700 (2009).

11. Cai, C. & Grabel, L. Directing the differentiation of embryonic stem cells to neural stem cells. *Developmental Dynamics* **236**, 3255–3266 (2007).

12. Fathi, A. *et al.* Quantitative proteomics analysis highlights the role of redox hemostasis and energy metabolism in human embryonic stem cell differentiation to neural cells. *Journal of Proteomics* **101**, 1–16 (2014).

13. Peng, J. *et al.* Differential response to lead toxicity in rat primary microglia and astrocytes. *Toxicol Appl Pharmacol* **363**, 64–71 (2019).

14. Hu, X. *et al.* Maternal High-Fat Diet Reduces Type-2 Neural Stem Cells and Promotes Premature Neuronal Differentiation during Early Postnatal Development. *Nutrients* **14**, 2813 (2022).

15. Zhang, Y. *et al.* Maternal sevoflurane exposure affects neural stem cell differentiation in offspring rats through NRF2 signaling. *Neurotoxicology* **93**, 348–354 (2022).

16. Swindell, W. R., Bojanowski, K., Kindy, M. S., Chau, R. M. W. & Ko, D. GM604 regulates developmental neurogenesis pathways and the expression of genes associated with amyotrophic lateral sclerosis. *Transl Neurodegener* **7**, 30 (2018).

17. Dreyer-Andersen, N. *et al.* Intermittent, low dose carbon monoxide exposure enhances survival and dopaminergic differentiation of human neural stem cells. *PLoS One* **13**, e0191207 (2018).

18. Shimizu, S. *et al.* Oral exposure to aluminum chloride for 28 days suppresses neural stem cell proliferation and increases mature granule cells in adult hippocampal neurogenesis of young-adult rats. *J Appl Toxicol* **42**, 1337–1353 (2022).

19. Takahashi, Y. *et al.* Oral exposure to high-dose ethanol for 28 days in rats reduces neural stem cells and immediate nascent neural progenitor cells as well as FOS-expressing newborn granule cells in adult hippocampal neurogenesis. *Toxicol Lett* **360**, 20–32 (2022).

20. Jiang, P., Hou, Z., Bolin, J. M., Thomson, J. A. & Stewart, R. RNA-Seq of Human Neural Progenitor Cells Exposed to Lead (Pb) Reveals Transcriptome Dynamics, Splicing Alterations and Disease Risk Associations. *Toxicol. Sci.* **159**, 251–265 (2017).

21. Wagner, P. J. *et al.* In Vitro Effects of Lead on Gene Expression in Neural Stem Cells and Associations between Up-regulated Genes and Cognitive Scores in Children. *Environ Health Perspect* **125**, 721–729 (2017).

22. Tasneem, S., Farrell, K., Lee, M.-Y. & Kothapalli, C. R. Sensitivity of neural stem cell survival, differentiation and neurite outgrowth within 3D hydrogels to environmental heavy metals. *Toxicol Lett* **242**, 9–22 (2016).

23. Davidovics, Z. & DiCicco-Bloom, E. Moderate lead exposure elicits neurotrophic effects in cerebral cortical precursor cells in culture. *J Neurosci Res* **80**, 817–825 (2005).

24. Shipley, M. M., Mangold, C. A. & Szpara, M. L. Differentiation of the SH-SY5Y Human Neuroblastoma Cell Line. *J Vis Exp* (2016) doi:10.3791/53193.

25. Ericson, B. *et al.* Blood lead levels in low-income and middle-income countries: a systematic review. *The Lancet Planetary Health* **5**, e145–e153 (2021).

26. Dominguez-Alfaro, A. *et al.* Toward Spontaneous Neuronal Differentiation of SH-SY5Y Cells Using Novel Three-Dimensional Electropolymerized Conductive Scaffolds. *ACS Appl Mater Interfaces* **12**, 57330–57342 (2020).

27. Latt, S. A., Stetten, G., Juergens, L. A., Willard, H. F. & Scher, C. D. Recent developments in the detection of deoxyribonucleic acid synthesis by 33258 Hoechst fluorescence. *J Histochem Cytochem* **23**, 493–505 (1975).

28. Jiang, Y. Q. & Oblinger, M. M. Differential regulation of beta III and other tubulin genes during peripheral and central neuron development. *J Cell Sci* **103 (Pt 3)**, 643–651 (1992).

29. Chung, D., Shum, A. & Caraveo, G. GAP-43 and BASP1 in Axon Regeneration: Implications for the Treatment of Neurodegenerative Diseases. *Front Cell Dev Biol* **8**, 567537 (2020).

30. Garner, C. C., Tucker, R. P. & Matus, A. Selective localization of messenger RNA for cytoskeletal protein MAP2 in dendrites. *Nature* **336**, 674–677 (1988).

31. BMDExpress. *Sciome* https://www.sciome.com/bmdexpress/.

32. Benchmark Dose Analysis - BMDExpress-2 Documentation. https://bmdexpress-2.readthedocs.io/en/feature-readthedocs/bmd_analysis/.

33. Create Elegant Data Visualisations Using the Grammar of Graphics. https://ggplot2.tidyverse.org/.

34. Fathi, E. & Farahzadi, R. Zinc Sulphate Mediates the Stimulation of Cell Proliferation of Rat Adipose Tissue-Derived Mesenchymal Stem Cells Under High Intensity of EMF Exposure. *Biol Trace Elem Res* **184**, 529–535 (2018).

35. Peng, Y. *et al.* Cysteine protease cathepsin B mediates radiation-induced bystander effects. *Nature* **547**, 458–462 (2017).

36. Colle, D., Farina, M., Ceccatelli, S. & Raciti, M. Paraquat and Maneb Exposure Alters Rat Neural Stem Cell Proliferation by Inducing Oxidative Stress: New Insights on Pesticide-Induced Neurodevelopmental Toxicity. *Neurotox Res* **34**, 820–833 (2018).

37. Huang, F. & Schneider, J. S. Effects of lead exposure on proliferation and differentiation of neural stem cells derived from different regions of embryonic rat brain. *Neurotoxicology* **25**, 1001–1012 (2004).

38. Caccamo, D. V. *et al.* An immunohistochemical study of neuropeptides and neuronal cytoskeletal proteins in the neuroepithelial component of a spontaneous murine ovarian teratoma. Primitive neuroepithelium displays immunoreactivity for neuropeptides and neuron-associated beta-tubulin isotype. *Am J Pathol* **135**, 801–813 (1989).

39. De Gendt, K. *et al.* Expression of Tubb3, a Beta-Tubulin Isotype, Is Regulated by Androgens in Mouse and Rat Sertoli Cells. *Biol Reprod* **85**, 934–945 (2011).

40. Kumari, A., Prassanawar, S. S. & Panda, D. β-III Tubulin Levels Determine the Neurotoxicity Induced by Colchicine-Site Binding Agent Indibulin. *ACS Chemical Neuroscience* (2022) doi:10.1021/acschemneuro.2c00324.

41. Chen, L. *et al.* Acute lead acetate induces neurotoxicity through decreased synaptic plasticity-related protein expression and disordered dendritic formation in nerve cells. *Environ Sci Pollut Res* **29**, 58927–58935 (2022).

42. Kosik, K. S. *et al.* Human GAP 43: Its deduced amino acid sequence and chromosomal localization in mouse and human. *Neuron* **1**, 127–132 (1988).

43. Ayyalasomayajula, N. *et al.* Inactivation of GAP-43 due to the depletion of cellular calcium by the Pb and amyloid peptide induced toxicity: An in vitro approach. *Chemico-Biological Interactions* **316**, 108927 (2020).

44. Santos, N. A. G. *et al.* The neuroprotection of cannabidiol against MPP+-induced toxicity in PC12 cells involves trkA receptors, upregulation of axonal and synaptic proteins, neuritogenesis, and might be relevant to Parkinson's disease. *Toxicology in Vitro* **30**, 231–240 (2015).

45. Song, Z. & Tao, A. The Neuroprotective Effects of Astragaloside IV against H_2O_2-Induced Damage in SH-SY5Y Cells are Associated with Synaptic Plasticity. *Journal of Chemistry* **2020**, e5343619 (2020).

46. Dayem, A. A. *et al.* Biologically synthesized silver nanoparticles induce neuronal differentiation of SH-SY5Y cells via modulation of reactive oxygen species, phosphatases, and kinase signaling pathways. *Biotechnology Journal* **9**, 934–943 (2014).

47. Dehmelt, L. & Halpain, S. The MAP2/Tau family of microtubule-associated proteins. *Genome Biology* **6**, 204 (2004).

48. Kanai, Y. & Hirokawa, N. Sorting mechanisms of Tau and MAP2 in neurons: Suppressed axonal transit of MAP2 and locally regulated microtubule binding. *Neuron* **14**, 421–432 (1995).

49. DeGiosio, R. A. *et al.* More than a marker: potential pathogenic functions of MAP2. *Front Mol Neurosci* **15**, 974890 (2022).

50. Lin, L. F. *et al.* Low dose lead exposure induces alterations on heterochromatin hallmarks persisting through SH-SY5Y cell differentiation. *Chemosphere* **264**, 128486 (2021).

51. Xie, C. & Miyasaka, T. The Role of the Carboxyl-Terminal Sequence of Tau and MAP2 in the Pathogenesis of Dementia. *Frontiers in Molecular Neuroscience* **9**, (2016).

52. Lv, M. *et al.* Effect of graphene oxide on undifferentiated and retinoic acid-differentiated SH-SY5Y cells line. *Nanoscale* **4**, 3861–3866 (2012).

53. Chan, M. C., Bautista, E., Alvarado-Cruz, I., Quintanilla-Vega, B. & Segovia, J. Inorganic mercury prevents the differentiation of SH-SY5Y cells: Amyloid precursor protein, microtubule associated proteins and ROS as potential targets. *Journal of Trace Elements in Medicine and Biology* **41**, 119–128 (2017).

54. Pak, E. J., Son, G. D. & Yoo, B. S. Cadmium inhibits neurite outgrowth in differentiating human SH-SY5Y neuroblastoma cells. *Int J Toxicol* **33**, 412–418 (2014).

55. Li, X., Li, X., Xiang, C. & Ye, F. Lead exposure represses mitochondrial metabolism by activation of heme-binding protein BACH1 in differentiated SH-SY5Y cell. *Sci Total Environ* **853**, 158665 (2022).

56. Feng, J. *et al.* Maternal exposure to cadmium impairs cognitive development of male offspring by targeting the Coronin-1a signaling pathway. *Chemosphere* **225**, 765–774 (2019).

57. Suzuki, Y., Jin, C., Iwase, T. & Yazawa, I. β-III Tubulin fragments inhibit α-synuclein accumulation in models of multiple system atrophy. *J Biol Chem* **289**, 24374–24382 (2014).

58. Jia, L. *et al.* Blood neuro-exosomal synaptic proteins predict Alzheimer's disease at the asymptomatic stage. *Alzheimers Dement* **17**, 49–60 (2021).

59. Kandimalla, R., Manczak, M., Yin, X., Wang, R. & Reddy, P. H. Hippocampal phosphorylated tau induced cognitive decline, dendritic spine loss and mitochondrial abnormalities in a mouse model of Alzheimer's disease. *Hum Mol Genet* **27**, 30–40 (2018).

60. Huang, H., Bihaqi, S. W., Cui, L. & Zawia, N. H. In vitro Pb exposure disturbs the balance between Aβ production and elimination: The role of AβPP and neprilysin. *NeuroToxicology* **32**, 300–306 (2011).

61. Zhao, Y. *et al.* Lead in Synergism With IFNγ Acts on Bone Marrow-Resident Macrophages to Increase the Quiescence of Hematopoietic Stem Cells. *Toxicological Sciences* **180**, 369–382 (2021).

62. Abdullah, M. *et al.* Diverse Effects of Lead Nitrate on the Proliferation, Differentiation, and Gene Expression of Stem Cells Isolated from a Dental Origin. *The Scientific World Journal* **2014**, e235941 (2014).

63. McCauley, P. T. *et al.* The effect of prenatal and postnatal lead exposure on neonatal synaptogenesis in rat cerebral cortex. *Journal of Toxicology and Environmental Health* **10**, 639–651 (1982).

64. Hu, F. *et al.* Developmental Lead Exposure Alters Synaptogenesis through Inhibiting Canonical Wnt Pathway In Vivo and In Vitro. *PLOS ONE* **9**, e101894 (2014).

65. Khwanraj, K., Phruksaniyom, C., Madlah, S. & Dharmasaroja, P. Differential Expression of Tyrosine Hydroxylase Protein and Apoptosis-Related Genes in

Differentiated and Undifferentiated SH-SY5Y Neuroblastoma Cells Treated with MPP^+. *Neurology Research International* **2015**, e734703 (2015).

66. Zhou, X., Bouitbir, J., Liechti, M. E., Krähenbühl, S. & Mancuso, R. V. Para-Halogenation of Amphetamine and Methcathinone Increases the Mitochondrial Toxicity in Undifferentiated and Differentiated SH-SY5Y Cells. *International Journal of Molecular Sciences* **21**, 2841 (2020).

67. Wenker, S. D. *et al.* Differential antiapoptotic effect of erythropoietin on undifferentiated and retinoic acid-differentiated SH-SY5Y cells. *Journal of Cellular Biochemistry* **110**, 151–161 (2010).

68. Purves, D. *et al.* Generation of Neurons in the Adult Brain. in *Neuroscience. 2nd edition* (Sinauer Associates, 2001).

69. Budtz-Jørgensen, E., Bellinger, D., Lanphear, B., Grandjean, P. & Investigators, on behalf of the I. P. L. S. An International Pooled Analysis for Obtaining a Benchmark Dose for Environmental Lead Exposure in Children. *Risk Analysis* **33**, 450–461 (2013).

70. Dignam, T., Kaufmann, R. B., LeStourgeon, L. & Brown, M. J. Control of Lead Sources in the United States, 1970-2017: Public Health Progress and Current Challenges to Eliminating Lead Exposure. *J Public Health Manag Pract* **25**, S13–S22 (2019).

71. McFarland, M. J., Hauer, M. E. & Reuben, A. Half of US population exposed to adverse lead levels in early childhood. *Proceedings of the National Academy of Sciences* **119**, e2118631119 (2022).

72. Penazzi, L., Bakota, L. & Brandt, R. Microtubule Dynamics in Neuronal Development, Plasticity, and Neurodegeneration. *Int Rev Cell Mol Biol* **321**, 89–169 (2016).

73. Michán, S. *et al.* SIRT1 Is Essential for Normal Cognitive Function and Synaptic Plasticity. *J. Neurosci.* **30**, 9695–9707 (2010).

74. Yoshida, G. J. & Saya, H. Molecular pathology underlying the robustness of cancer stem cells. *Regenerative Therapy* **17**, 38–50 (2021).

75. Encinas, M. *et al.* Sequential treatment of SH-SY5Y cells with retinoic acid and brain-derived neurotrophic factor gives rise to fully differentiated, neurotrophic factor-dependent, human neuron-like cells. *J Neurochem* **75**, 991–1003 (2000).

76. Ross, R. A., Spengler, B. A. & Biedler, J. L. Coordinate morphological and biochemical interconversion of human neuroblastoma cells. *J Natl Cancer Inst* **71**, 741–747 (1983).

Figures and Tables

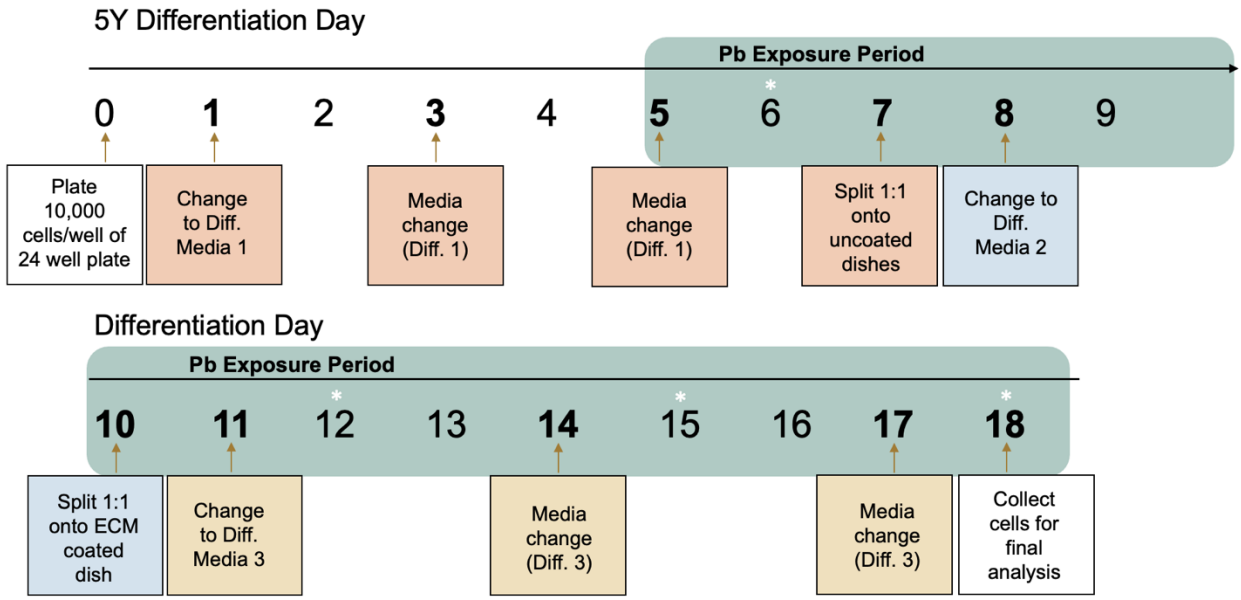

Figure 3.1: Overview of Experimental Workflow. SH-SY5Y cells were differentiated in the presence of retinoic acid (RA) for 18 days, with lead exposure beginning on Day 5. Cells were fixed and stained every three days, with the exception of Day 9, to assess changes in cellular and morphological measures of differentiation.

	0uM Pb			0.16uM Pb			1.26uM Pb			10uM Pb		
	Avg Cells per Image	StDev	p-value	Avg Cells per Image	StDev	p-value	Avg Cells per Image	StDev	p-value	Avg Cells per Image	StDev	p-value
Day 6	118.51	39.81	-	132.99	33.54	-	140.82	24.46	-	125.53	28.83	-
Day 12	17.32	6.46	0.001	23.91	4.82	0.0004	27.05	6.87	0.00004	87.57	75.05	0.29
Day 15	49.03	7.61	0.006	44.30	15.64	0.0005	40.86	10.92	0.00006	56.96	42.84	0.10
Day 18	41.11	20.72	0.002	31.91	9.10	0.0006	33.16	8.89	0.00004	85.69	117.12	0.61

*Table 3.1: Changes in Cell Number During SH-SY5Y Differentiation***.** Cell number was summed across each image and the average number of cells per well was calculated per well. A t-test was used to test for significant difference in cell number at each time point relative to Day 6 within each exposure condition. Significant changes in cell number per image are highlighted in red ($p < 0.05$).

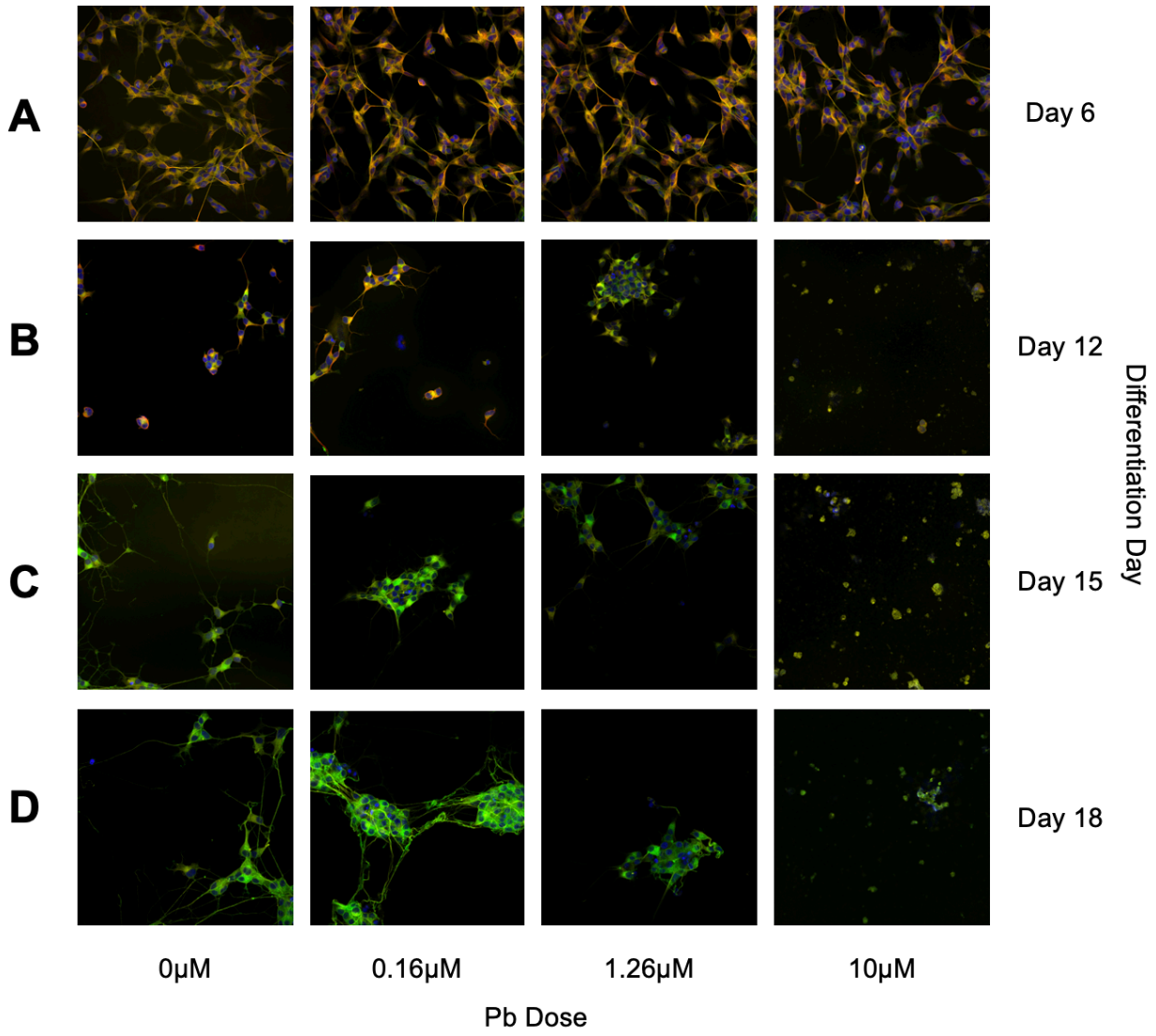

Figure 3.2: Immunofluorescent Images of SH-SY5Y Cells During Differentiation and by Lead Dose. Cells were fixed and stained with antibodies for B-tubulin III (yellow), GAP43 (green), and MAP2 (magenta), as well as Hoechst (blue) on A) Day 6, B) Day 12, C) Day 15, and D) Day 18.

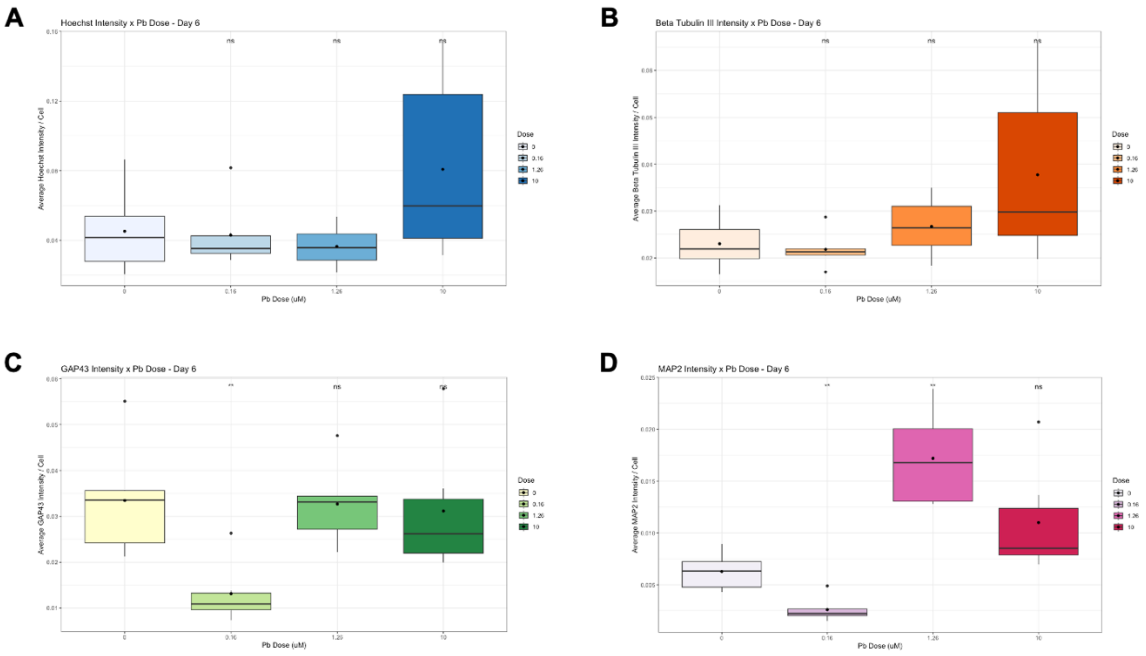

Figure 3.3: Quantification of Immunofluorescence on Day 6 of Differentiation. IF staining was performed to measure changes in A) Hoechst, B) β-tubulin III, C) GAP43, and D) MAP2. Statistically significant changes in expression, relative to control cells, was calculated via t-test, where * $p < 0.05$ and ** $p < 0.01$.

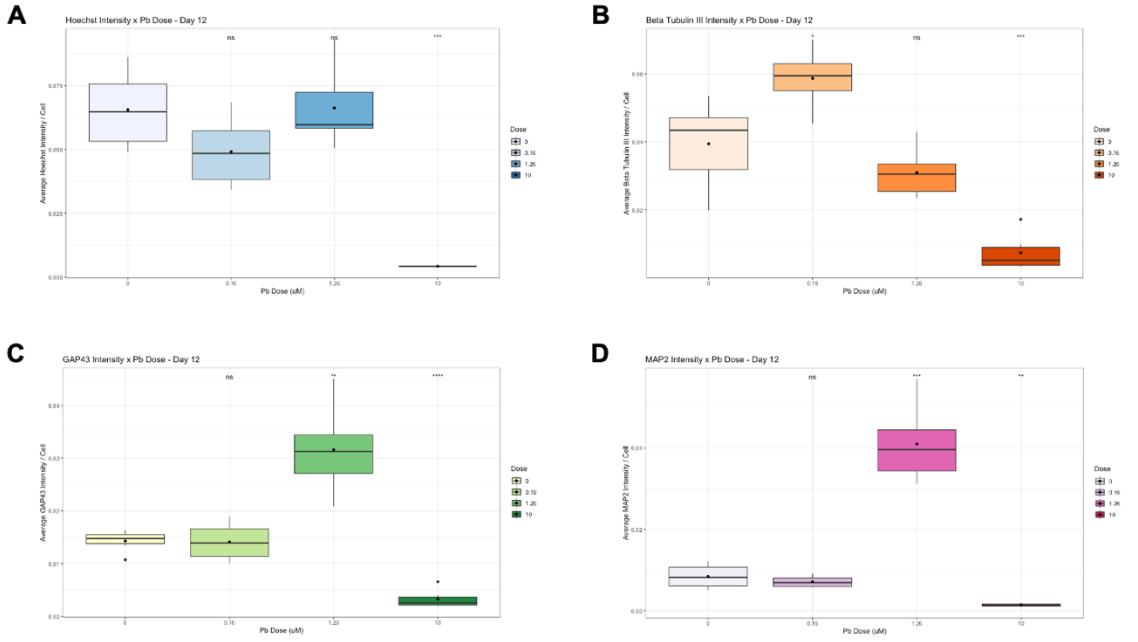

Figure 3.4: Quantification of Immunofluorescence on Day 12 of Differentiation. IF staining was performed to measure changes in A) Hoechst, B) β-tubulin III, C) GAP43, and D) MAP2. Statistically significant changes in expression, relative to control cells, was calculated via t-test, where * $p < 0.05$, ** $p < 0.01$, *** $p < 0.005$, and **** $p < 0.001$.

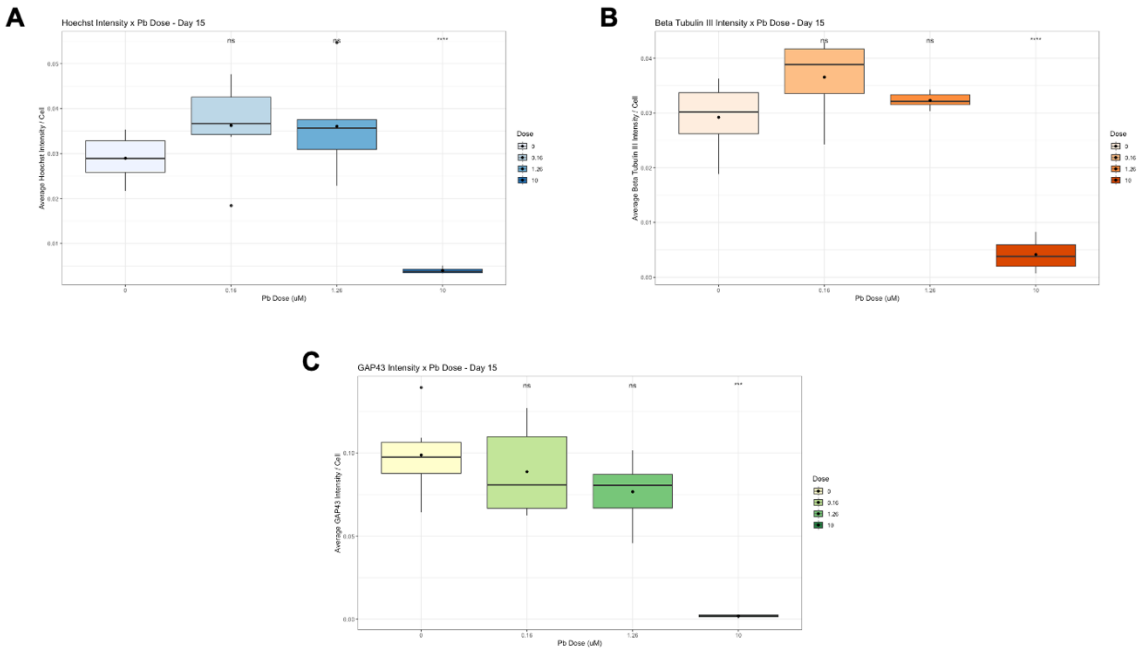

Figure 3.5:Quantification of Immunofluorescence on Day 15 of Differentiation. IF staining was performed to measure changes in A) Hoechst, B) β-tubulin III, and C) GAP43. Statistically significant changes in expression, relative to control cells, was calculated via t-test, where *** $p < 0.005$ and **** $p < 0.001$.

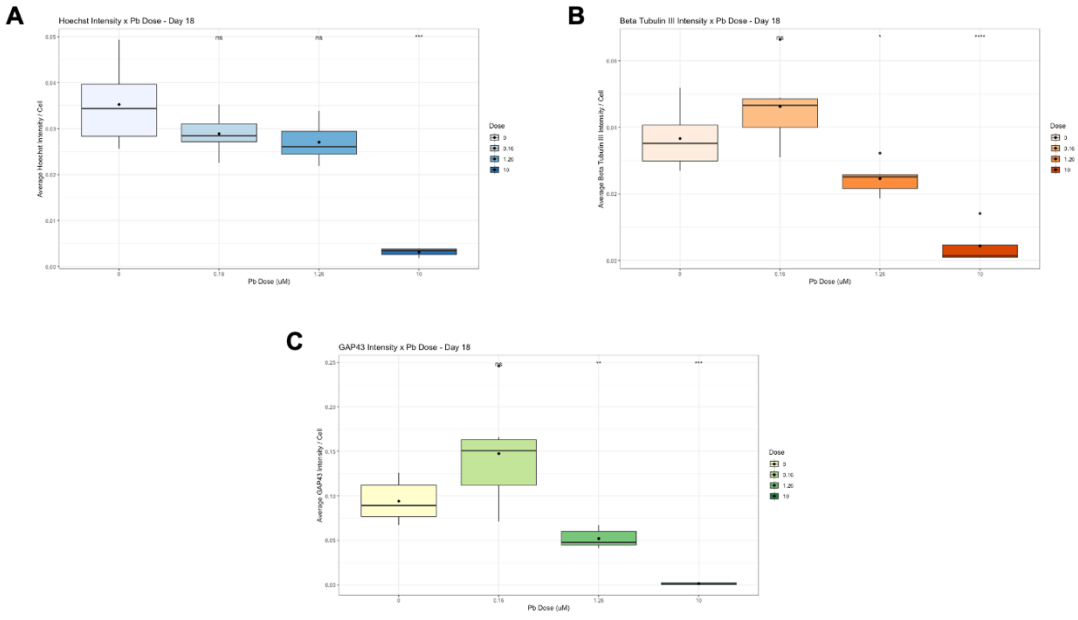

Figure 3.6: Quantification of Immunofluorescence on Day 18 of Differentiation. IF staining was performed to measure changes in A) Hoechst, B) β-tubulin III, and C) GAP43. Statistically significant changes in expression, relative to control cells, was calculated via t-test, where * $p < 0.05$, ** $p < 0.01$, *** $p < 0.005$, and **** $p < 0.001$.

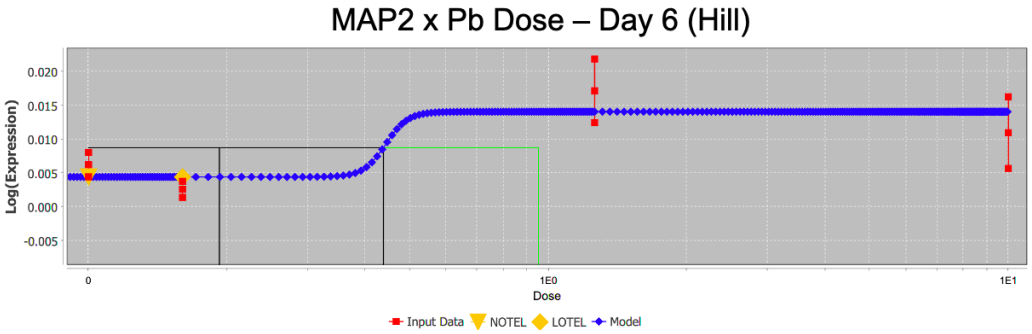

Figure 3.7: Dose-Response Relationship Between Lead Exposure and MAP2 Immunofluorescence on Day 6. Benchmark Dose Analysis was conducted using BMDExpress3 to characterize dose-response relationships.

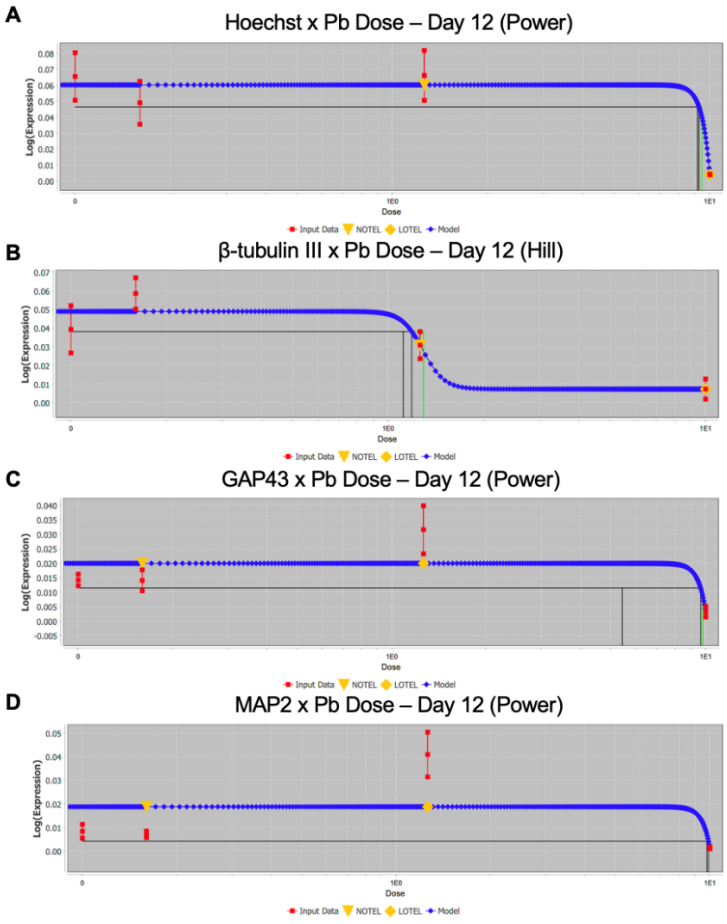

Figure 3.8: Dose-Response Relationship Between Lead Exposure and Immunofluorescence on Day 12. Benchmark Dose Analysis was conducted using BMDExpress3 to characterize dose-response relationships between Pb exposure and A) Hoechst, B) β-tubulin III, C) GAP43, and D) MAP2.

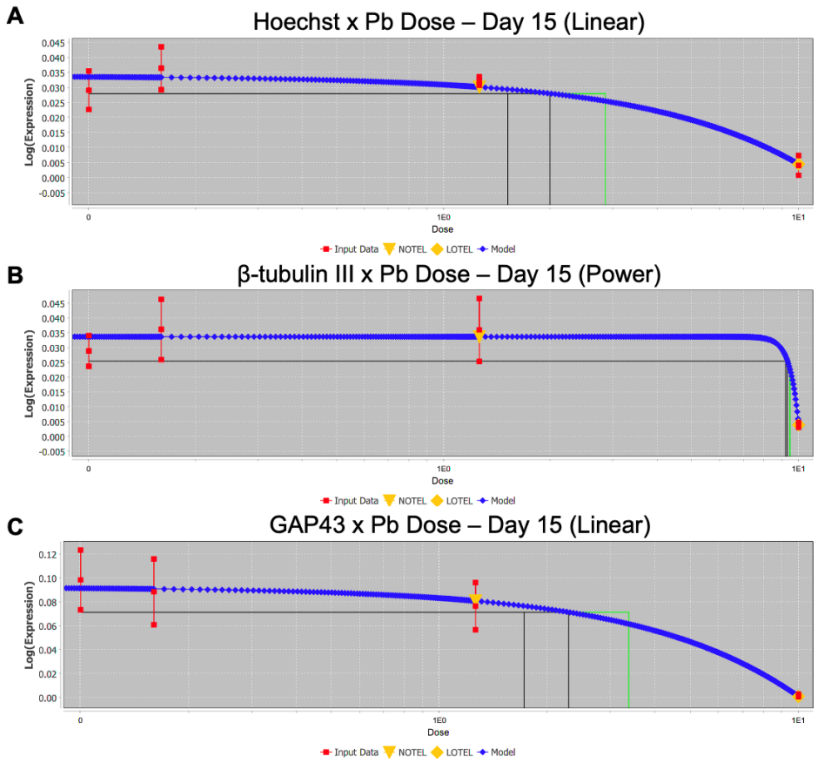

Figure 3.9: Dose-Response Relationship Between Lead Exposure and Immunofluorescence on Day 15. Benchmark Dose Analysis was conducted using BMDExpress3 to characterize dose-response relationships between Pb exposure and A) Hoechst, B) β-tubulin III, and C) GAP43.

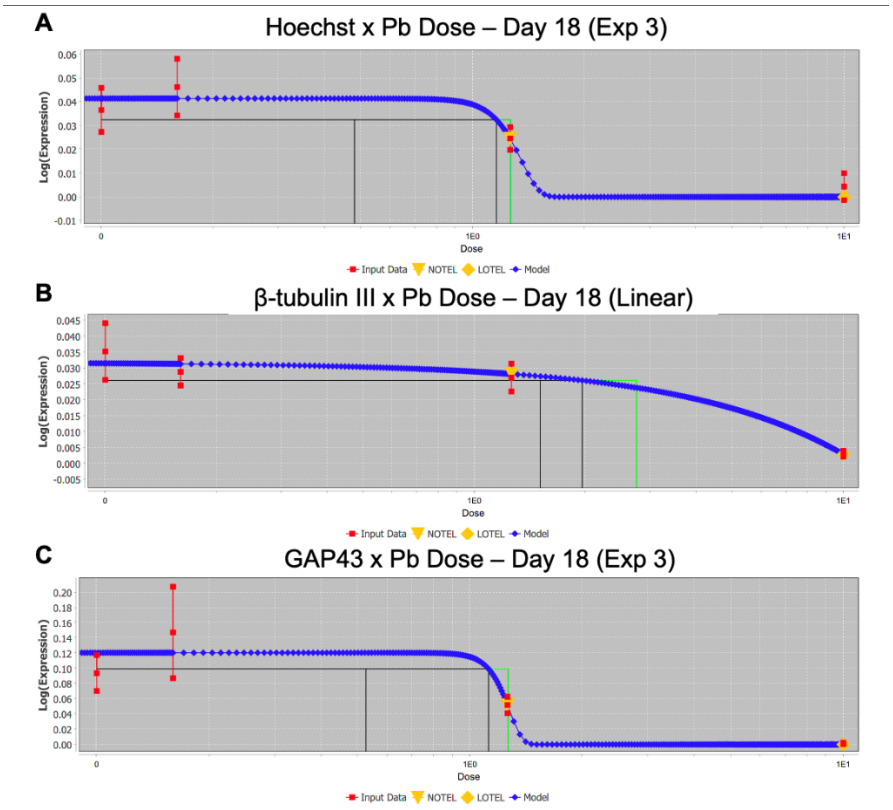

Figure 3.10: Dose-Response Relationship Between Lead Exposure and Immunofluorescence on Day 18. Benchmark Dose Analysis was conducted using BMDExpress3 to characterize dose-response relationships between Pb exposure and A) Hoechst, B) β-tubulin III, and C) GAP43.

Measure	Best Model	Best BMD (µM)	Best BMDL (µM)	Best BMDU (µM)	Best BMD (ug/dL)	Best BMDL (ug/dL)	Best BMDU (ug/dL)	Prefilter Adjusted P-Value	FC Dose Level 1	FC Dose Level 2	FC Dose Level 3
Day 6											
MAP2	Hill	0.437	0.192	0.951	9.064	3.988	19.710	9.801E-05	-2.411	2.740	1.754
Day 12											
β-tubulin III	Hill	1.186	1.114	1.292	24.567	23.090	26.774	5.729E-08	1.487	-1.274	-5.302
Hoechst (DNA)	Power	9.249	9.136	9.434	191.636	189.293	195.469	9.816E-08	-1.336	1.010	-15.620
GAP43	Power	9.628	5.419	9.780	199.499	112.291	202.634	3.711E-08	-1.011	2.211	-4.357
MAP2	Power	9.902	9.780	10.551	205.165	202.643	218.621	1.106E-10	-1.182	4.843	-5.850
Cell Area	Linear	1.000	0.795	1.318	20.715	16.464	27.301	6.070E-13	-1.124	-1.227	-25.544
Cytoplasm Area	Exp 3	0.383	0.265	0.745	7.931	5.484	15.440	5.047E-11	-1.188	-1.557	-34.389
Nuclei Area	Poly 2	2.063	0.928	3.140	42.739	19.232	65.057	6.106E-15	-1.079	-1.065	-14.919
Endpoints per Cell	Linear	2.188	1.684	3.072	45.344	34.887	63.642	7.059E-08	-1.333	-1.200	-Infinity
Branches per Cell	Linear	1.740	1.358	2.374	36.050	28.141	49.186	8.689E-09	-1.156	-1.156	-9.250
Total Branch Length per Cell	Linear	1.766	1.378	2.414	36.599	28.548	50.012	2.820E-09	-1.289	-1.259	-386.651
Day 15											
β-tubulin III	Linear	1.993	1.515	2.857	41.299	31.394	59.197	4.661004E-07	1.251	1.106	-7.060
Hoechst (DNA)	Power	9.308	9.189	9.453	192.859	190.387	195.859	3.882891E-05	1.251	1.245	-7.254
GAP43	Linear	2.290	1.719	3.368	47.446	35.621	69.787	1.871477E-05	-1.113	-1.288	-54.031
Cell Area	Power	9.103	8.988	9.245	188.622	186.229	191.549	5.725089E-07	1.038	1.123	-4.967
Cytoplasm Area	Power	9.168	9.051	9.310	189.956	187.546	192.903	4.627193E-06	1.006	1.074	-12.666
Nuclei Area	Power	9.199	9.083	9.342	190.607	188.192	193.561	4.126800E-06	1.054	1.162	-3.181
Endpoints per Cell	Power	7.650	2.551	9.326	158.515	52.865	193.234	4.769732E-07	1.214	1.214	-9.333
Branches per Cell	Power	5.453	1.462	9.007	112.986	30.292	186.616	1.725613E-09	1.000	1.000	-15.333
Total Branch Length per Cell	Power	7.414	1.948	9.269	153.610	40.354	192.059	4.661004E-07	1.185	1.126	-153.522
Day 18											
β-tubulin III	Exp 3	1.158	0.480	1.265	23.998	9.949	26.203	3.573759E-06	1.263	-1.489	-8.401
Hoechst (DNA)	Linear	1.960	1.507	2.750	40.617	31.230	56.987	8.787029E-07	-1.221	-1.304	-11.217
GAP43	Exp 3	1.121	0.526	1.266	23.226	10.906	26.224	1.313131E-05	1.569	-1.808	-65.234
Nuclei Area	Linear	2.581	1.938	3.802	53.479	40.152	78.774	2.501122E-05	-1.076	-1.220	-3.254
Endpoints per Cell	Exp 5	0.387	0.026	2.437	8.027	0.546	50.488	1.564943E-03	-1.167	-1.556	-2.917
Branches per Cell	Linear	2.020	1.550	2.845	41.854	32.119	58.958	1.917137E-06	-1.053	-1.250	-4.762
Total Branch Length per Cell	Exp 3	0.637	0.354	1.546	13.206	7.333	32.036	1.313131E-05	-1.258	-1.742	-34.762

Table 3.2: Summary of Benchmark Dose Analysis in Lead Exposed Differentiating SH-SY5Ys. Raw data was prefiltered using a One-Way ANOVA, and then assessed for best model fit using BMDExpress3. Benchmark Dose (BMD) reported in both µM and µg/dL and includes BMDL (BMD lower limit) and BMDU (BMD upper limit). Fold change in response reported at Dose 1 (0.16µM), Dose 2 (µM), and Dose 3 (µM).

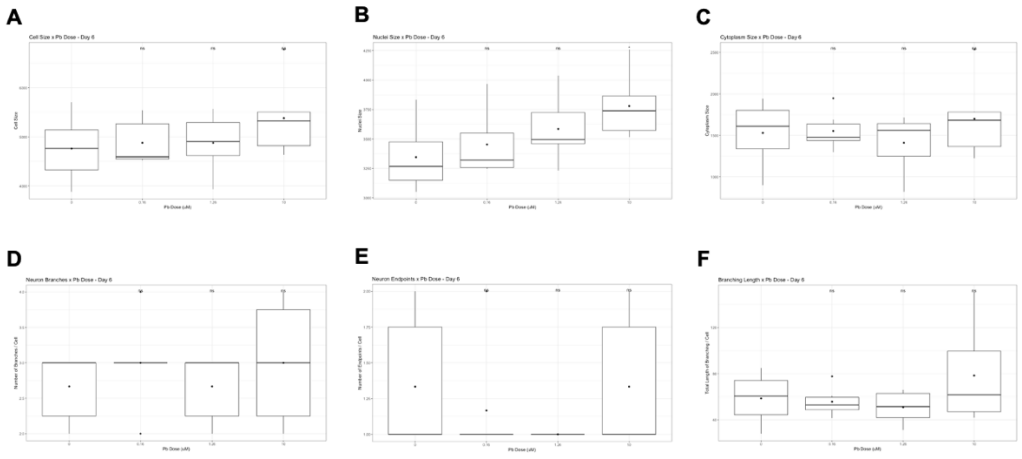

*Figure 3.11: Morphological Measures of SH-SY5Ys with Lead Exposure on Day 6. U*sing CellProfiler, Hoechst and GAP43 signal was used to identify primary objects (nuclei) and B-tubulin III was used to identify secondary objects (neuronal projections). These measures were converted into a skeleton which was then used to quantify additional morphological measures. Morphological measures include A) Cell Size, B) Nuclei Size, C) Cytoplasm Size, D) Neuron Branches per Cell, E) Neuron Endpoints per Cell, and F) Total Length of Branching. Statistically significant changes in expression, relative to control cells, was calculated via t-test, where * $p < 0.05$.

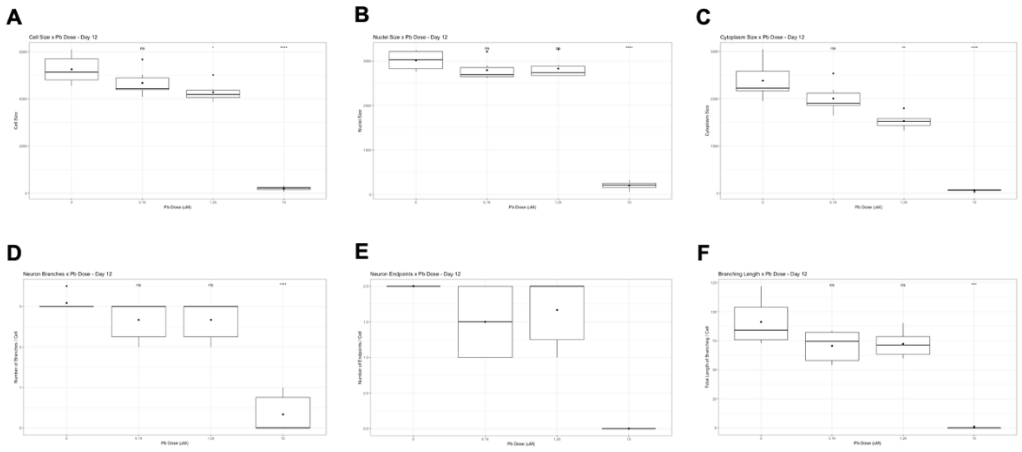

Figure 3. 12: Morphological Measures of SH-SY5Ys with Lead Exposure on Day 12. Using CellProfiler, Hoechst and GAP43 signal was used to identify primary objects (nuclei) and B-tubulin III was used to identify secondary objects (neuronal projections). These measures were converted into a skeleton which was then used to quantify additional morphological measures. Morphological measures include A) Cell Size, B) Nuclei Size, C) Cytoplasm Size, D) Neuron Branches per Cell, E) Neuron Endpoints per Cell, and F) Total Length of Branching. Statistically significant changes in expression, relative to control cells, was calculated via t-test, where * $p < 0.05$, ** $p < 0.01$, *** $p < 0.005$, **** $p < 0.001$.

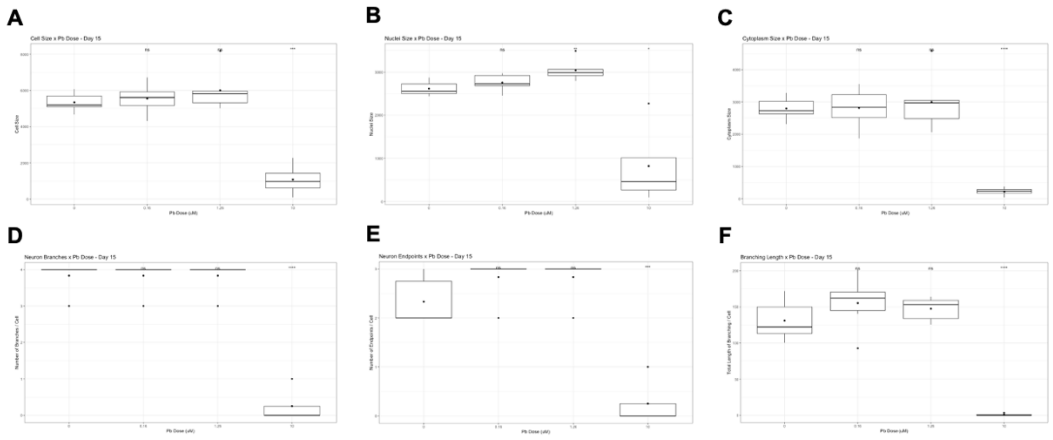

Figure 3.13: Morphological Measures of SH-SY5Ys with Lead Exposure on Day 15. Using CellProfiler, Hoechst and GAP43 signal was used to identify primary objects (nuclei) and B-tubulin III was used to identify secondary objects (neuronal projections). These measures were converted into a skeleton which was then used to quantify additional morphological measures. Morphological measures include A) Cell Size, B) Nuclei Size, C) Cytoplasm Size, D) Neuron Branches per Cell, E) Neuron Endpoints per Cell, and F) Total Length of Branching. Statistically significant changes in expression, relative to control cells, was calculated via t-test, where * $p < 0.05$, ** $p < 0.01$, *** $p < 0.005$, **** $p < 0.001$.

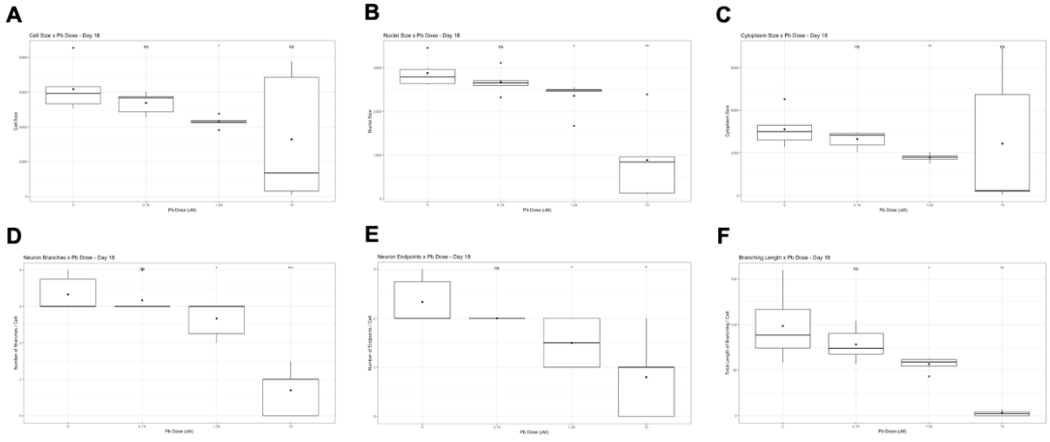

Figure 3.14: Morphological Measures of SH-SY5Ys with Lead Exposure on Day 18. Using CellProfiler, Hoechst and GAP43 signal was used to identify primary objects (nuclei) and B-tubulin III was used to identify secondary objects (neuronal projections). These measures were converted into a skeleton which was then used to quantify additional morphological measures. Morphological measures include A) Cell Size, B) Nuclei Size, C) Cytoplasm Size, D) Neuron Branches per Cell, E) Neuron Endpoints per Cell, and F) Total Length of Branching. Statistically significant changes in expression, relative to control cells, was calculated via t-test, where * $p < 0.05$, ** $p < 0.01$, *** $p < 0.005$, **** $p < 0.001$.

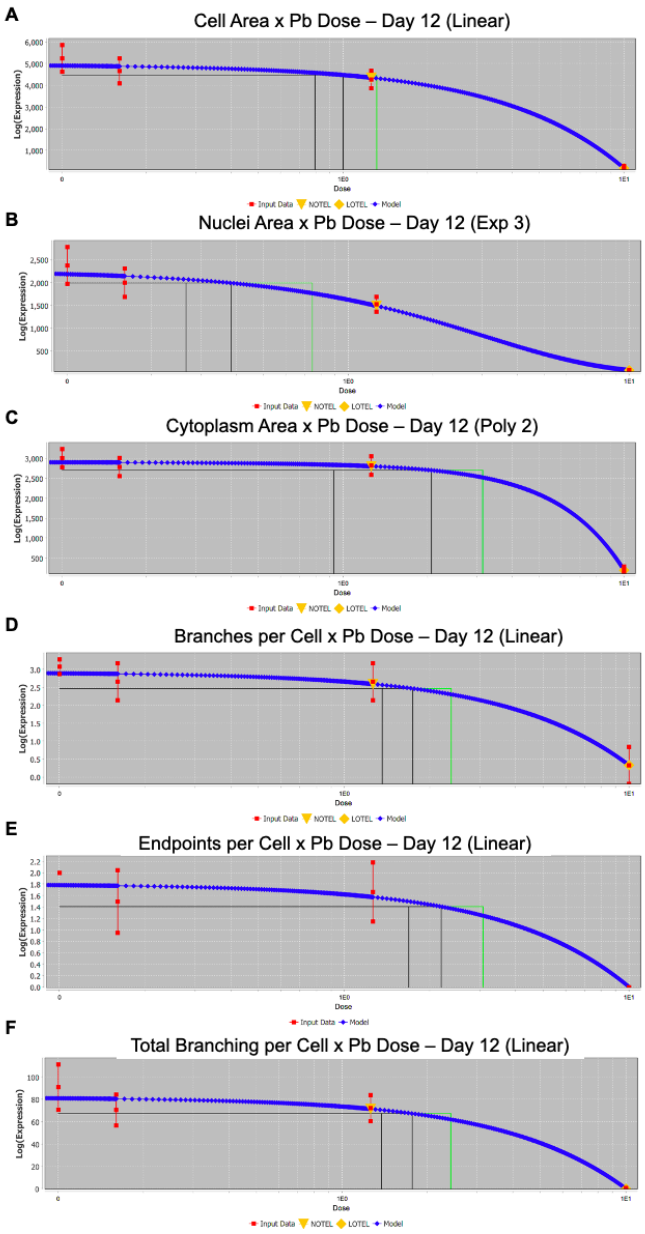

Figure 3.15: Dose-Response Relationship Between Lead Exposure and Morphological Measures on Day 12. Benchmark Dose Analysis was conducted using BMDExpress3 to characterize dose-response relationships between Pb exposure and A) Cell Size, B) Nuclei Size, C) Cytoplasm Size, D) Branches per Cell, E) Endpoints per Cell, and F) Total Branching per Cell.

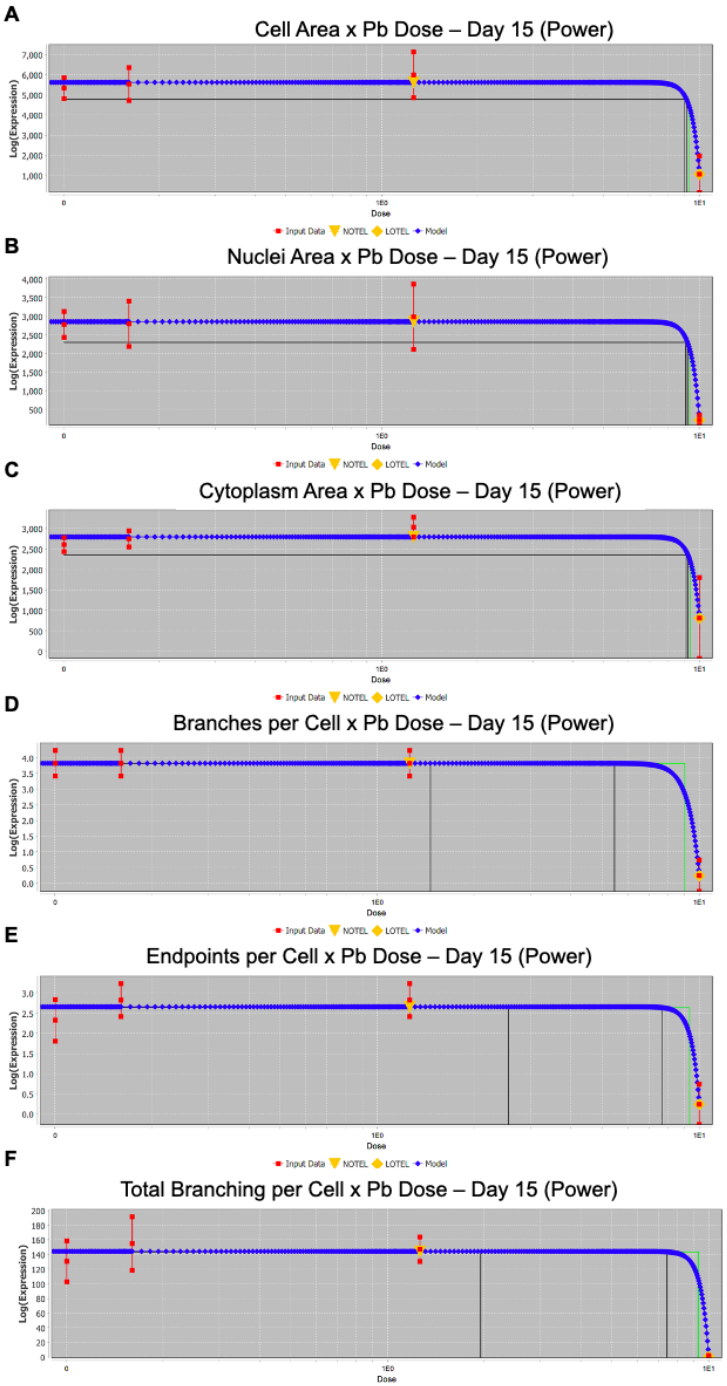

Figure 3.16: Dose-Response Relationship Between Lead Exposure and Morphological Measures on Day 15. Benchmark Dose Analysis was conducted using BMDExpress3 to characterize dose-response relationships between Pb exposure and A) Cell Size, B) Nuclei Size, C) Cytoplasm Size, D) Branches per Cell, E) Endpoints per Cell, and F) Total Branching per Cell.

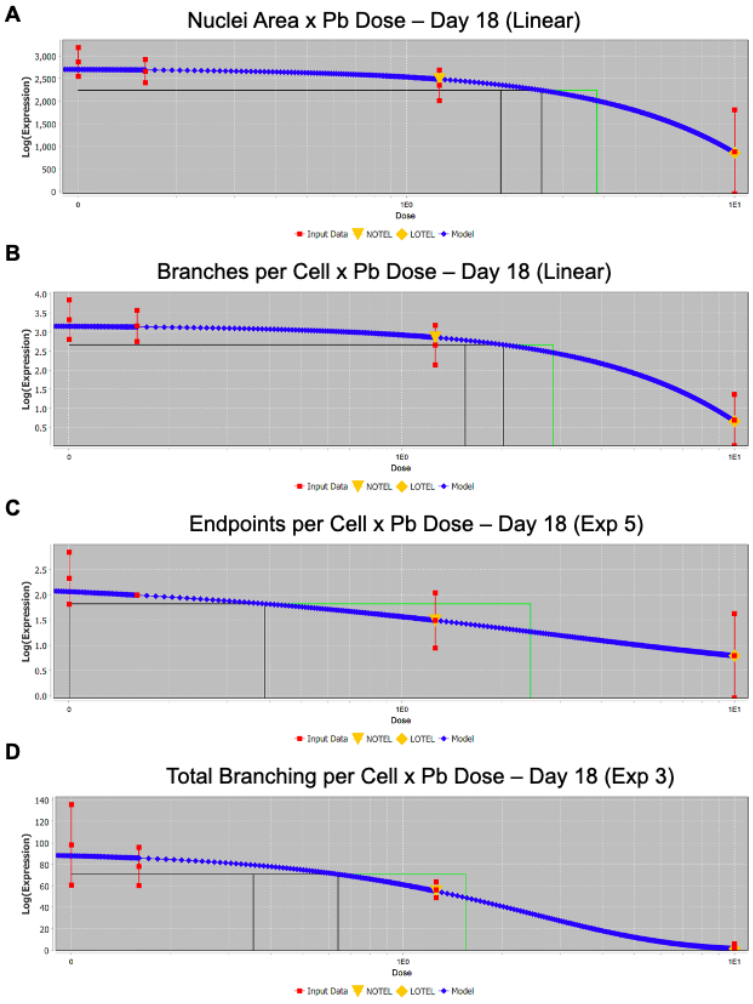

Figure 3.17: Dose-Response Relationship Between Lead Exposure and Morphological Measures on Day 18. Benchmark Dose Analysis was conducted using BMDExpress3 to characterize dose-response relationships between Pb exposure and A) Nuclei Size, B) Branches per Cell, C) Endpoints per Cell, and D) Total Branching per Cell.

Appendix

Basic Growth Media		
Component	**Volume for 500mL**	**Dilution**
EMEM	415mL	
15% hiFBS	75mL	
1x Pen/Strep	5mL	1:100
2mM Glutamine	5mL	1:100

Differentiation Media #1		
Component	**Volume for 50mL**	**Dilution**
EMEM	48mL	
2.5% hiFBS	1.3mL	
1x Pen/Strep	500µL	1:100
2mM Glutamine	500µL	1:100
10µM RA	100µL	1:500

Differentiation Media #2		
Component	**Volume for 50mL**	**Dilution**
EMEM	49mL	
1% hiFBS	500µL	
1x Pen/Strep	500µL	1:100
2mM Glutamine	500µL	1:100
10µM RA	100µL	1:500

Differentiation Media #3		
Component	**Volume for 50mL**	**Dilution**
Neurobasal	47mL	
1x B-27	1mL	1:50
20mM KCl	1mL	1:50
1x Pen/Strep	500µL	1:100
2mM Glutamaxl	500µL	1:100
50ng/mL BDNF	250µL	1:200
2mM db-cAMP	100µL	1:500
10µM RA	100µL	1:500

Table 3.A1: Differentiation Media, as adapted from Shipley et al., 2016.

Antibody/Stain	Host	Fluorophore	Dilution	Catalog Number	Staining Step
Hoechst 33342	-	-	1:2000	Thermo, H3570	Primary
β-tubulin conjugate	Mouse	eFluor660	1:150	Thermo, 50-4510-82	Primary
GAP43	Rabbit	-	1:200	Abcam, ab75810	Primary
MAP2	Chicken	-	1:500	Thermo, PA1-10005	Primary
Anti-Rabbit IgG	Goat	Alexa Fluor 488	1:333	Abcam, 150077	Secondary
Anti-Chicken IgY	Goat	Alexa Fluor 568	1:1000	Thermo, A11041	Secondary

Table 3.A2: Antibody Dilution Metrics.

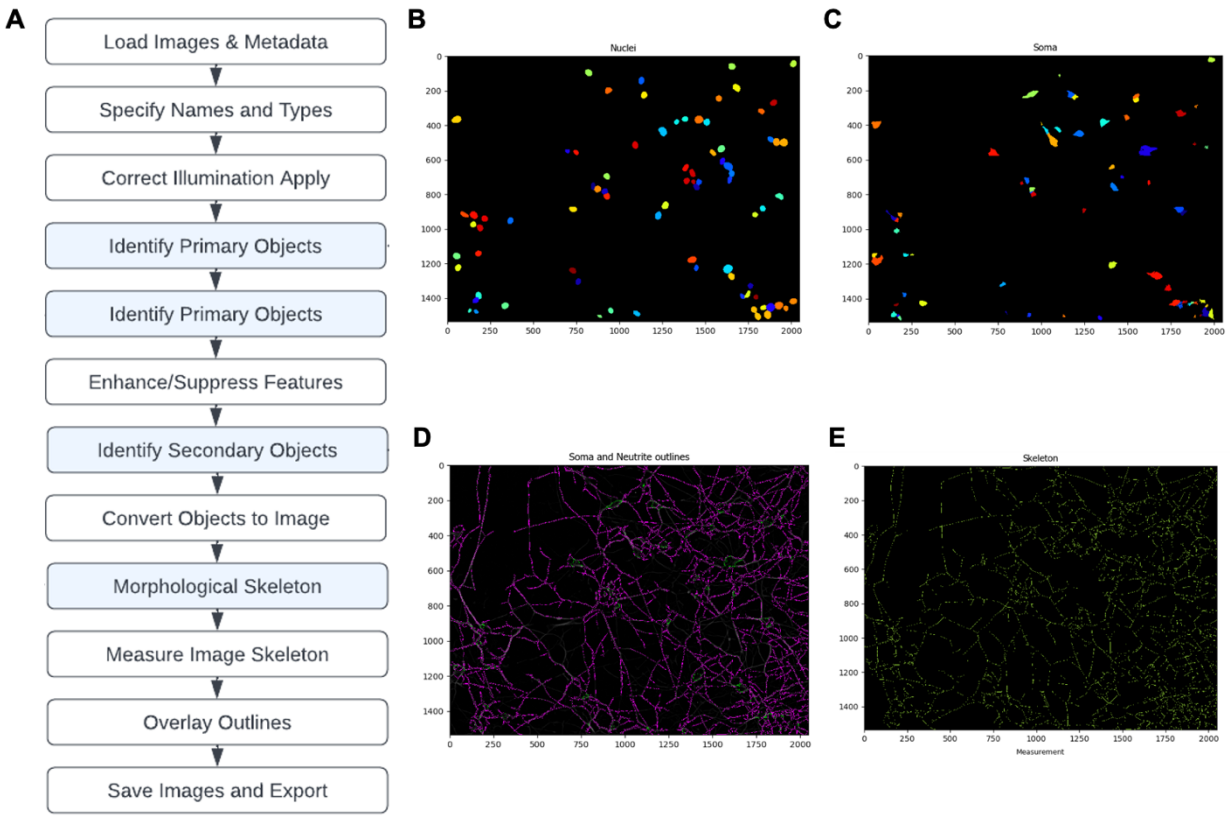

Figure 3.A1: Overview of Cell Profiler and Cell Profiler Analyst Workflow.

Chapter 4

Aim 3: Assessment of LINE-1 Epigenetic Regulation and Expression Associated with Lead (Pb) Exposure in Differentiating SH-SY5Y-Derived Neurons

Abstract

Long interspersed nuclear elements 1 (LINE-1) are a class of retrotransposable elements that require consistent regulation in order to reduce the effects they may otherwise have on the genome through insertional mutations. The repression of expression of these repetitive elements is orchestrated, in part, by piRNA-directed DNA methylation (DNAm). While this relationship has been extensively studied in the germline, there is relatively less research examining it in somatic tissues such as the brain. LINE-1 activity has been shown to be beneficial during early embryonic development and neurogenesis, when these elements contribute to cellular diversity and plasticity. Unregulated activity that persists past these stages however is associated with increased rates of DNA damage, mitochondrial dysfunction, and increases the risk for insertional mutations. Greater LINE-1 activity has been documented in several neurodegenerative diseases (NDs), such as Alzheimer's and Parkinson's, as well as with aging overall, as an aging epigenome is thought to have reduced capability to ensure maintained regulation of these elements. Developmental exposures to various toxicants alter LINE-1 regulation and expression, and it is theorized that such exposures may contribute to ND risk later in life due to early perturbations of this system. Here we explore changes in LINE-1 epigenetic regulation

and expression in response to lead (Pb) exposure during neurogenesis in differentiating SH-SY5Y cells. We examine Pb-associated changes in LINE-1 DNAm and mRNA expression, as well as of *PIWIL* gene expression, a main component of the piRNA system. We found that 0.16μM, 1.26μM, and 10μM Pb exposure during early differentiation (Days 9) were largely associated with decreased expression of *PIWIL1* mRNA with no changes detected in DNAm. During early differentiation we observed minimal changes in LINE-1 mRNA expression. As differentiation progressed into the later stages (days 12 and 15), 0.16μM and 1.26μM Pb exposure were associated with elevated LINE-1 DNAm, whereas 10μM Pb exposure was associated with decreased *5'UTR* and *ORF2* expression on D12 but increased expression of these mRNA on D15. Pb-associated elevation of *ORF2* expression was maintained through Day 18, whereas LINE-1 DNAm decreased somewhat with exposure. These results suggest that Pb exposure may disrupt LINE-1 expression during early neurogenesis, when its expression is thought to contribute to a stem-like state, whereas during later time points, exposure is associated with elevation of LINE-1 expression and inadequate epigenetic regulation. However, these results are not conclusive and additional work is needed to elucidate how LINE-1 epigenetic regulation and expression more clearly are affected by Pb exposure during a developmental process such as neural differentiation.

Introduction

A biomarker of neurodegenerative disease (ND) risk that has been gaining increased attention over the last decade is that of LINE-1 expression and regulation.[1,2] LINE-1 elements are a type of class I retrotransposable element and are capable of self-propagation within the genome.[3] Making up roughly 17% of the human genome,[4]

LINE-1 elements contain the capacity to, upon their transcription to an RNA intermediate, employ proteins (i.e., open reading frame proteins 1 and 2, ORF1p and ORF2p) encoded in their sequence, to reverse transcribe themselves back into the genome at a new location.[5,6] Additional LINE sequences exist in our genomes (LINE-2, LINE-3) however LINE-1 is the only remaining autonomous element.[4,7] Their mobile capacity has led to the classification of LINE-1 as a mutagen and dozens of disease-causing mutations have been linked to the reinsertion of these elements[8]. Many of these mutations have occurred in protein-coding regions,[9,10] directly disrupting the transcription of molecular factors that support normal cell health, while others have been documented in non-coding regions that have resulted in alterations in transcription initiation, disruption of gene splicing, as well as recombination of chromosomes.[11–13]

LINE-1 elements are regulated in part by the piRNA system.[14] PIWI-interacting RNA (piRNA) is a class of small, non-coding RNA (ncRNA) that work in concert with p-element induced wimpy testes (PIWI) proteins to maintain proper epigenetic control of LINE-1 elements.[15,16] Extensive work from the germline has demonstrated that piRNA activity lies upstream of and is required for the establishment of DNA methylation (DNAm) at LINE-1 elements, which in turn decreases the likelihood of their transcription and mobile activity.[17,18] This relationship of piRNA-directed DNAm of LINE-1 has not been as extensively explored in the soma, including the brain, wherein the regulation of LINE-1 has been shown to be important with regard to proper neurogenesis and neurodevelopment.[19,20]

LINE-1 activity has been shown to be greater during early embryonic development relative to later time points, particularly in proliferating neural progenitor

cells (NPCs).[21–23] The majority of LINE-1 activity seen in the developing embryo is eventually repressed as somatic differentiation progresses, with a notable exception being the brain, where LINE-1 activity continues in cell populations such as adult NSCs.[24,25] Several reports have documented associations between increased LINE-1 activity in developing neurons and greater cell diversity and plasticity.[26,27] LINE-1 activity has also been shown to be important in the shift forward from a 2-cell embryo, wherein the LINE-1 RNA itself acts as scaffolding for regulatory networks that represses activators of processes specific to this stage.[28,29] However, too much of a good thing, or activation that persists past the appropriate stages of development, can have deleterious effects on differentiating cells, with disease-causing mutations being notable effects.[30,31]

Many cellular processes that become more likely with age also contribute to reduced efficacy of LINE-1 regulation. Epigenetic age is a concept rooted in the theory that as we age, our epigenome shifts overtime, largely in response to our environment and lifestyle.[32,33] An aging epigenome is typically characterized by changes in DNAm, alterations in histone modifications, and a decrease in heterochromatin.[34] Many of these hallmarks of an aging epigenome promote greater LINE-1 activity, through hypomethylation and the formation of euchromatin which would otherwise sequester these elements and prevent their activation.[34–36] Oxidative stress and DNA damage are additional cellular conditions that increase with age and are also associated with greater LINE-1 activity, as they correspond with alterations in chromosome structure and provide more opportunities for LINE-1 insertions.[1,37–39]

Many disease states that are more likely to occur during later stages of life, including NDs such as Alzheimer's (AD) and Parkinson's disease (PD), are also correlated with greater rates of LINE-1 activity.[40,41] Hypomethylation of LINE-1 as well as differential expression of these elements has been documented across various NDs[42,43]. Furthermore, LINE-1 activity has been shown to be detrimental to the prognosis of such diseases. For example, abundant LINE-1 retrotransposition has been shown to be a source of DNA damage and neuroinflammation and this relationship is suspected to contribute to the rate of onset and prognosis of AD.[1,44] What's more, the accumulation of tau protein, a hallmark of AD, is suspected to contribute to LINE-1 activation, thus creating a cyclical loop of LINE-1 activation, tau accumulation, and cellular dysfunction that together accelerate the rate of AD progression.[45]

The epigenetic regulation and expression of LINE-1 elements has been studied in relation to environmental exposures, particularly those that occur during early development. Many of these exposures, such as radiation, cigarette smoke, particulate matter, and pesticides, are all associated with hypomethylation of LINE-1 elements.[46–49] Here we examine the effects of Pb exposure during the process of neural differentiation on LINE-1 epigenetic regulation and expression. We explore LINE-1 DNAm as well as the expression of PIWIL proteins, components of the piRNA system, in an effort to assess not only how LINE-1 epigenetic regulation happens in the developing brain, but also to what degree this pathway is perturbed by a classic neurotoxicant in ways that may contribute to ND risk later in life. As in Chapter 3, Aim 2, we employ the SH-SY5Y cell model to investigate this relationship. It is theorized that developmental exposures that alter LINE-1 regulation and expression create inadequately differentiated neurons

(such as those explored in Chapter 3 of this dissertation), which are then less resilient to additional stressors that contribute to ND risk throughout the life course. This dissertation, across Chapters 3 and 4, hypothesizes that Pb exposure during neural differentiation will result in changes to 5Y morphology (Chapter 3) as well as LINE-1 epigenetic regulation and expression (Chapter 4).

Methods

SH-SY5Y Differentiation and Lead Exposure

5Ys of the same passage (P39) as those used in Aim 2 were used for the purposes of this experiment. Slight modifications in culture conditions were made in order to generate enough nucleic acid for downstream applications, but the same overall differentiation protocol was used.[50] On Day 0 (D0), 1.2 million 5Ys were seeded per 10cm plate, with each plate representing one sample replicate. Beginning on D5, differentiating 5Ys were exposed to a range of Pb conditions (0μM, 0.16μM, 1.26μM, or 10μM Pb). Subsequent steps in differentiation mirror those outlined in Chapter 3 (**Figure 4.1** and **Table 3.A1**), with one additional time point included in this study (D9) due to our ability to effectively collect and lyse cells for genomic extractions on this day.

Nucleic Acid Extractions

On D6, D9, D12, D15, and D18, cells were collected for genomic extractions via the following procedure. Media was gently removed, and cells were detached from 10cm dishes using Tryp-LE Express Enzyme (Thermo, Cat. #12604013) with a 2–3-minute incubation at room temperature, or until cells were visibly detached under the microscope. Tryp-LE was quenched with a 5:1 volume of differentiation media and

suspended cells were spun down at 200g for 5 minutes. Media and Tryp-LE was aspirated, and pelleted cells were lysed in 600µL of 1% β-mercaptoethanol (Thermo, Cat. #21985023) diluted in Buffer RLT solution (Qiagen, Cat. #79216), according to manufacturer's recommendations. Lysed cells were then stored at -80ºC until genomic extractions could be completed. A total of n = 3 technical replicates were included per exposure and time point, with a final total sample size of N = 60. Lysed samples were homogenized using QIAShredder columns (Qiagen, Cat. #79656) prior to DNA and RNA extraction using the AllPrep DNA/RNA/Protein Mini Kit (Qiagen, Cat. #80004) according to manufacturer recommendations. DNA and RNA were stored at -80ºC until further use.

Gene Expression Analysis

1 µg of total RNA was reverse transcribed into cDNA using the iScript cDNA Synthesis Kit (BioRad, Cat. #1708890). mRNA expression of human *PIWILs 1-4*, as well as LINE-1 *5'UTR* and *ORF2*, and a reference gene (*GAPDH*) were quantified using the CFX Real-Time PCR using iTaq Universal SYBR Green Supermix (BioRad, Cat. #1725120) according to manufacturer's protocols with all samples run in triplicate. Primer sequences and amplicon sizes are described in **Table 4.A1** and primer efficiency was confirmed using cDNA serial dilutions. All qRT-PCR reactions were carried out for 40 cycles under standard PCR conditions. ΔCq values were calculated by subtracting the Cq triplicate average of a target sample from that of the reference gene. The fold difference in expression was then calculated using $2^{-\Delta Cq}$.[51]

DNA Methylation Analysis

Genomic DNA (gDNA) was bisulfite converted using the Epitect 96 Bisulfite Kit (Qiagen, Cat. #59110). Bisulfite conversion is important for DNAm analysis as it distinguishes unmethylated cytosines from methylated cytosines. Unmethylated cytosines are deaminated to uracil, which are then amplified as thymine during PCR, while methylated cytosines are resistant to this conversion, and are simply amplified as cytosines.[52] Bisulfite converted samples were then sequenced via pyrosequencing to assess DNAm of LINE-1, where site-specific methylation can be estimated by quantifying the relative proportion of cytosines to thymines at a given locus. A description of pyrosequencing parameters, primer sequences, and amplicon size and location in LINE-1 can be found in **Figure 4.2** and **Table 4.A2**.

Statistical Analysis

Three replicates for each exposure condition (n = 4) at each time point (n = 5) were included in each analysis. Replicates refer to one 10cm dish from which cells were collected on the appropriate day and extractions were performed on the entire cell population from that dish (therefore, no technical replicates were included in extractions) in order to optimize the amount of nucleic acid acquired per replicate. This sample size structure was maintained for subsequent analyses (i.e., 3 experimental replicates per dose and time condition in each assay). While gene expression analysis included technical replicates, the average of these was taken for statistical analysis, returning the sample size to the original format. Data are represented graphically as scatterplots using ggplot2.[53] Comparisons between each experimental group and control was performed using a two-sides t-test in R (v.4.1.2). Statistical significance was accepted

with $p < 0.05$ and is designated in figures as * $p < 0.05$, ** $p < 0.01$, *** $p < 0.005$, and **** $p < 0.001$.

Results

Dynamic Gene Expression and LINE-1 DNA Methylation During SH-SY5Y Differentiation

Significant changes in gene expression were observed during 5Y differentiation in the absence of Pb exposure with D6 serving as the reference measure. *PIWIL1* mRNA expression increased significantly ($p < 0.001$) on D12 relative to D6, 24 hours after the addition of terminal differentiation factors. Its expression decreased relative to D12 on D15 and D18, but on D18, expression was found to be significantly higher ($p < 0.05$) than that of D6 levels. *PIWIL4* expression was relatively stable between D6 and D12, after which it was elevated on D15 and D18, relative to D12 ($p < 0.05$) (**Figure 4.3A-B**). There was no detectable expression of *PIWIL2* or *PIWIL3* in these cells during this experiment and a summary of ΔCq values for all samples and targets is included in **Table 4.A3**.

Expression of multiple LINE-1 components also changed significantly during 5Y differentiation. The relative expression of LINE-1 *5'UTR* mRNA increased on D9 of differentiation, relative to D6 ($p < 0.01$), and then decreased steadily for the remainder of this process (D12-D18) ($p < 0.05$). The 5'UTR region of LINE-1 elements contains a transcription promoter site with affinity for transcription factors such as RNA polymerase II and YY1.[54] The relative expression of LINE-1 *ORF2* mRNA, on the other hand, increased steadily during differentiation, with significant increases measured beginning on D15 ($p < 0.01$) (**Figure 4.3C-D**). The LINE-1 ORF2 region encodes for the open

reading frame 2 protein (ORF2p), which has the capacity for endonuclease and reverse transcription activities.[6] Both the 5'UTR and ORF2 regions have important roles in LINE-1 mobility and interference of both has been associated with decreased LINE-1 activity.[55,56]

The pyrosequencing assay used in these experiments examined methylation at 4 CpG sites in the LINE-1 promoter region of the 5' UTR (Positions 1-4). DNAm of this region of LINE-1 was relatively stable during 5Y differentiation. There were no detectable changes in DNAm at Position 1 or 2 during differentiation (**Figure 4.4A-B**). The methylation of Positions 3 and 4 changed significantly towards the end of differentiation, with significant increases in the methylation of these positions on D18, relative to D15 (**Figure 4.4C-D**). Original data for pyrosequencing is included in **Table 4.A4**.

Lead Exposure Associated with Limited Changes PIWIL Expression

During the first two weeks of 5Y differentiation, Pb exposure largely had a depressive effect on *PIWIL1* expression, with consistent decreases in expression seen on D9, and D12 in the 0.16μM ($p < 0.01$, D9 only), 1.26μM ($p < 0.01$) and 10μM ($p < 0.01$) Pb exposed cells (**Figure 4.5A-C**). Interestingly, there was a reversal in this trend seen on D15, with greater expression in 0.16μM and 10μM ($p < 0.05$) Pb exposed cells relative to control (**Figure 4.5D**). No detectable changes in *PIWIL1* expression were found with Pb exposure on D18 (**Figure 4.5E**). There were substantially fewer significant changes in *PIWIL4* expression with Pb exposure compared to trends observed with *PIWIL1* expression. The only statistically significant change occurred on

D12, when *PIWIL4* expression was elevated in the 10μM Pb exposed cells, relative to control (**Figure 4.5H**).

High Lead Exposure Associated with Changes in LINE-1 mRNA Expression During SH-SY5Y Differentiation

Generally, only 10μM Pb exposure was associated with significant changes LINE-1 *5'UTR* and *ORF2* mRNA expression throughout 5Y differentiation. Changes in *5'UTR* expression were minimal on D6 and D9, and it was not until D12 that 10μM Pb exposure was associated with a reduction in its expression ($p < 0.05$) (**Figure 4.6A-C**). This trend was reversed on D15, when 10μM Pb exposure was associated with an increase in *5'UTR* expression ($p < 0.05$) (**Figure 4.6D**). No significant changes in *5'UTR* expression were detected with Pb exposure on D18 (**Figure 4.6E**). *ORF2* expression was more sensitive to Pb exposure during early differentiation, with greater expression on D6 in 1.26μM Pb exposed cells, relative to control ($p < 0.05$) (**Figure 4.6F**). Changes in expression on D12 mimicked those of *5'UTR*, wherein 10μM Pb exposed cells displayed a reduction in *ORF2* expression, relative to control ($p < 0.05$) (**Figure 4.6H**). This trend was also reversed as differentiation concluded, as on D15 and D18, *ORF2* expression was elevated in 10μM Pb exposed cells, relative to control ($p < 0.05$) (**Figure 4.6I-J**).

Lead Exposure Associated with Minimal Changes in LINE-1 DNA Methylation

DNAm levels were measured at 4 CpG positions within LINE-1 via pyrosequencing. No significant changes in DNAm were detected with Pb exposure until D12 of differentiation, when hypermethylation was detected at Positions 1 (1.26μM Pb

exposure, $p < 0.005$) and 4 (1.26μM Pb exposure, $p < 0.01$) (**Figure 4.7A** and **4.7D**). This trend was somewhat replicated on D15 at Positions 4, where 0.16μM Pb exposure was associated with hypermethylation ($p < 0.05$) (**Figure 4.8**). This association of hypermethylation in the presence of low and moderate Pb exposure largely disappeared as 5Y differentiation concluded on D18. At this time point, DNAm levels trended downward with Pb exposure at Positions 2-4, with a significant degree of hypomethylation detected at Position 3 in the 1.26μM Pb exposed cells ($p < 0.05$) (**Figure 4.9**). Remaining pyrosequencing results from D6 and D9 can be found in **Figure 4.A1-2**.

Discussion

Limited Correlation Between Baseline LINE-1 DNA Methylation and mRNA Expression. LINE-1 DNAm and mRNA expression were measured in the same cells with 0μM Pb exposure, and the DNA sequence assayed during pyrosequencing resides in the promoter region of the LINE-1 5' UTR.[57] DNAm in this region did not change substantially as 5Y differentiation progressed, with the only changes of significance being on D18, when the methylation of Positions 3 and 4 increased relative to D15 ($p < 0.05$) (**Figure 4.4**). With these patterns in mind, we would expect to see a positive correlation with *PIWIL* expression, that is relatively stable expression between D6 and D15 and an increase in expression on D18, given evidence of PIWIL-directed DNAm of LINE-1.[17] We would also expect to see an inverse relationship between LINE-1 DNAm and mRNA expression of *5' UTR* and *ORF2*, given previous work that found increased promoter methylation led to a decrease in mRNA expression.[58]

PIWIL4 expression increased on D15 and D18, relative to D12, and this increase appears to precede the observed increase in LINE-1 DNAm on D18 at Positions 3 and 4. Interestingly, *PIWIL1* expression was elevated on D12 relative to D6, and this precedes both the eventual increase in *PIWIL4* expression as well as the increase in LINE-1 DNAm on D18 (**Figure 4.3A-B**). The functional differences of the PIWIL proteins have not been well documented, particularly within the soma. Both PIWIL1 and PIWIL4 have been implicated not only in the regulation of LINE-1 elements, but also in stem cell maintenance and renewal.[59,60] It is possible that the differing patterns of expression that we see during 5Y differentiation are best explained by discordant roles in these cells at these timepoints. The elevated expression of *PIWIL1* on D12 and then decrease on D15 may reflect its role in stemness that is eventually turned off as these cells take on their terminal form, whereas the gradual rise in *PIWIL4* expression reflect piRNA-directed epigenetic control of TEs in terminally differentiated cells. However, given contradictory results in LINE-1 *5'UTR* and *ORF2* expression (discussed below), it is important that future work continue to investigate the roles of each PIWIL protein individually in somatic tissues such as the brain, so that their activity can be more thoroughly studied and interpreted in toxicological work.

There was also partial agreement between LINE-1 DNAm patterns and those of LINE-1 mRNA expression, with greater concordance seen with *5'UTR* expression compared to *ORF2*. LINE-1 *5' UTR* expression was significantly higher on D9 relative to D6, though no decrease in DNAm had been detected. Following this, LINE-1 5'UTR expression began to decline as observed on D12, and this decline continued into D15 and D18. This decline in 5'UTR expression preceded the observed modest increase in

LINE-1 DNAm detected on D18 and may reflect that the promoter that resides in the 5' UTR has limited self-regulatory capacity, and that the decrease in *5' UTR* expression may be better explained by DNAm changes in another regulatory region.[61] Relative stability in LINE-1 DNAm as well as of *ORF2* expression between D6 and D12 was not surprising. However, the modest increase in DNAm as Positions 3 and 4 between D15 and D18 was accompanied by a significant increase in *ORF2* expression, which was the opposite of the expected association. This is especially true given evidence that the LINE-1 promoter regulates the transcription of bicistronic LINE-1 mRNA which contains *ORF1* and *ORF2*.[62] It may be that more frequent analyses (i.e., daily) and/or a broader assessment of LINE-1 DNAm would have allowed for more thorough comparisons and the identification of changes in LINE-1 DNAm that better predict the observed change in *5'UTR* and *ORF2* expression. It may also be that other regulatory mechanisms besides PIWIL-directed DNAm of this specific region better explain the observed changes in LINE-1 expression during 5Y differentiation.

Minimal Correlation in Lead-Associated Changes in PIWIL Expression and LINE-1 DNA Methylation. *PIWIL1* expression decreased significantly with Pb exposure during early 5Y differentiation (D9-D12). On D6, there were no detectable changes in *PIWIL* expression or LINE-1 DNAm. By D9, *PIWIL1* expression was significantly suppressed by Pb exposure, but there were no corresponding changes observed in *PIWIL4* or DNAm levels. On D12, significant changes in DNAm included hypermethylated Positions 1 and 4 in exposed cells, while *PIWIL1* expression continued to decrease with exposure, which was the opposite of what was hypothesized. By D15, *PIWIL1* expression was elevated in exposed cells, and this was accompanied by an increase in

LINE-1 DNAm, and while few changes in DNAm reached statistical significance, this was one time point in which changes correlated in an expected way. *PIWIL1* expression showed no response to Pb exposure as differentiation concluded on D18. It is possible that depressed (D9 and D12) followed by elevated expression (D15) of *PIWIL1* during the course of 5Y differentiation in the presence of Pb is the result of compensatory mechanisms at work, and elevated *PIWIL1* expression has been quantified in disease states such as amyotrophic lateral sclerosis (ALS) and overexpression of this protein has been shown to rescue stem cell-like phenotypes in glioblastoma tissue.[63,64]

PIWIL4 expression appeared to be more resistant to Pb exposure during 5Y differentiation than *PIWIL1*, with the only significant change ($p < 0.05$) observed on D12, wherein 10 μM Pb exposure was associated with an increase in expression. *PIWIL4* has been shown to bind histone demethylases and induce the demethylation of piRNA-rich regions, thus increasing piRNA transcript production and subsequently promoting LINE-1 methylation in the germline.[65] Based on this, we would have expected to see a firmer correlation between *PIWIL4* expression and LINE-1 DNAm, but it is possible that the mechanisms by which PIWIL proteins coordinate LINE-1 methylation are different during neurogenesis than they are in the germline, and continued assessment of this relationship in this somatic tissue is needed.

Lead Exposure Associated with Inconsistent Changes in LINE-1 5' UTR Expression and DNA Methylation. The 5' UTR of LINE-1 contains a promoter region that directs LINE-1 transcription; however, this region is not self-regulated and instead is heavily influenced by upstream flanking sequences.[61] Interestingly, we did see some corresponding changes in 5' UTR DNAm and gene expression measures with Pb

exposure, most notably on D12 when LINE-1 DNAm increased with Pb exposure and *5' UTR* expression decreased, though significant effects were seen in different exposure groups. Generally, each time point included in this experiment provided preliminary evidence of increased as well as decreased *5' UTR* expression in the presence of Pb, which restricts our ability to make any strong conclusions as to how Pb exposure impacts the activity of this regulatory region (**Figure 4.6-4.9**). Previous work has documented increased LINE-1 5' UTR activity in the presence of mercury, however this work was conducted in non-differentiating cells.[66] It may be that the cellular environments inherent to differentiating cells respond differently to toxicant exposures and that variability in cell state during this process explains the variability in results seen here. Unsurprisingly, changes in *5' UTR* expression in the presence of Pb were similar to those of *ORF2*, which would be expected given that greater *5'UTR* activity would predict greater transcription of the downstream LINE-1 mRNA.[67]

These results highlight the need for continued assessment of the impact of environmentally relevant Pb exposure on LINE-1 promoter activity. Given the variability in *5' UTR* expression with Pb exposure, including on specific days as well as during the entire duration of differentiation, few conclusions can be drawn as to the effects of Pb exposure on LINE-1 5' UTR activity. It may be prudent to assay DNAm of the upstream flanking sequence, given its importance to LINE-1 promoter regulation, as well as the effects of Pb on other regulatory factors that have been implicated in 5' UTR activity in case changes in these measures better explain the effects seen on this promoter.

Lead Exposure Associated with Concordant Changes in LINE-1 Methylation and ORF2 Expression During Mid-to-Late Differentiation. Results on D12 and D18

demonstrated significant patterns in line with our overall hypothesis that Pb exposure will perturb LINE-1 regulation in ways that will correlate with corresponding changes in gene expression. On D12, DNAm increased modestly in the LINE-1 promoter region, and there is a concordant decrease in *ORF2* expression with Pb exposure, though these effects happen at different doses (**Figure 4.6-4.7**). D12 is a dynamic day for 5Y differentiation, being only 24 hours after the addition of terminal differentiation factors. It is plausible that a decrease in LINE-1 *ORF2* expression is a sign of dysregulation in these cells, as LINE-1 activity has been documented in NPCs and this activity is thought to be beneficial for stem cell maintenance.[23] It may be that while differentiation is still occurring, LINE-1 activity is supportive and that, upon Pb exposure and subsequent stress in these cells, this expression is decreased in favor of other compensatory mechanisms (such as metabolic pathways that mitigate reactive oxygen species and lessen the risk of cellular apoptosis).[68]

As 5Y differentiation concludes, these cells have largely taken on their terminal neural form and would not be expected to continue demonstrating phenotypes reminiscent of their stem cell precursors.[50] A somatic phenotype of LINE-1 repression would be considered the norm in these cells. Instead, in the presence of Pb, we saw a decrease in LINE-1 DNAm on D18 (significant at one position) and a corresponding elevation of *ORF2* expression (**Figure 4.6, 4.8-4.9**). The majority of currently available literature on Pb exposure and LINE-1 regulation pertains to that of LINE-1 DNAm, largely due to the use of LINE-1 DNAm as a proxy for global DNAm levels. The majority of this work finds that Pb exposure is associated with hypomethylation of LINE-1, and we saw preliminary evidence of this with the one measure of significant hypomethylation

on D18.[69,70] However, hypermethylation with Pb exposure was observed on D12 and D15, suggesting that the response of the developing nervous system to environmental toxicants may be dynamic and dependent on time point. Continued assessment of how LINE-1 DNAm changes during differentiation, in the presence of toxicants as well as without, perhaps at a wider range of CpG sites, would help expand our understanding of this dynamic developmental relationship.

The mechanisms thought to contribute to this association currently only extend as far as to DNMTs, specifically those than maintain DNAm such as DNMT1. DNMT1 is thought to be inhibited in a non-competitive manner by Pb, but corresponding work found no difference in the expression of *de novo* methyltransferase such as DNMT3A or 3B.[71] This may at least partially inform the results seen in this study, as early (D6 and D9) patterns of LINE-1 DNAm were not as disturbed by Pb exposure, perhaps in part because *de novo* methyltransferases may not be as susceptible to Pb exposure but also in that LINE-1 element expression is beneficial to these cells during differentiation and thus, DNAm levels are simply lower to begin with. However, by D12 and D15, Pb exposure is associated with hypermethylation of this LINE-1 region, and so previous work documenting Pb-associated inhibition of maintenance methyltransferases does not effectively explain this observation. It may be that other LINE-1 regulatory pathways or DNAm at other locations within these TEs contribute to the results seen here but were not quantified in this work.

Limitations

Limitations from Aim 2, Chapter 3 should also be considered here, as the SH-SY5Y cell line entails several caveats when interpreting results. Additionally, this work

was unable to assess changes in piRNA transcript expression as well as that of DNMTs, which would add to our understanding of how Pb exposure perturbs LINE-1 epigenetic regulation. This project was also limited in terms of the time points assessed. Continued work of this kind may consider increasing the frequency at which cells are collected, perhaps every 12 or 24 hours, in order to capture changes in DNAm that may more immediately precede changes in gene expression and would also allow for the opportunity to capture effects according to 5Y cell cycling.

It may be that larger sample sizes for each exposure group and time point are necessary in order to detected significant dose-response relationships in measures quantified using the assays described here. This may be especially true for gene expression analysis of *PIWILs*, as their expression is notably low overall.[72] Future work of this nature may do well to consider alternative methods that would be more forgiving of smaller sample sizes, such as RNA sequencing. It would also be beneficial to assess a greater array of CpGs in LINE-1 for changes in DNAm, as the four positions examined here may have provided a limited insight as to how Pb exposure alters the epigenetic regulation of this element.

Conclusion

This analysis provided evidence of differential expression of the LINE-1 *5' UTR* and *ORF2* in differentiating 5Ys exposed to environmentally relevant doses of Pb. While there was some evidence to suggest Pb disruption to PIWIL expression and LINE-1 DNAm may play a role in this relationship, no firm conclusions can be drawn due to the observance of several contradictory relationships. It is likely that Pb-induced disruption of LINE-1 epigenetic regulation and expression during this developmental process is not

explained by the factors measured here alone and additional work is needed to clarify this relationship. It would also be beneficial to assess Pb-associated changes in the expression of piRNA transcripts, the second component of the piRNA system. It may be that Pb exposure induces aberrant expression of piRNAs specific to LINE-1 elements and that this additional information would contribute to our understanding of the data presented here. Continued investigation into this relationship is warranted given previous work that has demonstrated a potential role of LINE-1 activity in ND as well as the capacity for environmental exposures to perturb the epigenetic regulation of these elements. It would also be beneficial to explore the effect of Pb on epigenetic regulation at other classes of TEs, such as Alu, the activity of which has also been implicated in ND.[73]

Acknowledgements

Thanks go out to those who helped design and facilitate these experiments, including Dr. Justin Colacino who was influential in experimental design, Katelyn Polemi who helped coordinate the massive number of cell culture vessels and media changes, and Elizabeth Tolrud who performed many of the genomic extractions. Gratitude is also due to Dr. Bek Pretoff for her guidance in how to assess DNAm at specific sites and Margaret Quaid for her help in executing the pyrosequencing experiments in this aim, as well as Dr. Bambarendage Perera for the design of the primers used in the qRT-PCR analysis. This work was supported by funding from the following sources: NIEHS Grant R35 (ES031686), NIEHS Grant K01 (ES032048), Institutional Training Grant T32 (ES007062), Institutional Training Grant T32 (HD079342), and National Institute of Aging (NIA) Grant R01 (AG072396).

References

1. Peze-Heidsieck, E. *et al.* Retrotransposons as a Source of DNA Damage in Neurodegeneration. *Front Aging Neurosci* **13**, 786897 (2022).

2. Takahashi, T. *et al.* LINE-1 activation in the cerebellum drives ataxia. *Neuron* **110**, 3278-3287.e8 (2022).

3. Wei, W. *et al.* Human L1 retrotransposition: cis preference versus trans complementation. *Mol Cell Biol* **21**, 1429–1439 (2001).

4. Lander, E. S. *et al.* Initial sequencing and analysis of the human genome. *Nature* **409**, 860–921 (2001).

5. Hafner, M. *et al.* Transcriptome-wide Identification of RNA-Binding Protein and MicroRNA Target Sites by PAR-CLIP. *Cell* **141**, 129–141 (2010).

6. Feng, Q., Moran, J. V., Kazazian, H. H. & Boeke, J. D. Human L1 Retrotransposon Encodes a Conserved Endonuclease Required for Retrotransposition. *Cell* **87**, 905–916 (1996).

7. Zhang, X., Zhang, R. & Yu, J. New Understanding of the Relevant Role of LINE-1 Retrotransposition in Human Disease and Immune Modulation. *Frontiers in Cell and Developmental Biology* **8**, (2020).

8. Chen, J.-M., Stenson, P. D., Cooper, D. N. & Férec, C. A systematic analysis of LINE-1 endonuclease-dependent retrotranspositional events causing human genetic disease. *Hum Genet* **117**, 411–427 (2005).

9. Wimmer, K., Callens, T., Wernstedt, A. & Messiaen, L. The NF1 gene contains hotspots for L1 endonuclease-dependent de novo insertion. *PLoS Genet* **7**, e1002371 (2011).

10. Miki, Y. *et al.* Disruption of the APC gene by a retrotransposal insertion of L1 sequence in a colon cancer. *Cancer Res* **52**, 643–645 (1992).

11. Schwahn, U. *et al.* Positional cloning of the gene for X-linked retinitis pigmentosa 2. *Nat Genet* **19**, 327–332 (1998).

12. Yoshida, K., Nakamura, A., Yazaki, M., Ikeda, S. & Takeda, S. Insertional mutation by transposable element, L1, in the DMD gene results in X-linked dilated cardiomyopathy. *Hum Mol Genet* **7**, 1129–1132 (1998).

13. Zamudio, N. *et al.* DNA methylation restrains transposons from adopting a chromatin signature permissive for meiotic recombination. *Genes Dev* **29**, 1256–1270 (2015).

14. Newkirk, S. J. *et al.* Intact piRNA pathway prevents L1 mobilization in male meiosis. *Proc Natl Acad Sci U S A* **114**, E5635–E5644 (2017).

15. Siomi, M. C., Miyoshi, T. & Siomi, H. piRNA-mediated silencing in Drosophila germlines. *Semin Cell Dev Biol* **21**, 754–759 (2010).

16. Senti, K.-A. & Brennecke, J. The piRNA pathway: a fly's perspective on the guardian of the genome. *Trends Genet* **26**, 499–509 (2010).

17. Zoch, A. *et al.* SPOCD1 is an essential executor of piRNA-directed de novo DNA methylation. *Nature* **584**, 635–639 (2020).

18. Aravin, A. A. *et al.* A piRNA Pathway Primed by Individual Transposons Is Linked to De Novo DNA Methylation in Mice. *Molecular Cell* **31**, 785–799 (2008).

19. Richardson, S. R., Morell, S. & Faulkner, G. J. L1 retrotransposons and somatic mosaicism in the brain. *Annu Rev Genet* **48**, 1–27 (2014).

20. Lf, O., Cf, M., Ed, S., V, S. & L, A.-C. LINE-1 specific nuclear organization in mice olfactory sensory neurons. *Molecular and cellular neurosciences* **105**, (2020).

21. Jachowicz, J. W. *et al.* LINE-1 activation after fertilization regulates global chromatin accessibility in the early mouse embryo. *Nat Genet* **49**, 1502–1510 (2017).

22. Vitullo, P., Sciamanna, I., Baiocchi, M., Sinibaldi-Vallebona, P. & Spadafora, C. LINE-1 retrotransposon copies are amplified during murine early embryo development. *Mol Reprod Dev* **79**, 118–127 (2012).

23. Jönsson, M. E. *et al.* Activation of neuronal genes via LINE-1 elements upon global DNA demethylation in human neural progenitors. *Nat Commun* **10**, 3182 (2019).

24. Coufal, N. G. *et al.* L1 retrotransposition in human neural progenitor cells. *Nature* **460**, 1127–1131 (2009).

25. Baillie, J. K. *et al.* Somatic retrotransposition alters the genetic landscape of the human brain. *Nature* **479**, 534–537 (2011).

26. Bodea, G. O., McKelvey, E. G. Z. & Faulkner, G. J. Retrotransposon-induced mosaicism in the neural genome. *Open Biol* **8**, 180074 (2018).

27. Bedrosian, T. A., Quayle, C., Novaresi, N. & Gage, F. H. Early life experience drives structural variation of neural genomes in mice. *Science* **359**, 1395–1399 (2018).

28. Wang, F. *et al.* Inhibition of LINE-1 retrotransposition represses telomere reprogramming during mouse 2-cell embryo development. *J Assist Reprod Genet* **38**, 3145–3153 (2021).

29. Spadafora, C. A LINE-1–encoded reverse transcriptase–dependent regulatory mechanism is active in embryogenesis and tumorigenesis. *Annals of the New York Academy of Sciences* **1341**, 164–171 (2015).

30. Della Valle, F. *et al.* LINE-1 RNA causes heterochromatin erosion and is a target for amelioration of senescent phenotypes in progeroid syndromes. *Sci Transl Med* **14**, eabl6057 (2022).

31. Grundy, E. E., Diab, N. & Chiappinelli, K. B. Transposable element regulation and expression in cancer. *FEBS J* **289**, 1160–1179 (2022).

32. Horvath, S. & Raj, K. DNA methylation-based biomarkers and the epigenetic clock theory of ageing. *Nat Rev Genet* **19**, 371–384 (2018).

33. Ryan, J., Wrigglesworth, J., Loong, J., Fransquet, P. D. & Woods, R. L. A Systematic Review and Meta-analysis of Environmental, Lifestyle, and Health Factors Associated With DNA Methylation Age. *J Gerontol A Biol Sci Med Sci* **75**, 481–494 (2020).

34. Pal, S. & Tyler, J. K. Epigenetics and aging. *Sci Adv* **2**, e1600584 (2016).

35. Jintaridth, P. & Mutirangura, A. Distinctive patterns of age-dependent hypomethylation in interspersed repetitive sequences. *Physiological Genomics* **41**, 194–200 (2010).

36. Van Meter, M. *et al.* SIRT6 represses LINE1 retrotransposons by ribosylating KAP1 but this repression fails with stress and age. *Nat Commun* **5**, 5011 (2014).

37. Yan, M. H., Wang, X. & Zhu, X. Mitochondrial defects and oxidative stress in Alzheimer disease and Parkinson disease. *Free Radic Biol Med* **62**, 90–101 (2013).

38. Schumacher, B., Pothof, J., Vijg, J. & Hoeijmakers, J. H. J. The central role of DNA damage in the ageing process. *Nature* **592**, 695–703 (2021).

39. Whongsiri, P. *et al.* Oxidative stress and LINE-1 reactivation in bladder cancer are epigenetically linked through active chromatin formation. *Free Radic Biol Med* **134**, 419–428 (2019).

40. Suarez, N. A., Macia, A. & Muotri, A. R. LINE-1 retrotransposons in healthy and diseased human brain. *Dev Neurobiol* **78**, 434–455 (2018).

41. Ravel-Godreuil, C., Znaidi, R., Bonnifet, T., Joshi, R. L. & Fuchs, J. Transposable elements as new players in neurodegenerative diseases. *FEBS Letters* **595**, 2733–2755 (2021).

42. Sae-Lee, C. *et al.* DNA methylation patterns of LINE-1 and Alu for pre-symptomatic dementia in type 2 diabetes. *PLoS One* **15**, e0234578 (2020).

43. Searles Nielsen, S. *et al.* LINE-1 DNA methylation, smoking and risk of Parkinson's disease. *J Parkinsons Dis* **2**, 303–308 (2012).

44. Shanbhag, N. M. *et al.* Early neuronal accumulation of DNA double strand breaks in Alzheimer's disease. *acta neuropathol commun* **7**, 77 (2019).

45. Ramirez, P. *et al.* Pathogenic tau accelerates aging-associated activation of transposable elements in the mouse central nervous system. *Progress in Neurobiology* **208**, 102181 (2022).

46. Cho, Y. H. *et al.* LINE-1 hypomethylation is associated with radiation-induced genomic instability in industrial radiographers. *Environ Mol Mutagen* **60**, 174–184 (2019).

47. Yang, J. *et al.* Urinary 1-hydroxypyrene and smoking are determinants of LINE-1 and AhRR promoter methylation in coke oven workers. *Mutat Res Genet Toxicol Environ Mutagen* **826**, 33–40 (2018).

48. Issah, I. *et al.* Association between global DNA methylation (LINE-1) and occupational particulate matter exposure among informal electronic-waste recyclers in Ghana. *Int J Environ Health Res* **32**, 2406–2424 (2022).

49. Alexander, M. *et al.* Pesticide use and LINE-1 methylation among male private pesticide applicators in the Agricultural Health Study. *Environ Epigenet* **3**, dvx005 (2017).

50. Shipley, M. M., Mangold, C. A. & Szpara, M. L. Differentiation of the SH-SY5Y Human Neuroblastoma Cell Line. *J Vis Exp* (2016) doi:10.3791/53193.

51. Winer, J., Jung, C. K., Shackel, I. & Williams, P. M. Development and validation of real-time quantitative reverse transcriptase-polymerase chain reaction for monitoring gene expression in cardiac myocytes in vitro. *Anal Biochem* **270**, 41–49 (1999).

52. Li, Y. & Tollefsbol, T. O. DNA methylation detection: Bisulfite genomic sequencing analysis. *Methods Mol Biol* **791**, 11–21 (2011).

53. Create Elegant Data Visualisations Using the Grammar of Graphics. https://ggplot2.tidyverse.org/.

54. Athanikar, J. N., Badge, R. M. & Moran, J. V. A YY1-binding site is required for accurate human LINE-1 transcription initiation. *Nucleic Acids Res* **32**, 3846–3855 (2004).

55. Moran, J. V. *et al.* High frequency retrotransposition in cultured mammalian cells. *Cell* **87**, 917–927 (1996).

56. Peddigari, S., Li, P. W.-L., Rabe, J. L. & Martin, S. L. hnRNPL and nucleolin bind LINE-1 RNA and function as host factors to modulate retrotransposition. *Nucleic Acids Res* **41**, 575–585 (2013).

57. Wu, Y. *et al.* Association of blood leukocyte DNA methylation at LINE-1 and growth-related candidate genes with pubertal onset and progression. *Epigenetics* **13**, 1222–1233 (2018).

58. Tahara, S. *et al.* Lower LINE-1 methylation is associated with promoter hypermethylation and distinct molecular features in gastric cancer. *Epigenomics* **11**, 1651–1659 (2019).

59. Juliano, C., Wang, J. & Lin, H. Uniting Germline and Stem Cells: The Function of Piwi Proteins and the piRNA Pathway in Diverse Organisms. *Annual Review of Genetics* **45**, 447–469 (2011).

60. Reeves, M. E. *et al.* RASSF1C modulates the expression of a stem cell renewal gene, PIWIL1. *BMC Research Notes* **5**, 239 (2012).

61. Lavie, L., Maldener, E., Brouha, B., Meese, E. U. & Mayer, J. The human L1 promoter: Variable transcription initiation sites and a major impact of upstream flanking sequence on promoter activity. *Genome Res* **14**, 2253–2260 (2004).

62. Scott, A. F. *et al.* Origin of the human L1 elements: proposed progenitor genes deduced from a consensus DNA sequence. *Genomics* **1**, 113–125 (1987).

63. Abdelhamid, R. F. *et al.* piRNA/PIWI Protein Complex as a Potential Biomarker in Sporadic Amyotrophic Lateral Sclerosis. *Mol Neurobiol* **59**, 1693–1705 (2022).

64. Wang, X. *et al.* MiRNA-154-5p inhibits cell proliferation and metastasis by targeting PIWIL1 in glioblastoma. *Brain Research* **1676**, 69–76 (2017).

65. Nagamori, I. *et al.* Relationship between PIWIL4-Mediated H3K4me2 Demethylation and piRNA-Dependent DNA Methylation. *Cell Reports* **25**, 350–356 (2018).

66. Habibi, L., Shokrgozar, M. A., Tabrizi, M., Modarressi, M. H. & Akrami, S. M. Mercury specifically induces LINE-1 activity in a human neuroblastoma cell line. *Mutat Res Genet Toxicol Environ Mutagen* **759**, 9–20 (2014).

67. Briggs, E. M. *et al.* RIP-seq reveals LINE-1 ORF1p association with p-body enriched mRNAs. *Mobile DNA* **12**, 5 (2021).

68. Zeybek, N. D., Baysal, E., Bozdemir, O. & Buber, E. Hippo Signaling: A Stress Response Pathway in Stem Cells. *Curr Stem Cell Res Ther* **16**, 824–839 (2021).

69. Goodrich, J. M. *et al.* Adolescent epigenetic profiles and environmental exposures from early life through peri-adolescence. *Environ Epigenet* **2**, (2016).

70. Issah, I. *et al.* Global DNA (LINE-1) methylation is associated with lead exposure and certain job tasks performed by electronic waste workers. *Int Arch Occup Environ Health* **94**, 1931–1944 (2021).

71. Sanchez, O. F. *et al.* Lead (Pb) exposure reduces global DNA methylation level by non-competitive inhibition and alteration of dnmt expression†. *Metallomics* **9**, 149–160 (2017).

72. Perera, B. P. U. *et al.* Somatic expression of piRNA and associated machinery in the mouse identifies short, tissue-specific piRNA. *Epigenetics* **14**, 504–521 (2019).

73. Larsen, P. A. *et al.* The Alu neurodegeneration hypothesis: A primate-specific mechanism for neuronal transcription noise, mitochondrial dysfunction, and manifestation of neurodegenerative disease. *Alzheimer's & Dementia* **13**, 828–838 (2017).

Figures and Tables

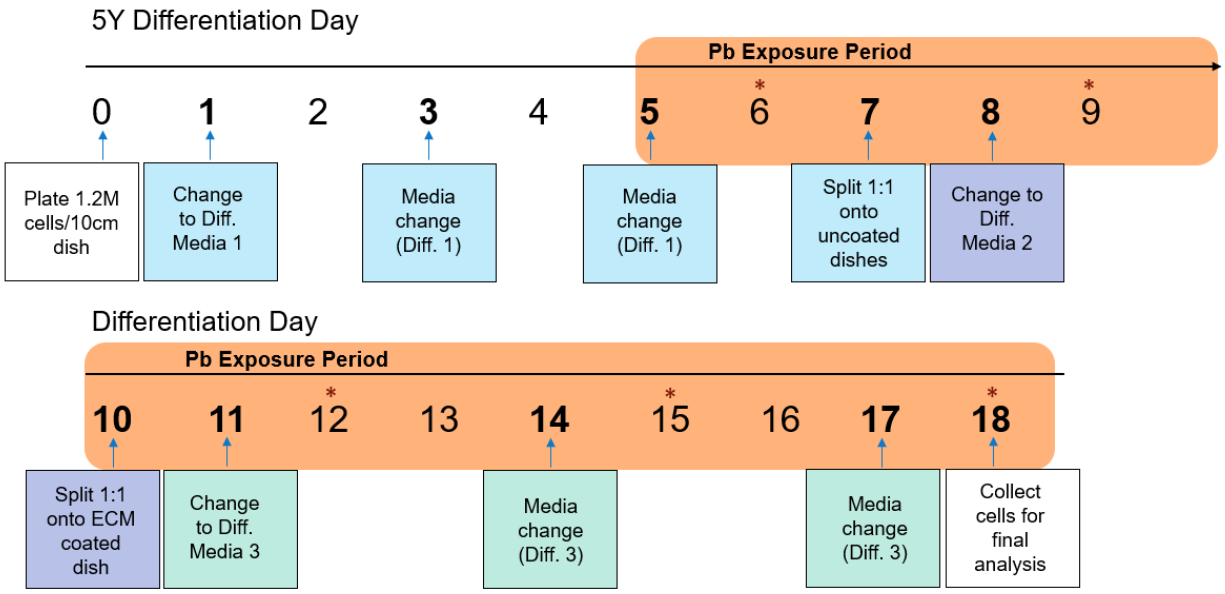

Figure 4.1: SH-SY5Y Differentiation Protocol. SH-SY5Y cells were differentiated in the presence of retinoic acid (RA) for 18 days, with lead exposure beginning on Day 5. *Indicates days on which cells were collected for genomic extraction and subsequent analysis.

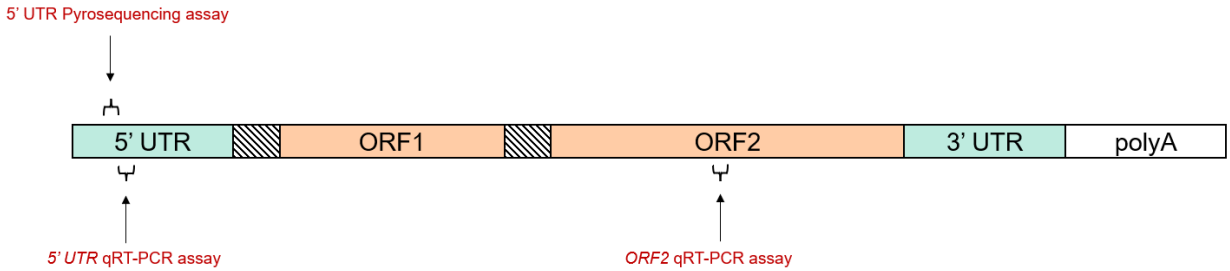

Figure 4.2: Location of LINE-1 Pyrosequencing and qRT-PCR Assays. Pyrosequencing region includes bases 302-327 of LINE-1, which reside in the promoter region of the 5' UTR. qRT-PCR 5'UTR and ORF2 amplicons are ~98 and ~131 nucleotides in length and primer sequences were obtained from Wissing et al., 2012.

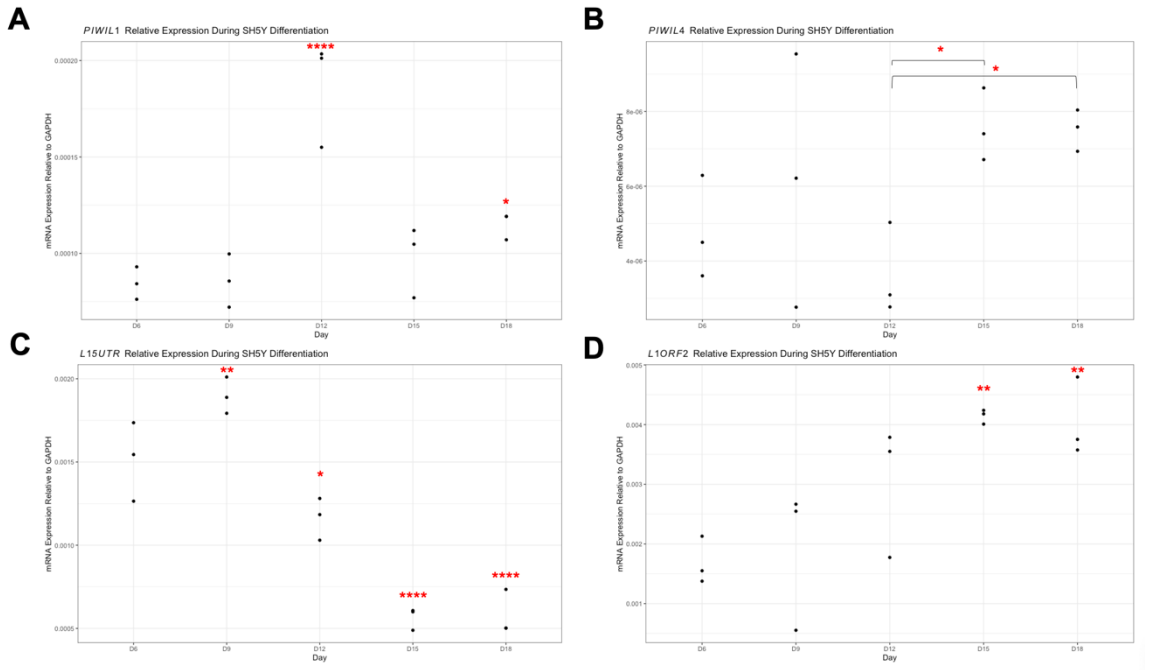

Figure 4.3: Baseline PIWIL and LINE-1 Gene Expression During SH-SY5Y Differentiation. A) *PIWIL1*, B) *PIWIL4*, C) *L15'UTR* and D) *L1ORF2* were quantified during SH-SY5Y differentiation via qRT-PCR using SYBR Green chemistry in the absence of Pb exposure (*p < 0.05, ** p < 0.01, **** p < 0.001).

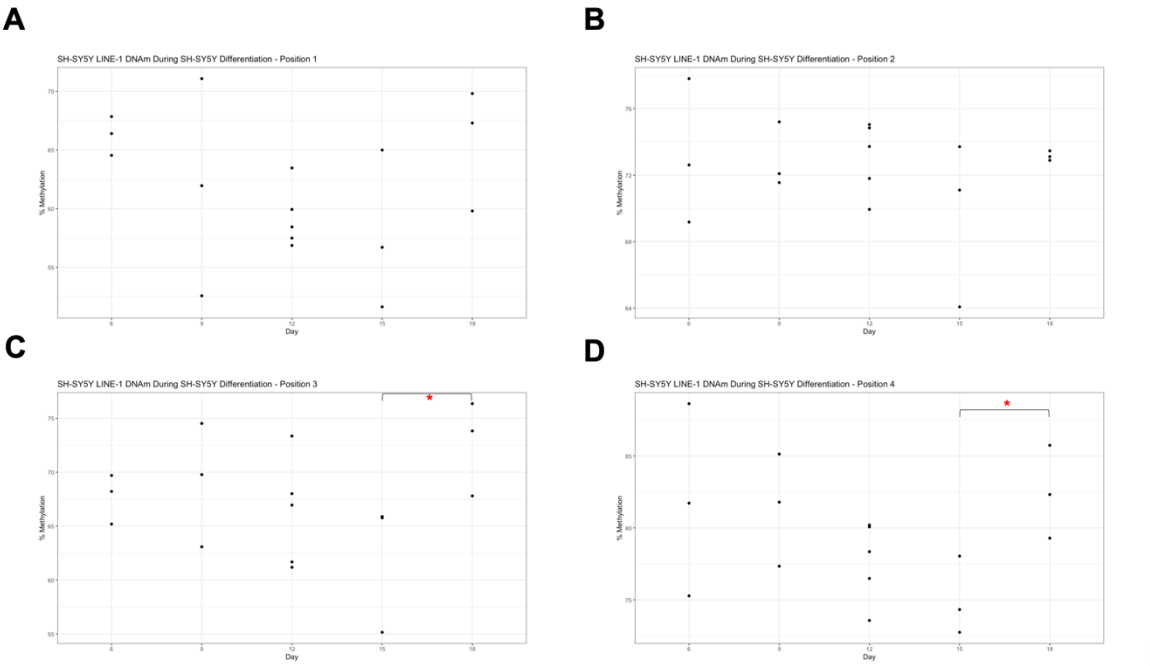

Figure 4.4: Baseline DNA Methylation of LINE-1 During SH-SY5Y Differentiation. LINE-1 methylation was quantified in the promoter of the 5' UTR via pyrosequencing at A) Position 1, B) Position 2, C) Position 3, and D) Position 4 in cells during differentiation and in the absence of Pb exposure (* p < 0.05).

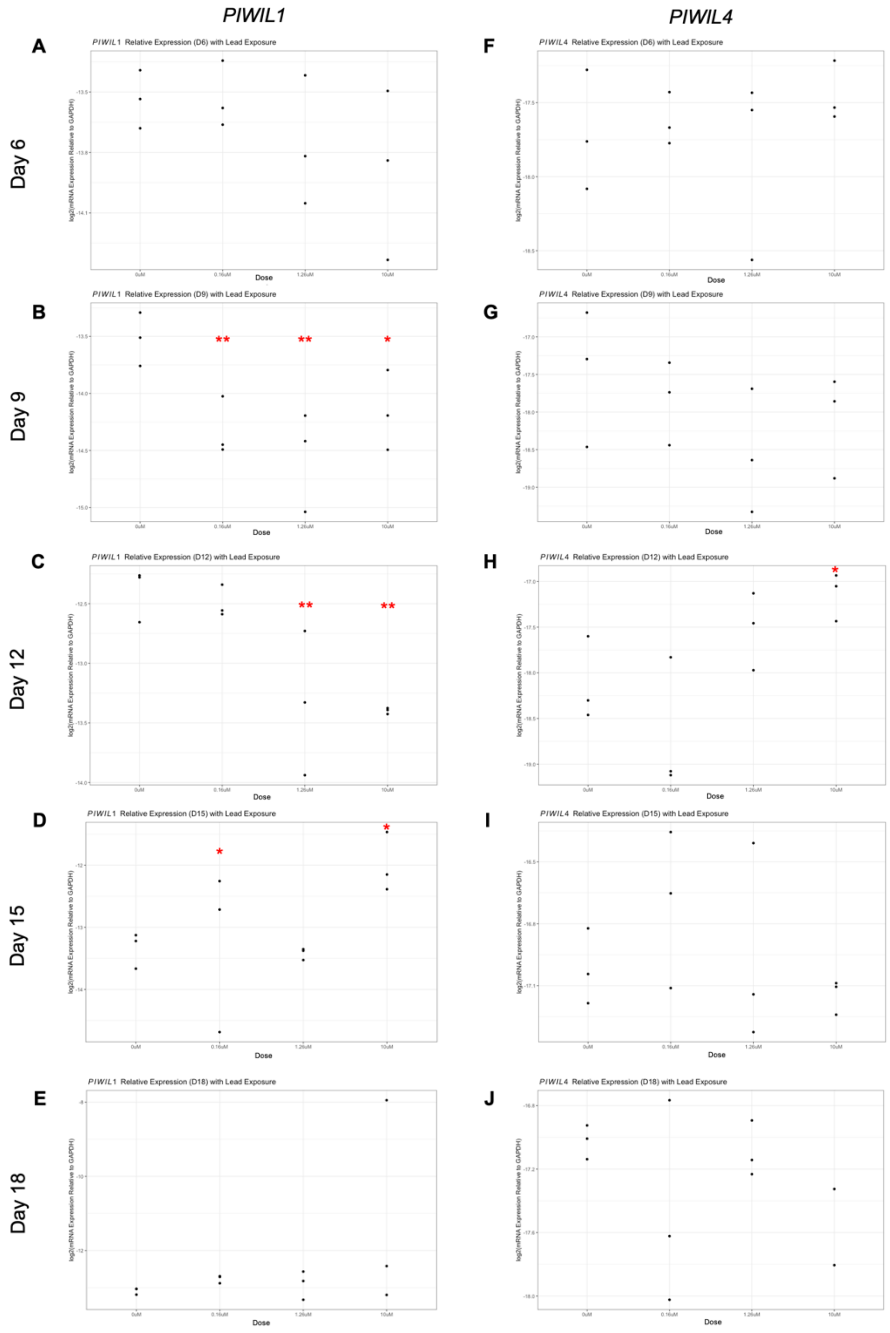

Figure 4.5: PIWIL Expression with Lead Exposure in Differentiating SH-SY5Y. Changes in PIWIL1 (A-E) and PIWIL4 (F-J) expression with 0.16μM, 1.26μM, and 10μM Pb exposures quantified every three days beginning on Day 6 (* $p < 0.05$, ** $p < 0.01$).

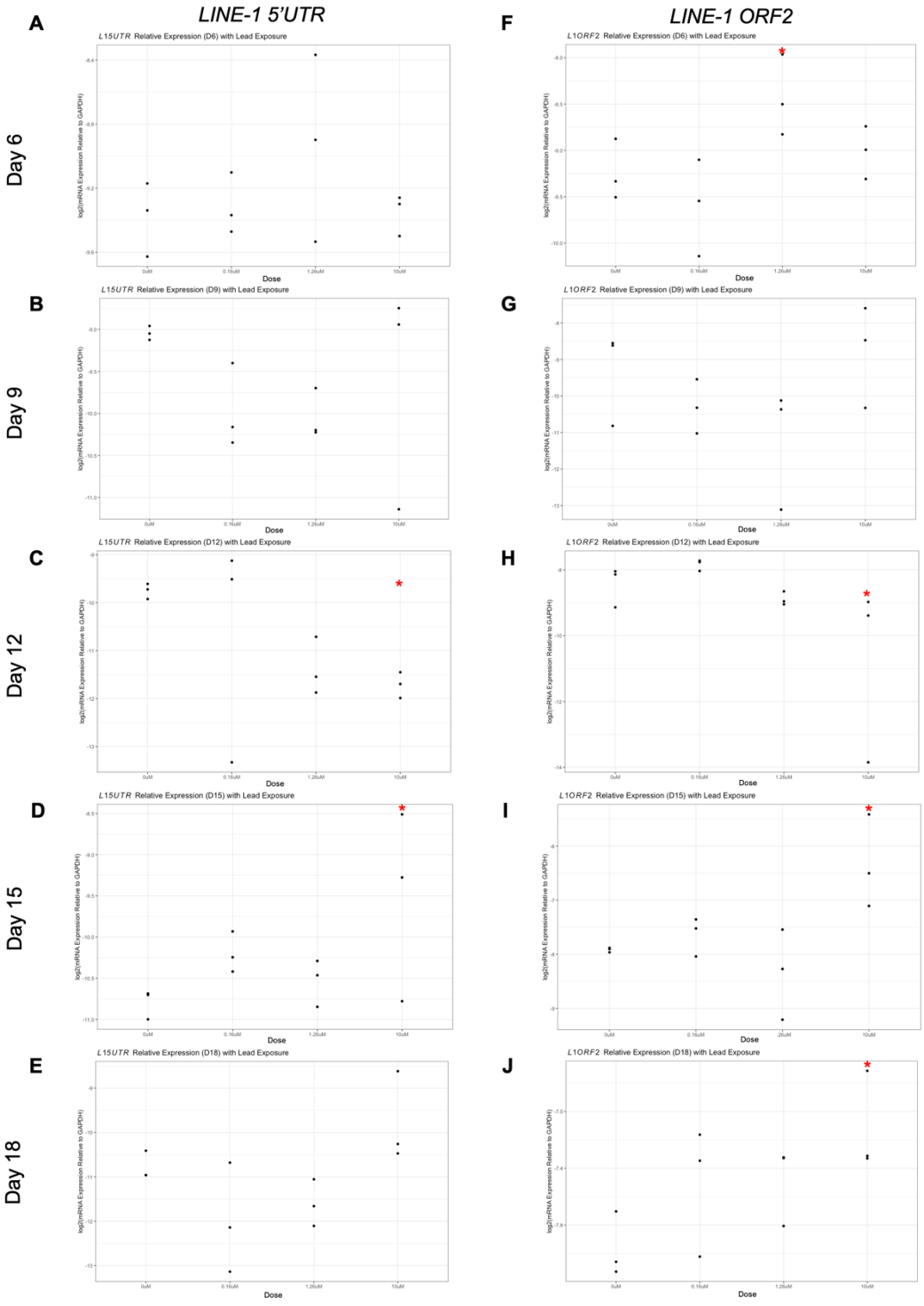

Figure 4.6: LINE-1 Expression with Lead Exposure in Differentiating SH-SY5Y. Changes in L15'UTR (A-E) and L1ORF2 (F-J) expression with 0.16μM, 1.26μM, and 10μM Pb exposures quantified every three days beginning on Day 6 (* $p < 0.05$).

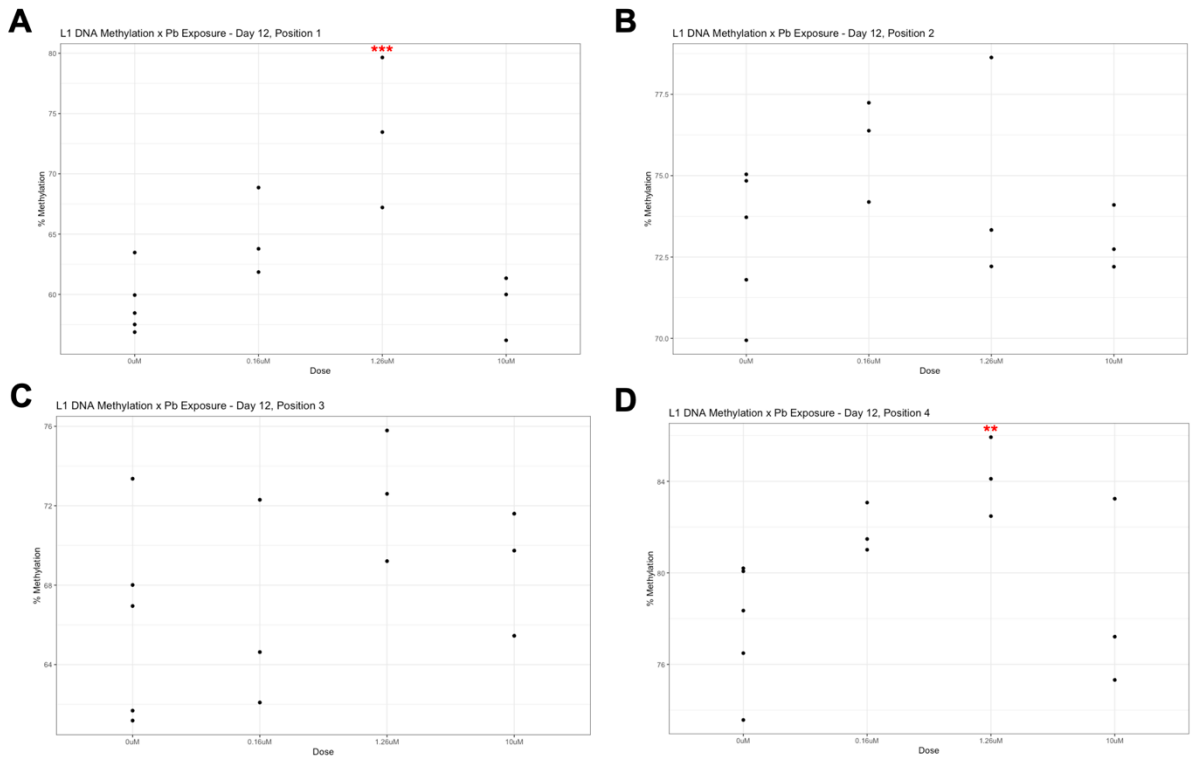

Figure 4.7: LINE-1 DNA Methylation on Day 12 with Lead Exposure. DNA methylation quantified via pyrosequencing at A) Position 1, B) Position 2, C) Position 3, and D) Position 4 in the LINE-1 promoter (** $p < 0.01$, *** $p < 0.005$).

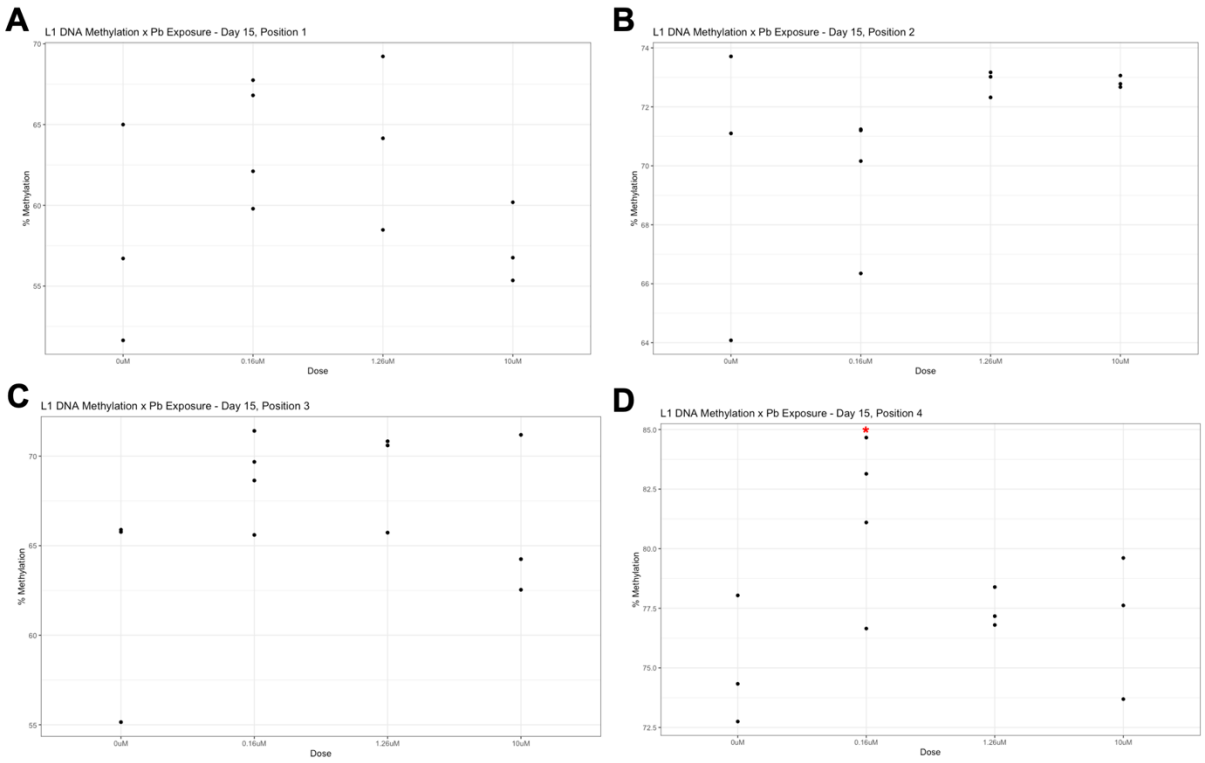

Figure 4.8: LINE-1 DNA Methylation on Day 15 with Lead Exposure. DNA methylation quantified via pyrosequencing at A) Position 1, B) Position 2, C) Position 3, and D) Position 4 in the LINE-1 promoter (* $p < 0.05$).

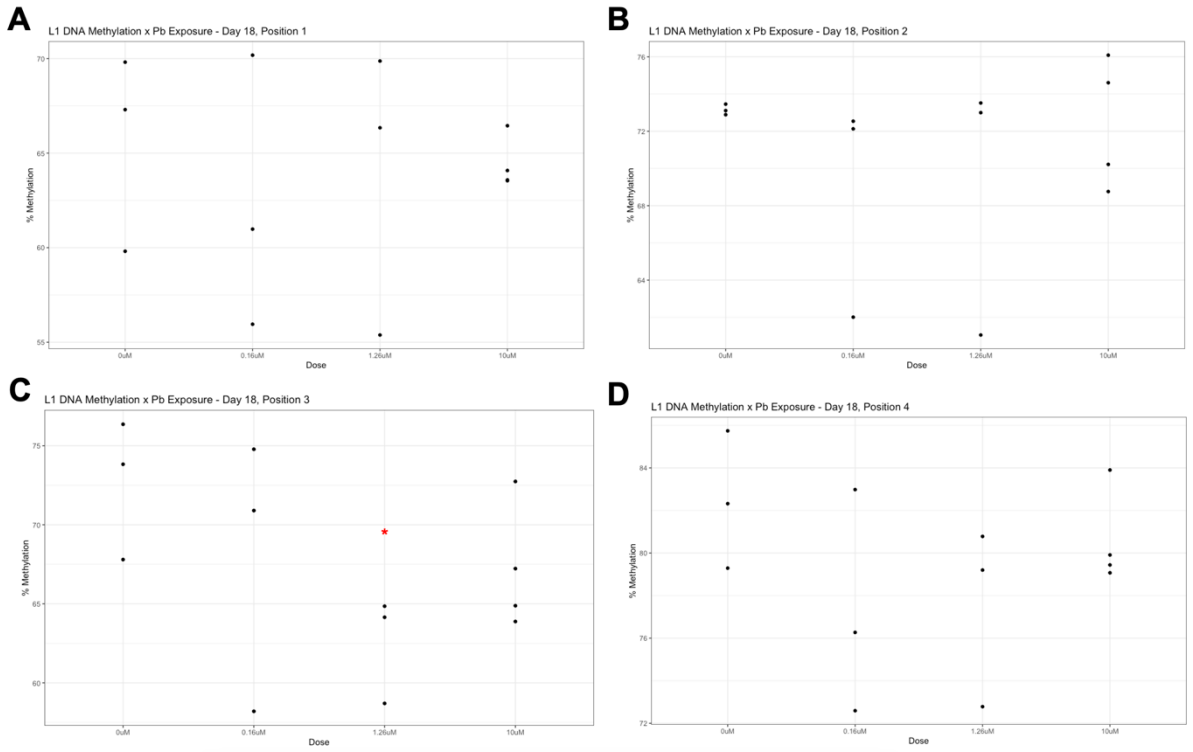

Figure 4.9: LINE-1 DNA Methylation on Day 18 with Lead Exposure. DNA methylation quantified via pyrosequencing at A) Position 1, B) Position 2, C) Position 3, and D) Position 4 in the LINE-1 promoter (* $p < 0.05$).

Appendix

Experiment ID	Primer ID	Primer Sequence	Length	Amplicon Size	Vendor
PIWIL1	PIWIL1_F	ACGAAGTGCCACAGTTTTTGG	21	124	IDT
	PIWIL1_R	AGTCTTCCTCCAGACTGAGC	20		IDT
PIWIL2	PIWIL2_F	GCCTGGGTTGAACTAAAGGA	20	106	IDT
	PIWIL2_R	CCATGATGATGCAAACAACC	20		IDT
PIWIL3	PIWIL3_F	TCAGATGGCAGCAAAATCAC	20	129	IDT
	PIWIL3_R	ACGTTGTGTACCCGTTAGGC	20		IDT
PIWIL4	PIWIL4_F	ATGGCACCGAGATCACCTAT	20	126	IDT
	PIWIL4_R	GCTGAGCCTCACTGTTGTCA	20		IDT
L15'UTR*	L15UTR_F	ACGGAATCTCGCTGATTGCTA	21	98	IDT
	L15UTR_R	AAGCAAGCCTGGGCAATG	18		IDT
L1ORF2*	L1ORF2_F	GAGAGGATGCGGAGAAATAGGA	22	131	IDT
	L1ORF2_R	GGATGGCTGGGTCAAATGGT	20		IDT
Predesigned qRT-PCR Assay					
GAPDH	Assay ID: qHsaCEP0041396				Bio-Rad

Table 4.A1: Primers used for qRT-PCR. Assays indicated by * previously validated by Wissing et al., 2012.

Oligo Name	5' – sequence – 3'	length	size	Position (Hg 19)
FWD PCR Primer	5'- TTGAGTTAGGTGTGGGATATAGTT-3'	24	~150	Many – repetitive element
REV PCR Primer	5'-[biotin]-CAAAAAATCAAAAAATTCCCTTTCC-3'	25		
Sequencing Primer	5'-AGGTGTGGATATAGT-3'	15		
Assayed Sequence				
CTCGTGGTGCGCCGTTTCTTAAGCCG				

Table 4.A2: Pyrosequencing parameters.

Sample ID	PIWIL1		PIWIL2		PIWIL3		PIWIL4		L1 5' UTR		L1 ORF2		GAPDH	
Day_Dose_Replicate	Cq_Mean	Cq_STD	Cq_Mean	Cq_STD	Cq_Mean	Cq_STD	Cq_Mean	Cq_STD	Cq_Mean	Cq_STD	Cq_Mean	Cq_STD	Cq_Mean	Cq_STD
D6_0uM_1	29.14	0.080	0.00	0.000	0.00	0.000	33.02	0.433	24.91	0.313	24.62	0.538	15.74	0.345
D6_0uM_2	29.37	0.142	0.00	0.000	0.00	0.000	33.91	1.867	25.17	0.310	25.17	0.758	15.83	0.408
D6_0uM_3	29.26	0.154	0.00	0.000	0.00	0.000	33.34	0.623	25.21	0.301	25.08	0.515	15.58	0.307
D6_0.16uM_1	29.43	0.345	0.00	0.000	0.00	0.000	33.44	0.946	25.24	0.109	25.31	0.663	15.77	0.122
D6_0.16uM_2	29.34	0.178	0.00	0.000	0.00	0.000	33.77	1.071	25.10	0.266	25.10	1.233	16.00	0.308
D6_0.16uM_3	29.53	0.485	0.00	0.000	0.00	0.000	33.38	0.865	25.32	0.380	26.09	1.706	15.95	0.285
D6_1.26uM_1	29.63	0.478	0.00	0.000	0.00	0.000	34.77	1.659	24.58	0.249	24.18	0.298	16.21	0.667
D6_1.26uM_2	29.79	0.427	0.00	0.000	0.00	0.000	33.28	0.662	24.63	0.222	24.24	0.486	15.73	0.450
D6_1.26uM_3	30.09	0.385	0.00	0.000	0.00	0.000	33.70	0.413	25.81	0.232	25.10	0.653	16.27	0.402
D6_10uM_1	29.89	0.479	0.00	0.000	0.00	0.000	33.59	0.454	25.35	0.254	24.79	0.203	16.05	0.287
D6_10uM_2	30.02	0.358	0.00	0.000	0.00	0.000	33.74	0.329	25.79	0.265	25.52	0.074	16.53	0.516
D6_10uM_3	30.51	0.471	0.00	0.000	0.00	0.000	33.77	0.337	25.68	0.115	25.49	0.204	16.18	0.148
D9_0uM_1	30.15	0.314	0.00	0.000	0.00	0.000	34.85	2.450	25.44	0.250	27.21	0.760	16.39	0.338
D9_0uM_2	29.61	0.176	0.00	0.000	0.00	0.000	33.00	0.195	25.28	0.278	24.87	0.203	16.32	0.450
D9_0uM_3	29.79	0.197	0.00	0.000	0.00	0.000	33.57	0.795	25.40	0.410	24.90	0.232	16.28	0.534
D9_0.16uM_1	30.29	0.659	0.00	0.000	0.00	0.000	34.70	0.462	26.61	0.666	27.29	1.794	16.26	0.135
D9_0.16uM_2	30.32	0.623	0.00	0.000	0.00	0.000	33.56	0.851	25.23	0.645	25.37	0.711	15.83	0.235
D9_0.16uM_3	30.01	0.380	0.00	0.000	0.00	0.000	32.91	0.782	25.72	0.964	25.89	0.827	15.56	0.253
D9_1.26uM_1	30.49	0.518	0.00	0.000	0.00	0.000	33.99	1.247	26.00	0.573	26.67	1.188	16.30	0.075
D9_1.26uM_2	30.46	0.410	0.00	0.000	0.00	0.000	35.37	1.398	26.24	0.467	26.16	1.216	16.04	0.299
D9_1.26uM_3	30.54	0.588	0.00	0.000	0.00	0.000	34.14	0.931	25.73	0.554	28.62	2.990	15.51	0.347
D9_10uM_1	30.65	0.452	0.00	0.000	0.00	0.000	35.04	0.882	27.30	0.676	26.49	0.983	16.16	0.319
D9_10uM_2	30.15	0.511	0.00	0.000	0.00	0.000	34.21	1.051	25.30	0.343	23.95	0.519	16.35	0.510
D9_10uM_3	30.43	0.602	0.00	0.000	0.00	0.000	33.84	0.814	24.99	0.442	24.71	0.320	16.24	0.198
D12_0uM_1	27.79	0.521	0.00	0.000	0.00	0.000	33.81	0.429	25.23	0.551	23.55	0.217	15.51	0.188
D12_0uM_2	27.91	0.431	0.00	0.000	0.00	0.000	33.72	0.688	25.18	0.355	24.39	0.780	15.26	0.294
D12_0uM_3	28.07	0.416	0.00	0.000	0.00	0.000	33.41	0.377	25.42	0.591	23.95	0.302	15.81	0.420
D12_0.16uM_1	28.18	0.443	0.00	0.000	0.00	0.000	34.71	0.623	25.11	0.379	23.63	0.227	15.59	0.458
D12_0.16uM_2	28.39	0.971	0.00	0.000	0.00	0.000	34.91	0.618	29.16	3.410	23.55	0.455	15.83	0.183
D12_0.16uM_3	28.16	0.793	0.00	0.000	0.00	0.000	33.65	0.360	24.94	0.529	23.58	0.501	15.82	0.517
D12_1.26uM_1	29.40	0.656	0.00	0.000	0.00	0.000	33.44	1.376	27.34	0.533	24.51	0.385	15.47	1.025
D12_1.26uM_2	29.11	0.169	0.00	0.000	0.00	0.000	33.24	0.996	27.32	0.788	24.74	0.705	15.78	1.384
D12_1.26uM_3	29.12	0.236	0.00	0.000	0.00	0.000	33.53	0.510	27.11	0.194	25.05	0.869	16.40	2.570
D12_10uM_1	29.37	0.271	0.00	0.000	0.00	0.000	32.88	0.467	27.64	0.819	24.92	0.677	15.95	0.551
D12_10uM_2	29.19	0.378	0.00	0.000	0.00	0.000	32.86	0.387	27.25	0.901	25.19	0.493	15.80	0.568
D12_10uM_3	28.96	0.296	0.00	0.000	0.00	0.000	33.02	0.216	27.57	0.783	29.43	1.075	15.58	0.157
D15_0uM_1	29.51	0.196	0.00	0.000	0.00	0.000	33.20	1.036	27.07	1.370	24.29	0.536	16.38	0.535
D15_0uM_2	29.85	0.293	0.00	0.000	0.00	0.000	33.22	0.233	27.18	0.851	24.06	0.281	16.18	0.432
D15_0uM_3	29.52	0.115	0.00	0.000	0.00	0.000	33.49	0.353	27.01	0.324	24.27	0.255	16.30	0.272
D15_0.16uM_1	28.82	0.369	0.00	0.000	0.00	0.000	32.75	0.390	26.35	0.940	24.14	0.506	16.10	0.901
D15_0.16uM_2	31.29	0.222	0.00	0.000	0.00	0.000	33.72	0.233	27.02	0.747	24.13	0.595	16.60	0.753
D15_0.16uM_3	29.10	0.154	0.00	0.000	0.00	0.000	33.20	0.763	26.78	0.587	24.20	0.851	16.84	1.412
D15_1.26uM_1	30.07	1.568	0.00	0.000	0.00	0.000	33.11	0.213	26.99	0.233	24.24	0.400	16.70	0.929
D15_1.26uM_2	29.93	1.161	0.00	0.000	0.00	0.000	33.90	0.910	27.04	0.877	24.85	1.015	16.58	0.730
D15_1.26uM_3	29.87	1.023	0.00	0.000	0.00	0.000	33.49	1.001	27.19	1.285	25.55	0.781	16.35	0.332
D15_10uM_1	29.43	0.563	0.00	0.000	0.00	0.000	35.20	2.094	26.47	0.365	23.37	0.803	17.96	0.639
D15_10uM_2	29.36	0.812	0.00	0.000	0.00	0.000	34.30	0.988	26.49	1.038	23.72	1.030	17.21	1.642
D15_10uM_3	29.41	0.689	0.00	0.000	0.00	0.000	34.12	0.302	27.80	2.948	24.13	0.891	17.02	1.096
D18_0uM_1	29.15	0.405	0.00	0.000	0.00	0.000	33.10	0.393	26.92	1.190	24.02	0.927	15.96	0.308
D18_0uM_2	29.67	0.877	0.00	0.000	0.00	0.000	33.56	0.672	27.05	0.974	24.77	1.557	16.64	0.435
D18_0uM_3	29.99	0.645	0.00	0.000	0.00	0.000	33.96	0.594	27.92	0.983	24.66	0.785	16.95	0.527
D18_0.16uM_1	29.65	0.576	0.00	0.000	0.00	0.000	33.71	0.481	29.08	3.938	24.96	0.803	16.94	0.506
D18_0.16uM_2	29.48	0.896	0.00	0.000	0.00	0.000	34.22	0.908	29.74	3.817	23.95	0.536	16.60	0.418
D18_0.16uM_3	29.50	0.932	0.00	0.000	0.00	0.000	34.83	2.184	27.49	1.653	23.97	0.680	16.81	0.487
D18_1.26uM_1	29.44	0.270	0.00	0.000	0.00	0.000	33.76	0.902	28.28	3.029	23.94	0.141	16.62	0.204
D18_1.26uM_2	30.25	0.795	0.00	0.000	0.00	0.000	34.16	0.741	29.03	3.516	24.73	0.625	16.93	0.544
D18_1.26uM_3	29.78	0.540	0.00	0.000	0.00	0.000	34.10	0.180	28.26	2.262	24.54	0.439	17.21	0.470
D18_10uM_1	30.23	2.168	0.00	0.000	0.00	0.000	34.84	1.301	27.50	0.707	24.34	0.784	17.03	0.821
D18_10uM_2	29.70	0.773	0.00	0.000	0.00	0.000	34.60	0.682	27.54	0.708	24.61	0.462	17.28	0.653
D18_10uM_3	38.27	0.111	0.00	0.000	0.00	0.000	0.00	0.000	38.95	1.162	37.04	0.461	30.33	2.590

Table 4.A3: Summary of ΔCq values.

Sample ID	Percent Methylation			
Day_Dose_Replicate	Position 1	Position 2	Position 3	Position 4
6_0uM_1	66.4	77.8	69.7	88.63
6_0uM_2	64.55	69.18	68.22	75.28
6_0uM_3	67.85	72.61	65.19	81.72
6_0.16uM_1	72.03	76.36	65.02	82.78
6_0.16uM_2	65.22	73.04	61.58	79.71
6_0.16uM_3	69.3	70.19	65.2	81.75
6_1.26uM_1	72.76	75.45	64.51	80.48
6_1.26uM_2	59.05	71.8	61.85	78
6_1.26uM_3	63.13	71.95	63.19	79.52
6_10uM_1	61.23	70.49	64.59	80.82
6_10uM_2	68.71	72.78	70.68	79.58
6_10uM_3	62.59	70.08	58.43	78.69
9_0uM_1	61.96	72.09	74.53	85.13
9_0uM_2	52.58	71.55	69.78	77.34
9_0uM_3	71.08	75.2	63.08	81.79
9_0.16uM_1	68.13	75.99	63.74	84.66
9_0.16uM_2	66.9	73.93	66.52	79.39
9_0.16uM_3	62.69	76.29	68.15	77.02
9_1.26uM_1	64.23	70.42	63.18	75.18
9_1.26uM_2	60.56	68.74	66.29	73.85
9_1.26uM_3	59.99	73.33	76.47	83.22
9_10uM_1	70.07	72.85	72.38	75.98
9_10uM_2	67.66	72.34	70.95	79.97
9_10uM_3	65.51	72.04	70.75	81.96
12_0uM_1	59.94	74.84	73.36	78.35
12_0uM_2	63.47	75.04	68.01	76.49
12_0uM_3	56.87	71.8	66.95	73.57
12_0.16uM_1	61.85	76.38	64.63	83.07
12_0.16uM_2	68.86	74.19	62.09	81.48
12_0.16uM_3	63.78	77.24	72.3	81.01
12_1.26uM_1	79.65	78.63	72.6	84.11
12_1.26uM_2	67.21	73.33	75.79	85.93
12_1.26uM_3	73.46	72.21	69.21	82.48
12_10uM_1	56.19	74.1	71.6	77.21
12_10uM_2	61.34	72.74	65.45	83.24
12_10uM_3	59.99	72.2	69.74	75.32
15_0uM_1	65	73.71	65.77	78.04
15_0uM_2	51.64	64.08	55.15	72.75
15_0uM_3	56.71	71.1	65.89	74.33
15_0.16uM_1	62.11	66.35	65.6	76.65
15_0.16uM_2	66.81	71.24	68.64	81.1
15_0.16uM_3	59.79	71.2	71.41	84.66
15_1.26uM_1	58.48	73.17	70.6	77.17
15_1.26uM_2	69.22	72.32	70.83	76.8
15_1.26uM_3	64.15	73.02	65.73	78.39
15_10uM_1	60.19	72.67	64.25	77.62
15_10uM_2	56.76	73.06	71.19	79.61
15_10uM_3	55.35	72.78	62.54	73.69
18_0uM_1	59.81	72.89	67.8	79.29
18_0uM_2	69.81	73.46	73.83	82.32
18_0uM_3	67.3	73.11	76.36	85.74
18_0.16uM_1	55.95	62.01	58.2	72.59
18_0.16uM_2	70.18	72.54	70.9	76.27
18_0.16uM_3	60.98	72.13	74.78	82.98
18_1.26uM_1	66.34	73	64.85	79.2
18_1.26uM_2	69.87	73.52	64.15	80.78
18_1.26uM_3	55.38	61.05	58.7	72.78
18_10uM_1	63.54	68.76	67.23	79.91
18_10uM_2	66.45	74.61	72.74	79.07
18_10uM_3	64.08	76.09	63.88	83.9

Table 4.A4: Summary of L1 DNA methylation pyrosequencing results per sample.

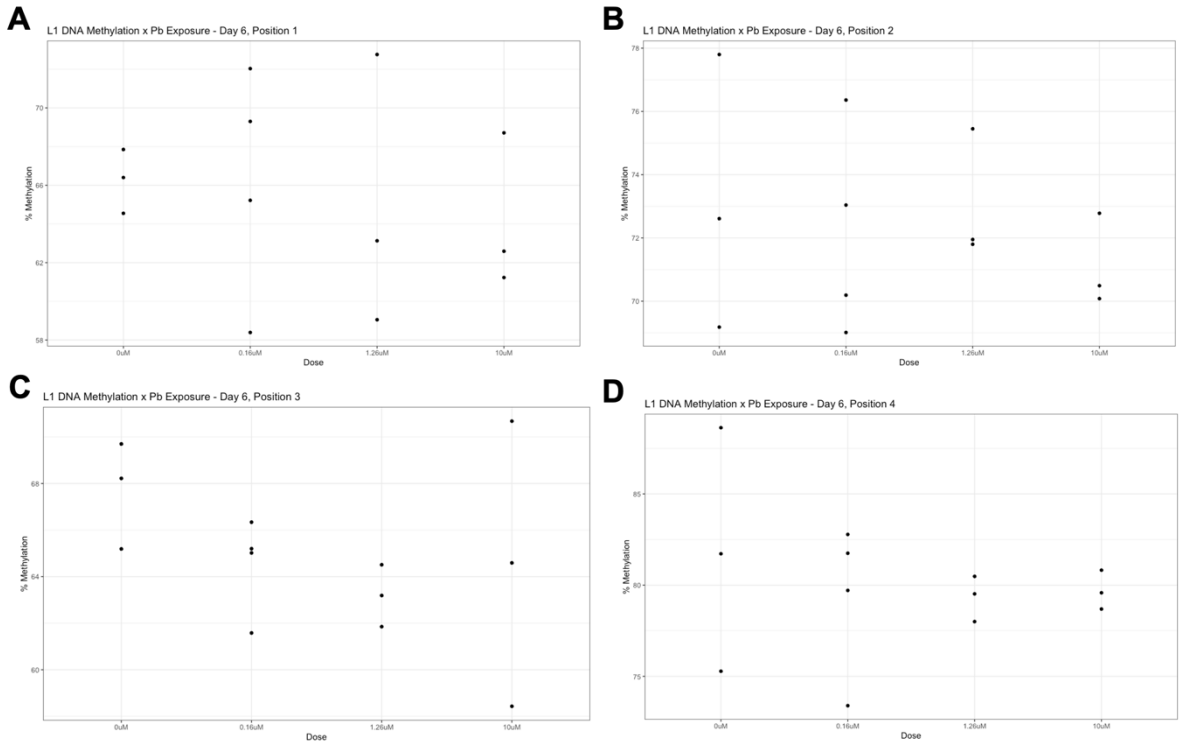

Figure 4.A1: L1 DNA Methylation on Day 6 with Lead Exposure.

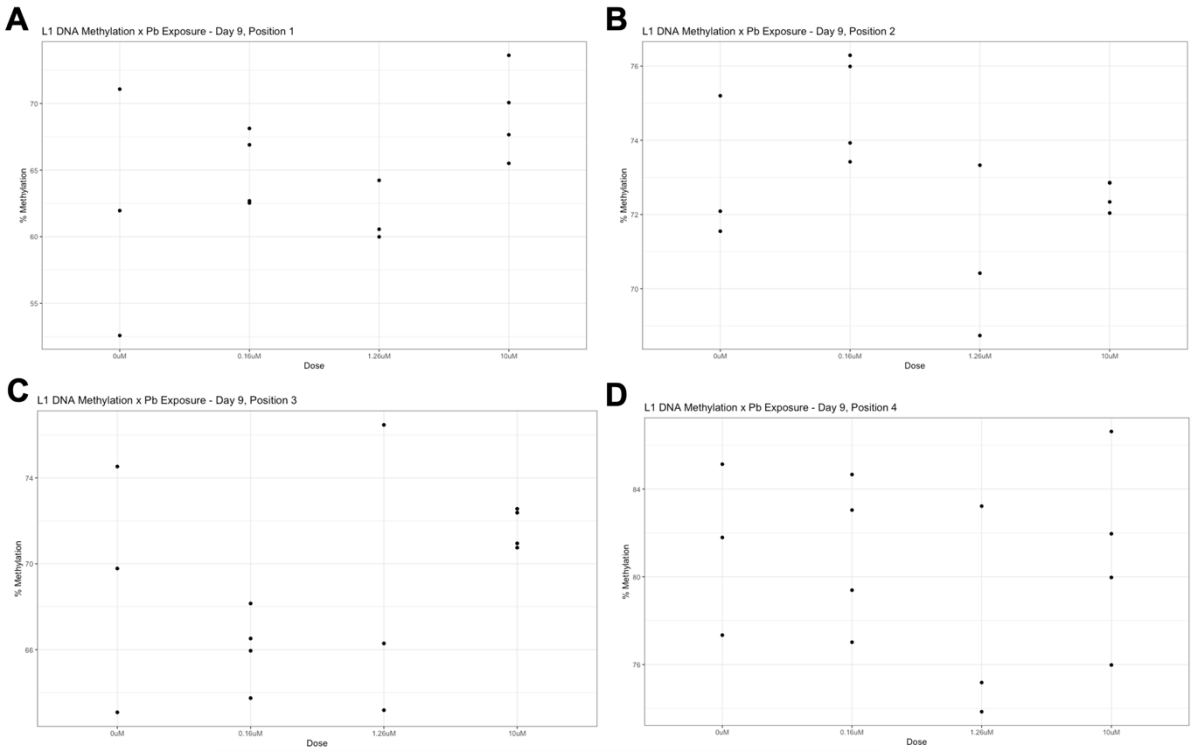

Figure 4.A2: L1 DNA Methylation on Day 9 with Lead Exposure.

Chapter 5

Aim 4: Characterization of piRNA and PIWIL Expression in the Human Soma Reveals Tissue- and Sex-Specific Patterns During Early Development

Abstract

PIWI-interacting RNA (piRNA) are a class of small, non-coding RNA (ncRNA) that, along with PIWI proteins, regulate the expression and patterns of DNA methylation of transposable elements (TEs). This function has been thoroughly characterized in the germline, where piRNA-directed silencing of TEs has been found to be important for gametogenesis and reproductive function in several model organisms. There is relatively little work exploring the presence and function of piRNAs in somatic tissues, though what does exist supports the notion that this class of ncRNA may be important to cellular plasticity and differentiation. Recent work from our group has demonstrated notable expression of this system in murine somatic tissues and while overall expression was found to be lower than that of the germline, there were distinct profiles and targets of piRNA transcripts in each tissue, suggesting tissue-specific functions of this class. Here we expand upon this work, characterizing the expression of piRNA and *PIWIL* mRNA in several human somatic tissues (brain, heart, lung, liver, and kidney) alongside the gonads from an early developmental period (gestational days 90-105), in 5 males and 5 females per tissue type. We identified *PIWIL1* and *PIWIL2* expression, most notably in the brain, heart, and kidney, that was significantly less than that of the gonads ($p < 0.05$) We found *PIWIL3* and/or *PIWIL4* expression to be comparable to ($p >$

0.05) to that of the gonads in nearly all included tissues. Sodium periodate treatment followed by small RNA sequencing allowed for the enrichment of piRNAs in each sample. Sequencing results were cross-referenced with a set of piRNAs previously identified using similar enrichment techniques considered to be gold-standard (e.g., sodium periodate or PIWI co-immunoprecipitation) to determine whether our samples contained piRNAs that have been previously identified. Differential expression analysis was used to define piRNAs by identifying sequences preferentially expressed in treated or untreated samples. The brain contained 1,808 piRNAs, while the heart contained 1,441, the lung contained 1,456, the liver contained 1,562, the kidney contained 1,662, and the gonad contained 1,586. Within each tissue, there was overlap in piRNA presence between the sexes, however each sex-tissue combination did have its own subset of piRNAs that were exclusively expressed in that category, supporting the idea that piRNA may have tissue-specific roles in sexually dimorphic development. Further analysis found overlap of piRNAs within each sex across the somatic tissues, with 706 and 511 piRNAs found in all somatic tissues in males and females, respectively. When the gonads were included, 120 piRNAs were detected in all tissues regardless of sex. Differential expression analysis between the tissues further demonstrated that each somatic tissue contained a number of piRNAs that were significantly expressed relative to others, though this difference was lessened when comparing expression levels in each tissue to the gonads alone. Multi-mapped and uniquely mapped piRNAs in the soma mapped to similar targets as those of the gonads, with LINE-1 elements and regulatory region common targets. These results suggest that while much of our characterization of piRNA has occurred in the gonads, their presence and function may

not be as specific to the germline as previously thought, particularly during early development. A thorough characterization of piRNA expression in the soma will contribute significantly to future toxicological work pertaining to small ncRNA, as well as research on epigenome editing.

Introduction

Non-coding RNA (ncRNA) play important roles in gene expression regulation at the pre- and post-transcriptional levels, and there are several subclasses with distinct biology and modes of action.[1,2] Small ncRNA, those shorter than 200 nucleotides (nt) in length, such as microRNA (miRNA), short interfering RNA (siRNA), and PIWI-interacting RNA (piRNA), regulate gene expression and protein translation in distinct ways.[3] These systems rely on a ncRNA guide, which acts as chaperone for effector proteins, directing them to regions of the genome (constituting RNA-induced transcriptional silencing (RITS) complex) or specific mRNAs (constituting RNA-induced silencing complexes (RISC)).[4,5] Of these, piRNA represent the largest subclass, but is also the least studied in terms of its expression and function in all tissues.[6]

piRNAs have been classically characterized in the germline, where they are potent regulators of transposable elements (TEs).[7] These ncRNA primarily associate with a subset of Argonaute proteins, p-element induced wimpy testis (PIWI) proteins, named for their discovery and relevance in *Drosophila* gametogenesis.[8,9] PIWI proteins in the *Drosophila* are Piwi, Aubergine, and Argonaute3, while those of the mouse are Piwi1 (Miwi), Piwi2 (Mili), and Piwi4 (Miwi2).[10,11] Humans have a fourth protein, with the PIWI-like proteins being PIWIL1 (HIWI), PIWIL2 (HILI), PIWIL3, and PIWIL4 (HILI2).[12] Across species, PIWI proteins play dual roles in the piRNA gene expression regulatory

system. They act in the regulatory function of this class of ncRNA, in that they have been shown to recruit DNA methylation (DNAm) machinery such as DNA methyltransferases (DNMTs) to and to induce chromatin modifications at TEs to minimize their transcription, as well as degrade mRNA once it has been transcribed.[13] PIWI proteins contain several important domains, including the PAZ domain which binds the guide piRNA transcript, the MID domain that attaches to target mRNA, and the PIWI domain which contains endonuclease capabilities and cleaves target mRNA.[14–16]

PIWI proteins are also essential to the biogenesis of piRNA transcripts themselves.[6] piRNA are initially transcribed as precursor RNAs that are processed, in part by PIWI proteins. Primary and secondary piRNA processing pathways have been extensively characterized in *Drosophila*, wherein the primary pathway employs the endonuclease capacity of PIWI/Ago proteins to produce intermediate piRNAs roughly 24-32 nucleotides in length from their precursors, and in the germline, these sequences have a preference for a uridine at the 5' end as well as an adenosine at position 10.[17] These intermediates are eventually methylated at their 3' end by the conserved methyltransferase Hen1 to create a mature and stable piRNA.[18] piRNAs produced via this pathway most often act as guides to piRNA clusters and active transposons in the genome. Transcripts from these locations, along with piRNAs from the primary processing pathway, enter into the "ping-pong- cycle, wherein both transcripts are passed back and forth between PIWI proteins and are eventually also methylated by Hen1, to produce additional piRNA.[19] piRNA biogenesis is a Dicer-independent process, which is notably different from that of miRNA and siRNA, which rely on this enzyme extensively.[20]

The piRNA system has been well characterized in the germline, where this class of ncRNA is essential for proper gamete development and maturation.[21,22] Several landmark studies have characterized increased expression of TEs as well as severe perturbations to gametogenesis with PIWI protein mutations.[23] Given the immense importance of piRNA in the germline, it was long assumed that this was the only location of their expression and function. However, there is mounting evidence of piRNA presence and activity in several somatic tissues, and this has been documented within several experimental models, including the sea slug, mouse, and macaque.[24–26] Our group has previously identified the expression of piRNA and PIWI proteins in the soma of adult mice, with distinct patterns observed in tissues from all three germ layers (e.g., brain, heart, liver, and kidney). This study also employed a rigorous method of isolating piRNAs from other classes of small ncRNA (sodium periodate treatment) meaning that while levels of expression were lower than that of the germline, the reliability of what was identified is robust.[26] An overview of the each component of the piRNA system in humans is described in **Figure 5.1**.

We employed a similar method in an attempt to characterize piRNA and PIWIL expression in human somatic tissues from early development. Here we present evidence of piRNA and *PIWIL* mRNA expression during gestational development, notably with expression comparable to or exceeding that of the germline in some somatic tissues. Given the increasing attention being paid to the differential expression and potential function of piRNA in various disease states and with regard to environmental exposures, as well as its potential use in epigenetic editing, it is essential that a comprehensive baseline of expression in the soma be established.[27–29]

Methods

Somatic Tissues Acquisition

Human gestational tissues were obtained via an NIH-funded biobank through the University of Washington (2R24 HD000836-47), including brain, heart, lung, liver, kidney, and gonadal tissue. Healthy tissues were collected from volunteers undergoing elective pregnancy termination during the first or second trimester, as previously reported on.[30] For the purposes of this work, tissues from gestational days 90-105 were used. Following surgery and donation consent, tissues were flash frozen in liquid nitrogen in polycarbonate-free polypropylene tubes and stored at -80ºC. Samples were shipped to the University of Michigan on dry ice. A total of n = 5 male and n = 5 female samples were used per each of 6 tissues, for a total sample size of n = 60.

RNA Isolation and Gene Expression Analysis

RNA was isolated using the AllPrep DNA/RNA/Protein Mini Kit (Qiagen, Cat. #80004) according to manufacturer protocols. This kit isolates RNA >200nts in length which was subsequently used for *PIWIL* mRNA expression analysis. RNA concentration was quantified using the NanoPhotomoeter system and quality and integrity (RIN) scores were calculate using the QIAxcel Advanced Instrument. RNA quality scores are summarized in **Table 5.A1**.

RNA was reverse transcribed into cDNA using the iScript cDNA Synthesis Kit (Bio-Rad, Cat. #1708890). cDNA was used to quantify *PIWIL* expression in each tissue using custom primer sets from Integrated DNA Technologies (IDT) and primer efficiency was optimized using serial cDNA dilutions. Primer sequences and amplicon sizes are

reported in **Table 5.A2**. mRNA expression was quantified via qRT-PCR on the Applied Biosystems StepOne Real-Time PCR system using SsoAdvanced Universal SYBR Green Supermix (Bio-Rad, Cat. #1725270) and reactions were carried out for 40 cycles and according to standard SYBR Green PCR protocols. mRNA expression was assessed alongside reference gene *ACTG1* (Bio-Rad, assay #qHsaCEP0025243) and blank controls.

Cq values for each sample were obtained in triplicate (n = 3 technical replicates per gene per sample) and the average was taken from these for further analysis. The ΔCq value was calculated by subtracting the mean Cq value of each reference triplicate for a given sample from that of the testing triplicate. The fold difference in *PIWIL* expression relative to that of *ACTG1* was calculated by raising the ΔΔCq as a negative power of 2 ($2^{-\Delta\Delta Cq}$). Differences in the ΔCq of *PIWIL1-4* mRNA in each somatic tissue relative to control was computed using a two-sides t-test in R (v.4.1.2). Statistical significance was accepted with $p < 0.05$ and is designated in figures as * $p < 0.05$, ** $p < 0.01$, *** $p < 0.005$, and **** $p < 0.001$. Data are represented graphically as boxplots, with the median indicated in the box as a horizontal line, using ggplot2.[31] The size of the box represents the interquartile range (IQR), with the 25th and 75th percentile indicated by the lower and upper limits, respectively. The lines extending above and below these plots represent measures that fall within 1.5 times the IQR in either direction, and values that fall beyond these points are those that lie outside of this limit and are represented by dots.

smRNA Isolation, Sodium Periodate Treatment, and smRNA Sequencing

smRNA was isolated using the RNeasy MinElute Cleanup Kit (Qiagen, Cat. #74204) to isolate those RNA transcripts shorter than 200nt in length. Fully mature piRNA transcripts are resistant to β-elimination via sodium periodate treatment due to the presence of the 2'O-methylation modification on their 3' end. Upon treatment, those transcripts without this modification are degraded, leaving an overrepresentation of 2'O-methylated transcripts.[32] Each smRNA sample was divided into 4 aliquots of 400ng each, with 3 undergoing sodium periodate treatment and 1 serving as an untreated control. Sodium periodate treatment consisted of reactions including freshly prepared sodium periodate (Sigma, Cat. #BCBS5360V), 5X borate buffer generated from 150mM borax (Alfa Aesar, Cat. #T29C533) and 150mM boric acid (Fluka Analytics, Cat. #SZBG1280V), adjusted to a pH of 8.6 using sodium hydroxide (Thermo, Cat. #A4782902). A full description of sodium periodate reaction preparation is described in previously published protocols.[26] Sodium periodate treatment technical replicates (n = 3 per sample) were recombined following treatment and, including sodium periodate untreated controls, the final smRNA sample size for library preparation and sequencing was n = 120.

smRNA libraries were prepared at the University of Michigan Advanced Genomics Core using the SMARTer smRNA-Seq Kit (Takara, Cat. #635031) using Takara smRNA Indexing Primer Set HT, which allowed for the pooling of the entire 120-sample library onto one sequencing lane. This kit employs polyadenylation and template switching by extension steps, before adding adapters by PCR. The smRNA library was

cleaned and size-selected using AMPure XP Beads (Fisher, Cat. #NC9933872) and sequenced on a NovaSeq S4 flowcell as a 1x100bp run.

Bioinformatics Identification of piRNA Transcripts

FastQC (v0.11.15)[33] and MultiQC (v1.8)[34] were used to assess quality of all sequenced samples. Trimming, including that of sequencing adapters, was performed according to Takara recommended protocols in order to remove sequencing adapters, poly-adenylated tails, and the first three nucleotides added during the template switching step.[35] Additionally, all reads shorted than 20nt and longer than 45nt in length were removed from downstream analysis. After this quality control and processing, remaining reads were mapped to the reference genome (hg38) using bowtie2 (v2.2.9),[36] with no mismatches allowed. An upper limit of mapping locations was set to 10,000 to maximize the capture of transcripts targeting repetitive elements while also maintaining efficiency in the bioinformatic pipeline. We next wanted to determine whether our samples contained any piRNAs that have been previously identified. To do this, we generated a GTF file of sequences previously documented using methods considered to be gold-standard in the identification of piRNAs (e.g., sodium periodate treatment or PIWI-co-immunoprecipitation).[37] This list contains roughly 77 thousand piRNAs and is publicly available through piRBase. This GTF file was employed as the feature to generate a counts matrix, wherein -O was specified to allow for reads to be assigned to more than one matched meta-feature, -M was specified to ensure multi-mapping reads were counted, and --fraction thus returned counts of 1/(x*y), wherein x is the total number of alignments for a given read and y is the total number of features overlapping with that read.[37,38]

The generated counts matrix for each tissue and sex combination was used to determine which sequences we regarded as true piRNAs in the samples included in this study. While this approach provided us with a summary of what sequences in our data had been previously identified in other work aimed at assessing piRNA expression, we wanted to further refine what we considered to be a piRNA given what we know about gold-standard identification methods. Therefore, we next employed differential expression (DE) analysis using edgeR to determine which sequences were enriched in our treated versus untreated samples (logFC > 0, FDR < 0.05), for each tissue and sex combination, and used these sequences in subsequent analyses.[39] For some analyses, we included those sequences that showed no significant difference in expression between treated and untreated samples (FDR > 0.05), as we regarded these as potential piRNAs and in need of further consideration, and those analyses are designated as such.

Evaluation of piRNA Sequence Overlap Between Tissues and Sexes

The total profiles of piRNAs (including those found to be enriched in the treated samples as well as those for which no difference in expression was detected) in each tissue-sex combination were utilized in initial broad comparisons. For this analysis, we only considered whether a piRNA was detected in a given sample (that is, the list of piRNA IDs in a given matrix) rather than the counts matrix itself, in order to assess general trends in whether tissues and sexes contained overlapping piRNAs with other sample types. Lists of piRNA IDs were generated for each tissue-sex combination and the overlap of IDs between each category of samples was evaluated and illustrated using VennDiagram (v1.7.3).[40] For those piRNAs detected in a given tissue, we

assessed whether there was commonality between the sexes, which provided a sense of the uniqueness of piRNA profiles in a tissue between the sexes. Following this, we used a similar approach to examine the overlap in piRNAs between each somatic tissue for a given sex. In order to most efficiently illustrate the overlap in piRNAs detected in all tissues and sexes, including those of the gonads, we utilized an UpSet plot using UpSetR (v1.4.0),[41] with the same list of IDs employed above, a total nsets of 12, and ordered by frequency.

Enrichment of piRNAs by Tissue and Sex

Our remaining assessments of in which tissues and sexes each piRNA were expressed was conducted utilizing the count matrices generated via the GTF described above. We compiled all count data for each sample into one matrix and performed an initial assessment of sample groupings using multidimensional scaling (MDS) via limma (v3.50.3), with groupings characterized by tissue (col) and sex (pch). The counts matrix was further utilized in the generation of a heatmap using pheatmap (v1.0.12).[42] Counts were converted to counts per million (CPM) and further log transformed (logCPM) for visualization. Final map was clustered by piRNAs (cluster_rows = T) and annotated by tissue type.

Identification of piRNA Targets

piRNA target analysis was split between those deemed to be multi-mapping transcripts (mapped to > 1 location in the genome) and uniquely-mapping transcripts (mapped to one location in the genome). Multi-mapping piRNAs were annotated using Repeat Masker, which is publicly available through UCSC Genome Browser.[43,44]

Uniquely-mapping piRNAs were annotated using annotatr to determine the genomic region they fell within.[45] An overview of the bioinformatics pipeline used for the purposes of this work is described in **Figure 5.2**.

Results

Tissue- and Sex-Specific Patterns of PIWIL mRNA Expression

PIWIL proteins play dual roles in the piRNA system, in that while they elicit much of the regulatory capacity, they are also vital to the biogenesis of piRNA transcripts themselves.[10] We measured mRNA expression of PIWIL proteins using qRT-PCR and SYBR Green chemistry and found detectable levels of these mRNAs in several somatic tissues. A summary of average ΔCq values for each *PIWIL* target, stratified by tissue and sex, can be found in **Table 5.A3**, and a visual representation of this data in **Figure 5.3** has been transformed for adequate visualization.

PIWIL1 expression was greatest in the gonads and significantly exceeded expression levels detected in the somatic tissues, with average ΔCq values of 11.33 ($p < 0.001$) and 9.41 ($p < 0.05$), in males and females, respectively. The somatic tissue with the greatest *PIWIL1* expression was the male and female kidney (average ΔCq values of 14.22 and 14.02, respectively), followed by male and female heart (average ΔCq values of 15.23 and 14.99, respectively). The remaining somatic tissues demonstrated notably lower levels of expression with ΔCq values ranging from 18.12 to 20.42 in the brain, lung, and liver. Overall, while *PIWIL1* was detected in several somatic tissues, its expression was significantly lower than that of the gonads (**Figure 5.3A**).

PIWIL2 expression demonstrated similar overall patterns to that of *PIWIL1*, with the greatest expression seen in the male ($p < 0.05$) and female gonad ($p < 0.001$) (average ΔCq values of 12.66 and 10.79, respectively) and moderate levels of expression among the somatic tissues documented. Male and female brain, heart, and kidney all had average ΔCq values between 14.5 and 16.16, while male and female lung and liver had the lowest levels of *PIWIL2* expression, with ΔCq averages of 16.72 to 16.70 and 16.33 to 16.62, respectively, indicating especially low expression in these tissues (**Figure 5.3B**).

We found relatively low levels of *PIWIL3* expression across all tissues assessed, including the gonads, wherein average ΔCq values for males and females were 19.45 and 17.72, respectively. Comparable levels ($p > 0.05$) were found in the male and female liver (average ΔCq values of 18.44 and 19.16, respectively), as well as brain (average ΔCq values of 19.24 and 19.00, respectively). Lower levels of expression were detected in the kidney (average ΔCq values of 20.39 and 19.91 in males and females, respectively), heart (average ΔCq values of 19.66 and 20.1, respectively), and lung (average ΔCq values of 20.53 and 20.80, respectively), though only that of male kidney was determined to be significantly different from gonadal expression in that sex ($p < 0.05$) (**Figure 5.3C**).

Expression of *PIWIL4* in several somatic tissues was also comparable to that of the gonads, in both males and females. There was no significant difference ($p > 0.05$) in ΔCq values for *PIWIL4* in the brain, heart, kidney, or liver in either sex (average ΔCq range of 12.27 to 14.36 in males and 12.72 to 13.28 in females), relative to the gonads (average ΔCq values of 13.28 and 12.76 in males and females, respectively). Only male

and female liver were determined to have significantly less *PIWIL4* expression, relative to the gonads ($p < 0.01$), with average ΔCq values of 15.85 and 16.06, respectively (**Figure 5.3D**).

Detection of piRNAs in Treated and Untreated Sodium Periodate Samples

Sequenced reads from treated and untreated samples were mapped to the human genome (hg38) and then aligned to piRNAs in piRBase which were previously identified via gold-standard methods. This allowed us to identify sequences in our data that have been reported using techniques that enrich for piRNAs (i.e., PIWI co-immunoprecipitation and/or sodium periodate treatment).[46] A number of individual transcripts were identified as being significantly expressed in the treated versus untreated samples (2,925 in gonad, 2,080 in brain, 1,968 in heart, 2,131 in lung, 2,067 in liver, and 1,670 in kidney) ($FC > 1$ and $FDR < 0.05$) (**Table 5.1**). This analysis also found numerous previously identified piRNAs in the untreated samples, which was unexpected as sodium periodate treatment is expected to enrich for true piRNAs based on their 2'-O methylation on the 3' end, which is resistant to this oxidation reaction. A visual summary of DE analysis between treated and untreated samples in each tissue and sex are presented in **Figure 5.A1-3**.

This approach identified sequences that were present to a significant degree in the untreated versus treated samples ($logFC < 0$ and $FDR < 0.05$), as well as sequences that had no detectable significant difference in expression between these two sample types ($FDR > 0.05$). Sequences with no significant difference in DE between treated and untreated samples were included in some of the downstream analyses below (and are indicated as such), as they were regarded to be "likely" piRNA

transcripts and deserving of additional attention in future work given their previous identification using methods of piRNA enrichment, as indicated by their inclusion in the reference list. Sequences determined to be significantly expressed in the untreated versus treated samples were omitted from subsequent analyses in this study, as they were regarded as unlikely to be piRNAs based on our inability to identify them in our enriched sample set.

Sex-Specificity of Detected piRNAs

Catalogued piRNAs, those determined to be either significantly expressed in the treated samples or those for which no significant difference in expression was found, were compared between males and females of each sex, in order to assess to what degree these transcripts overlapped between the sexes. In the brain, 1,319 piRNAs were identified in both males and females, with 685 detected only in male brain and 76 in female brain (**Figure 5.4A**). A similar pattern presented in the lung and liver, wherein a notable number of piRNAs were identified in both sexes (1,266 in lung and 1,003 in liver), and males had transcripts in the lung (791) and liver (1,019) compared to female lung (74) and liver (45) (**Figure 5.4C-D**). A reversal of this trend was seen in the heart, as there were many piRNAs identified in both sexes (1,031), however females contained a greater number of transcripts detected only in that sex (875) compared to males (62) (**Figure 5.4B**). The kidney contained 1,194 piRNAs that were identified in male and females, with 308 found only in males and 168 found only in females (**Figure 5.4E**). The gonads had the greatest degree of overlap in detected piRNAs with 1,839 identified in both sexes, while male gonad contained 713 piRNAs that females did not, while female gonad contained 373 (**Figure 5.4F**).

piRNA Overlap Between Human Somatic Tissues

Sequences used in the above comparisons were further applied to an assessment of overlap between all five somatic tissues (brain, heart, lung, liver, and kidney) in each sex, and hundreds of piRNAs were observed in both the male and female somatic tissue sets. 706 piRNAs detected in males were detected in all five somatic tissues included in this study, with varying degrees of overlap between other combinations of tissues. Interestingly, the male heart and lung contained the least number of piRNAs specific to those tissues, with 93 and 88 identified in each, respectively. Following these, male brain contained 175 transcripts specific to that somatic tissue, while the liver and kidney contained 196 and 200, respectively (**Figure 5.5**). In the female soma, there appeared to be more tissue-specificity in piRNA expression compared to that of males, particularly within the heart were 614 piRNAs were identified but not in any other somatic tissue examined, whereas 511 piRNAs were detected in all five female somatic tissues included in this study. As in males, the female brain and lung contained few piRNAs specific to each tissue (50 and 112, respectively). Conversely to trends seen in males, fewer transcripts were detected in the female kidney alone (154) as well as the liver (44) (**Figure 5.6**).

In order to evaluate the overlap in identified piRNAs across all tissues studied (somatic tissues as well as the gonads) and between the sexes, an UpSet plot was used. This analysis found 108 previously identified piRNAs to be present in all tissues and both sexes considered in this work. There was notable overlap in several extensive combinations of these variables, such as 64 piRNAs found in all tissues other than male brain, while a further 45 were identified in all samples aside from female gonad, lung,

and liver. The greatest degree of specificity continued to be detected in the female heart, as 101 piRNAs were identified in these tissues and no other combination. Additional female tissues such as gonad, kidney, and lung contained relatively high numbers of piRNAs that were not found in other sex and tissue combinations, with 58 and 48 piRNAs identified in only these tissues, respectively. A full illustration of these comparisons is presented in **Figure 5.7**.

Differential Expression of Detected piRNAs Between Tissues

This broad analysis was motivation to explicitly assess piRNA profiles in each tissue based on counts. To do this, we utilized a curated list of 1,963 piRNAs that were found to be significantly expressed in the treated samples, relative to untreated (FC > 0, FDR < 0.05), omitting those that displayed no significant difference in expression between the treatment groups (FDR > 0.05) from further analysis. This counts-based analysis using pheatmap demonstrated that piRNA profiles in each sample clustered primarily by tissue with distinct groupings that were further subset by sex (**Figure 5.8**). Interestingly, the only sex and tissue combination to not cluster entirely together was female brain, with the piRNA profiles of some samples clustering with female gonad and liver, and another with male gonad and liver. When considering whether both sexes from a given tissue clustered together, only the liver, lung, and kidney had greater degrees of similarity in piRNA profiles between males and females compared to the gonads, brain, and heart. While a number of piRNAs were detected to some degree in the majority of all samples, there are smaller groupings of piRNAs that were detected almost exclusively in certain tissues. For example, female brain and heart both contained a number of piRNAs that were not detected in their respective male

counterparts. Multidimensional scaling was used to identify general trends in sample clustering based on counts of piRNAs in each tissue type and this analysis provided similar trends as those seen in clustering using pheatmap, with liver, kidney, and lung all clustering together and subtler separation based on sex within each cluster. Brain, heart, and gonad samples clustered together, with some separation between the sexes of each group (**Figure 5.A3**).

This broader analysis was motivation to explicitly assess what piRNAs are expressed to a significant degree in one tissue relative to the others. A summary table of the number of piRNAs found to be significantly expressed to a greater degree in one tissue relative to the others is described in **Table 5.A4**. Interestingly, only 131 piRNAs were found to be differentially expressed in the gonads relative to the remaining tissues (**Figure 5.9F**), and all somatic tissues had greater numbers of this measure (340 in brain, 658 in heart, 266 in lung, 171 in liver, and 373 in kidney) (**Figure 5.9A-E**). Relatively few piRNAs were detected in the brain (1), heart (7), lung (16), liver (10), kidney (40), and gonad (15) to a significantly lesser degree than other tissue types, suggesting that while each tissue type has a subset of enriched piRNAs, the remaining transcripts in each tissue profile were likely found to some degree in other tissues studied. When we repeated this analysis for each tissue relative to the gonads alone, we identified fewer piRNAs enriched in each somatic tissue, with 66 detected in the brain, 211 in heart, 46 in lung, 42 in liver, and 284 in kidney (**Table 5.A5** and **Figure 5.10A-E**). These findings reinforce the conclusion that many piRNAs identified in the gonads are found to some degree in various somatic tissue types.

Differentially Expressed piRNAs in the Soma Previously Identified in Existing Databases.

We compared the top differentially expressed piRNAs in the soma to previously existing literature using piRBase to assess whether previous research has identified these transcripts (**Table 5.A6**). We limited this analysis to fifty piRNAs with the highest significant (FDR < 0.05) fold-change in expression, relative to the gonads, and this list included differentially expressed transcripts from brain, heart, lung, and liver. All fifty piRNA have been previously identified in reports utilizing sodium periodate treatment when assessing piRNA expression in either human ovary from a similar developmental period (mid-gestation) or ovaries retrieved during reproductive age. All piRNAs considered in this comparison (50) were previously detected in gestational ovary samples, whereas only 2 were also detected in ovary from reproductive age, suggesting that somatic piRNA expression during periods of development significantly resembles that of the germline.

Targets of Somatic versus Gonadal piRNAs

Lastly, we took the piRNAs that were determined to be significantly expressed in each tissue and determined where they mapped to in the genome (hg38). A summary of target breakdown for multi-mapped as well as unique piRNAs are included in **Tables 5.A7** and **5.A8**. Multi-mapping transcripts mapped to more than 1 location, whereas uniquely mapping transcripts were limited to those that mapped to no more than 1 location.

The targets of multi-mapped piRNAs were broken down by repetitive element families (TE family) included in UCSC Repeat Masker (**Figure 5.11**).[44] The vast majority

of multimapping piRNAs detected in this study were found to map to LINE-1 elements, with the highest proportion seen in the brain (94%), followed by the kidney (84%), heart (83%), liver (81%), and gonad (75%). The lung had comparatively less of these piRNAs map to LINE-1 elements, with only 64% (**Table 5.A7**). Remaining multi-mapped piRNAs in the gonads largely mapped to LTRs, with a small percentage mapping to SINE(Alu (2.2%) or TcMar-Trigger elements (0.1%). While all somatic tissues contained piRNAs that mapped to SINE/Alu elements and at least one LTR family, there were several notable patterns regarding the remaining TE families. Nearly a third (32%) of multi-mapped piRNAs in the lung and 9.3% in the liver mapped to hAT-Tip100 elements, whereas the heart was the only tissue to contain piRNAs that mapped to hAT-Charlie repetitive elements.

The targets of uniquely mapped piRNAs were summarized by genomic region (**Figure 5.12**) and found introns to be the most common designation for brain (49%), heart (56%), lung (34%), liver (33%), kidney (55%), and gonad (55%) (**Table 5.A8**). Genomic regions important to gene expression regulation were the next most mapped-to categories. 1 to 5kb regions, those immediately upstream from promoters were the targets of 10-17% of uniquely mapped piRNAs, depending on tissue. 6-11% of unique piRNAs were found to target CpG shores as well as CpG intergenic regions, with smaller percentages in each tissue targeting other CpG regions such as shelves and islands. There were notable tissue differences in the percentage of unique piRNAs that mapped to promoter regions, with 8-13% in brain, lung, and liver, whereas this fraction in gonad, kidney, and heart was between 0.7% and 5%.

Discussion

PIWIL-Specific Expression in the Soma is Comparable to that of the Gonads. Relative expression of *PIWIL1* and *PIWIL2* in nearly all somatic tissues was lower than that of the gonads, with the exception of *PIWIL1* expression in male kidney as well as *PIWIL2* expression in male brain, heart, and kidney which were all much more comparable. Surprisingly, the expression of *PIWIL3* and *PIWIL4* in many somatic tissues was comparable to or even exceeded that of the gonads, most notably male and female brain, heart, and kidney. To our knowledge, these findings are unique in that it is the first characterization of *PIWIL* expression across an array of somatic tissue types that are not cancerous in nature. Indeed, the expression of *PIWIL* proteins has been well-documented in numerous cancerous tissues, such as bladder, breast, head and neck, and skin cancers.[47–50] Recent studies have begun to draw correlations between *PIWIL* expression and cancer progression and prognosis, with many concluding that elevated *PIWIL* levels are associated with greater rates of malignancy and treatment resistance.[47,51,52] It is suspected that this relationship is at least partially explained by the apparent relevance of PIWIL proteins to stem cell populations.[53] Several studies of PIWIL expression in the soma, in humans as well as several model organisms, has found expression to be associated with stemness, cellular differentiation, and regeneration.[54,55] Cancer is often described as stemness and development gone awry, and so it is unsurprising to see *PIWIL* expression implicated in both of these endpoints.[56]

Given this context, our results demonstrating detectable (*PIWIL1* and *PIWIL2*) expression, as well as levels comparable to or exceeding that of the gonads (*PIWIL3*

and *PIWIL4*) are somewhat expected, as these samples were obtained during a highly dynamic developmental period (gestational days 90-105), wherein stem cell differentiation is happening in earnest in a variety of tissue types throughout the body.[57] What's more, we saw elevated expression of *PIWIL*3 and *PIWIL4* in the developing brain and heart, where notable stem cell populations exist throughout the life course, suggesting that these tissues in particular may maintain this elevated expression past this developmental stage.[58,59] Corresponding work examining *PIWI* expression in several somatic tissues of the adult also found notable levels in the brain and heart, adding confidence to the idea that PIWI proteins may support certain stem cell populations throughout life.[26] This current work also identified notable *PIWIL* expression in the developing kidney and liver, however that of the adult mouse was not as prominent as that of the brain and heart. This may be informed by additional work that has demonstrated the adult kidney and liver to be supported by mesenchymal cells originating from bone marrow,[60,61] and so these tissues in adulthood may have less specific need of the stem-cell supporting function of PIWIL proteins compared to during development.

Previously Identified piRNAs Detected in Somatic Tissues. piRNA make up only a subset of small ncRNA expressed in any given tissue, and there may be ambiguity as to what class a given sequence belongs to if steps to enrich one class over another are not taken. For this reason, we employed sodium periodate treatment, which enriches for sequences with a 2'O-methylation on the 3' end. Given this treatment, we would expect to see substantially more piRNA detection via the employed bioinformatic pipeline in the treated versus untreated samples. This work utilized a list of piRNAs previously

identified using one of two methods considered to be gold-standard (i.e., sodium periodate treatment or PIWI co-immunoprecipitation), available through piRBase. Because of this approach, this work does not include piRNAs that exist in these developing tissues that have not been previously documented, and it would be beneficial to complement this work with additional analyses that attempt to complete this as has been previously described.[26] Upon differential expression analysis between these two sample types, we found that while several hundred of these previously identified piRNAs were detected in the treated samples, a good many were also found to be significantly expressed in the untreated samples and that even more were determined to show no significant expression in either treatment category.

It may be that some sequences included in this list of previously identified piRNAs from co-immunoprecipitation experiments are actually siRNA or miRNA. While piRNA are named for their exclusive interaction with PIWI proteins, it is not a given that PIWI proteins only interact with piRNA, and there is evidence to suggest that PIWI domains may have the capacity to bind other forms of small ncRNA.[62] There is also extensive similarity between PIWI and other Argonaute proteins, in that their domains have been heavily conserved and they are all roughly 90kDa in size.[63] It may be that, without incredibly efficient antibodies, that other Argonaute proteins may be pulled down during co-immunoprecipitation experiments, and their associated small ncRNA may be inadvertently classified as piRNAs. It should also be noted that siRNA have been found to be 2'O-methylated as well, making their degradation by sodium periodate treatment less likely.[64] It is not known whether this gold-standard list of piRNAs was developed using a size-selection step, which would help differentiated the 23-24nt siRNA from the

longer 24-32nt piRNAs. With these considerations in mind, we excluded sequences found to be significantly expressed in the untreated samples from further analysis as it is possible that they are not in fact piRNAs.

Some Sex-Specificity of piRNA Profiles in Each Tissue. There was significant overlap in detected piRNAs between males and females within each tissue, with 63% (1,319/2,080) sequences in common in brain, 52% in heart (1,031/1,968), 59% in lung (1,266/2,131), 48% in liver (1,003/2,067), 71% in kidney (1,194/1,670), and 63% in gonad (1,839/2,925). While this overlap is significant, with roughly half or more of all sequences detected in a given tissue shared between males and females, notable patterns in sex-specific profiles remain. Male brain (685), lung (791), and liver (1,019) all contained more piRNA sequences than their female counterparts (76, 74, and 45, respectively), whereas female heart (875) contained 14 times the number of piRNAs as male heart samples (62). There is evidence of sexually dimorphic gene expression in the development of each of these tissues, and so it is of no surprise that there are distinct profiles of piRNAs between males and females during development as well, though it is worth noting that piRNA presence in both sexes may have been missed due to false negatives.[65–68] It would be prudent to assess whether there is a delineation between where sex-specific and shared piRNAs map to in the genome. It may be that shared sequences are more likely to map to repetitive elements, which require regulation regardless of sex, whereas sex-specific piRNAs may map to particular genes related to the organ development along sex-specific patterns.

Differential Expression of piRNAs Greater in the Soma than in the Gonads. Differential expression analysis between tissue types was conducted in two ways. First,

expression differences of in each tissue were calculated relative to all other tissues studied (including the gonads), and second, differential expression in each somatic tissue was calculated relative to the gonads alone. No significant differences in expression were found for the majority of piRNAs between tissue types, much as was seen in the comparison of expression profiles across sex. 83% (1,622/1,963) of piRNAs in the brain demonstrated no significant differential expression when compared to remaining tissues, and this trend was replicated in the heart (66%, 1,298/1,963), lung (86%, 1,681/1,963), liver (91%, 1,782/1,963), kidney (79%, 1,550/1,963), and the gonads (93%, 1,817/1,963).

We found an even greater degree of overlap when we examined the number of non-differentially expressed piRNAs in each somatic tissue relative to only the gonads. 96% (1,889/1,963) of sequences identified in the brain were also found in the gonads, with similar trends seen across remaining somatic tissues. Previous work in adult mice found hippocampal and testicular piRNA distributions to be similar, in that they had the highest levels of piRNA expression as well as the greatest number of piRNAs mapping to repetitive elements.[26] The hippocampus is a major location of neural stem cells, both during development as well as throughout life, and it may be that the significant degree of overlap in piRNAs identified in this work is informed by an elevated need for the orchestration of stemness and TE regulation.[69] Interestingly, previous work has also documented similarities in piRNA profiles between the brain and testis in mice at several developmental time points and found greater correlation in adult tissues relative to those from post-natal days 10 and 14.[70] The work presented here entailed the use of

whole brain samples, and as such, our results may mask region-specific correlations with the gonads that explain the discrepancy with this previously published work.

As with the sex-specific profiles discussed above, the remaining piRNAs that were found to be differentially expressed in each tissue type cannot be discounted. The proportion of piRNAs expressed to a significant degree in one tissue relative to the others ranged from 7% and 9% in the gonads (131/1,963) and liver (171/1,963), to 14%, 17%, and 19% in the lung (266/1,963), brain (340/1,963), and kidney (373/1,963), respectively, and got as high as 33% in the heart (685/1,963). As with previous work that found tissue-specific profiles of piRNAs in various somatic tissues, these results highlight that there is likely tissue- and/or cell-type specific roles for this class of ncRNA. Much of the available literature conducted in adult tissues found relatively little overlap, either via general comparisons of piRNA presence between somatic tissues and the gonads, or via differential expression analysis relative to what was found here.[25,26] As such, it is hypothesized that the degree of uniqueness in piRNA profiles in individual tissues intensifies with age, and developmental periods contain much more similarity in sequences between the soma and that of the germline.

Differentially Expressed piRNAs Previously Documented in Developing Ovary. In our comparison of the top differentially expressed piRNAs to the currently available literature, we found significant overlap with previous work cataloging piRNA in developmental ovary samples.[71] The similarities between these two studies are not surprising given the significant overlap between piRNAs and the gonads identified in this current work, the utilization of tissues from comparable time points, and also that both studies employed the same method of piRNA enrichment. The roughly one-third of

piRNAs identified in this previous work mapped to repetitive elements, suggesting that the remaining piRNA have other regulatory functions in that tissue during early development.

piRNAs in the Soma Primarily Target LINE-1 Elements and Introns. Our analysis of genomic targets of both multimapping and unique piRNAs presented evidence that, at least for those piRNAs detected in this study that have been previously identified in the germline, there is a good deal of similarity between the soma and the germline in terms of where these transcripts map. Multimapping piRNAs, that is those sequences that map to repetitive elements in the genome, largely mapped to LINE-1 elements (65-94% of multi-mapped piRNAs, depending on tissue). This suggests that during early development in the soma, these transcripts contain LINE-1 specific silencing functions similar to those in the developing germline.[22,74] There were also similar proportions of multi-mapped piRNAs mapping to SINE/Alu elements and TcMar, again suggesting similar functions between the soma and the germline during this developmental window. Several tissues, most commonly brain and kidney, contained LTR-specific piRNAs, along with the gonads. Alternatively, whereas hAT-targeted piRNAs were exclusively detected in the heart, and TcMar-targeted piRNAs were only detected in the kidney, liver, and lung, and while these TE families are considered to be inactive,[75] there may be tissue-specific biology during early development that explains why these patterns emerged.

Uniquely mapping (those that did not map to a repetitive element) piRNAs largely targeted introns in the brain, heart, kidney, and gonad, with a reduced fraction targeting these regions in the liver and lung. Comparable proportions of piRNAs in the soma and

gonads mapped to 1 to 5kb regions, as well as CpG-rich regions, suggesting that in both the soma and the germline during early development, uniquely mapping piRNAs may play regulatory roles in the expression of non-TE genes. This function of piRNA has been explored with regard to cancer biology, with several studies documenting piRNAs targeting CpG and transcriptional regulatory regions,[76,77] though additional work is needed to understand how these unique piRNAs function in healthy and developing somatic tissues. One study does document piRNA-directed methylation of a conserved CpG island in the CREB2 promoter, an important factor in memory formation,[78] however we identified 873 genes to which unique piRNAs mapped (**Table 5.A9**). Considering that this work does not include piRNAs in these tissues that have not yet been documented, there may be additional non-TE targets of piRNAs in the soma, emphasizing the need for continued research into the role of piRNA regulation outside of repetitive elements.

Limitations

Studies in human tissues are difficult in that tissue collection and storage can pose significant challenges to downstream applications (as demonstrated by the RIN scores of the total RNA, **Table 5.A1**) due to sample quality. Moreover, whole organ tissues were collected, preventing the assessment of region- or cell-specific expression patterns. Additionally, while the gonads served as our measure of germline expression, it should be noted that the gonads themselves contain somatic tissues, which may have affected the results seen here.[79] Finally, given the use of a reference catalogue of piRNAs previously identified using gold standard methods, we were unable to identify any new piRNA transcripts in this study. Future work would benefit from efforts to

employ methods aimed at discovering previously unidentified piRNAs in order to create a full profile of expression in these tissues.

Conclusion

To our knowledge, this study if the first of its kind to rigorously evaluate the expression of *PIWIL* expression and piRNA profiles in several somatic tissues from an early developmental period. These results highlight apparent similarities in piRNA expression in developing tissues and the germline, suggesting previous conclusions that the germline was the main site of piRNA expression may be incorrect, especially when considering developmental stages. This work also demonstrates that there are, to some degree, unique piRNA profiles in each tissue and sex, and these tissue-specific transcripts may play roles in sexually dimorphic development. This hypothesis can be further evaluated by exploring the targets of both multi- and uniquely mapped piRNAs in order to ascertain whether regulatory patterns are unique to certain tissues and sexes. Taken together, this study emphasizes the importance of considering piRNA in future toxicological work, as developmental exposures in particular may alter this system in ways that have repercussions for tissue development and function. This work also highlights the potential for piRNA use in epigenomic editing, as the identification of tissue-specific piRNAs may provide avenues for editing that are targeted and specific to a tissue or cell type of interest.

Acknowledgements

This work was supported and guided in large part by Dr. Dana Dolinoy, who provided extensive advice and feedback to the development of the experiments

described here as well as of this chapter, and her support throughout this process is greatly appreciated. Dr. Bambarendage Perera provided additional support and guidance in getting this project off the ground, including qRT-PCR primer design. Dr. Kai Wang and Dr. Justin Colacino were immensely helpful in the smRNA sequencing analysis and helped ensure the bioinformatics analysis of this data was thorough. Given the obstacles faced during the completion of this work, the people mentioned above were integral to ensuring this study was completed. I would also like to thank Katelyn Polemi and Tamara Jones for this assistance in the bench work that was required as a part of this study, including sorting through boxes of samples, optimizing assays, and research support. Finally, thanks go out to Melissa Coon and the UM Advanced Genomics Core, for their assistance in the preparation of and sequencing of the smRNA libraries. This work was supported by funding from the following sources: NIEHS Grant R35 (ES031686), NIEHS Grant K01 (ES032048), NIEHS Grant R01 (ES028802), the Michigan Lifestage Environmental Exposures and Disease (M-LEEaD) NIEHS Core Center (P30 ES017885), Institutional Training Grant T32 (ES007062), Institutional Training Grant T32 (HD079342), and National Institute of Aging (NIA) Grant R01 (AG072396).

References

1. Mattick, J. S. & Makunin, I. V. Non-coding RNA. *Hum. Mol. Genet.* **15 Spec No 1**, R17-29 (2006).

2. Zhang, P., Wu, W., Chen, Q. & Chen, M. Non-Coding RNAs and their Integrated Networks. *J. Integr. Bioinforma.* **16**, 20190027 (2019).

3. Shi, J., Zhou, T. & Chen, Q. Exploring the expanding universe of small RNAs. *Nat. Cell Biol.* **24**, 415–423 (2022).

4. Bhattacharjee, S., Roche, B. & Martienssen, R. A. RNA-induced initiation of transcriptional silencing (RITS) complex structure and function. *RNA Biol.* **16**, 1133–1146 (2019).

5. Iwakawa, H.-O. & Tomari, Y. Life of RISC: Formation, action, and degradation of RNA-induced silencing complex. *Mol. Cell* **82**, 30–43 (2022).

6. Czech, B. *et al.* piRNA-Guided Genome Defense: From Biogenesis to Silencing. *Annu. Rev. Genet.* **52**, 131–157 (2018).

7. Tóth, K. F., Pezic, D., Stuwe, E. & Webster, A. The piRNA Pathway Guards the Germline Genome Against Transposable Elements. *Adv. Exp. Med. Biol.* **886**, 51–77 (2016).

8. Lin, H. & Spradling, A. C. A novel group of pumilio mutations affects the asymmetric division of germline stem cells in the Drosophila ovary. *Dev. Camb. Engl.* **124**, 2463–2476 (1997).

9. Grivna, S. T., Beyret, E., Wang, Z. & Lin, H. A novel class of small RNAs in mouse spermatogenic cells. *Genes Dev.* **20**, 1709–1714 (2006).

10. Thomson, T. & Lin, H. The Biogenesis and Function of PIWI Proteins and piRNAs: Progress and Prospect. *Annu. Rev. Cell Dev. Biol.* **25**, 355–376 (2009).

11. Ding, D. *et al.* Mitochondrial membrane-based initial separation of MIWI and MILI functions during pachytene piRNA biogenesis. *Nucleic Acids Res.* **47**, 2594–2608 (2019).

12. Ross, R. J., Weiner, M. M. & Lin, H. PIWI proteins and PIWI-interacting RNAs in the soma. *Nature* **505**, 353–359 (2014).

13. Mann, J. R. & Mattiske, D. M. RNA interference in mammalian DNA methylation. *Biochem. Cell Biol. Biochim. Biol. Cell.* **90**, 70–77 (2012).

14. Simon, B. *et al.* Recognition of 2'-O-methylated 3'-end of piRNA by the PAZ domain of a Piwi protein. *Struct. Lond. Engl. 1993* **19**, 172–180 (2011).

15. Parker, J. S., Parizotto, E. A., Wang, M., Roe, S. M. & Barford, D. Enhancement of the seed-target recognition step in RNA silencing by a PIWI/MID domain protein. *Mol. Cell* **33**, 204–214 (2009).

16. Jin, S., Zhan, J. & Zhou, Y. Argonaute proteins: structures and their endonuclease activity. *Mol. Biol. Rep.* **48**, 4837–4849 (2021).

17. Huang, X., Fejes Tóth, K. & Aravin, A. A. piRNA Biogenesis in Drosophila melanogaster. *Trends Genet. TIG* **33**, 882–894 (2017).

18. Horwich, M. D. *et al.* The Drosophila RNA methyltransferase, DmHen1, modifies germline piRNAs and single-stranded siRNAs in RISC. *Curr. Biol. CB* **17**, 1265–1272 (2007).

19. Czech, B. & Hannon, G. J. One Loop to Rule Them All: The Ping-Pong Cycle and piRNA-Guided Silencing. *Trends Biochem. Sci.* **41**, 324–337 (2016).

20. Yadav, R. P. & Kotaja, N. Small RNAs in spermatogenesis. *Mol. Cell. Endocrinol.* **382**, 498–508 (2014).

21. Dai, P. *et al.* A Translation-Activating Function of MIWI/piRNA during Mouse Spermiogenesis. *Cell* **179**, 1566-1581.e16 (2019).

22. Zhang, H. *et al.* The piRNA pathway is essential for generating functional oocytes in golden hamsters. *Nat. Cell Biol.* **23**, 1013–1022 (2021).

23. Théron, E. *et al.* The interplay between the Argonaute proteins Piwi and Aub within Drosophila germarium is critical for oogenesis, piRNA biogenesis and TE silencing. *Nucleic Acids Res.* **46**, 10052–10065 (2018).

24. Moazed, D. A piRNA to remember. *Cell* **149**, 512–514 (2012).

25. Yan, Z. *et al.* Widespread expression of piRNA-like molecules in somatic tissues. *Nucleic Acids Res.* **39**, 6596–6607 (2011).

26. Perera, B. P. U. *et al.* Somatic expression of piRNA and associated machinery in the mouse identifies short, tissue-specific piRNA. *Epigenetics* **14**, 504–521 (2019).

27. Liu, Y. *et al.* The emerging role of the piRNA/piwi complex in cancer. *Mol. Cancer* **18**, 123 (2019).

28. Toth, G. P. *et al.* Development of omics biomarkers for estrogen exposure using mRNA, miRNA and piRNAs. *Aquat. Toxicol. Amst. Neth.* **235**, 105807 (2021).

29. Perera, B. P. U. *et al.* PIWI-Interacting RNA (piRNA) and Epigenetic Editing in Environmental Health Sciences. *Curr. Environ. Health Rep.* **9**, 650–660 (2022).

30. Nahar, M. S., Liao, C., Kannan, K. & Dolinoy, D. C. Fetal Liver Bisphenol A Concentrations and Biotransformation Gene Expression Reveal Variable Exposure and

Altered Capacity for Metabolism in Humans. *J. Biochem. Mol. Toxicol.* **27**, 116–123 (2013).

31. Create Elegant Data Visualisations Using the Grammar of Graphics. https://ggplot2.tidyverse.org/.

32. Ohara, T. *et al.* The 3′ termini of mouse Piwi-interacting RNAs are 2′-O-methylated. *Nat. Struct. Mol. Biol.* **14**, 349–350 (2007).

33. Andrews. FastQC A Quality Control tool for High Throughput Sequence Data. https://www.bioinformatics.babraham.ac.uk/projects/fastqc/ (2010).

34. Ewels, P., Magnusson, M., Lundin, S. & Käller, M. MultiQC: summarize analysis results for multiple tools and samples in a single report. *Bioinforma. Oxf. Engl.* **32**, 3047–3048 (2016).

35. SMARTer smRNA-Seq Kit for Illumina—sequence small RNAs with high sensitivity and minimal bias. https://www.takarabio.com/products/next-generation-sequencing/epigenetics-and-small-rna-sequencing/small-rna-seq-kit.

36. Langmead, B. & Salzberg, S. L. Fast gapped-read alignment with Bowtie 2. *Nat. Methods* **9**, 357–359 (2012).

37. Wang, J. *et al.* piRBase: a comprehensive database of piRNA sequences. *Nucleic Acids Res.* **47**, D175–D180 (2019).

38. bedtools: a powerful toolset for genome arithmetic — bedtools 2.31.0 documentation. https://bedtools.readthedocs.io/en/latest/.

39. Chen, Y. *et al.* edgeR: Empirical Analysis of Digital Gene Expression Data in R. (2023) doi:10.18129/B9.bioc.edgeR.

40. pheatmap function - RDocumentation. https://www.rdocumentation.org/packages/pheatmap/versions/1.0.12/topics/pheatmap.

41. Taubert, H. *et al.* Piwil 2 expression is correlated with disease-specific and progression-free survival of chemotherapy-treated bladder cancer patients. *Mol. Med. Camb. Mass* **21**, 371–380 (2015).

42. Qian, L. *et al.* Piwi-Interacting RNAs: A New Class of Regulator in Human Breast Cancer. *Front. Oncol.* **11**, 695077 (2021).

43. Chattopadhyay, T., Biswal, P., Lalruatfela, A. & Mallick, B. Emerging roles of PIWI-interacting RNAs (piRNAs) and PIWI proteins in head and neck cancer and their potential clinical implications. *Biochim. Biophys. Acta Rev. Cancer* **1877**, 188772 (2022).

44. Pammer, J. *et al.* PIWIL-2 and piRNAs are regularly expressed in epithelia of the skin and their expression is related to differentiation. *Arch. Dermatol. Res.* **312**, 705–714 (2020).

45. Al-Janabi, O. *et al.* Piwi-like 1 and 4 gene transcript levels are associated with clinicopathological parameters in renal cell carcinomas. *Biochim. Biophys. Acta* **1842**, 686–690 (2014).

46. Heng, Z. S. L. *et al.* The role of 17β-estradiol-induced upregulation of Piwi-like 4 in modulating gene expression and motility in breast cancer cells. *Oncol. Rep.* **40**, 2525–2535 (2018).

47. Ma, X. *et al.* Piwi is required in multiple cell types to control germline stem cell lineage development in the Drosophila ovary. *PloS One* **9**, e90267 (2014).

48. Yakushev, E. Y., Sokolova, O. A., Gvozdev, V. A. & Klenov, M. S. Multifunctionality of PIWI proteins in control of germline stem cell fate. *Biochem. Biokhimiia* **78**, 585–591 (2013).

49. Rojas-Ríos, P. & Simonelig, M. piRNAs and PIWI proteins: regulators of gene expression in development and stem cells. *Development* **145**, (2018).

50. Aponte, P. M. & Caicedo, A. Stemness in Cancer: Stem Cells, Cancer Stem Cells, and Their Microenvironment. *Stem Cells Int.* **2017**, (2017).

51. Reynolds, L. P. *et al.* Developmental Programming of Fetal Growth and Development. *Vet. Clin. North Am. Food Anim. Pract.* **35**, 229–247 (2019).

52. Kalamakis, G. *et al.* Quiescence Modulates Stem Cell Maintenance and Regenerative Capacity in the Aging Brain. *Cell* **176**, 1407-1419.e14 (2019).

53. Laflamme, M. A. & Murry, C. E. Heart Regeneration. *Nature* **473**, 326–335 (2011).

54. Grange, C., Skovronova, R., Marabese, F. & Bussolati, B. Stem Cell-Derived Extracellular Vesicles and Kidney Regeneration. *Cells* **8**, 1240 (2019).

55. Pittenger, M. F. *et al.* Multilineage potential of adult human mesenchymal stem cells. *Science* **284**, 143–147 (1999).

56. Parker, J. S., Roe, S. M. & Barford, D. Crystal structure of a PIWI protein suggests mechanisms for siRNA recognition and slicer activity. *EMBO J.* **23**, 4727–4737 (2004).

57. Farazi, T. A., Juranek, S. A. & Tuschl, T. The growing catalog of small RNAs and their association with distinct Argonaute/Piwi family members. *Development* **135**, 1201–1214 (2008).

58. Dimitrova, D. G., Teysset, L. & Carré, C. RNA 2′-O-Methylation (Nm) Modification in Human Diseases. *Genes* **10**, 117 (2019).

59. Deegan, D. F., Karbalaei, R., Madzo, J., Kulathinal, R. J. & Engel, N. The developmental origins of sex-biased expression in cardiac development. *Biol. Sex Differ.* **10**, 46 (2019).

60. Savic, I., Garcia-Falgueras, A. & Swaab, D. F. Chapter 4 - Sexual differentiation of the human brain in relation to gender identity and sexual orientation. in *Progress in Brain Research* (ed. Savic, I.) vol. 186 41–62 (Elsevier, 2010).

61. Lowe, R., Gemma, C., Rakyan, V. K. & Holland, M. L. Sexually dimorphic gene expression emerges with embryonic genome activation and is dynamic throughout development. *BMC Genomics* **16**, 295 (2015).

62. Gortner, L., Shen, J. & Tutdibi, E. Sexual dimorphism of neonatal lung development. *Klin. Padiatr.* **225**, 64–69 (2013).

63. Kirby, E. D., Kuwahara, A. A., Messer, R. L. & Wyss-Coray, T. Adult hippocampal neural stem and progenitor cells regulate the neurogenic niche by secreting VEGF. *Proc. Natl. Acad. Sci. U. S. A.* **112**, 4128–4133 (2015).

64. Ghosheh, Y. *et al.* Characterization of piRNAs across postnatal development in mouse brain. *Sci. Rep.* **6**, 25039 (2016).

65. Roovers, E. F. *et al.* Piwi Proteins and piRNAs in Mammalian Oocytes and Early Embryos. *Cell Rep.* **10**, 2069–2082 (2015).

66. Sabbah, N. A. *et al.* piRNA-823 Is a Unique Potential Diagnostic Non-Invasive Biomarker in Colorectal Cancer Patients. *Genes* **12**, 598 (2021).

67. Yin, J. *et al.* Small RNA sequencing revealed aberrant piRNA expression profiles in colorectal cancer. *Oncol. Rep.* **42**, 263–272 (2019).

68. Aravin, A. A. *et al.* A piRNA Pathway Primed by Individual Transposons Is Linked to De Novo DNA Methylation in Mice. *Mol. Cell* **31**, 785–799 (2008).

69. Kojima, K. K. Human transposable elements in Repbase: genomic footprints from fish to humans. *Mob. DNA* **9**, 2 (2018).

70. Zhang, L. *et al.* piR-31470 epigenetically suppresses the expression of glutathione S-transferase pi 1 in prostate cancer via DNA methylation. *Cell. Signal.* **67**, 109501 (2020).

71. Fu, A., Jacobs, D. I. & Zhu, Y. Epigenome-wide analysis of piRNAs in gene-specific DNA methylation. *RNA Biol.* **11**, 1301–1312 (2014).

72. Rajasethupathy, P. *et al.* A Role for Neuronal piRNAs in the Epigenetic Control of Memory-Related Synaptic Plasticity. *Cell* **149**, 693–707 (2012).

73. Piprek, R. P., Rams-Pociecha, I., Zdanowski, R., Kloc, M. & Kubiak, J. Z. Desmoplakin (Dsp) conditional knockout in NR5A1+ somatic cells affects germ cell survival in developing mouse gonads. *Reprod. Camb. Engl.* **163**, 199–207 (2022).

Figures and Tables

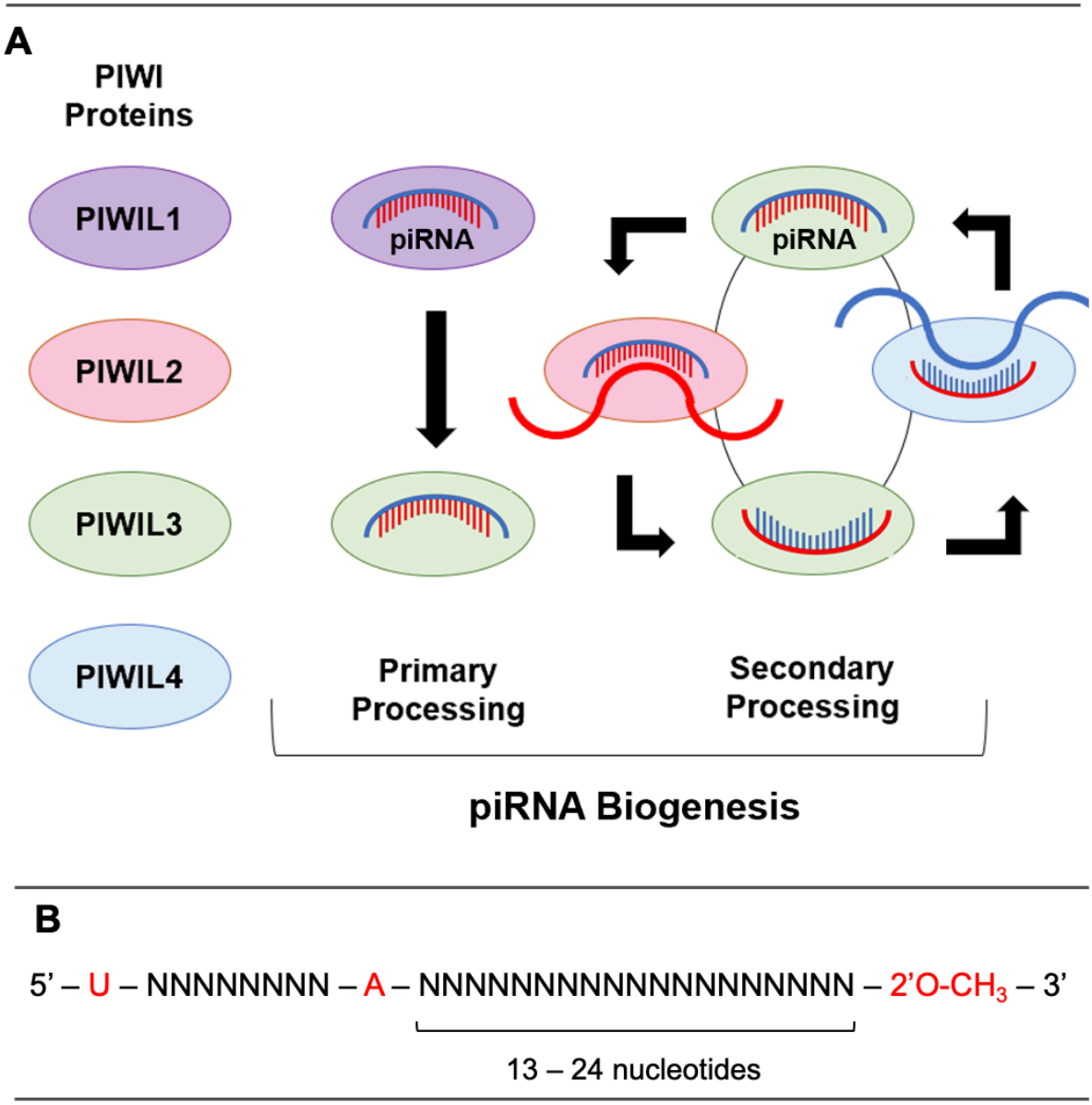

Figure 5.1: Overview of the Human piRNA System. A) PIWIL proteins 1-4 are important players in the biogenesis of piRNAs, via a primary and secondary processing pathway. B) Fully mature piRNA transcripts are 24-35 nucleotides in length, have a preference for a 5' uridine signature and an adenosine at position 10, and are 2'O-methylated on the 3' end.

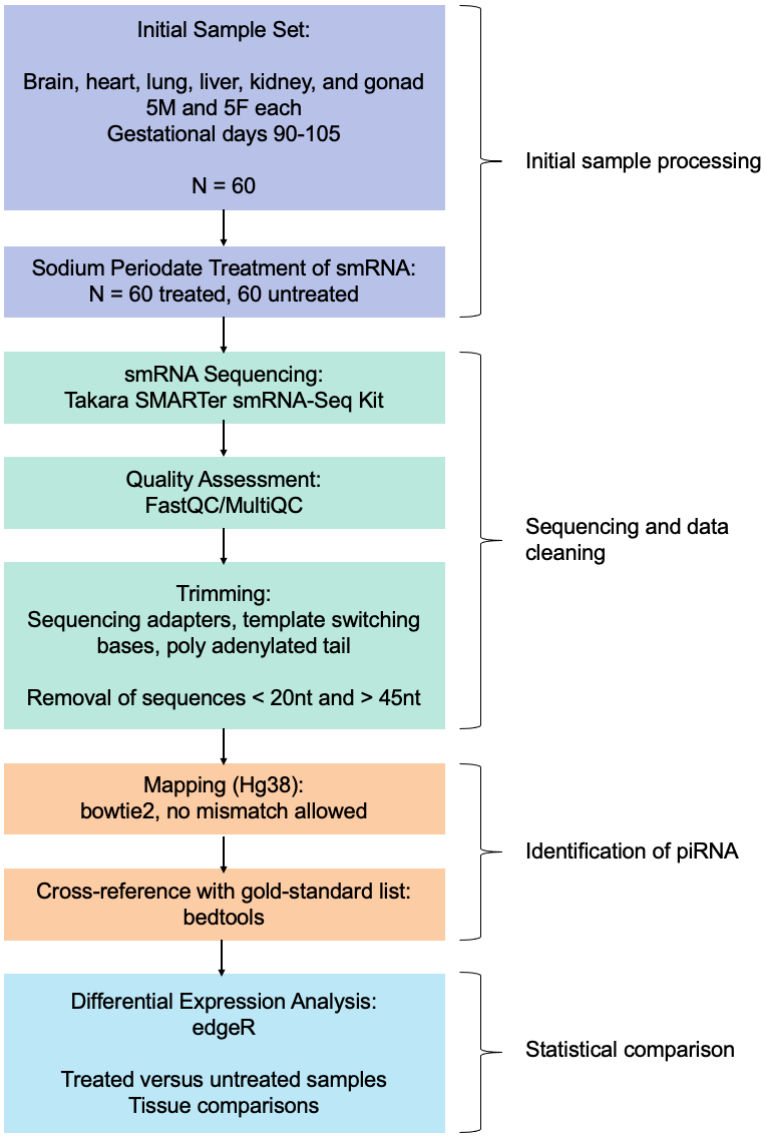

Figure 5.2: Sample Processing and Bioinformatics Pipeline. Brain, heart, lung, liver, kidney, and gonad tissues were collected from 5 males and 5 females each at gestational days 90-105. smRNA was extracted and subjected to sodium periodate treatment, after which samples were sequenced via smRNA sequencing. Sequencing results were quality controlled and trimmed according to manufacturer recommendations, and subsequent reads were mapped to hg38. Mapped reads were cross-referenced with a gold-standard set of piRNAs from piRBase to identify piRNAs. Differential expression analysis was conducted to assess expression in treated versus untreated samples as well as between tissue types.

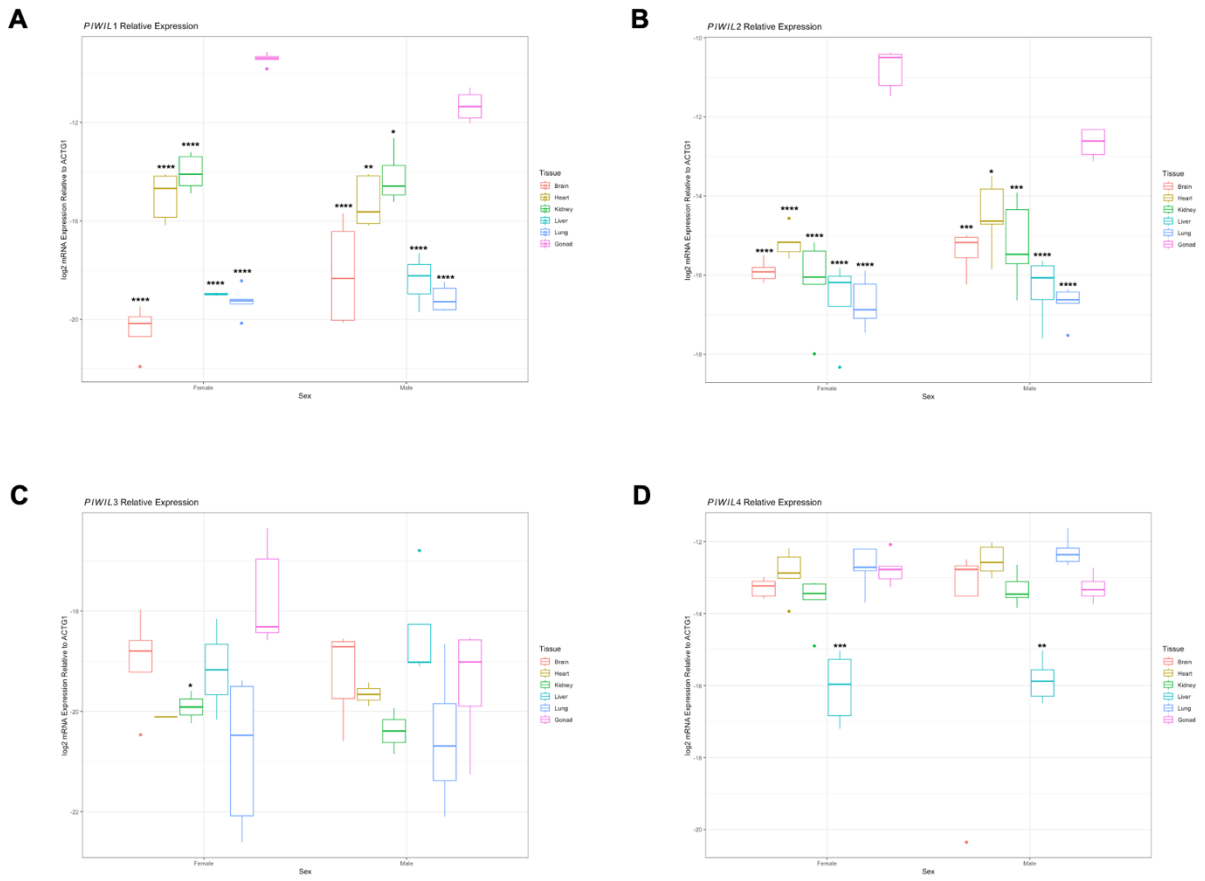

Figure 5.3: Relative mRNA Expression of PIWIL1-4. mRNA expression of A) PIWIL1, B) PIWIL2, C) PIWIL3, and D) PIWIL4 was quantified via qRT-PCR, relative to ACTG1. Significant differences are indicated as * $p < 0.05$, ** $p < 0.01$, *** $p < 0.005$, and **** $p < 0.001$.

	Gonad		Brain		Heart		Lung		Liver		Kidney	
	M	F	M	F	M	F	M	F	M	F	M	F
Sig. Exp. In Treated	840	746	971	837	534	907	837	619	963	599	889	773
No Sig. Difference	1712	1466	839	558	559	999	1220	721	1059	449	613	589
Sig. Exp. In Untreated	708	1229	1087	1132	985	1303	924	942	744	1576	1718	1416

Table 5.1: Summary of Differentially Expressed piRNA in Treated versus Untreated Samples. edgeR was used to assess the number of piRNAs detected to a significant degree in treated versus untreated samples (dark blue), as well as those expressed to a significant degree in untreated samples (white) and those for which no significant difference in expression was detected (light blue). Significance was determined via a combined fold change > 0 and $p < 0.05$.

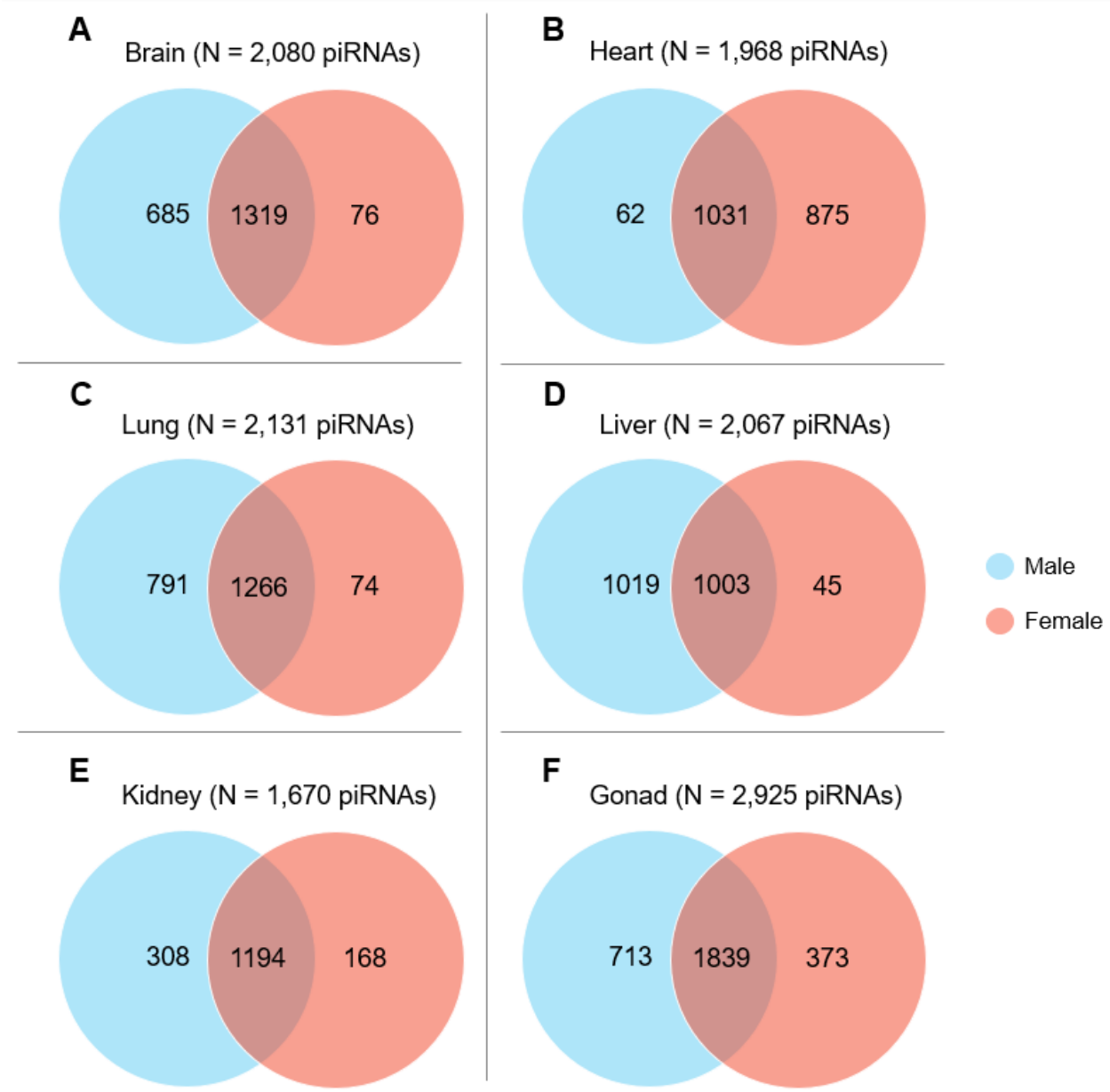

Figure 5.4: Overlap of Detected piRNAs Between Males and Females. Catalogues of male and female piRNAs in A) brain, B) heart, C) lung, D) liver, E) kidney, and F) gonad were compared to assess degrees of overlap.

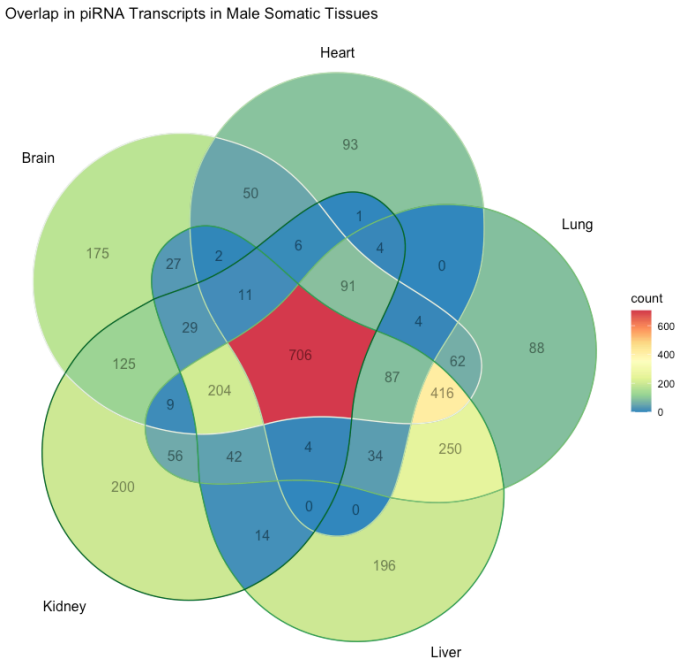

Figure 5.5: Overlap in piRNAs Detected in Male Somatic Tissues. piRNAs in male brain, heart, lung, liver, and kidney were compared to assess degrees of overlap.

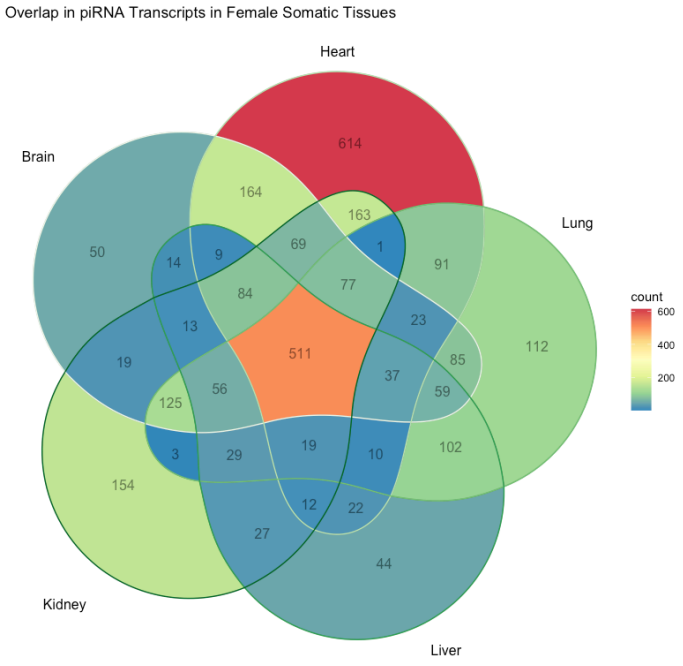

Figure 5.6: Overlap in piRNAs Detected in Female Somatic Tissues. piRNAs in female brain, heart, lung, liver, and kidney were compared to assess degrees of overlap.

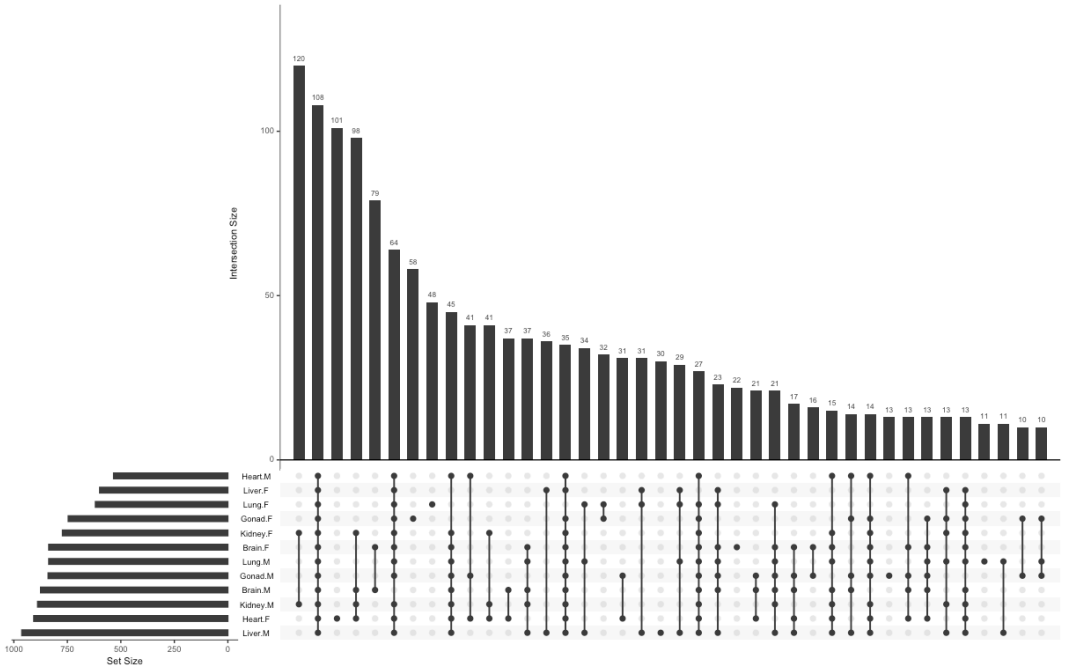

Figure 5.7: UpSet Plot of piRNA Detection Across All Tissues and Sexes. Tissue- and sex-specific catalogues of piRNAs were compared to assess overlap.

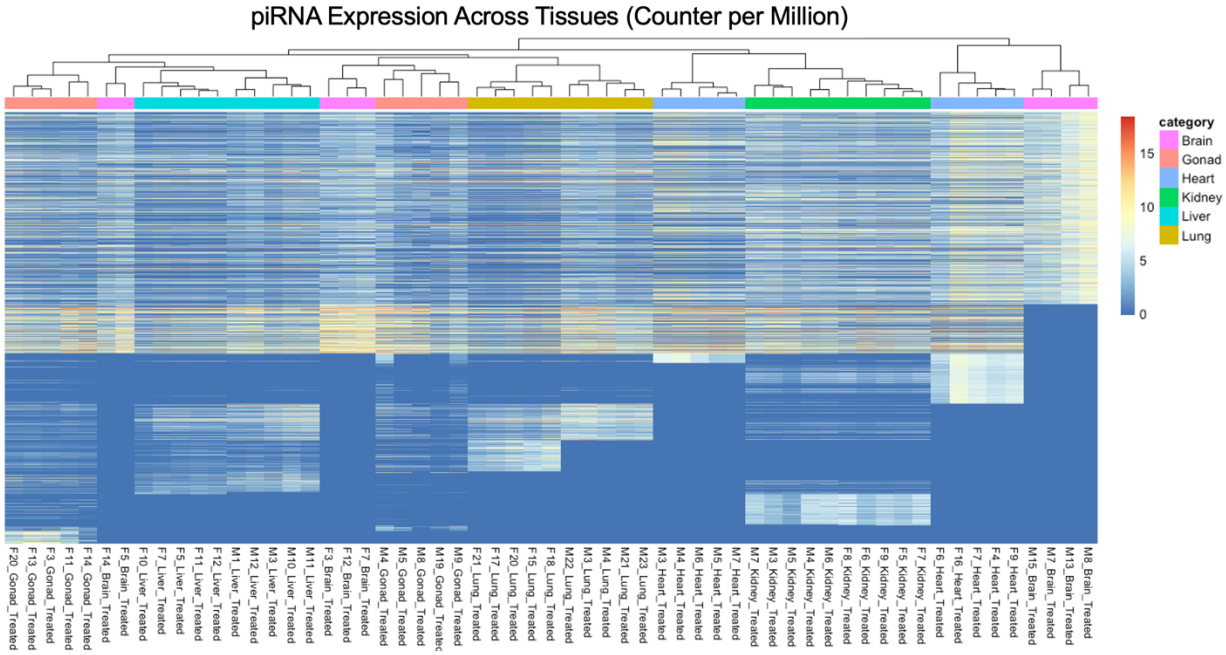

*Figure 5.8: Comparison of Expression of Each piRNA Across Tissues***.** Heatmap of piRNA expression in each sex-tissue combination, as quantified by counts per million (cpm) in brain (pink), gonad (orange), heart (blue), kidney (green), liver (teal), and lung (gold).

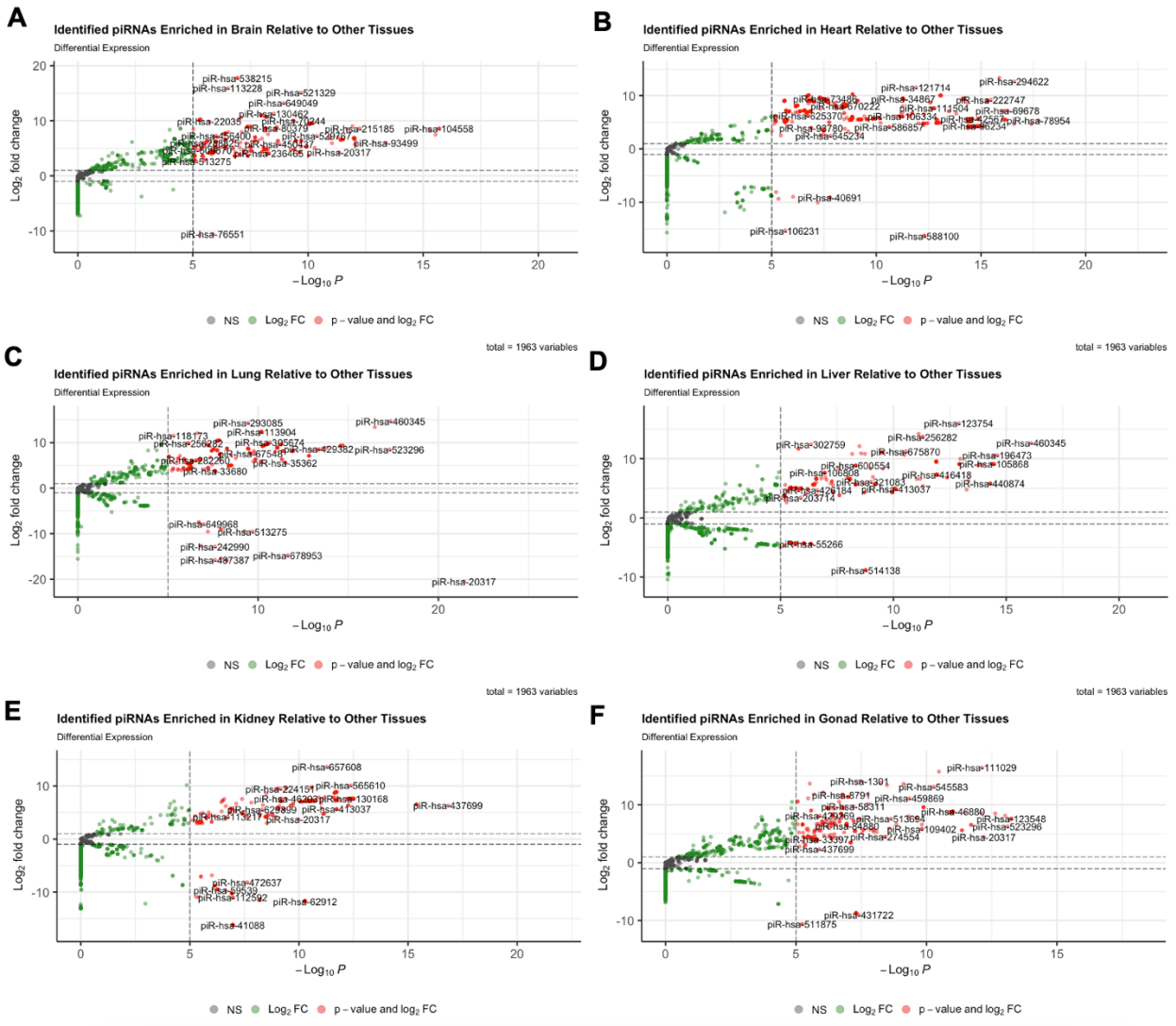

Figure 5.9: Enrichment of piRNA in Each Tissue. Enrichment of piRNAs in A) brain, B) heart, C) lung, D) liver, E) kidney, and F) gonad relative to other tissues was assessed using edgeR.

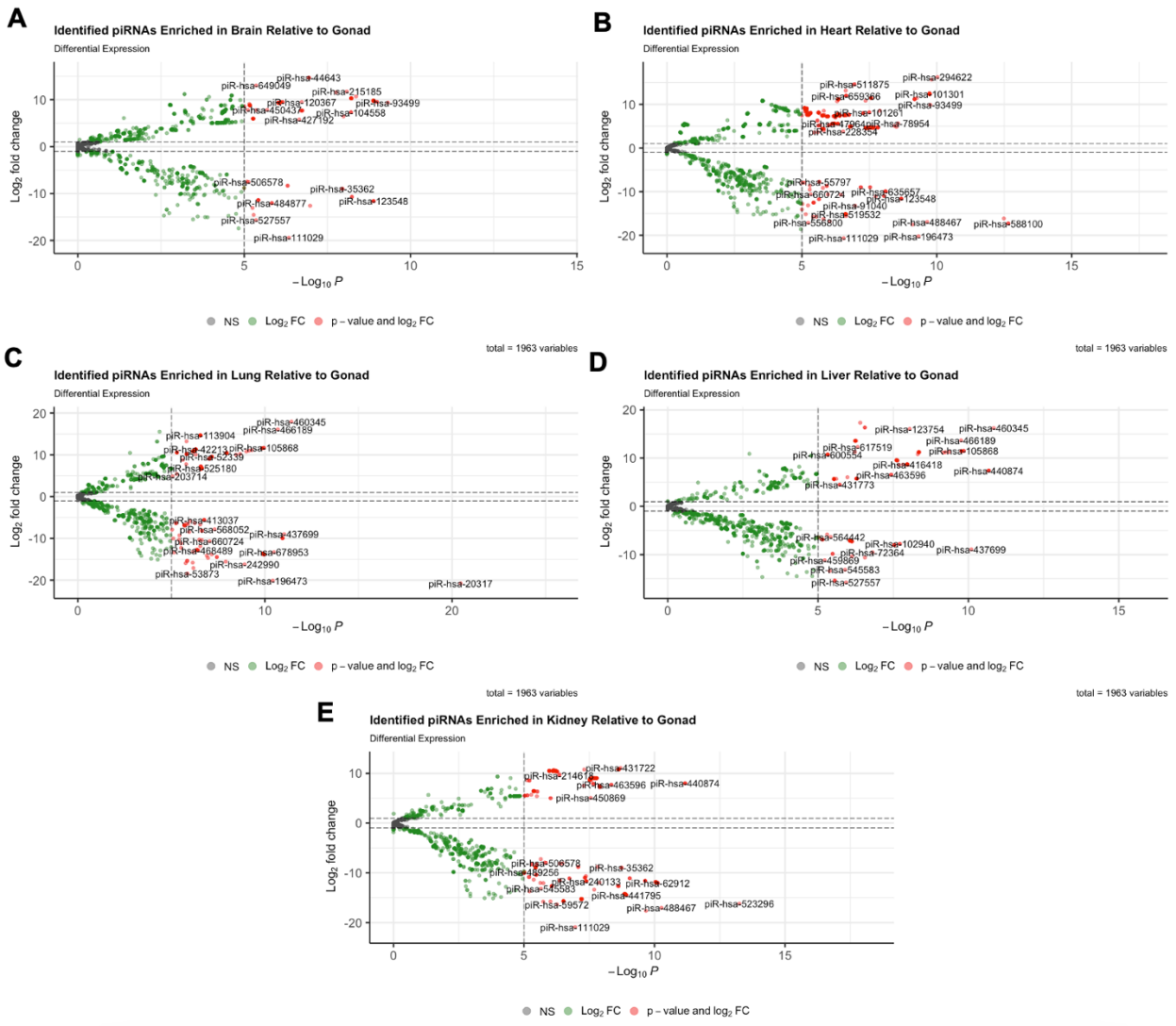

Figure 5.10: Enrichment of piRNA in Each Tissue Relative to Gonad. Enrichment of piRNAs in A) brain, B) heart, C) lung, D) liver, and E) kidney relative to gonad was assessed using edgeR.

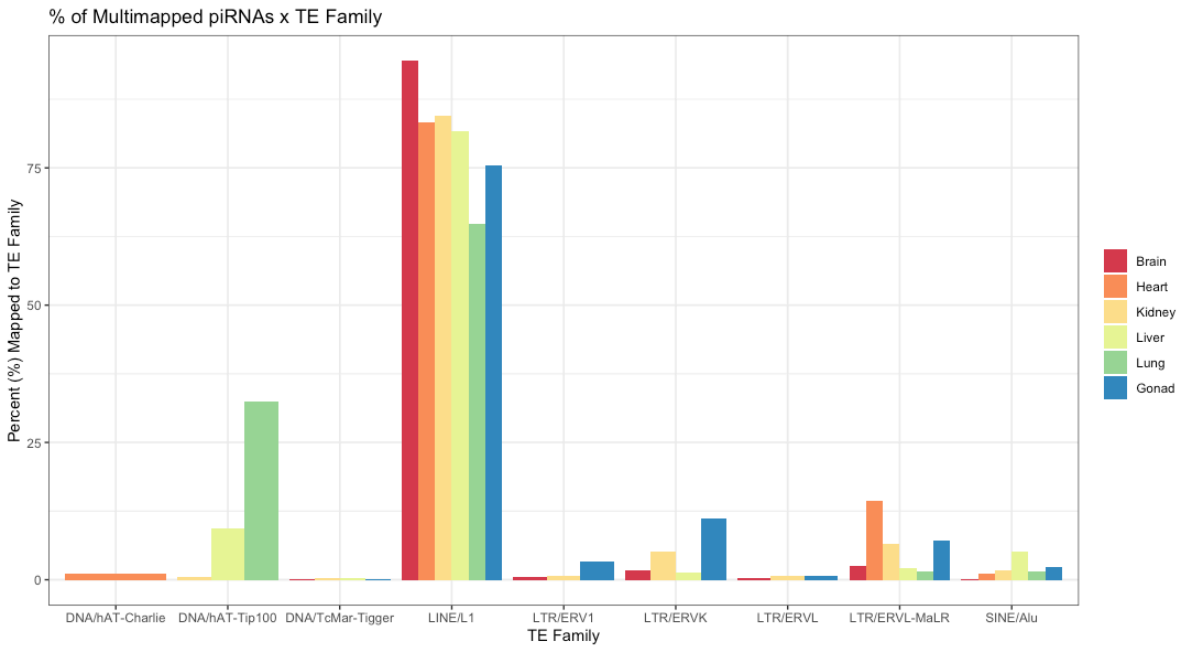

Figure 5.11: Multi-mapped piRNAs Represented by Various Repeat Classes. Multi-mapping piRNAs were categorized by the transposable element family to which they mapped in the brain (red), heart (orange), lung (green), liver (light green), kidney (gold), and gonad (blue).

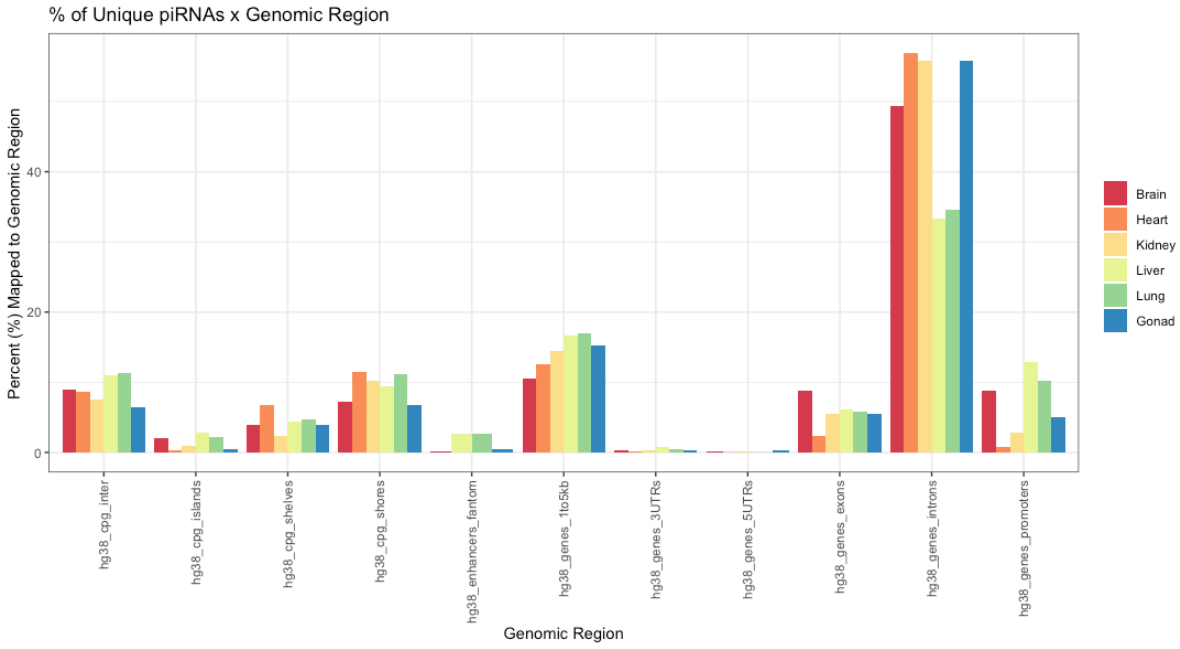

*Figure 5.12: Uniquely-mapped piRNAs Represented by Various Genomic Regions. U*niquely-mapping piRNAs were categorized by the genomic region to which they mapped in the brain (red), heart (orange), lung (green), liver (light green), kidney (gold), and gonad (blue).

Appendix

Tissue	Sex	Average RNA integrity number (RIN)
Brain	M	6.88
	F	5.72
Heart	M	7.3
	F	6.2
Lung	M	4.28
	F	5.75
Liver	M	5.92
	F	6.34
Kidney	M	5.75
	F	4.85
Gonad	M	7.54
	F	7.52

Table 5.A1: Summary of RNA Integrity Number (RIN) scores for each sex and tissue.

Experiment ID	Primer ID	Primer Sequence	Length	Amplicon Size	Vendor
PIWIL1	PIWIL1_F	ACGAAGTGCCACAGTTTTTGG	21	~124	IDT
	PIWIL1_R	AGTCTTCCTCCAGACTGAGC	20		IDT
PIWIL2	PIWIL2_F	GCCTGGGTTGAACTAAAGGA	20	~106	IDT
	PIWIL2_R	CCATGATGATGCAAACAACC	20		IDT
PIWIL3	PIWIL3_F	TCAGATGGCAGCAAAATCAC	20	~129	IDT
	PIWIL3_R	ACGTTGTGTACCCGTTAGGC	20		IDT
PIWIL4	PIWIL4_F	ATGGCACCGAGATCACCTAT	20	~126	IDT
	PIWIL4_R	GCTGAGCCTCACTGTTGTCA	20		IDT

Table 5.A2: Primers used for gene expression analysis of *PIWIL1-4*.

A

PIWIL1				
Tissue	Sex	Avg ΔCq	Avg Rel Expression	Avg log2(Rel Expression)
Gonad	M	11.33	4.21E-04	-11.33
	F	9.41	1.48E-03	-9.42
Brain	M	18.12	7.58E-06	-18.12
	F	20.42	8.35E-07	-20.43
Heart	M	15.23	3.17E-05	-15.23
	F	14.99	3.59E-05	-15.00
Lung	M	19.14	1.82E-06	-19.15
	F	19.27	1.69E-06	-19.27
Liver	M	18.41	4.71E-06	-17.77
	F	18.97	1.95E-06	-18.97
Kidney	M	14.22	6.57E-05	-14.22
	F	14.02	6.63E-05	-14.02

B

PIWIL2				
Tissue	Sex	Avg ΔCq	Avg Rel Expression	Avg log2(Rel Expression)
Gonad	M	12.66	1.59E-04	-12.67
	F	10.79	5.89E-04	-10.80
Brain	M	15.40	2.42E-05	-15.40
	F	15.89	1.66E-05	-15.90
Heart	M	14.50	4.98E-05	-14.50
	F	15.17	2.78E-05	-15.18
Lung	M	16.72	9.57E-06	-16.73
	F	16.70	1.01E-05	-16.71
Liver	M	16.33	1.34E-05	-16.33
	F	16.62	1.18E-05	-16.63
Kidney	M	15.21	3.27E-05	-15.22
	F	16.16	1.64E-05	-16.17

C

PIWIL3				
Tissue	Sex	Avg ΔCq	Avg Rel Expression	Avg log2(Rel Expression)
Gonad	M	19.45	1.75E-06	-19.45
	F	17.72	5.66E-06	-17.73
Brain	M	19.24	1.84E-06	-19.24
	F	19.00	2.25E-06	-19.01
Heart	M	19.66	1.22E-06	-19.66
	F	20.10	8.84E-07	-20.11
Lung	M	20.53	9.71E-07	-20.53
	F	20.80	7.76E-07	-20.81
Liver	M	18.44	3.50E-06	-18.44
	F	19.16	1.99E-06	-19.16
Kidney	M	20.39	7.63E-07	-20.39
	F	19.91	1.04E-06	-19.91

D

PIWIL4				
Tissue	Sex	Avg ΔCq	Avg Rel Expression	Avg log2(Rel Expression)
Gonad	M	13.28	1.04E-04	-13.29
	F	12.76	1.49E-04	-12.77
Brain	M	14.36	1.11E-04	-14.36
	F	13.28	1.02E-04	-13.28
Heart	M	12.51	1.76E-04	-12.52
	F	12.88	1.43E-04	-12.89
Lung	M	12.27	2.09E-04	-12.28
	F	12.72	1.58E-04	-12.72
Liver	M	15.85	1.81E-05	-15.85
	F	16.06	1.72E-05	-16.06
Kidney	M	13.32	1.02E-04	-13.32
	F	13.65	8.41E-05	-13.66

Table 5.A3: Summary of PIWIL ΔCq values, relative expression, and log2 transformed relative expression.

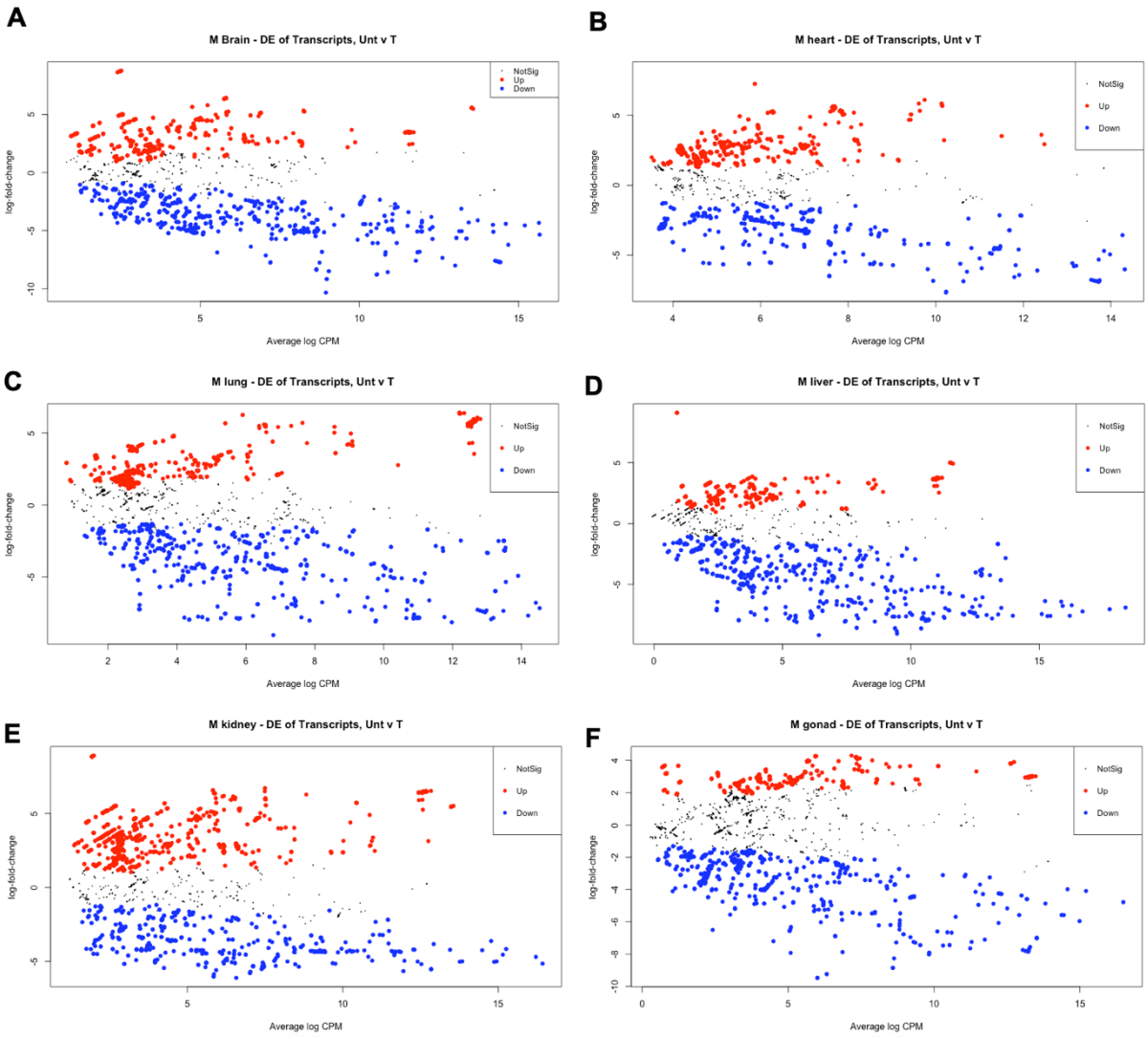

Figure 5.A1: Summary of differential expression analysis in male A) brain, B) heart, C) lung, D) liver, E) kidney, and F) gonad. Significantly expressed transcripts in treated (blue) as well as untreated samples (red) indicated.

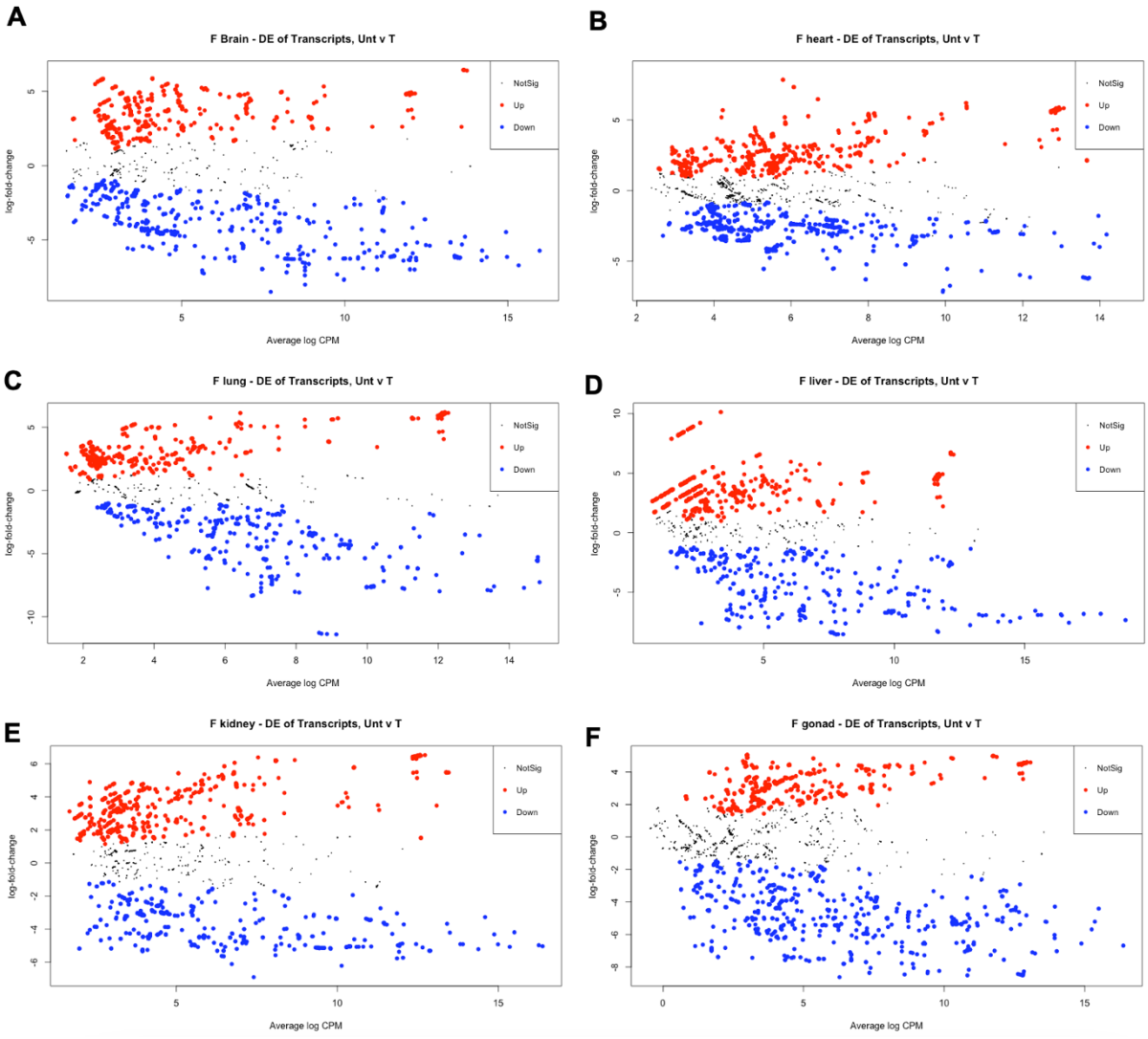

Figure 5.A2: Summary of differential expression analysis in female A) brain, B) heart, C) lung, D) liver, E) kidney, and F) gonad. Significantly expressed transcripts in treated (blue) as well as untreated samples (red) indicated.

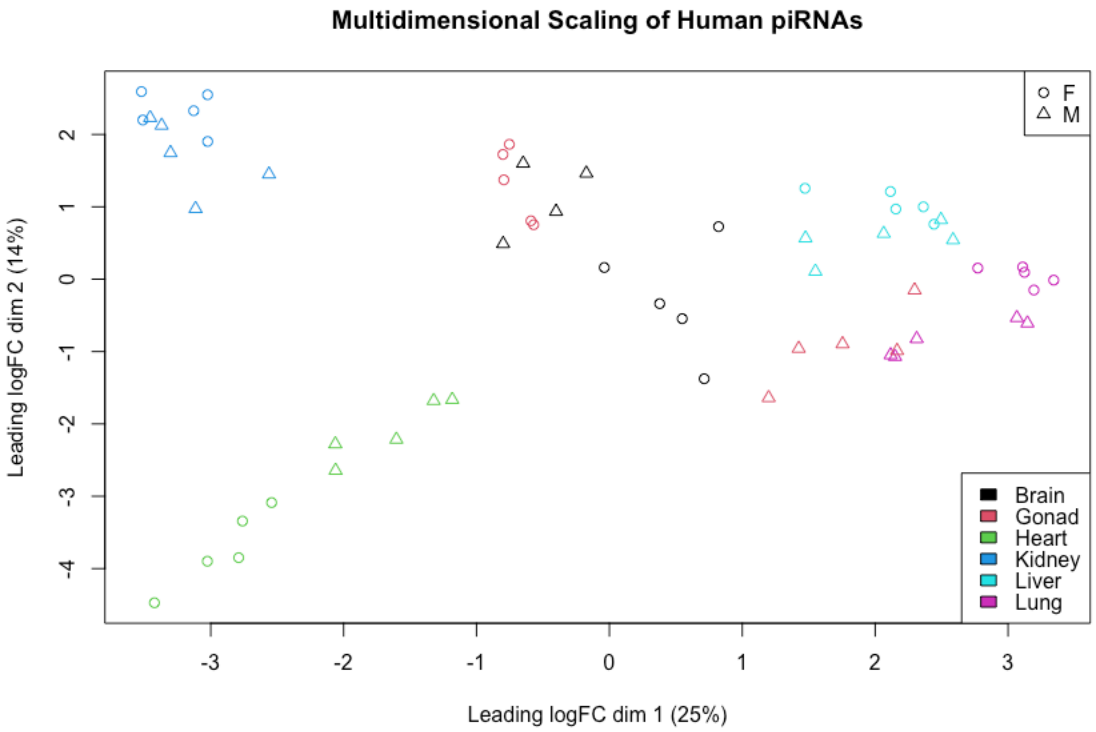

Figure 5.A3: Multidimensional scaling of each tissue and sex according to piRNA expression profiles.

	Differentially Expressed piRNAs in Each Tissue Relative to Total					
	Brain	Heart	Lung	Liver	Kidney	Gonad
Increased Expression	340	658	266	171	373	131
No Sig. Difference	1622	1298	1681	1782	1550	1817
Decreased Expression	1	7	16	10	40	15

Table 5.A4: Summary of differentially expressed piRNAs in each tissue relative to all others.

	Differentially Expressed piRNA in Each Tissue Relative to Gonad				
	Brain	Heart	Lung	Liver	Kidney
Increased Expression	66	211	46	42	284
No Sig. Difference	1889	1702	1874	1914	1582
Decreased Expression	8	50	43	7	97

Table 5.A5: Summary of differentially expressed piRNAs in each tissue relative gonad.

piRBase ID	logFC	Pvalue	FDR	Tissue of Significant Expression	Species	Sequence	Length	Dataset	PubMed ID	Number of References
piR-hsa-511875	14.69494	1.14E-07	3.28E-06	Brain	Human	GCTTTGGTGAC TCTAGATAACCT CGGGCTGATC	33	169:2 170: 2	25818294	1
piR-hsa-44643	14.68972	1.14E-07	3.28E-06	Brain	Human	GCTTTGGTGAC TCTAGATAACCT CGGGCT	29	167:1 168: 1 169:2 17 0:9 171:2 1 73:1	25818294	1
piR-hsa-974412	14.67026	2.87E-07	6.71E-06	Lung	Human	AGATTGCACCAT CAGTAGGGAAA CTGGAAAGTTT	34	7.084028	25818294	1
piR-hsa-627582	14.66945	2.87E-07	6.71E-06	Lung	Human	CAGAAGAGATAT GAGGAATTGTT AAGGAAGTC	33	169:1 170: 1 175:1	25818294	1
piR-hsa-446431	14.54397	1.19E-07	2.21E-06	Heart	Human	TTCCTAGAGACT TGGAGGGCTTA GAAGAC	29	7.042361	25818294	1
piR-hsa-974413	13.57491	5.79E-07	1.46E-05	Liver	Human	TACTTGGCAAGT GGGATAAAAAAA GAGA	28	7.084722	25818294	1
piR-hsa-627583	13.57442	5.80E-07	1.46E-05	Liver	Human	CATCTGGAAGA AGCCACATGCC TTGCCTCA	31	7.042361	25818294	1
piR-hsa-649049	13.02525	4.37E-06	5.36E-05	Brain	Human	TGGCTGGTCCG AGTGCAGTGGT GT	24	169:3 170: 1	25818294	1
piR-hsa-1013011	12.37602	1.81E-10	1.77E-08	Heart	Human	CATATTGCTCAG AACGTATCCTTG TCTTTAAGCA	34	7.084028	25818294	1
piR-hsa-636551	12.37416	1.88E-10	1.77E-08	Heart	Human	AGGATCCTTAAC ATTGTCAAAGAC T	25	7.042361	25818294	1
piR-hsa-1009561	12.3727	1.84E-10	1.77E-08	Heart	Human	GTTCCCTGGTG GTCTAGTGGTTA GG	25	7.084028	25818294	1
piR-hsa-497871	12.3727	1.84E-10	1.77E-08	Heart	Human	GGCAAACCAGA GCTCAGAAAAA AGG	25	7.042361	25818294	1
piR-hsa-535981	12.3727	1.84E-10	1.77E-08	Heart	Human	CAGAACCGACT ACGGCTTTCAAT C	24	7.042361	25818294	1
piR-hsa-538681	12.3727	1.84E-10	1.77E-08	Heart	Human	TACTCAATATCG GGAGGTCTGCA AGG	26	169:1 175: 4 176:1 17 7:30 178:1	25818294	1
piR-hsa-821731	12.3727	1.84E-10	1.77E-08	Heart	Human	TTTATTGAATTG GGCTCTGGTTT CAGGC	28	7.084028	25818294	1
piR-hsa-842371	12.3727	1.84E-10	1.77E-08	Heart	Human	TCTGCACCTTCA GTTCTCAGGAC ACAATG	29	7.084028	25818294	1
piR-hsa-215185	11.73967	6.18E-09	2.63E-07	Brain	Human	CTGGCGCTGCG GGATGAACCGA ACGCCGGG	30	168:1 169: 1 170:6 17 2:1	25818294	1
piR-hsa-489802	11.68209	1.14E-10	1.00E-08	Lung	Human	CTGCAGCGGGC TTGGCTTTGTGA GGA	26	169:1 177: 1	25818294	1
piR-hsa-333912	11.60424	1.43E-10	1.00E-08	Lung	Human	CTACATACAGAG CTCCTACAACTT	24	7.000694	25818294	1
piR-hsa-294622	11.56735	1.71E-08	5.16E-07	Brain	Human	CTGGCGCTGCG GGATGAACCGA ACGCCGGGT	31	168:2 169: 1 170:10 1 71:4 172:1 173:1 176: 1 177:1 17 8:1	25818294	1
piR-hsa-489803	11.49581	1.43E-10	3.12E-08	Liver	Human	TTTCTGGGTACA TAGAGCTGTACA TTGAGCTC	32	169:1 170: 2 269	25818294 31358756	2
piR-hsa-333913	11.46361	1.70E-10	3.12E-08	Liver	Human	TATAGGCTTAAG ACACCAATTGTG CAATGTGA	32	168:2 169: 2 170:12 1 75:4 176:3 177:22 269 270	25818294 31358756	2
piR-hsa-336761	11.45965	2.72E-08	7.80E-07	Heart	Human	GATTTCCCCAAA TGTGGGAAACT CGACTGCATTA	34	7.000694	25818294	1
piR-hsa-475371	11.44284	2.75E-08	7.80E-07	Heart	Human	TGCCTAAGATTG AATGTGTTCACC CCAAGC	30	7.042361	25818294	1
piR-hsa-740251	11.44284	2.75E-08	7.80E-07	Heart	Human	TTGAGAAAAGCT GCCAGTGAGAC TACCAC	29	7.042361	25818294	1
piR-hsa-422132	11.32953	5.01E-07	1.03E-05	Lung	Human	GGCATCAGGGA GATTCTGACAGT AGAAAG	29	7.042361	25818294	1
piR-hsa-695142	11.32953	5.01E-07	1.03E-05	Lung	Human	CACATTTTTCTG AGGCTATGAATG CTGTG	29	169:1 170: 1	25818294	1
piR-hsa-459063	11.24222	4.41E-10	7.21E-08	Liver	Human	ATGAGCTCTGTA GGTCCGCCGGT	24	7.042361	25818294	1
piR-hsa-1034211	11.24014	6.66E-10	4.92E-08	Heart	Human	TTAAGCTAGAAA ACATTTATATTTG ACCCCTTT	33	7.084028	25818294	1
piR-hsa-815953	11.22364	4.37E-09	4.64E-07	Liver	Human	TCTTGAACTCCT GACCTCAAGCA GT	25	7.084028	25818294	1
piR-hsa-528863	11.22033	4.44E-09	4.64E-07	Liver	Human	GCTGAAGGAAA AGATTGATCGCC GTT	26	7.042361	25818294	1
piR-hsa-435241	11.19415	6.64E-10	4.92E-08	Heart	Human	TTTTACAGAACT AGGATATGTGGA AA	26	7.042361	25818294	1
piR-hsa-779781	11.18529	4.52E-07	4.36E-06	Heart	Human	GAGAACTTTGAA GGCCGAAGTGG AGATGGGTT	32	7.042361	25818294	1
piR-hsa-496691	11.17731	6.77E-10	4.92E-08	Heart	Human	TCGATCTCCTGA CCTCGTGATGT GCCCGCT	30	7.042361	25818294	1
piR-hsa-538215	11.17431	6.22E-04	2.27E-03	Brain	Human	CGGCTGGTCCG ATGGTAGTGGG TTATC	27	7.045833	25818294	1
piR-hsa-677732	11.17431	6.22E-04	2.27E-03	Brain	Human	CGGCTGGTCCG ATGGTAGTGGG TTATCAGA	30	169:3 170: 2	25818294	1
piR-hsa-459062	11.12135	5.04E-10	3.41E-08	Lung	Human	GACAGAGTAGA CCTTGACCAAAT CTCAAGC	30	7.042361	25818294	1
piR-hsa-504172	11.0258	6.17E-07	1.18E-05	Lung	Human	TTTCCAAACAAA GTCACATTATGA GATGCTGGG	33	7.042361	25818294	1
piR-hsa-511892	11.0258	6.17E-07	1.18E-05	Lung	Human	CATTAGTTAGAC GTTGAACTTAGC CG	26	7.042361	25818294	1
piR-hsa-674852	11.0258	6.17E-07	1.18E-05	Lung	Human	ATGCCACTGAA CTCCAGCCTGG GTGAGAGT	30	7.042361	25818294	1
piR-hsa-549092	10.90884	6.65E-07	1.20E-05	Lung	Human	TCTGAGGCTAC ATTTGGGCATGA TTCAGACC	31	7.042361	25818294	1
piR-hsa-589652	10.90884	6.65E-07	1.20E-05	Lung	Human	GACGAGGTGAT GAACCAAAATT GGCCTATTATG	34	7.042361	25818294	1
piR-hsa-618402	10.90884	6.65E-07	1.20E-05	Lung	Human	TGATCCTGCTGA AGATCGGCCTG GCCAT	28	169:1 177: 1	25818294	1
piR-hsa-961482	10.90884	6.65E-07	1.20E-05	Lung	Human	ATTCAAAGTGTA ATAGGAGAGTTA AAAGATGT	32	7.084028	25818294	1
piR-hsa-35526	10.90013	2.32E-05	2.23E-04	Brain	Human	CGGCTGGTCCG AGTGCAGTGGT GTTTAC	26	167:1 169: 8 170:1 17 6:1	25818294	1
piR-hsa-298988	10.87926	2.39E-05	2.26E-04	Brain	Human	CGGCTGGTCCG AGTGCAGTGGT GTTT	26	168:1 169: 7 170:6 17 1:1 177:1	25818294	1
piR-hsa-88436	10.87764	2.41E-05	2.28E-04	Brain	Human	CGGCTGGTCCG AGTGCAGTGGT GTT	25	167:2 169: 12 170:4 1 71:3 173:1 177:1 178: 1	25818294	1
piR-hsa-40481	10.87345	2.44E-05	2.28E-04	Brain	Human	CGGCTGGTCCG AGTGCAGTGGT GT	24	167:1 168: 1 169:7 17 0:6 171:3 1 76:1	25818294	1
piR-hsa-910261	10.8664	2.86E-04	8.58E-04	Heart	Human	TTTTGATCTGCA TTTCCCTAATGA TTAG	28	7.084028	25818294	1

Table 5.A6: Summary of top 50 differentially expressed piRNA in somatic tissues.

Transposable Element Family	Tissue	# of multi-mapped piRNAs	Total multi-mapped piRNAs/tissue	Percent mapping to each TE family
LINE/L1	Brain	528		94.45%
LTR/ERVK	Brain	10		1.78%
LTR/ERVL-MaLR	Brain	14		2.50%
SINE/Alu	Brain	1	559	0.17%
LTR/ERV1	Brain	3		0.53%
DNA/TcMar-Tigger	Brain	1		0.17%
LTR/ERVL	Brain	2		0.35%
LINE/L1	Heart	75		83.33%
LTR/ERVL-MaLR	Heart	13	90	14.44%
DNA/hAT-Charlie	Heart	1		1.11%
SINE/Alu	Heart	1		1.11%
DNA/hAT-Tip100	Lung	22		32.35%
LINE/L1	Lung	44	68	64.70%
LTR/ERVL-MaLR	Lung	1		1.47%
SINE/Alu	Lung	1		1.47%
DNA/hAT-Tip100	Liver	36		9.37%
LINE/L1	Liver	314		81.77%
LTR/ERVK	Liver	5		1.30%
SINE/Alu	Liver	20	384	5.20%
LTR/ERVL-MaLR	Liver	8		2.08%
DNA/TcMar-Tigger	Liver	1		0.26%
LINE/L1	Kidney	520		84.55%
LTR/ERVK	Kidney	31		5.04%
DNA/TcMar-Tigger	Kidney	2		0.32%
DNA/hAT-Tip100	Kidney	3	615	0.48%
LTR/ERVL-MaLR	Kidney	40		6.50%
LTR/ERV1	Kidney	4		0.65%
SINE/Alu	Kidney	11		1.78%
LTR/ERVL	Kidney	4		0.65%
LTR/ERVK	Gonad	63		11.09%
LINE/L1	Gonad	428		75.35%
LTR/ERVL-MaLR	Gonad	40		7.04%
LTR/ERV1	Gonad	19	568	3.34%
SINE/Alu	Gonad	13		2.28%
LTR/ERVL	Gonad	4		0.70%
DNA/TcMar-Tigger	Gonad	1		0.17%

Table 5.A7: Summary of multi-mapping piRNAs and TE families.

Table 5.A8: Summary of uniquely mapped piRNAs and genomic regions, per tissue.

Table 5.A9: Summary of gene targets of uniquely mapping piRNAs.

Chapter 6
Discussion

Summary and Synthesis of Research Findings

In this dissertation research, we performed three toxicological studies examining the effects of developmental lead (Pb) exposure on neural outcomes: A longitudinal mouse model of perinatal exposure in the developing brain, and two studies employing a cell model which assessed changes in cell morphology and epigenetic regulation during neural differentiation. These studies were intended to explore how early developmental Pb exposure may contribute to neurodegenerative disease (ND) risk later in life through perturbations in the establishment of epigenetic patterns governing gene expression and neural differentiation. The final study characterized the expression of an understudied class of non-coding RNA (ncRNA), piRNA, in several human somatic tissues during early development, in order to support future work aimed at exploring how environmental exposures perturb the expression and function of this class.

In Aim 1, we found that perinatal exposure to 32 ppm Pb via drinking water was associated with differential methylation at imprinted genes as well as an important class of transposable elements, LINE-1, during adulthood. Males and females perinatally exposed to Pb displayed differential methylation in cortex and blood in genomic regions associated with gene expression regulation, with relatively little overlap in differentially methylated regions between the sexes. Pathway analysis revealed imprinting genes as

a class of interest and of these, *Gnas* and *Grb10*, two imprinted genes for which monoallelic expression is important during brain development[1,2], contained Pb-associated alterations in DNA methylation (DNAm) in both tissues and sexes. This association was notably present in the imprinting control regions (ICRs) of these two genes, and it was observed that Pb-associated changes in DNAm in the *Grb10* ICR were detected in both male blood and cortex, suggesting this locus may be a candidate for future biomarker work. In addition to imprinted genes, we found that LINE-1 methylation was also perturbed with Pb exposure, particularly within the cortex, and that there was no overlap in DNAm changes between males and females. Assessment of both gene classes highlighted in this aim emphasize the importance of considering sex-specific effects of environmental exposures on epigenetic mechanisms, which has been previously documented.[3] These results of Pb-associated changes in DNAm at two gene classes important for neural functioning throughout the life course in an animal model were motivation to explore how Pb affects the vital process of neurogenesis and whether there are any mechanistic links between exposure and altered epigenetic regulation in an *in vitro* setting.

In Aim 2, we found that Pb exposure perturbs neural differentiation in the SH-SY5Y cell model. This experimental design was an opportunity to assess changes in cell morphology and differentiation throughout this developmental process, as opposed to limiting the exposure period to before or after differentiation had occurred. Pb exposure was associated with changes in protein expression during early neurogenesis, such as GAP43, β-tubulin III, and MAP2, which has been previously documented.[4] During the later stages of differentiation, Pb exposure was associated with hindered

development of neural axonal and dendritic projections, as quantified by immunofluorescence, as well as the number and length of such projections. This study provided evidence that Pb exposure affects differentiating cells differently during various stages of this process and suggests that early effects may predict reduced neuronal growth and development at a later timepoint. While we have long known Pb to be a potent neurotoxicant,[5] this work provided additional insights into how the timing of exposure may affect neural differentiation. In addition to this, benchmark dose analysis provided evidence that current guidelines set by the US government as to unacceptable levels of Pb exposure may not be stringent enough to prevent exposure-associated effects on neurogenesis.

Aim 3 employed the same experimental framework as Aim 2, with differentiating SH-SY5Y cells exposed to Pb and a time course analysis of effects. In this aim, we assessed Pb-associated changes in the epigenetic regulation of LINE-1 and found that, as in Aim 2, Pb exposure had differentiation stage-specific effects on these outcomes. LINE-1 activity is suspected to be beneficial in multipotent cells, contributing to stemness and plasticity, but its expression is typically repressed in terminally differentiated cells, minimizing the risk of insertional mutations as well as associated DNA damage, oxidative stress, and apoptosis.[6–9] During early neural differentiation, Pb exposure was associated with down-regulation of LINE-1 expression, whereas during later differentiation exposure was associated with increased expression, suggesting that the timing and degree of LINE-1 expression is significantly perturbed by Pb exposure. LINE-1 expression is regulated, in part, by piRNA and PIWI-directed DNA methylation,[10] and we found Pb exposure to be largely associated with a decrease in *PIWIL1*

expression during early differentiation and increased expression during later stages. We were surprised to see minimal changes in LINE-1 methylation with Pb exposure, at any stage in this process, given the association between Pb exposure and LINE-1 hypomethylation observed in Aim 1. However, it may be that this *in vitro* aim was not powered enough to detected significant differences in DNAm via pyrosequencing or that a larger scope of DNAm analysis would have provided evidence of association. Regardless, it is suspected that Pb-associated changes in *PIWIL* expression contributed to the observed dysregulation of LINE-1 expression, and that this increased LINE-1 expression during late stages of differentiation may inform the observed effects in Aim 2 on cell morphology, as the maintenance of neural outgrowth may have been perturbed by cellular stress brought on by prolonged LINE-1 expression.[11] We were unable to evaluate this relationship at imprinted genes, which would expand upon the results acquired in Aim 1, and this is an area for continued exploration in this experimental model.

The observed associations between developmental Pb exposure and aberrant LINE-1 regulation in Aims 1 and 3 furthered our hypothesis that future work exploring the piRNA system may help elucidate the mechanisms behind this relationship. This is especially true as Aims 2 and 3 demonstrated that Pb exposure has stage-specific effects on neural differentiation, and the PIWI proteins are suspected to be involved in stem cell maintenance and differentiation.[12] In order to effectively carry out these toxicological studies, a baseline characterization of the expression of this class of ncRNA, in the brain as well as other somatic tissues where this relationship may extend, during human development is needed. Aim 4 evaluated the expression of piRNA and

PIWIL expression in developing (gestational days 90-105) brain, heart, lung, liver, and kidney, alongside the gonads. We found *PIWIL1* and *PIWIL2* mRNA expression in all included somatic tissues, though this expression was lower than that of the gonads. *PIWIL3* and *PIWIL4* expression was comparable to that of the gonads in nearly all tissues examined.

We further explored piRNA profiles using a list of previously identified transcripts using gold-standard methods (i.e., PIWI co-immunoprecipitation or sodium periodate treatment). An analysis of piRNA profiles in each tissue revealed that while many piRNAs were shared between males and females, there were also sex-specific groupings in each tissue. Given what is known about sexually dimorphic development in many organ systems,[13–15] it is suspected that these unique piRNA profiles may play a role in these processes. Differential piRNA expression in the developing brain may also begin to inform the sex-specific changes in LINE-1 DNA methylation in Aim 1 following Pb exposure, as alterations in piRNA profiles that are unique to males and females would likely result in sex-specific changes in their genomic targets as well. However, this hypothesis would need to be explicitly evaluated in a mouse model, as was used for Aim 1, as the trends observed in developmental piRNA expression described here come from human tissues.

We also found that there was a significant overlap in piRNAs in the gonads relative to each somatic tissue type, with relatively few piRNAs differentially expressed in the gonads, though these piRNAs had all been previously identified in the germline, which may at least partially explain these trends. We also found that the locations to which multi-mapping and unique piRNAs mapped in the soma were similar to that of the

gonads, with LINE-1 elements and gene expression regulatory regions being common targets. These results suggest that the presence and function of piRNA may not be as restricted to the germline as previously thought,[16] especially during early development, but additional work determining whether there are as yet undiscovered piRNAs in these tissues will help solidify our understanding of piRNA expression in the soma versus the germline. This work provides a thorough baseline of piRNA and *PIWIL* expression in several tissue types, laying the groundwork for future toxicological work focused on this class of ncRNA.

This dissertation corroborates previous work that has found Pb exposure to be associated with abnormal neural differentiation[17] and development,[18] and builds upon this literature by expanding these analyses to perturbations of epigenetic mechanisms and of gene classes known to be associated with ND risk. The longitudinal aspect of Aim 1 allowed us to explore how developmental Pb exposure alters the epigenome and whether these associations persist into adulthood at imprinted genes as well as LINE-1 elements. The cell model employed in this dissertation allowed us to explore how continuous Pb exposure during a fundamental process such as neurogenesis affects both the success of neural differentiation as well as epigenetic and gene expression changes that occur in these cells in a time-course manner. These studies provided evidence that perturbations to LINE-1 epigenetic regulation and expression happen alongside changes in protein expression and cellular morphology, and that, regardless of the type of measure, the effects of Pb on neural differentiation appear to be stage-dependent. Taken together, these toxicological aims provide evidence that Pb exposure perturbs patterns of epigenetic regulation and LINE-1 expression during

neurodevelopment. This work also contributes to our hypothesis that exposure to neurotoxicants such as Pb during critical windows of development may contribute to ND risk later in life through perturbations of normal neurodevelopment. It is suspected that the dysregulation at the epigenetic level of important gene classes such as LINE-1 during neurogenesis contribute to cellular stress and create suboptimal neural populations that are primed to take on neurodegenerative phenotypes later in life. The final aim of this dissertation provides a reference point for future work examining this relationship, as disruption to piRNA expression and function is hypothesized to be a mechanistic link between Pb exposure and many of the effects observed in the previous three aims. A summary of research aims and the evidence they provided to the overall hypothesis that developmental Pb exposure contributes to ND risk through perturbation of LINE-1 element regulation and the generation of suboptimal neural populations is provided in **Figure 6.1**.

Relevance to Human Health

A major goal of this dissertation was to employ mouse and cell models in a way that accurately reflected human exposures. Pb exposure in the mouse model was delivered via drinking water, a relevant route of exposure given current trends in Pb exposure events[19] and resulted in a continuous exposure model rather than one large exposure event each day. Levels of Pb in water were set to 32 ppm, which produces blood lead levels (BLLs) in mice of roughly 16-60μg/dL and reflects a significant exposure level in humans by today's standards.[20,21] 16-60μg/dL BLLs would have been much more common 50 years ago, prior to stricter Pb legislation in the US, and thus is an accurate representation of developmental exposures experienced by those who are

now in their 50s and 60s.[22] Given that Aim 1 was conducted in 5-month-old mice, this provides evidence that exposures that occurred during early development at historically relevant Pb doses likely resulted in effects that persist into adulthood and may be contributing to health risks in these currently aging populations. This is true for effects seen at both LINE-1 elements as well as imprinted genes as both classes have been implicated as requiring well-orchestrated expression regulation via DNAm during processes such as neurodevelopment.[23,24]

Experiments conducted in cells also utilized environmentally relevant Pb exposures based on current and historical BLL benchmarks set by the US CDC, as Pb exposure via blood was thought to be the most relevant to the cellular environment. 0.16μM Pb exposure correlates to a BLL of roughly 3.5μg/dL, the current actionable level set by the CDC,[25] while the moderate dose of 1.26μM Pb is analogous to BLLs of approximately 26μg/dL, which was more commonly seen prior to strict Pb legislation enacted in the 1970s and correlates to the lower end of BLLs observed with the 32 ppm exposure model in Aim 1.[22] The use of these environmentally relevant doses provided two important insights; first, that both historical and current BLLs significantly impact neurogenesis at the morphological and epigenetic levels. This suggests that while older populations in the US are at risk of health outcomes related to suboptimal neural populations generated in the presence of Pb during early development, the same can be said for younger generations who have generally been exposed to lower levels. Benchmark dose modeling of these outcomes also demonstrated that the current actional BLL set by the CDC of 3.5μg/dL may not be strict enough to avoid Pb-associated changes in neural differentiation and LINE-1 regulation.

Given the toxicological evidence of Pb-associated effects on LINE-1 regulation and expression, there is a need for continued evaluation of what mechanisms explain these relationships. This is especially true given the lack of decisive findings in Aim 3, from which no strong conclusions could be made as to the role of the piRNA system in the observed perturbations to LINE-1 regulation in this aim or that of Aim 1.The characterization of piRNA in the human soma during early development will support such work in the future, as this class of ncRNA is so closely tied to LINE-1 epigenetic regulation. In addition to this, the findings of Aim 4 change our understanding of piRNA expression in humans and challenges the previously held notion that this system is predominantly expressed in the germline. The presence of this system in various somatic tissues during early development raises many questions as to its function in each tissue, whether there are sexually dimorphic trends in its activity, and how its perturbation by developmental environmental exposures may modify disease risk throughout life.

Impact and Innovation

To our knowledge, this dissertation includes the first study to assess the effects of developmental Pb exposure on genome-wide patterns of DNAm in the cortex in adulthood. This work allowed for unbiased exploration of changes in DNAm and led to the identification of imprinted genes as a class of interest, which may not have been realized otherwise. This dissertation also includes two complementary aims that assess Pb exposure during neural differentiation, wherein exposure occurred during this developmental process as opposed to before or after, which has been common in much of the previously published literature. This experimental set up also allowed us to

assess changes in classic markers of neural differentiation (such as protein expression and morphology) alongside changes in the epigenetic regulation of LINE-1 expression. This allowed us to make preliminary conclusions as to how LINE-1 dysregulation may inform the changes seen in neural differentiation progression in the presence of neurotoxicants and is motivation to take a continued look at this relationship.

Finally, to our knowledge, this dissertation includes the first attempt to characterize piRNA expression in developing human (or other species) somatic tissues. Much of the available literature on piRNA and PIWI expression and function concludes that the germline is the major site of activity,[26] and work exploring this class in the soma has largely focused on adult time points.[27] This study provides novel evidence of piRNA expression in the developing soma and that patterns within each tissue may be somewhat dependent on sex. Additionally, this work demonstrates that piRNA expression and function is likely relevant to developing tissues, in the soma as much as the germline, which significantly motivates continued work evaluating how developmental exposures impact this class of ncRNA in an array of tissue types.

Recommendation for Future Research

Future work that would further inform the conclusions drawn in Aims 1 and 3 would be an analysis of piRNA expression in such samples. Given the association between Pb exposure and LINE-1 methylation, documented here as well in previously published literature,[28,29] it would be prudent to assess how piRNA profiles change both in cortical tissue from developmentally exposed mice as well as in differentiating neurons. It would be informative to explore whether Pb exposure induces differential expression of piRNA that map to LINE-1 elements in directions that correlate with

observed trends in DNAm. To this end, it would also be beneficial to extend the analysis conducted in Aim 4 to include an assessment of piRNAs that may not have been previously identified, using previously published methods,[27] to ascertain whether there are piRNAs unique to the developing brain that contribute to LINE-1 regulation and may be subject to differential expression upon Pb exposure.

An additional analysis that would complement much of the work conducted in this dissertation would be an evaluation of chromatin state and histone modifications in these experimental models. piRNA and PIWI proteins are known to coordinate epigenetic regulation through modifications to these factors,[30,31] in addition to that of DNAm, and it is likely that changes in LINE-1 expression observed in Aim 3 are not entirely explained by changes in DNAm alone. It would be reasonable to explore how DNAm, piRNA expression, and chromatin states change in the same animals or cells in response to Pb exposure and whether one or more of these factors correlate with observed trends in LINE-1 expression.

Finally, generalizability of these findings could be improved with additional experimental models. The relevance of differential DNA methylation in Aim 1 to ND risk would be better interpreted if future efforts in animal models examined changes in behavioral patterns following developmental Pb exposure. It is possible to quantify behavioral traits associated with neurodegenerative outcomes in mice,[32,33] and it would be interesting to follow perinatally exposed mice throughout life, measuring behaviors related to neurological function and decline into old age, and upon death, assess the epigenetic regulation of LINE-1 in regions of the brain such as the cortex and hippocampus. Additionally, future cell line work of this nature would benefit from a truly

pluripotent stem cell model, such as human embryonic stem cells, from which the generation of neurons is possible in a timeframe similar to that of the SH-SY5Y cell line used here. While the cell line in this dissertation provided a robust model of neural differentiation, their origin from cancerous tissue limits our ability to draw firm conclusions pertaining to normal neurons, and the use of hESCs would eliminate this consideration.[34] The use of hESCs would also provide the opportunity to differentiate stem cells into multiple neural cell types, thus increasing our ability to assess effects in different neural populations as well as examine how the effects of Pb exposure change when there is more than one neural cell type present in a given environment.[35]

References

1. Mouallem, M. *et al.* Cognitive impairment is prevalent in pseudohypoparathyroidism type Ia, but not in pseudopseudohypoparathyroidism: possible cerebral imprinting of Gsalpha. *Clin. Endocrinol. (Oxf.)* **68**, 233–239 (2008).

2. Plasschaert, R. N. & Bartolomei, M. S. Tissue-specific regulation and function of Grb10 during growth and neuronal commitment. *Proc. Natl. Acad. Sci. U. S. A.* **112**, 6841–6847 (2015).

3. Montrose, L., Faulk, C., Francis, J. & Dolinoy, D. C. Perinatal lead (Pb) exposure results in sex and tissue-dependent adult DNA methylation alterations in murine IAP transposons. *Environ. Mol. Mutagen.* **58**, 540–550 (2017).

4. Strużyńska, L., Chalimoniuk, M. & Sulkowski, G. Changes in expression of neuronal and glial glutamate transporters in lead-exposed adult rat brain. *Neurochem. Int.* **47**, 326–333 (2005).

5. Lidsky, T. I. & Schneider, J. S. Lead neurotoxicity in children: basic mechanisms and clinical correlates. *Brain* **126**, 5–19 (2003).

6. Jachowicz, J. W. *et al.* LINE-1 activation after fertilization regulates global chromatin accessibility in the early mouse embryo. *Nat. Genet.* **49**, 1502–1510 (2017).

7. Terry, D. M. & Devine, S. E. Aberrantly High Levels of Somatic LINE-1 Expression and Retrotransposition in Human Neurological Disorders. *Front. Genet.* **10**, 1244 (2019).

8. Peze-Heidsieck, E. *et al.* Retrotransposons as a Source of DNA Damage in Neurodegeneration. *Front. Aging Neurosci.* **13**, 786897 (2022).

9. Gamdzyk, M. *et al.* cGAS/STING Pathway Activation Contributes to Delayed Neurodegeneration in Neonatal Hypoxia-Ischemia Rat Model: Possible Involvement of LINE-1. *Mol. Neurobiol.* **57**, 2600–2619 (2020).

10. Zoch, A. *et al.* SPOCD1 is an essential executor of piRNA-directed de novo DNA methylation. *Nature* **584**, 635–639 (2020).

11. Belgnaoui, S. M., Gosden, R. G., Semmes, O. J. & Haoudi, A. Human LINE-1 retrotransposon induces DNA damage and apoptosis in cancer cells. *Cancer Cell Int.* **6**, 13 (2006).

12. Apostolou, P. *et al.* Involvement of retrotransposon L1 in stemness and cellular plasticity. *Cell Commun. Adhes.* **22**, 1–7 (2015).

13. Yang, C. F. *et al.* Sexually dimorphic neurons in the ventromedial hypothalamus govern mating in both sexes and aggression in males. *Cell* **153**, 896–909 (2013).

14. Deegan, D. F., Nigam, P. & Engel, N. Sexual Dimorphism of the Heart: Genetics, Epigenetics, and Development. *Front. Cardiovasc. Med.* **8**, 668252 (2021).

15. Gortner, L., Shen, J. & Tutdibi, E. Sexual dimorphism of neonatal lung development. *Klin. Padiatr.* **225**, 64–69 (2013).

16. Iwasaki, Y. W., Siomi, M. C. & Siomi, H. PIWI-Interacting RNA: Its Biogenesis and Functions. *Annu. Rev. Biochem.* **84**, 405–433 (2015).

17. Tiffany-Castiglioni, E. Cell culture models for lead toxicity in neuronal and glial cells. *Neurotoxicology* **14**, 513–536 (1993).

18. Dórea, J. G. Environmental exposure to low-level lead (Pb) co-occurring with other neurotoxicants in early life and neurodevelopment of children. *Environ. Res.* **177**, 108641 (2019).

19. Hanna-Attisha, M., LaChance, J., Sadler, R. C. & Champney Schnepp, A. Elevated Blood Lead Levels in Children Associated With the Flint Drinking Water Crisis: A Spatial Analysis of Risk and Public Health Response. *Am. J. Public Health* **106**, 283–290 (2016).

20. Faulk, C., Barks, A., Liu, K., Goodrich, J. M. & Dolinoy, D. C. Early-life lead exposure results in dose- and sex-specific effects on weight and epigenetic gene regulation in weanling mice. *Epigenomics* **5**, 487–500 (2013).

21. Biomonitoring - Lead | US EPA. https://www.epa.gov/americaschildrenenvironment/biomonitoring-lead.

22. McFarland, M. J., Hauer, M. E. & Reuben, A. Half of US population exposed to adverse lead levels in early childhood. *Proc. Natl. Acad. Sci.* **119**, e2118631119 (2022).

23. Fontana, C. *et al.* Early maternal care restores LINE-1 methylation and enhances neurodevelopment in preterm infants. *BMC Med.* **19**, 42 (2021).

24. Davies, W., Isles, A. R. & Wilkinson, L. S. Imprinted gene expression in the brain. *Neurosci. Biobehav. Rev.* **29**, 421–430 (2005).

25. Blood Lead Reference Value | Lead | CDC. https://www.cdc.gov/nceh/lead/data/blood-lead-reference-value.htm (2022).

26. Dai, P. *et al.* A Translation-Activating Function of MIWI/piRNA during Mouse Spermiogenesis. *Cell* **179**, 1566-1581.e16 (2019).

27. Perera, B. P. U. *et al.* Somatic expression of piRNA and associated machinery in the mouse identifies short, tissue-specific piRNA. *Epigenetics* **14**, 504–521 (2019).

28. Yohannes, Y. B. *et al.* Methylation profiles of global LINE-1 DNA and the GSTP1 promoter region in children exposed to lead (Pb). *Epigenetics* **17**, 2377–2388 (2022).

29. Goodrich, J. M. *et al.* Adolescent epigenetic profiles and environmental exposures from early life through peri-adolescence. *Environ. Epigenetics* **2**, dvw018 (2016).

30. Akulenko, N. *et al.* Transcriptional and chromatin changes accompanying de novo formation of transgenic piRNA clusters. *RNA N. Y. N* **24**, 574–584 (2018).

31. Burgess, D. J. Probing a piRNA paradox. *Nat. Rev. Genet.* **18**, 639–639 (2017).

32. Hoffman, J. L. *et al.* Alcohol drinking exacerbates neural and behavioral pathology in the 3xTg-AD mouse model of Alzheimer's disease. *Int. Rev. Neurobiol.* **148**, 169–230 (2019).

33. Cleal, M. *et al.* The Free-movement pattern Y-maze: A cross-species measure of working memory and executive function. *Behav. Res. Methods* **53**, 536–557 (2021).

34. Hoffmann, L. F. *et al.* Neural regeneration research model to be explored: SH-SY5Y human neuroblastoma cells. *Neural Regen. Res.* **18**, 1265–1266 (2022).

35. Shan, W. *et al.* Evaluation of atrazine neurodevelopment toxicity in vitro-application of hESC-based neural differentiation model. *Reprod. Toxicol. Elmsford N* **103**, 149–158 (2021).

Figures

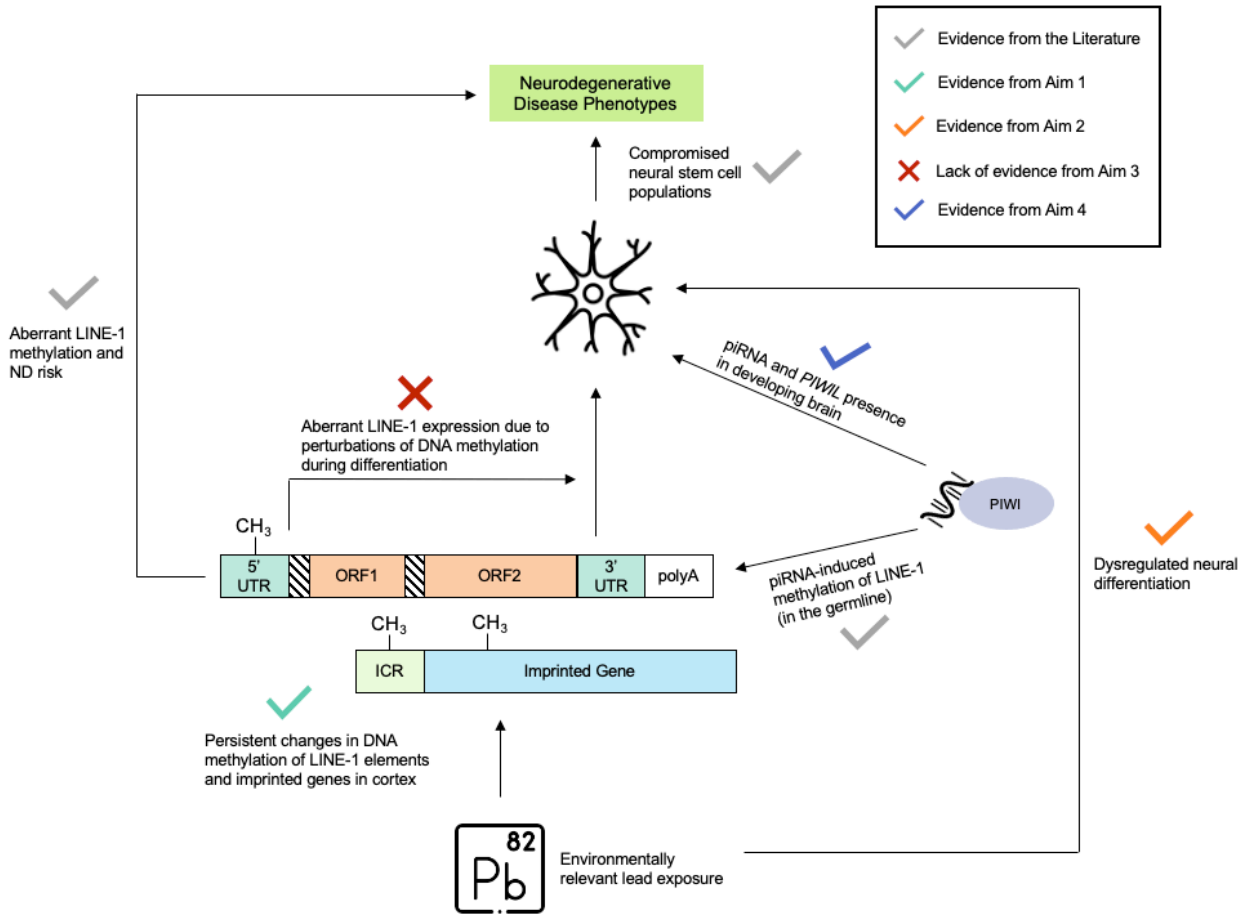

Figure 6.1: Proposed mechanism linking developmental lead (Pb) exposure and neurodegenerative disease risk later in life. Hypomethylation of LINE-1 elements has been associated with increased ND risk, and increased LINE-1 retrotransposition is detrimental to developing neurons. Suboptimal neurons have also been documented as associated with ND risk. LINE-1 epigenetic regulation occurs, in part, through piRNA-directed DNA methylation (DNAm). In Aim 1, we found evidence that perinatal Pb exposure is associated with aberrant adult brain and blood DNAm patterns at LINE-1 elements and imprinted genes, indicating that Pb exposure may modulate the expression of these genes. In Aim 2, we demonstrated that Pb exposure significantly perturbs differentiating neurons, which are suspected to contribute to ND risk, per the available literature. In Aim 4 we demonstrated that piRNA and PIWIL mRNA are expressed within the developing human brain and that many piRNAs expressed in this tissue to a significant degree map to LINE-1 elements, suggesting that this regulatory function by this class of ncRNA may not be limited to the germline. In Aim 3, we did not acquire convincing evidence that hypomethylation and overexpression of LINE-1 elements following Pb exposure is related to dysregulation of the piRNA system, suggesting that other regulatory pathways may better explain the observations we made in Aim 1.